UiT The Arctic University of Norway

Faculty of Science and Technology
Department of Geosciences

Lithostratigraphy and chemostratigraphy of Triassic black shales on Edgeøya, eastern Svalbard

Implications for understanding Triassic source rock formation on the Norwegian Barents Shelf

Fredrik Wesenlund

A dissertation for the degree of Philosophiae Doctor, January 2022

C

Lithostratigraphy and chemostratigraphy of Triassic black shales on Edgeøya, eastern Svalbard

Implications for understanding Triassic source rock formation on the Norwegian Barents Shelf

Fredrik Wesenlund
ARCEx - Research Centre for Arctic Petroleum Exploration
Department of Geosciences
Faculty of Science and Technology
UiT The Arctic University of Norway
P.O. box 6050 Langnes
9037 Tromsø, Norway

A dissertation submitted for
the degree of *Philosophiae Doctor*
Tromsø 2022

D

Supervisors:

Associate Professor Dr. Sten-Andreas Grundvåg
ARCEx - Research Centre for Arctic Petroleum Exploration
Department of Geosciences
Faculty of Science and Technology
UiT The Arctic University of Norway
P.O. box 6050 Langnes
9037 Tromsø, Norway

Dr. Olaf Thießen
Equinor ASA
Margrethe Jørgensens vei 4
9406 Harstad, Norway

Dr. Jon Halvard Pedersen
Lundin Energy Norway AS
Strandveien 4
1326 Lysaker, Norway

Jon Erik Skeie
Aker BP ASA
Storåkeren 11
9411 Harstad, Norway

Front page image: A polar bear sow and cub in front of the steep, black shales of the Middle Triassic Botneheia Formation. The picture was taken in the Muen locality (77°49’18.9"N, 21°22’36.6"E) during a field expedition in August 2018 to western Edgeøya, eastern Svalbard.

To the memory of my dear friend, Robin Orre Svennungsen

“If you wish to make an apple pie from scratch,
you must first invent the universe.”
–Carl E. Sagan

“Civilization exists by geological consent,
subject to change without notice.”
–William J. Durant

“Essentially, all models are wrong,
but some are useful.”
–George E. P. Box

Abstract

The Norwegian Barents Shelf (NBS) is an Arctic petroleum province with a complex geological history. Current geochemical work on oil discoveries in the region has identified Triassic mudstones as important petroleum source rocks. A review of the published literature found that several source rock-forming processes have been suggested as contributors to their formation. The aim of this thesis is thus to further understand the paleoenvironmental factors that affected Triassic source rock formation and potential on the NBS. This was done by investigating the lithostratigraphy and organic/inorganic chemostratigraphy of the organic-rich Spathian–Carnian outcrops on Edgeøya, eastern Svalbard. These exposures represent uplifted and exhumed strata of the northwestern NBS that are equivalent to Triassic source rocks on the southern NBS. Paper I characterizes the mudstone facies and bulk organic properties of the Anisian–Ladinian Botneheia Formation to investigate benthic redox conditions, productivity, and organic richness. Paper II performs a multi-elemental chemostratigraphic analysis to further clarify how these environmental factors affected Spathian–Carnian source rock formation. Paper III documents source- and maturity-specific biomarker compounds of the investigated succession and their correlation with oils from the *Alta*, *Gohta*, *Wisting Central* and *Hanssen* discoveries on the NBS. These papers consider the reported climate-induced transition from warmer to cooler oceans at the Spathian–Anisian boundary to have an important impact on Spathian vs. Anisian–Ladinian source rock formation in the region. The early Carnian pro-deltaic mudstones terminated formation of oil-prone source rocks due to the prograding Triassic Boreal Ocean delta system in the south. Spathian mudstone extracts from Svalbard and the Spathian-sourced *Wisting Central/Hanssen* oils show strong biomarker correlations, indicating that these age-equivalent source rocks have comparable organic facies. This challenges the idea that Spathian mudstones on the southern NBS are lateral facies equivalents to the Anisian–Ladinian mudstones in Svalbard. These findings have important implications for conceptualizing the Lower–Upper Triassic source rock models on the NBS.

Acknowledgements

First and foremost, I would like to express my deepest appreciation to my main supervisor Sten-Andreas Grundvåg. I'm very grateful that I was given the opportunity to embark on a PhD degree at UiT The Arctic University of Norway as a part of ARCEx. Together we have scaled howling mountains, icy valleys and treacherous coasts in the Arctic wilderness of Svalbard, luckily with all our limbs still attached at the end of the day. Your approach to this project has been highly professional, supportive and with great spirit. Your patience and constructive criticism have been paramount, and I cannot emphasize enough my appreciation.

To my co-supervisors Olaf Thießen, Jon Halvard Pedersen, and Jon Erik Skeie: I'm deeply indebted to your input and keen interest in this project. Your extensive knowledge provided a beacon of light for an inexperienced PhD-student. I greatly value your ideas, comments, guidance and overall discussions, which I have learned a lot from. Thank you very much.

The completion of my dissertation would not have been possible without my main fieldwork companions and fellow scientists Victoria Sjøholt Engelschiøn and Sofie Bernhardsen. I look back with fond memories of our many hikes together hunting for the best outcrops, and I could not have asked for better camaraderie in the field. I would like to extend my sincere thanks to the organizers Snorre Olaussen and Atle Mørk during field work in 2017 and 2018 on Edgeøya respectively. The skippers Martin, Gisle and Daniel from The Dale Oen Experience on board RV Youexplore are thanked for safe passage and good company. Lastly, I thank the Norwegian Petroleum Directorate (NPD) for helpful discussions during and after the field work on Edgeøya.

I also had great pleasure of working together with the lab-staff Trine, Karina, Ingvild and Matteus. Without your help with sample preparations, use of lab equipment, and geochemical analyses, this work could not have been fulfilled. I really appreciate your expertise and I'm happy to have been a part of your including working environment in the lab. Many thanks to you all.

I would like to thank my UiT ARCEx inmates Alfred, Amando, Andreas, Ellen, Iver, JB, Julian, Mathias, Max, Renate, Rowan, Sigrun, Stine—as well as Kim, Tom and Peter at UNIS—for providing a fun and friendly working environment that I will definitely miss. Furthermore, I thank all my colleagues and friends in Tromsø with whom I have shared hikes, ski trips, quizzes, lunches, discussions, coffee, beers and more. Your friendliness and presence made this project unfold with positivism.

I want to thank my family back home for always being there and for always believing in me. You have kept me going, and this thesis would not have been possible without your continuous encouragement.

Last, but not least, I could not have completed this study without my beloved Nikoline. The PhD project has been a roller coaster of advancements and setbacks, but your never-ending support and understanding made this ride as painless as possible, and for that I am eternally grateful.

Preface

This thesis is the outcome of a four-year PhD project that commenced in April 2017. The project was funded by the Research Centre for Arctic Petroleum Exploration (ARCEx), which is a research collaboration between academia and industry with financial support from the Norwegian Research Council (grant no. 228107) and Norwegian authorities. UiT The Arctic University of Norway is the degree-awarding institution. The work was supervised by Associate Professor Dr. Sten-Andreas Grundvåg (ARCEx, UiT), Dr. Olaf Thießen (Equinor), Dr. Jon Halvard Pedersen (Lundin Energy Norway), and Jon Erik Skeie (Aker BP).

The main objective of the project is to geochemically and sedimentologically characterize and discuss the formation of significant Triassic source rock units in Svalbard and compare these to inferred time- and facies-equivalent source rocks in the subsurface of the Barents Shelf. This work therefore combines facies descriptions, inorganic and organic chemostratigraphy, source–oil correlations, as well as statistical techniques to distinguish and evaluate the paleodepositional processes and products necessary for source rocks to form. The project included approximately six weeks of field work in Svalbard for logging and sampling, and a significant amount of time in the lab processing and analyzing the collected samples. Parts of the work in this thesis have been presented at national and international conferences, either as posters or oral presentations. These publications are registered in the Current Research Information System in Norway (person ID: 540128), available here: `https://app.cristin.no/persons/show.jsf?id=540128`.

One year of the four-year PhD period was dedicated to duty work. This was mainly fulfilled by assisting with seminar exercises and field work for MSc students enrolled in the GEO-3112 "Sedimentary processes and products" course and the GEO-3113 "Field course in exogene geology" course. I also assisted with hosting the weekly Friday seminars at the department, which aim to display the scientific diversity at the department and facilitate scientific discussion between colleagues.

The following ECTS-accredited courses were completed to fulfill the educational component of the PhD degree: AG-834 "Arctic Basins and Petroleum Provinces" (UNIS, 10 ECTS), SVF-8600 "Philosophy of Science and ethics" (UiT, 6 ECTS), "PYREX: Geological Field Trip to the Spanish Pyrenees" (NFiP, 2 ECTS), "World Heritage Jurassic Coast of Dorset" (NFiP, 2 ECTS), and AG-836 "Rift Basin Reservoirs: From Outcrop to Model" (UNIS, 10 ECTS).

Although the current study is strongly tied to petroleum exploration, it relies heavily on principles derived from many other geoscientific disciplines. This includes—among others—organic geochemistry, paleoclimatology, paleoecology, paleoceanography and carbon cycle studies, biogeochemistry, ichnology, lithostratigraphy, sequence stratigraphy and elemental chemostratigraphy. Workers that have a background in these disciplines may therefore find this study intriguing.

This thesis consists of an introduction to why the study was carried out and the geological background (Chapter 1), the scientific approach (Chapter 2), a summary of the three included research papers of which I am the first author (Chapter 3), the three papers (Chapters 4 to 6), and a synthesis (Chapter 7). The three papers (labeled I–III) presented in this thesis are:

I Wesenlund, F., Grundvåg, S.-A., Engelschiøn, V.S., Thießen, O., & Pedersen, J. H. (2021). **Linking facies variations, organic carbon richness and bulk bitumen content – A case study of the organic-rich Middle Triassic shales from eastern Svalbard.** *Marine and Petroleum Geology* 132, 105168. DOI: `https://doi.org/10.1016/j.marpetgeo.2021.105168`.

II Wesenlund, F., Grundvåg, S.-A., Engelschiøn, V.S., Thießen, O., & Pedersen, J. H. **Multi-elemental chemostratigraphy of Triassic mudstones in eastern Svalbard: implications for source rock formation in front of the World's largest delta plain.** *Manuscript accepted for publication in* The Depositional Record *and is currently in copyediting, typesetting or proofreading*.

III Wesenlund, F., Grundvåg, S.-A., Thießen, O., Engelschiøn, V.S., Lerch, B., & Pedersen, J. H. **Organic chemostratigraphy of Triassic black shales in Svalbard: implications for Triassic source facies development, thermal maturity evaluations, and correlations with Barents Sea oils.** *Manuscript in preparation, planned for submission to* Journal of Petroleum Geology.

Contents

List of Abbreviations

AOM amorphous organic matter

APT Applied Petroleum Technology

ARCEx Research Centre for Arctic Petroleum Exploration

CRediT Contributor Roles Taxonomy

DOI Digital Object Identifier

DOP degree of pyritization

ECTS European Credit Transfer and Accumulation System

EF enrichment factor

EOM extractable organic matter

ETR extended tricyclic terpane ratio

FID flame ionization detector

Fm Formation

GC gas chromatography

GR gamma ray

HC hydrocarbon

HCA hierarchical cluster analysis

HI Hydrogen Index

ICP inductively coupled plasma

IEA International Energy Agency

JR-1 Jet Rock - 1

m/z mass-to-charge ratio

Mb Member

MDBT methyldibenzothiophene

MFS maximum flooding surface

MP methylphenanthrene

MPDF1 methylphenanthrene distribution factor 1

MPDF2 methylphenanthrene distribution factor 2

MPI-1 methylphenanthrene index 1

MPR methylphenanthrene ratio

MS mass spectrometer

NBS Norwegian Barents shelf

NCS Norwegian Continental shelf

NFiP Petroleum Research School of Norway

NIGOGA the Norwegian Industry Guide to Organic Geochemical Analyses

NPD Norwegian Petroleum Directorate

NSO-1 North Sea Oil - 1

OES optical emission spectrometry

OI Oxygen Index

OM organic matter

OMZ oxygen minimum zone

PAAS Post-Archean Australian Shale

PCA principal component analysis

PCC Pearson correlation coefficient

Ph Phytane

PI production index

PP petroleum potential

Pr Pristane

REE rare earth element

SAR saturate/aromatic ratio

SCI spore coloration index

SD standard deviation

SIM selected ion monitoring

sm^3 standard cubic meter

SPI source potential index

SR-1 Svalbard Rock - 1

TA-DMC triaromatic dimethylcholesteroid

TAR terrigenous/aquatic ratio

TBO Triassic Boreal Ocean

TC total carbon

TIC total inorganic carbon

TLC thin layer chromatograph

TOC total organic carbon

TR transgressive–regressive

TS total sulfur

UiO University of Oslo

UiT University of Tromsø

UNIS University Centre in Svalbard

VR vitrinite reflectance

WD wave dispersive

XRF X-ray fluorescence

1

Introduction

1.1 Rationale - the global demand for energy

Petroleum (from Latin *petra*, rock, and *oleum*, oil) is the second most abundant liquid on the Earth and has played a paramount role in the development of human society (Islam, 2020). Following the invention of the modern kerosene lamp in Poland in 1853, which sparked a widespread demand for petroleum (Wołkowicz et al., 2017), the high energy density and complex chemical nature of petroleum have served humanity in many ways. This includes fuels for light, transportation, heating and electricity, and as a raw material for chemicals, plastics and other synthetic products that are present in nearly everything we use. Petroleum has been and still is essential for food production and conservation, as well as the development of pharmaceutical products, and thus plays a significant role with respect to sustaining the growth and existence of the human kind. Naturally, the huge financial implications of the petroleum industry remains a prominent driver for hydrocarbon exploration. In Norway, much of the revenue from the oil and gas industry is transferred to the Government Pension Fund Global, informally known as the "oil fund" (NBIM, 2021). This fund has currently reached c. 12 trillion NOK and will serve as a financial reserve for current and future generations (NBIM, 2021). It is also anticipated that the fund will play an important role in the ongoing transition to renewable and sustainable energy sources.

In Norway, the financial contributions from the petroleum industry to academia, and its law-imposed obligations to support research, have contributed immea-

surably to basic research. However, petroleum-related research at Norwegian universities has become increasingly controversial and debated (e.g., NENT, 2014), particularly as Norway is expected to take on a leading role in the ongoing campaign to reduce emissions of greenhouse gases. The international community has agreed that the global fossil fuel consumption must decline in the near future if we (i.e., the human society) are serious about meeting the ambitious goals of the Paris Agreement, the legally-binding international treaty on climate change (Nogrady, 2021).

A recent report by DNV (2021) forecasts that the electrification of final energy demand will change from 19% to 38% by 2050, dominantly through wind and solar power (Fig. 1.1). However, fossil fuels are still expected to account for c. 50% of the world primary energy demand in 2050 (Fig. 1.1). Petroleum will therefore have a substantial role in the decades to come, both as an energy source and feedstock for various products. As petroleum is a non-renewable energy source, it can only be replenished by making new discoveries. The total world consumption of c. 15 million standard cubic meter (sm^3) petroleum and liquid fuels in 2021 is expected to increase in the near future (EIA, 2021). The historic and future demand creates a strong incentive for the energy industry to continue with petroleum production and exploration. This is despite the estimate that nearly 58% of oil, 59% of fossil methane gas, and 89% of coal (relative to the 2018 reserve base) must remain in the ground to achieve a global 1.5°C temperature target as pledged in the Paris Agreement (Welsby et al., 2021).

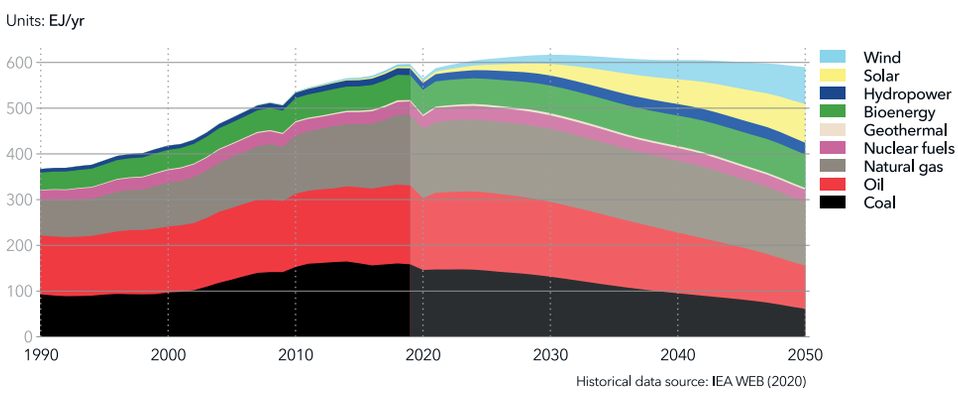

Figure 1.1: Historical and forecast world primary energy supply by source (DNV, 2021). Historical data up to and including 2018 is based on data and statistics from the International Energy Agency (IEA) (see DNV, 2021, for more info). Year 2020 marks the onset of the COVID-19 pandemic, causing an abrupt decline in world energy demand.

An important topic that has gotten considerable less attention than climate change is the geopolitical role Norway has as a European fossil fuel and feedstock provider. Norway, a European Free Trade Association (EFTA) state, is

clearly a less controversial petroleum-producing European nation compared to, e.g., Russia, especially after the EU and U.S. condemned the Russian annexation of the Crimea peninsula in Ukraine in 2014. Following this, the Nord Stream 2 gas pipeline from Russia to Germany, currently being finalized, has been highly debated and even sanctioned by the U.S. Department of State (Blinken, 2021). While it is beyond the scope of this thesis to provide an extensive analysis of European geopolitics, it is apparent that Norway's decision to continue or discontinue oil and gas exploration and production on the Norwegian Continental shelf (NCS) has serious potential geopolitical ramifications.

Consequently, petroleum activity on the NCS is ongoing and simultaneously contributing to the welfare state of Norway. During the last 10 years, significant investigations have been made to increase our understanding of the petroleum potential on the NBS. This is due to the fact that the NBS is generally an underexplored petroleum province. In response, ARCEx was formed, partly funded by the Research Council of Norway, a Norwegian government agency. This study is thus a part of the governmental mission to understand the geological prerequisites and processes that allow petroleum accumulations to occur on the NBS.

1.2 Why study source rocks?

Petroleum source rocks, or simply source rocks, are sedimentary rocks containing organic matter (OM) that are capable of, may become, or have been able to generate and expel petroleum (Tissot and Welte, 1984). For the exploration geologist, mapping and documenting the presence of source rocks and establishing their source potential are key objectives, because without a source rock, petroleum cannot be generated (Selley and Sonnenberg, 2015). The existence of a source rock is therefore the minimum requirement for a *petroleum system* to occur, i.e., all the essential elements and processes necessary for petroleum accumulations to exist (*sensu* Magoon and Dow, 1994). "*Do we have a source rock?*" should therefore be among the very first questions in any play or prospect evaluation (Selley and Sonnenberg, 2015). For a source rock to exist, petroleum-generating OM must have been created, deposited, and preserved in sufficient quanta (Bohacs et al., 2005). Thus, the paleodepositional environment—in which the source rock was deposited—has the ultimate control on source rock thickness, quality, and richness of OM. For this very reason, understanding the many factors governing the source rock depositional model and formation are other key objectives for the petroleum explorationist (Peters and Cassa, 1994).

1.3 Why study source rocks on Svalbard and the Barents Shelf?

On the NBS, c. 130 wildcat wells have been drilled to date, contrasting the more than 750 wildcat wells drilled in the North Sea (norskpetroleum.no, 2021). Still, the NBS is estimated to contain 64% of the remaining undiscovered resources on the NCS (NPD, 2017). This amounts to c. 2.5 of 3.9 billion sm^3 of recoverable oil equivalents and includes the (currently) non-commercial acreage in the Northern NBS (norskpetroleum.no, 2021). In a recent resource-estimate report by the NPD (2017) it is suggested that the Middle Triassic mudstones are the most important oil-prone source rock succession offshore in the northern parts of the NBS. The largest oil discovery on the NBS during the last 10 years of exploration effort is the Wisting Discovery (2013), which is presumably sourced by Lower–Middle Triassic organic-rich mudstones (Lerch et al., 2018; norskpetroleum.no, 2021). Facies-equivalent Lower–Middle Triassic mudstones are proven to be oil-prone and the source of the petroleum hosted within the Triassic (Kobbe Formation (Fm)) reservoir in the Goliat Field (2000), which was put into production in 2016 (e.g., Lundschien et al., 2014; Tsikalas et al., 2018). These two oil accumulations, which are located more than 250 km apart from each other, demonstrate that Lower–Middle Triassic oil-prone source rocks are regionally distributed.

However, it is difficult to investigate Triassic source rock material from the NBS, as recovered core material is relatively scarce. This is a primary limitation concerning further documentation and interpretation of their stratigraphic and lateral facies variability. The core sections of well 7323/07 from the Svalis Dome area, drilled during the 1980s, penetrate Triassic organic-rich mudstones and thus serve as a key reference section to investigate the Lower–Middle Triassic source rocks on the commercially available part of the NBS (Mørk and Elvebakk, 1999). According to the NPD (2021b), it was only until recently (2016) that Lower–Middle Triassic source rocks were penetrated during commercial exploration (i.e., the 7222/1-1 *Aurelia* wildcat well operated by Eni Norge AS, now Vår Energi AS). Although penetrated, the inferred Triassic source rock unit was not cored. As oil companies focus mostly on characterizing their petroleum-filled reservoirs (and rarely the source rocks) there is an overall lack of core material necessary for proper source rock evaluation. This is less than ideal, as visual and geochemical assessments of mudstone samples from either core or outcrop provide the best circumstances to investigate how the paleoenvironmental conditions developed and thus the source potential (Percy and Pedersen, 2020). This is where the high-Arctic archipelago of Svalbard comes into play.

Svalbard represents an exhumed and exposed part of the NBS, thus providing an

onshore window into the subsurface of the NBS, which allows field geologists to observe, smell, chew and sample the Lower–Middle Triassic source rock system. In Svalbard, the Middle Triassic Botneheia Fm represents a slightly younger facies equivalent to the prolific Lower–Middle Triassic source rock units offshore (Lundschien et al., 2014). However, despite previous source rock investigations of the Lower Triassic strata (e.g., Abdullah, 1999; Brekke et al., 2014; Hammer et al., 2019; Mørk et al., 1999b) and especially the Middle Triassic strata in Svalbard (e.g., Abay et al., 2018; Abdullah, 1999; Brekke et al., 2014; Hubred, 2006; Krajewski, 2008; Krajewski, 2013; Leith et al., 1993; Mørk et al., 1982; Mørk and Bjorøy, 1984; Vigran et al., 2008), their paleodepositional conditions are still not entirely understood. In particular, the regional understanding and the link between the onshore (Svalbard) and offshore (e.g., Svalis Dome) parts of the succession is poorly understood.

1.4 What factors govern source rock formation and potential?

While many processes and their combinations affect source rock formation (Katz, 2005), the following three factors are considered the most important in terms of investigating source rock formation and potential (Bohacs et al., 2005; Katz, 2005; Tyson, 1995; Walters, 2006):

- Organic productivity, i.e., the creation or lack thereof of OM (e.g., Pedersen and Calvert, 1990)
- Preservation potential, i.e., the preservation or destruction of OM (e.g., Demaison and Moore, 1980)
- Sedimentation or burial rate, i.e., the condensation or dilution of OM (e.g., Creaney and Passey, 1993)

OM-rich rocks, including source rocks, are thus formed when the OM production is high, destruction is low, and dilution/condensation by clastic input and/or biogenic material (e.g., silicates, phosphates and/or carbonates) is balanced (Fig. 1.2). The sections below (Sections 1.4.1 to 1.4.3) briefly describe how these factors may vary based on the depositional environment.

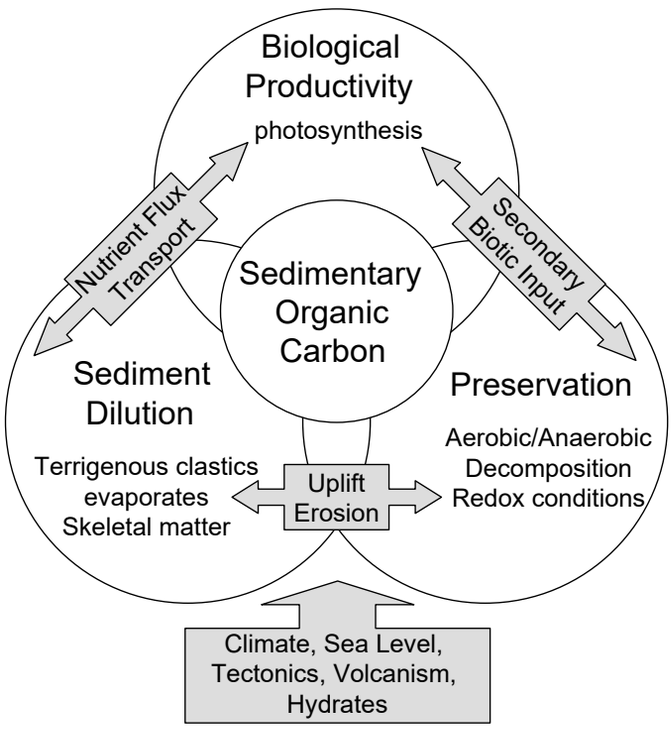

Figure 1.2: The interplay between the three major factors affecting sedimentary organic carbon accumulation and thus source rock deposition: production, preservation and dilution. Collected from Walters (2006).

1.4.1 Organic productivity

While several previous publications predating the 20th century argued that petroleum could have originated from abiotic sources, there is now overwhelming amounts of evidence proving that petroleum originates from biogenic sources (see discussion in Peters et al., 2005b, their chapter 9). In order for OM to be deposited and eventually form source rocks, it must first be produced. In the marine environment, phytoplankton—i.e., algae produced in the photic zone through photosynthesis—are the primary source of marine OM (Demaison and Moore, 1980), however bacterial biomass may represent a significant part of the deposited OM (Bordovskiy, 1965). Primary produced terrestrial OM, including wood, roots, spores, pollen, leaves, etc. can also be transported into the marine environment by rivers and be deposited with the marine OM (Demaison and Moore, 1980). As a result, the absolute and relative abundance of marine vs. terrestrial OM and the resulting kerogen content in a source rock can vary significantly, ultimately affecting the source rock quality (Table 1.1). As the macerals derived from algal bodies (kerogen type I and II) are oil-prone (Table 1.1), the degree of marine primary productivity and the processes which

causes this to occur are central in terms of understanding the source rock formation and its potential. The review on source rock development by Katz (2005) considered the two following processes to be typically associated with elevated marine primary productivity:

- Upwelling, causing nutrient-rich bottom waters to flow upwards in the water column and eventually to the photic zone.

- Fluvial discharge from rivers and streams, providing nutrient-rich waters into the basin.

In both scenarios, the availability of nutrients—which generally is a limiting factor for marine primary productivity—is elevated, resulting in increased production of marine OM (Demaison and Moore, 1980). Furthermore, as the amount of primary produced OM in the photic zone is roughly proportional to that which is exported to the sea floor surface (Tribovillard et al., 2006), the degree of primary productivity has a direct influence on the richness of OM in the sediment.

Table 1.1: Relationship between organic petrographic nomenclature, Rock-Eval kerogen type, the probable origin of the macerals and their main expelled petroleum product at peak maturity. Note that source rocks often host a mix of marine and terrestrial OM, resulting in a mixed kerogen type (e.g., type III/II), being both gas-prone and oil-prone. *Assuming immature source rocks only. Adapted from Peters et al. (2005b) and Peters and Cassa (1994).

Maceral group	Kerogen type*	Maceral type	Probable origin	Main petroleum product
Liptinite	II	Resinite	Plant resins/degraded macerals	Oil
	II	Sporinite	Spores/pollens	Oil
	II	Cutinite	Plant cuticles	Oil
	II	Bituminite	Degraded algae	Oil
	I	Alginite	Algae	Oil
	II	Liptodetrinite	Mixed origin/aliphatic biological materials	Oil
Vitrinite	III	Vitrinite	Woody tissues	Gas
Inertinite	IV	Semifusinite	Partially heated woody tissues	None
	IV	Fusinite	Carbonized woody tissues	None
	IV	Micrinite	Woody tissues/uncertain	None
	IV	Macrinite	Woody tissues/uncertain	None
	IV	Inertodetrinite	Carbonized woody tissue fragments	None
	IV	Sclerotinite	Fungal hyphae	None

1.4.2 Preservation potential

As the reactive OM necessary to form source rocks is deposited on the sea floor, it serves as an important energy and nutrient source for living organisms, as well as being thermodynamically unstable (Demaison and Moore, 1980;

Peters et al., 2005b). In order for the marine and terrestrial OM to take part in source rock formation, it is crucial that it is minimally oxidized during deposition and subsequent diagenesis. During oxic conditions, oxidizing bacteria in combination with benthic scavengers will efficiently degrade (i.e., metabolize and oxidize) the deposited OM, while during anoxic conditions, the lack of oxidizing bacteria but presence of sulfate-reducing or methanogenic bacteria results in less efficient OM degradation (Demaison and Moore, 1980). The benthic oxygen content therefore has direct implications on OM degradation and consumption (Fig. 1.3a), hence also the quality and quantity of the deposited OM.

Anoxic conditions take place when the oxygen demand exceeds the supply (Katz, 2005). For instance, obstructed oxygen supply due to the bathymetric configuration or water mass stratification induced by chemical or thermal contrasts may cause oxygen depletion, potentially preserving oil-prone OM (Fig. 1.3b). Furthermore, algal blooms formed by high nutrient supply through fluvial discharge or upwelling results in higher than normal oxygen demand, reinforced by the following bacterial degradation of the produced algae (Demaison and Moore, 1980). These scenarios may result in waters so depleted in oxygen that an oxygen minimum zone (OMZ) or "dead zone" is formed, allowing sufficient preservation of oil-prone OM (Fig. 1.3c). Thus, paleoceanographic and paleogeographic investigations of the source rock and the associated basin could provide important implications for understanding variations in the preservation potential.

1.4.3 Sedimentation rate

In a marine basin with anoxic conditions, it has been shown that low sedimentation rates yield higher total organic carbon (TOC) content that is oil-prone, while high sedimentation rates yield lower TOC content and more gas-prone kerogen (Creaney and Passey, 1993). However, too low sedimentation rates might also increase the exposure time of the deposited OM, leading to greater possibility of degradation as well as thinner source rock successions (Bohacs et al., 2005). Several factors can affect the sedimentation rate, e.g., the amount and type of sediment that is transported into the basin, the distance to the sediment source, the biogenic production in the basin, the degree of bioturbation, and the hydrological/hydrodynamic regimes (e.g., Szmytkiewicz and Zalewska, 2014). While the interplay between these processes are complicated, perhaps even impossible to determine in ancient rocks (Tyson, 2001), sedimentary sites may have optimal sedimentation rates in which the TOC content is maximized (Fig. 1.4). Thus, an assessment of the biogenic vs. detrital input into the basin and distance to the sediment source may help to understand how the sedimentation rate affects the source rock potential.

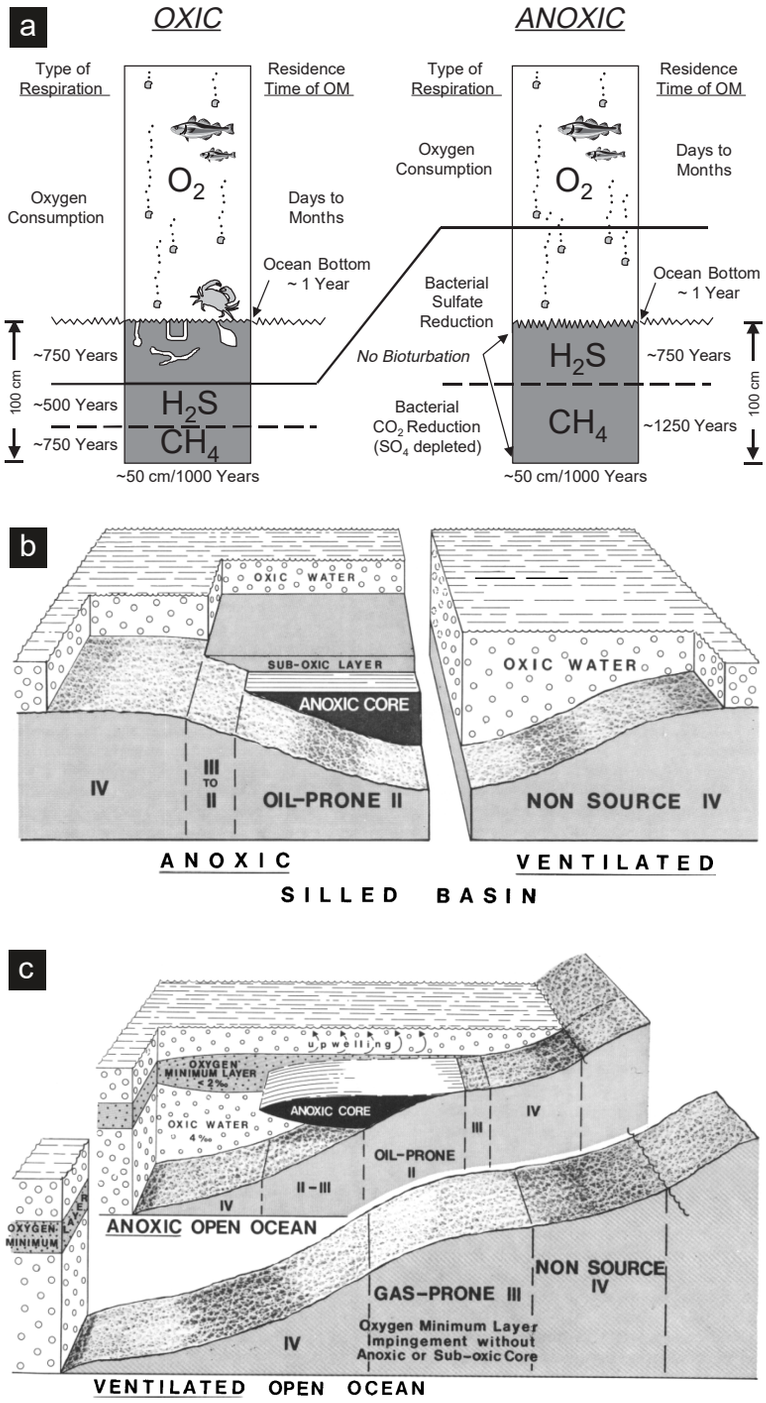

Figure 1.3: (a) The effects of oxic and anoxic conditions on benthic hospitality and associated OM degradation. Collected from Peters et al. (2005b), originally from Demaison and Moore (1980). **(b)** A comparison of an oxic (ventilated) and anoxic (stagnant) silled basin setting and their effect on source rock quality (kerogen type). Collected from Demaison et al. (1983). **(c)** A comparison of an oxic (ventilated) and anoxic (upwelled) open ocean basin setting and their effect on source rock quality (kerogen type). Collected from Demaison et al. (1983).

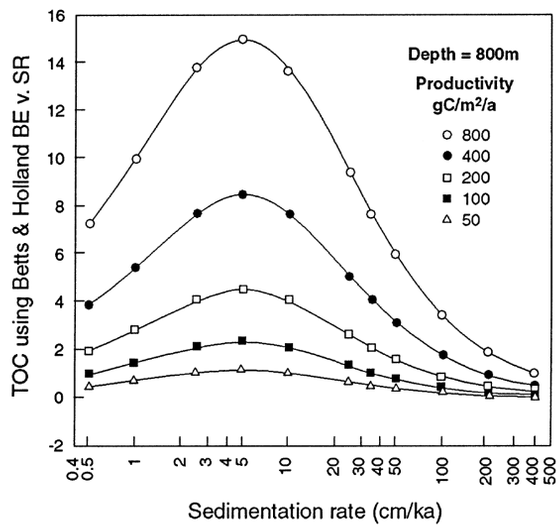

Figure 1.4: An example of a modeled relationship between TOC using the burial efficiency (BE) vs. sedimentation rate (SR) relationship of Betts and Holland (1991) plotted against sedimentation rate. Water depth is set at 800 m, the burial efficiency is assumed to be independent of carbon delivery flux, and the TOC is assumed to be marine only. For this given configuration, a sedimentation rate of c. 5 cm/ka maximizes the TOC content of the sediment. Collected from Tyson (2001).

1.5 Aim and objectives

Mapping the thickness, richness and quality of source rocks and how they where formed provides new knowledge to evaluate the probability of oil and gas formation on the NBS. As a result, the overall aim of this PhD thesis is investigate how the Lower–Middle Triassic source rock properties and petroleum products were affected by the variable and changing paleodepositional conditions, ultimately governing source rock quality and their final source potential.

More specifically, the objectives of this study are to:

- Characterize and document lithology, kerogen and bitumen contents of the Triassic source rocks in Svalbard, and evaluate how organic productivity, OM preservation, and sedimentation/burial rates have influenced these parameters (main focus of Paper I).

- Establish an elemental chemostratigraphic- and proxy-based framework to specifically evaluate how paleoredox conditions, paleoproductivity, and sedimentation rates changed from the late Early Triassic to the earliest

Late Triassic, and tentatively correlate this framework with inferred age- and facies-equivalent mudstones on the Barents Shelf (main focus of Paper II).

- Characterize the aliphatic, aromatic and biomarker compounds of mudstone extracts from Svalbard to identify how paleoredox conditions, paleoproductivity and lithology variations affect commonly applied source facies and thermal maturity parameters. The analyzed extracts are compared to oils from selected discoveries on the NBS, which previously have been linked to inferred Triassic sources (main focus of Paper III).

1.6 Geologic setting

The Triassic development in Svalbard and the greater Barents Sea is strongly linked with the inherited marine epicontinental shelf that formed during the Permian ((Henriksen et al., 2011b; Mørk, 2015). This relatively shallow basin, here referred to as the Triassic Boreal Ocean (TBO), was bounded by the Fennoscandian Shield in the south, Greenland in the west and Novaya Zemlya in the southeast, facing the open waters of the Panthalassic Ocean in the North (Fig. 1.5). The Uralian orogen, which started to develop during the Permian in the southeast, formed the dominant sediment source for much of the region during the Triassic and provided huge amounts of sediments that were transported more than 1500 km within the TBO (Klausen et al., 2019), eventually reaching Svalbard during the Carnian (Figs. 1.6 and 1.7). The Svalbard area is generally considered to be tectonically quiescent throughout the entire Triassic (Leith et al., 1993; Riis et al., 2008), however studies performed on the Upper Triassic growth faults on western Edgeøya (Høy and Lundschien, 2011) could indicate deep-rooted normal fault activity (Anell et al., 2013; Osmundsen et al., 2014), suggesting some tectonic activity during the Late Triassic. Klausen (2013) argued that they could just as well represent depositional gravity driven collapse of the unconsolidated delta front. Still, recent work suggests that far-field tectonics caused by the late Triassic Uralide orogeny could have reactivated deep-rooted Carboniferous tectonic faults, which combined with localized shallow diagenesis and liquidation, resulted in mechanical instabilities and formation of these Upper Triassic growth fault systems (Ogata et al., 2018). Similarly, Muller et al. (2019) linked angular unconformities between Upper Triassic and Jurassic strata on the southern Barents Shelf with compression induced by the Novaya Zemlya Fold and Thrust Belt, which developed during the Late Triassic as the northern extension of the Uralian orogenic wedge. Thus apparently, the Early and Middle Triassic in Svalbard were generally unaffected by tectonism.

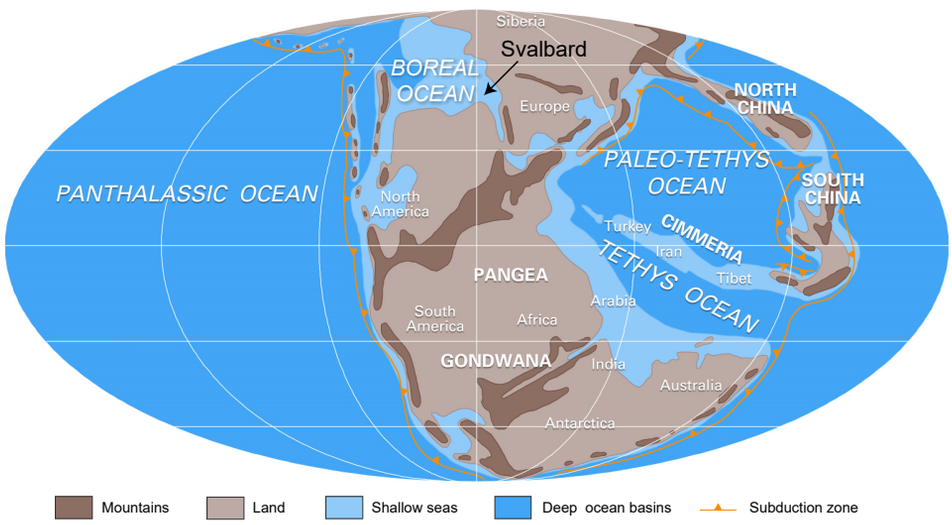

Figure 1.5: Early Triassic paleogeographic reconstruction, showing the epicontinental setting of the Boreal Ocean at c. 40–60 °N and the likely placement of Svalbard. Modified from Logan (2020).

The Early Triassic is interpreted to represent a period with hothouse conditions that reduced marine productivity and nutrient supply, possibly resulting in an Early Triassic nutrient gap in the TBO (Grasby et al., 2016; Grasby et al., 2020). The mudstone-dominated Lower Triassic succession in central–eastern Svalbard is assigned to the Vikinghøgda Fm, which were deposited in a marine shelf environment with northeastern Greenland acting as the most important source area (Mørk et al., 1982). In central Spitsbergen, the lowermost part of the Vikinghøgda Fm contains abundant siltstones and sandstones with hummocky cross-lamination, which suggests deposition on a shelf mainly above storm wave base (Mørk et al., 1999b). Such deposits do not occur in the Lower Triassic in eastern Svalbard, possibly because the Edgeøya Platform was uplifted and subaerially exposed during the Induan (Vigran et al., 2014). The Edgeøya Platform was flooded during an early Smithian transgression, establishing moderately deep shelf environments, allowing the deposition of fine-grained mudstones assigned to the Lusitaniadalen Member (Mb) (Mørk et al., 1999b). During the Spathian, the basin deepened even further, resulting in the deposition of darker and more OM-rich silty mudstones assigned to the Vendomdalen Mb. (Mørk et al., 1999b). Based on the finely laminated character of these mudstones, they are suggested to have been deposited below storm wave base in an oxygen deficient setting (Mørk et al., 1999b). On the southern NBS, age-equivalent mudstones are assigned to the lower Steinkobbe Fm. These mudstones were apparently deposited in a deep and restricted shelf environment, eventually promoting the formation of important oil-prone source rocks (Mørk and Elvebakk, 1999).

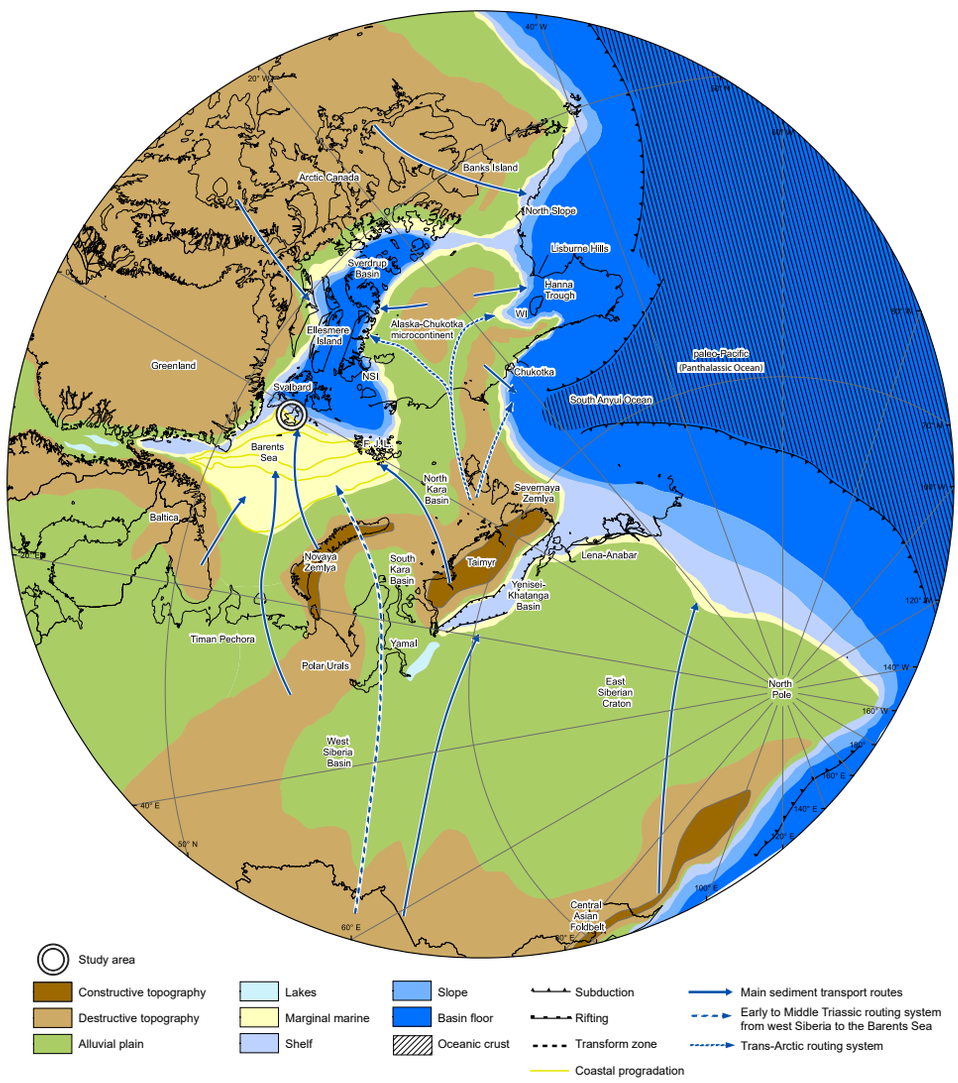

Figure 1.6: Late Triassic paleogeographic reconstruction, showing how the TBO delta system prograded. Modified from Sømme et al. (2018).

During the earliest Anisian, regional transgression associated with a pan-Arctic flooding event marks the onset of the Middle Triassic (Mørk et al., 1994; Mørk et al., 1982; Mørk et al., 1989). The resulting regionally-extensive flooding surface has been traced from Svalbard southward to the Svalis Dome on the southern NBS, westwards to the Sverdrup Basin in Arctic Canada (Mørk et al., 1989), southeastwards into the southern Barents Basin in Russia (Gilmullina et al., 2021), and perhaps to the Wandel Sea Basin in northeastern Greenland towards the southwest (Bjerager et al., 2019). In Svalbard, the Middle Triassic is assigned to the Botneheia Fm, which comprises the Muen (Anisian) and the Blanknuten (Anisian-Ladinian) members (Krajewski, 2008; Mørk et al., 1999a). The lower–

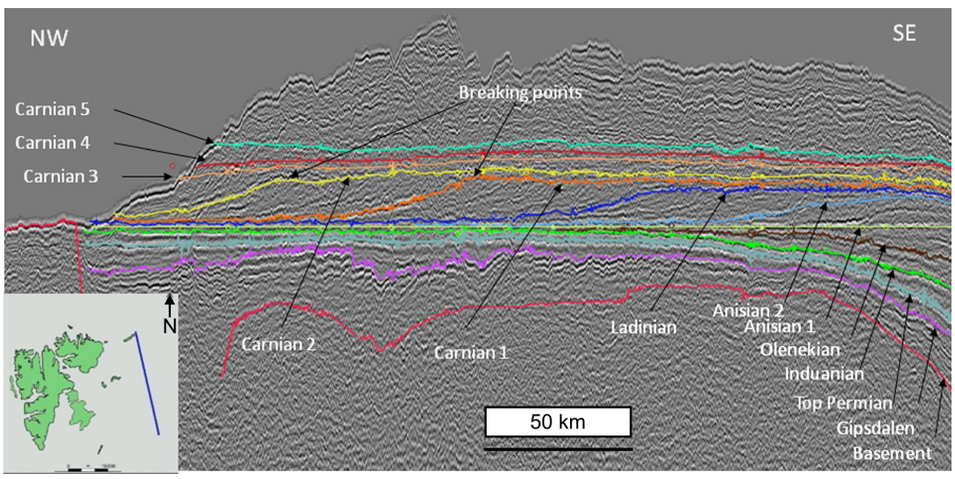

Figure 1.7: A northwest to southeast seismic line c. 300 km east of the western shore of Edgeøya. The seismic line is flattened on a seismic reflector of Anisian age to illustrate the northwestwards progradation of the TBO delta system. Modified from Høy and Lundschien (2011).

middle Muen Mb consists of dark gray and soft mudstones with authigenic P-nodules, but with negligible P content within the mudstone matrix (Krajewski, 2008). It has previously been interpreted to represent deep and restricted (oxygen deficient) shelf deposits (Høy and Lundschien, 2011; Vigran et al., 2014). However, the unit also shows evidence of ventilated, oxic–dysoxic and hospitable benthic conditions (Krajewski, 2008; Krajewski, 2013; Wesenlund et al., 2021). On the southern NBS, gray silt- and mudstones of the middle Steinkobbe Fm (lower Anisian) also indicate deposition in open well-ventilated shelf environments (Mørk and Elvebakk, 1999). This regional Spathian–Anisian facies transition may thus be attributed to lowered OM preservation potential due to the global climate change from warm and restricted oceans during the Spathian to cooler and ventilated oceans during the Anisian (Grasby et al., 2016; Grasby et al., 2020; Sun et al., 2012).

The middle–upper Anisian marks the onset of increasingly enhanced upwelling and nutrient supply, resulting in intense marine productivity and the formation of an OMZ (Krajewski, 2008; Krajewski, 2013). This allowed deposition of black, brittle and mudstones with elevated and H-rich OM content, abundant P-nodules, and P-filled mudstone matrix that belong to the middle–upper Muen and lower Blanknuten members on Edgeøya (Krajewski, 2008; Krajewski, 2013; Wesenlund et al., 2021). During the early Ladinian sea-level highstand, the combined effect of these processes reached a maximum, promoting the formation of highly oil-prone, non-bioturbated and phosphatic mudstones assigned to the Blanknuten Mb (Krajewski, 2013). On the southern NBS, the extensive deltaic progradation continued during the Ladinian, resulting in the development of

well-ventilated pro-delta settings (Lundschien et al., 2014). Thus, while the conditions to form highly oil-prone source rocks were ideal in the northern NBS during this time, they had already ended in the Svalis Dome area on the southern NBS (Leith et al., 1993). Shoaling of the TBO during the late Ladinian resulted in increasingly oxygenated bottom conditions and diminished OM preservation potential in Svalbard, but still deposition of oil-prone black shales belonging to the upper Blanknuten Mb (Krajewski, 2013).

In Svalbard, the early Carnian marks an important shift in the main sediment source, from Greenland in the west to Novaya Zemlya in the southeast (Vigran et al., 2014). This relates to the continued progradation of the approaching TBO delta system, which resulted in the deposition of prodelta muds that eventually blanketed the Lower-Middle Triassic sediments in Svalbard (e.g., Riis et al., 2008). These prodelta mudstones are assigned to the Tschermakfjellet Fm (lower Carnian) (Mørk et al., 1982) and are thus diachronous, lateral facies equivalents to the Ladinian lower Snadd Fm mudstones on the southern NBS (Lundschien et al., 2014). The Tschermakfjellet Fm consists of dark gray–gray mudstones with characteristic siderite-cemented nodules and beds that have a red weathering hue attributed to the increasingly shallowing basin and influx of riverine input (Mørk et al., 1982; Vigran et al., 2014), reflecting the upwards-shallowing offshore shelf to pro-deltaic environment (Nagy et al., 2011; Vigran et al., 2014). The continuous progradation of the TBO delta system introduced the genetically related delta topset part represented by the overlying and topmost formation in Edgeøya, the Carnian De Geerdalen Fm (Fig. 1.8). This unit consists of sandstones and mudstones from a dominantly paralic depositional environment (Lord et al., 2017; Mørk et al., 1982; Vigran et al., 2014). This exemplifies that the vast TBO delta plain eventually reached Svalbard, more than 1000 km northwest of the southeastern initial position of the delta front (Klausen et al., 2019).

The Sverdrup Basin region was still in a distal position (relative to the delta front), which promoted ideal conditions for OM preservation and source rock deposition (Fig. 1.6). Here, the upper Triassic Murray Harbour Fm represents a facies-equivalent unit to the Middle Triassic Botneheia Fm (Leith et al., 1993). In the North Slope Basin, northern Alaska, the phosphatic, calcareous and organic-rich middle–upper Triassic Shublik Fm also demonstrate that similar conditions were widespread at these times, allowing oil-prone source rocks to form. (Parrish et al., 2001; Parrish and Curtis, 1982; Yurchenko et al., 2018). Thus, the oceanic conditions during the late Triassic were still favorable for marine oil-prone source rock deposition in the TBO and along the northern Pangean shelf margin, even though these conditions were terminated in Svalbard at the arrival of the TBO delta system (Leith et al., 1993).

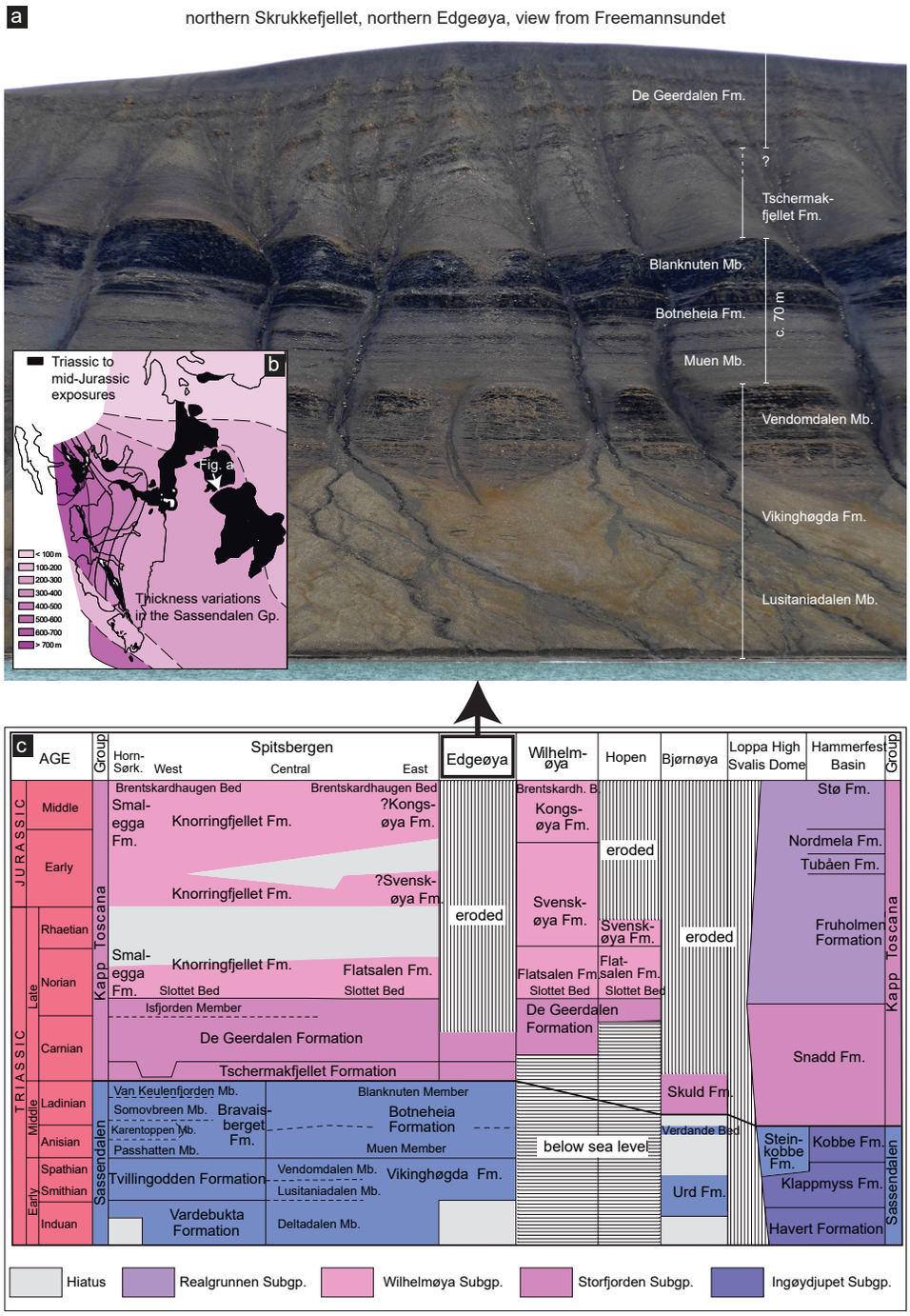

Figure 1.8: (a) Outcrop overview of the Vikinghøgda, Botneheia, Tschermakfjellet and De Geerdalen formations in northern Edgeøya, eastern Svalbard. **(b)** Thickness map of the Sassendalen Group (Vikinghøgda and Botneheia formations in central–eastern Svalbard), showing the gradual thinning eastwards, away from the main sediment source in the west. Collected from Vigran et al. (2014). **(c)** Lithostratigraphic overview of the Sassendalen and Kapp Toscana groups. Collected from Vigran et al. (2014), initially modified from Mørk et al. (1999a).

2

Scientific approach

This study combines field work with geochemical analyses and multivariate statistics of sampled mudstones from Edgeøya, eastern Svalbard, and crude oil samples from the 7220/11-1 *Alta*, 7120/1-3 *Gohta*, 7324/8-1 *Wisting Central* and 7324/7-2 *Hanssen* discoveries on the NBS. This chapter documents the scientific approach and geochemical analyses that was undertaken in this study, and describes the rationale of the applied methods.

2.1 Field work and localities

Approximately five weeks of field work split into four field expeditions were carried out in Svalbard between 2017–2018 (Table 2.1). The objectives of these campaigns were to log and document the lithostratigraphical development of the Triassic mudstone succession in eastern Svalbard, and simultaneously collect samples for geochemical analyses. These samples form the foundation for the geochemical database that was later used to interpret the source rock properties and paleodepositional conditions. The Blanknuten, Skrukkefjellet and Muen localities (Fig. 2.1) provided excellent stratigraphic control which allowed clear recognition of the Lower, Middle and Upper Triassic parts of the succession and sub-unit differentiation of the Botneheia Fm, following the nomenclature of Krajewski (2008), Krajewski (2013), and Vigran et al. (2014). Samples from the late mature–postmature Muen locality (Brekke et al., 2014) were analyzed using organic geochemical techniques, however the biomarker data were un-

fortunately of insufficient resolution or quality to interpret chemostratigraphic variations through the Middle Triassic Botneheia Fm. Luckily, the excellent exposures of the Botneheia Fm in the marginally mature to mature Blanknuten and Skrukkefjellet localities (Krajewski, 2013) allowed clear identification of organic chemostratigraphic variations, lithostratigraphic sub-units and boundaries. Given the completeness of the succession in eastern Svalbard and the favorable thermal maturity, the dataset in Papers I–III are solely based on the coupled litho- and chemostratigraphic database acquired from the Blanknuten and Skrukkefjellet localities. The fieldwork and remaining geochemical results from the other localities (Table 2.1) are therefore not considered here.

Table 2.1: Summary of field expeditions carried out as a part of this study.

Field season	Item	Description
Summer 2017	Duration (days)	3
	Localities	Festningen, Hornsund, Muen
	Stratigraphic units	Botneheia Fm, Bravaisberget Fm
	Organizer	Snorre Olaussen
	Main field party	Fredrik Wesenlund, Sten-Andreas Grundvåg, Olaf Thießen
	Transportation	RV Stålbas
	Sponsor	Statoil (now Equinor ASA)
Summer 2017	Duration (days)	2
	Localities	Miseryfjellet
	Stratigraphic units	Urd Fm, Skuld Fm
	Organizer	Atle Mørk
	Main field party	Fredrik Wesenlund, Sten-Andreas Grundvåg, Sigrun M. Kvendbø Hegstad
	Transportation	RV Stålbas
	Sponsor	NPD
Spring 2018	Duration (days)	2
	Localities	Milne Edwardsfjellet
	Stratigraphic units	Botneheia Fm
	Organizer	Sten-Andreas Grundvåg
	Main field party	Fredrik Wesenlund, Sten-Andreas Grundvåg
	Transportation	Snow mobile
	Sponsor	ARCEx
Summer 2018	Duration (days)	28
	Localities	Blanknuten, Drivdalen, Muen, Skrukkefjellet
	Stratigraphic units	Vikinghøgda Fm, Botneheia Fm, Tschermakfjellet Fm
	Organizer	Atle Mørk
	Main field party	Fredrik Wesenlund, Victoria Sjøholt Engelschiøn, Sofie Bernhardsen, Atle Mørk
	Transportation	RV Youexplore by The Dale Oen Experience
	Sponsor	Lundin Energy Norway, NPD

2.2 Stratigraphic logging and facies characterization

The excellently exposed outcrops on Edgeøya, eastern Svalbard, allowed detailed lithostratigraphic investigation and correlation of the studied Lower–

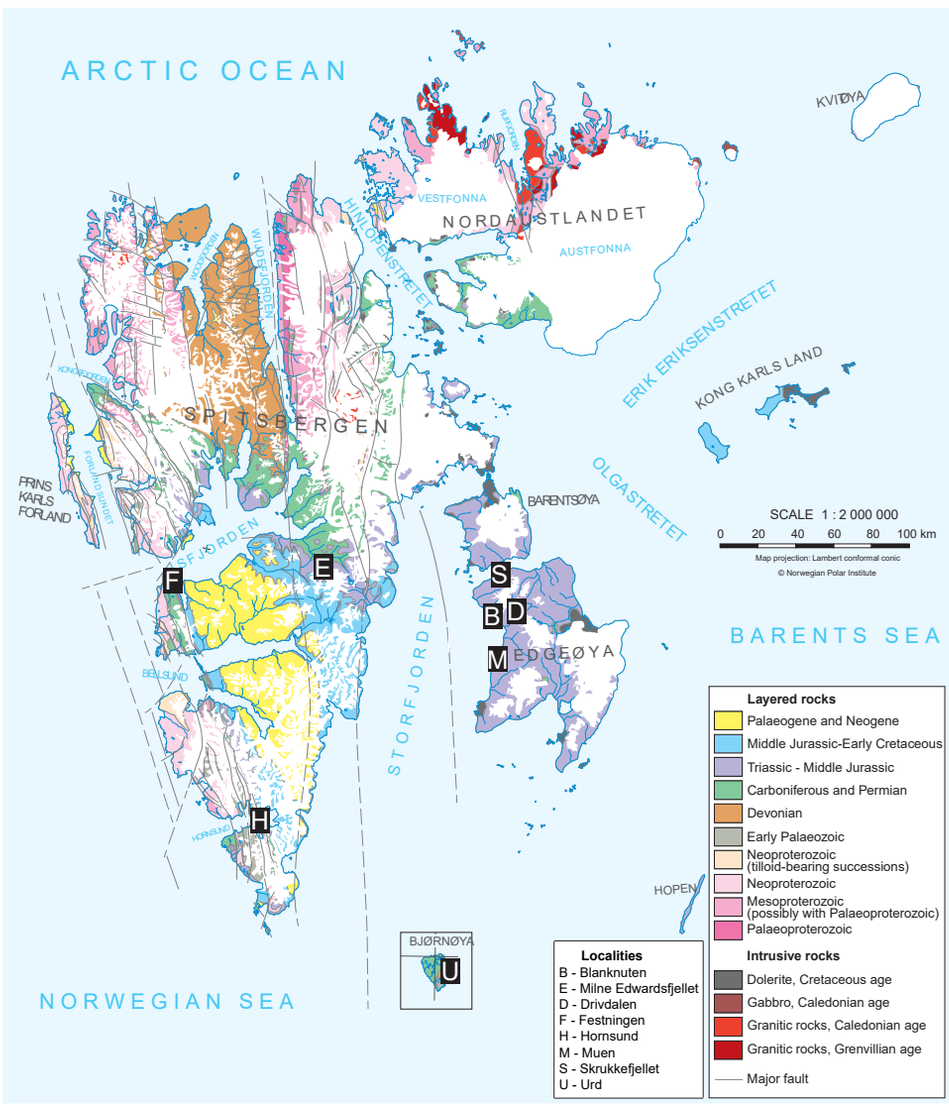

Figure 2.1: Overview map of Svalbard and the investigated localities. Note that Bjørnøya (locality U), i.e., the island representing the southernmost part of the Svalbard archipelago, is repositioned to fit in the figure. Modified from Dallmann and Elvevold (2015).

Upper Triassic mudstones. A lithostratigraphic log that covers the Lower–Upper Triassic mudstones of the Blanknuten section is included in Papers I and III. Paper II includes a composite log, combining the above Blanknuten log with a lithostratigraphic log of the Skrukkefjellet section. Careful lithostratigraphic correlation by close-up and overview photographs were sufficient to correlate the defined lithostratigraphic units and facies with high confidence between the Blanknuten and Skrukkefjellet sections. The logging focused on documenting litho- and biostratigraphic variations, including sedimentary structures, event beds, degree of bioturbation, trace fossils, authigenic nodules and concretions of variable mineralogy, cementation, color, cliff-forming ability, outcrop weathering expression, and brittleness. These macroscopic properties were used to generate a mudstone facies classification scheme that was applied throughout Papers I–III.

Due to the overall fine-grained nature and varying degree of cementation in the investigated mudstones, it was not possible to macroscopically determine their grain size in a consistent and objective manner. However, the macroscopic facies classification is shown to be sufficient to determine all of the lithostratigraphic boundaries, as well as the previously defined Lower–Upper Triassic mudstones (Papers I–III). It is also directly linked to the detailed lithostratigraphy of Krajewski (2008) and Krajewski (2013), who performed exhaustive sedimentological and petrographical microfacies descriptions and interpretations of the mudstones of the Botneheia Fm. Thus, the provided lithostratigraphic log and the defined mudstone facies show that only a minimum of tools are required to sufficiently distinguish the defined lithostratigraphic sub-units and therefore also the main source rock intervals in the study area (Paper I).

The ages of the defined lithostratigraphic units are based on lithostratigraphic correlations of the Skrukkefjellet and Blanknuten sections using palynozones from the Skrukkefjellet locality (Table 2.2) (Vigran et al., 2014). As the investigated Lower–Middle Triassic successions in these localities show extremely low stratigraphic variation, as well as being only c. 20 km apart, it is assumed that the palynozones in the Skrukkefjellet section are also present in the Blanknuten section and that these are lithostratigraphically correlated.

Table 2.2: Approximate age relationships between the defined lithostratigraphic units used in this study and identified palynozones from the Skrukkefjellet locality (Vigran et al., 2014).

		Lithostratigraphic units		
Palynozone	Age	Svalbard	Svalis Dome	Core
Pechorosporites disertus	early Spathian	Vendomdalen Mb	Klappmyss Fm	7323/7–U–4
Jerseyiaspora punctispinosa	late Spathian	Vendomdalen Mb	lower Steinkobbe Fm	7323/7–U–4
Anapiculatisporites spiniger	early Anisian	lower–middle Muen Mb	lower Steinkobbe Fm	7323/7–U–4
Triadispora obscura	middle Anisian	middle–upper Muen Mb, lower Blanknuten Mb	middle Steinkobbe Fm	7323/7–U–1
Protodiploxypinus decus	late Anisian	lower Blanknuten Mb	upper Steinkobbe Fm	7323/7–U–7, 7323/7–U–9
Echinitosporites iliacoides	Ladinian	middle Blanknuten Mb, upper Blanknuten Mb	Snadd Fm	7323/7–U–10, 7323/7–U–5, 7323/7–U–2
Aulisporites astigmosus	early–middle Carnian	Tschermakfjellet Fm	Snadd Fm	7430/7–U–1

2.3 Geochemical analyses

A range of analytical techniques was applied to determine organic and inorganic properties of the collected mudstone samples. Collectively, the acquired analytical data serve as the geochemical foundation to evaluate the source rock properties and the paleoenvironmental conditions. A short description of the applied instruments, what type of data they provide and which lab they belong to is given below.

A **LECO™ CS744** carbon/sulfur determinator was used to determine total carbon (TC), total inorganic carbon (TIC), TOC, and total sulfur (TS). These analyses were performed at the Department of Geoscience, Faculty of Science and Technology, UiT. The instrument combusts the sample using radio-frequency induction, forming CO_2 and SO_2. These two gases absorb infrared energy at unique wavelengths, and can therefore be separately quantified as they pass through infrared absorption cells within the instrument. TOC is widely used to as an indicator of source rock richness (e.g., Bohacs et al., 2005; Peters and Cassa, 1994), TIC is a proxy for carbonate content (e.g., Song et al., 2014), and TS is often related to the paleoenvironmental redox conditions (Berner, 1984; Berner and Raiswell, 1983; Raiswell et al., 1988). To acquire TOC, the sample was treated with HCl to remove carbonate. This was repeated until no reaction between the sample and HCl could be observed, indicating that carbonate (i.e. the inorganic carbon) has dissolved and that only organic carbon remains in the sample. TC and TS were determined by analyzing non-acid treated samples. TIC was then calculated by subtracting the TOC from TC. More details concerning this analytical method are present in Paper I.

In the same lab, a **Bruker S8 Tiger** wave dispersive (WD) X-ray fluorescence (XRF) spectrometer was used to determine a variety of major, minor and trace elements, ranging from Na to U. As black shales are commonly enriched in elements that are affected by variations in redox conditions and paleoproductivity, the elemental assemblage may provide important information on these depositional processes (Algeo and Maynard, 2004; Algeo and Maynard, 2008; Craigie, 2018; Tribovillard et al., 2006). Elemental chemostratigraphic variations may also be used to identify chemostratigraphic units within homogeneous mudstone sections for correlation purposes (Craigie, 2018). The powdered mudstone samples were homogeneously mixed with binder wax and subsequently pressed at 20 t to yield a press pellet ready for analysis. The elements Si, Al, K, Ca, Mg, Na, P and Se were calibrated using the the semi-quantitative Bruker QUANT-EXPRESS™ method, while Sc, Ti, V, Cr, Mn, Fe, Co, Ni, Cu, Zn, Ga, As, Rb, Sr, Y, Zr, Nb, Mo, Cs, Ba, La, Ce, Pb, Th, U were calibrated against the quantitative Bruker GEO-QUANT T™ method.

Normalization against an average shale standard is a common procedure to

determine if the studied samples are enriched or depleted relative to representative background concentrations (Tribovillard et al., 2006). To evaluate if the mudstone samples were enriched or depleted in any of these elements, the enrichment factor (EF) of each element were calculated following Eq. (2.1) (Tribovillard et al., 2006):

$$X_{EF} = \frac{\left(\frac{X}{Al}\right)_{\text{sample}}}{\left(\frac{X}{Al}\right)_{\text{standard}}} \tag{2.1}$$

where X_{EF} is the EF of the element of interest, and X and Al are the weight concentrations of the element of interest and Al. This study uses the commonly used Post-Archean Australian Shale (PAAS) standard (Taylor and McLennan, 1985) for all elements except As, which lack in their study. For As, the average shale in Wedepohl (2004) was used, however with the Al value from the PAAS (Taylor and McLennan, 1985) for consistency.

The organic geochemical analyses were performed at the organic geochemical laboratory at the Department of Geosciences, Faculty of Mathematics and Natural Sciences, University of Oslo (UiO). Prior to the organic geochemical analyses, the crushed mudstone samples were extracted with a **FOSS ST 243 Soxtec™** manual extraction system using 50 ml dichloromethane:methanol (93:7 vol./vol.) The samples were boiled for 1 hour and rinsed for 2 hours, and the remaining total extract was subsequently concentrated to 0.5 ml by fume hood evaporation.

An **Iatroscan™ MK-5** thin layer chromatograph (TLC) flame ionization detector (FID) was used to quantify the saturate, aromatic and polar fractions (resins + asphaltenes) of the total extracts (further described in Karlsen and Larter, 1991). These properties are useful to determine organic richness and the OM type hosted within the source rocks (Le Tran and Philippe, 1993; Tissot and Welte, 1984; Waples and Curiale, 1999). 2.0 or 3.0 µl (specified in the online supplementary materials for Paper I) of a 3.85 % strength analyte of the above 0.5 ml total extract concentrate was then applied onto silica gel-coated rods (type Chromarod IV). Through elutions with cyclohexane and toluene, the saturated hydrocarbons, aromatic hydrocarbons and polar compounds (resins + asphaltenes) were separated along the silica rods. The silica rods were then evaporated a final time to remove any residual solvents and subsequently analyzed by the Iatroscan™ instrument. Peak areas were manually interpreted and absolute bitumen content was calculated using in-house response factors. More details regarding this method is available in Paper I.

A **Varian™ CP-3800** gas chromatography (GC)-FID was used to quantify the relative concentration of the C_{13}–C_{20} acyclic isoprenoids (excluding C_{17}) and the C_9–C_{44} *n*-alkanes. Collectively, these compounds are commonly used in oil–source rock correlation, maturity assessments and to determine the source rock depositional environment (Peters et al., 2005a; Tissot and Welte, 1984). Five pasteur pipette drops of the total extract concentrate were inserted into sample vials, subsequently put into an autosampler ready for analysis. The compounds above were quantified relative to each other—i.e., without an internal standard—by measuring the peak heights from manually interpreted baselines from each GC-FID chromatograms.

A **Thermo Scientific™ Trace™ 1310** GC coupled to a **Thermo Scientific™ TSQ™ 8000 Triple Quadrupole** GC-mass spectrometer (MS) was used to determine a selection of biomarkers, phenanthrene, methylphenanthrenes and methyldibenzothiophenes. These compounds and ratios thereof are heavily applied to evaluate thermal maturity, source rock depositional environment, and/or the the age of the source rock, all which contribute to improved source rock understanding (Kvalheim et al., 1987; Peters et al., 2005a; Radke, 1988; Tissot and Welte, 1984). Prior to the analysis, a five Å molecular sieve and five pasteur pipette drops of the total extract concentrate was mixed together with cyclohexane to remove *n*-alkanes and polar compounds. the resulting analyte was concentrated in a sample vial and analyzed using the following mass-to-charge ratios (m/zs): 142, 156, 170, 177, 178, 184, 191, 192, 198, 205, 206, 217, 218, 219, 231, 253 and 259 (Weiss et al., 2000).

A set of specific analytical methods not offered by academic institutions was outsourced to Applied Petroleum Technology (APT) in Oslo, Norway. This includes Rock-Eval pyrolysis (Peters, 1986), vitrinite reflectance analysis (Dow, 1977), and analysis of the visual kerogen composition (Tyson, 1995).

A flow chart of the analytical procedures is shown in Figure 2.2. For further information on the analytical procedures, see Papers I–III.

2.4 Source–oil and oil–oil correlations

Source–oil correlation is an integral part of understanding the petroleum system, as it allows the petroleum geologist to determine the genetic relationship between the source rock and the migrated oil or reservoir extract (Peters et al., 2005a). Similarly, an oil–oil correlation is made by comparing the geochemistry of reservoired oils, making it is possible to assess the source and maturity properties of the oils (Peters et al., 2005a). This is important, as knowing if the oils were sourced from the same or different source rocks and their mat-

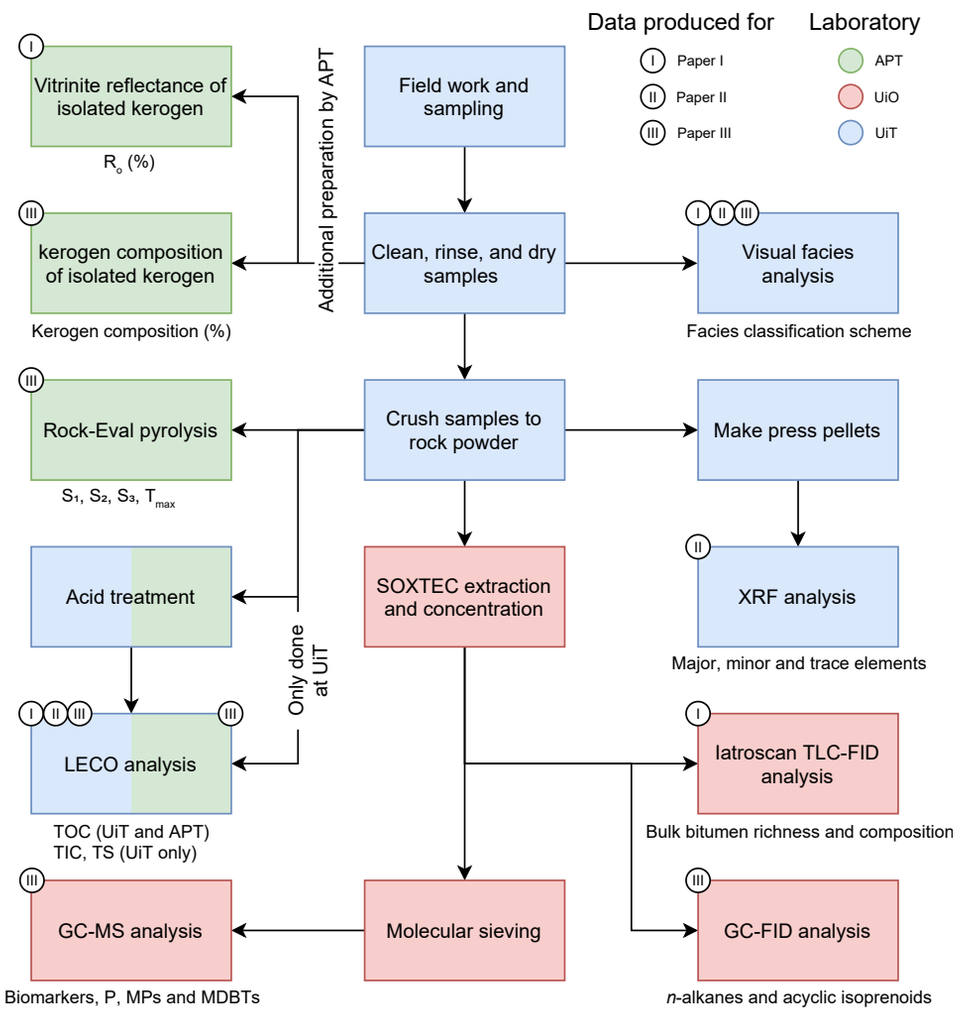

Figure 2.2: A simplified flowchart summarizing the geochemical analyses performed in this study. For an explanation of the abbreviations, see page xvi.

uration levels has major implications towards understanding the petroleum system.

The chromatograms of the mudstone extracts were compared with selected NBS oils previously analyzed by Benedict Lerch at the organic geochemical laboratory at the Department of Geosciences, Faculty of Mathematics and Natural Sciences, UiO, and generously provided for Paper III (Table 2.3). As these oils were analyzed using the same equipment and instruments as the mudstone extracts, they are assumed to be readily comparable and without need for correction due to variations in interlaboratory procedures or results. As with the extracts, the organic geochemical compounds identified in the GC-FID and GC-MS chromatograms of the oils were quantified using manual

baseline interpretation and peak height measurements.

Table 2.3: Summary of selected oils from the NBS included for source–oil and oil–oil correlations

Discovery	Well	Sample type	Measured depth (m)	Formation	Stratigraphy
Alta	7220/11-1	Oil (DST-1A)	1946.5	Falk	Carboniferous
Alta	7220/11-1	Oil (DST-1B)	1921.0	Triassic conglom.	Triassic
Gohta	7120/1-3	Oil	2315.7	Røye	Permian
Wisting Central	7324/8-1	Oil	664.0	Stø	Middle Jurassic
Hanssen	7324/7-2	Oil	715.0	Stø	Middle Jurassic

2.5 Exploratory data analysis and repeatability

The PYTHON programming language coupled with the PANDAS data analysis and manipulation library were used to import and wrangle the geochemical data and to calculate geochemical parameters. The MATPLOTLIB, NUMPY, SCIKIT-LEARN, SEABORN and PLOTLY data analysis libraries were consistently used for all the bi- and multivariate plots and analyses included in this study.

The recent call for openness and availability of scientific work and the introduction of Plan S, which is an initiative stating that results from scientific research funded by public grants *must* be published open access, is strongly supported by UiT The Arctic University of Norway. In an effort to promote transparency and repeatability, the PYTHON scripts written for this study are or will be available in the following GitHub repository: `https://github.com/fredrwes/Publications`. As this PYTHON-based approach is powerful, flexible, and open source, these scripts could pose as an alternative to proprietary software for other workers concerned with similar research questions.

For Paper I, all the geochemical data is accessible in the supplementary materials on the article webpage. It can be accessed via the DOI in Paper I (see Chapter 4). Similarly, all the analytical data for Paper II will be accessible through the *The Depositional Record* article webpage when published. For Paper III, the raw GC-FID and GC-MS data will eventually be uploaded to the DataverseNO open research data repository maintained by UiT The Arctic University of Norway: `https://dataverse.no/dataverse/uit`.

In Papers I and II, multivariate analyses were performed, namely principal component analysis (PCA) and hierarchical cluster analysis (HCA). These analyses are commonly used to gain insight into the correlation between the

organic and inorganic geochemical properties of source rocks and oils (Garcia et al., 2020; Peters et al., 2005a; Wang et al., 2018). Before performing the PCA and HCA, the data were transformed into the tidy data format (see discussion on tidy data formatting by Wickham, 2014). Each column was then scaled to the range of [0,1] using min–max feature scaling according to Eq. (2.2):

$$x' = \frac{x - \min(x)}{\max(x) - \min(x)} \tag{2.2}$$

where x is an original value, and x' is the normalized value. The PCA performs linear dimensionality reduction to project it to a lower dimensionality space, ideally allowing the main features of the multivariate dataset to be displayed using bivariate plots. The applied PCA algorithm is documented in the SKLEARN documentation (Scikit-learn, 2021). The HCA performs hierarchical/agglomerative clustering using the unweighted pair group method with arithmetic mean algorithm. The applied HCA algorithm is further described in the SEABORN documentation (seaborn, 2021) and the SCIPY documentation (SciPy, 2021).

3

Summary of research papers

3.1 Paper I

Wesenlund, F., Grundvåg, S.-A., Engelschiøn, V.S., Thießen, O., & Pedersen, J. H. (2021). **Linking facies variations, organic carbon richness and bulk bitumen content – A case study of the organic-rich Middle Triassic shales from eastern Svalbard.** *Marine and Petroleum Geology* 132, 105168. DOI: `https://doi.org/10.1016/j.marpetgeo.2021.105168`.

In Paper I, Middle–Upper Triassic strata on Edgeøya, eastern Svalbard, were logged and sampled. The samples were analyzed for TOC, TIC, and TS content (LECO analysis) and bulk bitumen characterization (Iatroscan TLC-FID analysis). Optical vitrinite reflectance analyses by APT of a small sample subset were included. The collected samples were grouped into specific mudstone facies based on their macroscopic and geochemical properties. This paper establishes a stratigraphic framework which has subsequently been applied in Papers II and III. Previous work by Krajewski (2008), Krajewski (2013), and Vigran et al. (2014) of the Botneheia Fm was fundamental in order to get an overview of the Middle Triassic lithostratigraphy in the study area. The main aim of this paper is to document the Middle Triassic organic chemostratigraphic development and discuss their variations in light of the evolving Triassic source rock depositional environment in the TBO. This is further integrated with the pan-Arctic Middle

Triassic 2nd order transgressive–regressive (TR) cycle. The geochemical data was utilized in multivariate analyses to see if they could be used to distinguish the determined lithostratigraphic units using geochemistry alone.

The results show that the mudstones of the lower–middle Muen Mb (lower Anisian) were deposited in oxic–dysoxic benthic conditions with relatively poor preservation potential. This is based on relatively low median TOC, TS and absolute bitumen content, high saturate/aromatic ratio (SAR), and the presence of *Helminthopsis* and *Chondrites* trace fossils. In contrast, the phosphogenic upper Muen Mb (middle–upper Anisian) shows substantially larger median TOC, TS, absolute bitumen, and a significantly lower SAR. This unit marks the onset of extensive marine OM production, deposition and preservation during increasingly oxygen deficit conditions. The lower Blanknuten Mb (upper Anisian) shows similar facies characteristics and organic/inorganic geochemical content, marking a continued deepening of the basin. The middle Blanknuten Mb (lower Ladinian) is the unit with highest TOC, TS, absolute bitumen content and the lowest SAR. This reflects deposition during the maximum flooding phase of the Middle Triassic TR-sequence, causing sediment starvation but also high nutrient supply promoted by well-established upwelling. Ultimately, this resulted in high marine productivity and subsequent oxygen demand, triggering oxygen deficiency and thus good preservation of the deposited oil-prone marine OM. The upper Blanknuten Mb mudstones (upper Ladinian) denote the onset of basin shoaling, seen by increased relative amounts of terrestrial OM and lowered preservation potential inferred from higher SAR and lower TOC contents. The mudstones of the lowermost meters of the Tschermakfjellet Fm are shown to be organic geochemically similar to the mudstones of the lower–middle Muen Mb.

Multivariate analyses of these stratigraphic units using the obtained geochemical data allow a clear distinction of the non-phosphogenic lower–middle Muen Mb and the phosphogenic upper Muen Mb and entire Blanknuten Mb. This is important, as the former unit hosts mostly mixed oil/gas source rocks while the latter units host dominantly oil-prone source rocks.

The findings of this study are compared with former, contradicting interpretations of the benthic redox conditions during deposition of the Muen Mb mudstones in eastern Svalbard. Krajewski (2008) and Krajewski (2013) considered the mudstones of the lower–middle Muen Mb to have been deposited during oxic–dysoxic benthic conditions, while Lundschien et al. (2014) and Vigran et al. (2014) considered the entire Muen Mb to be deposited in dominantly anoxic benthic conditions. This study considers these mudstones to be deposited during oxic–dysoxic benthic conditions, evidenced by the amount and composition of the kerogen and bitumen content, as well as the presence of *Chondrites* and *Helminthopsis* trace fossils. Thus, while the lower–middle

Muen Mb unit contains P-nodules that indicate phosphogenesis due to upwelling, the productivity was not intense enough to form a persistent OMZ that allowed good preservation of H-rich OM. The bulk bitumen composition and richness of the mudstone extracts of the phosphogenic upper Muen Mb and entire Blanknuten Mb are also shown to be in good agreement with Rock-Eval pyrolysis data from Krajewski (2013) and Mørk and Bjorøy (1984), further strengthening the fact that these units are the best Triassic source rock units in Svalbard.

Conclusively, this study generally agrees with the previous paleoenvironmental interpretations, but considers the lower–middle Muen Mb to be deposited in oxic–dysoxic benthic conditions, in agreement with Krajewski (2008) and Krajewski (2013).

3.2 Paper II

Wesenlund, F., Grundvåg, S.-A., Engelschiøn, V.S., Thießen, O., & Pedersen, J. H. **Multi-elemental chemostratigraphy of Triassic mudstones in eastern Svalbard: implications for source rock formation in front of the World's largest delta plain.** *Manuscript accepted for publication in* The Depositional Record *and is currently in copyediting, typesetting or proofreading*.

In Paper II, the Lower–Upper Triassic mudstones on Edgeøya, eastern Svalbard, were characterized for their major, minor and trace element composition using WD-XRF analysis. The lithostratigraphy introduced in Paper I was applied and expanded to include the Vendomdalen Mb (Spathian) of the Vikinghøgda Fm (Lower Triassic). The TOC, TIC and TS data of the Botneheia and Tschermakfjellet formations from Paper I were included and also determined for the Vendomdalen Mb following the analytical methods outlined in Paper I. The main aim of this paper is to establish an elemental chemostratigraphic framework and apply the elemental data as proxies to investigate how marine productivity (OM generation), benthic paleoredox conditions (OM preservation), and changing sedimentation rates (OM concentration or dilution) affected OM accumulation and source rock formation in the TBO. Similar to Paper I, the obtained geochemical data from this study were utilized in multivariate analyses to check whether the previously identified lithostratigraphic units could be identified based on their elemental assemblage.

The results show that the silty mudstones of the Vendomdalen Mb are enriched in TOC, TS and exhibit elevated EFs of U, Co, Fe, Mo and Pb, indicating deposition during intermittent euxinic benthic waters. Their relatively low values of TOC and EFs of Ni, Cu, Ba and P further suggest that Spathian primary

productivity was overall low. The lower–middle Muen Mb shows lower TOC content, negligible EFs of Mo, U and P, but a higher EF of Ba and common *in situ* P-nodules in the mudstone matrix. Thus, the early Anisian may mark the onset of a cooler climate with less restricted waters, enhanced upwelling, nutrient supply and marine productivity, but the production was not sufficient to form a persistent OMZ with good preservation potential. Intense phosphogenesis was not well-established before deposition of the upper Muen Mb and the lower Blanknuten Mb mudstones, which show a sharp increase in productivity, redox and phosphate proxies (i.e., TOC, TS and EFs of Ba, Cr, Cu, Ni, Si, U, P, Sc, Y, La and Ce). The Middle Blanknuten Mb mudstones exhibit the strongest enrichment in most of the paleoredox and -productivity proxies, including TOC, TS and EFs of V, Zn, U, P, Si, Ba, Cr, Ni and Cu. The reducing (euxinic) benthic conditions appear to be mainly driven by metabolic demand, as EFs of Mo and U indicate an unrestricted and less stratified basin setting, perhaps caused by the cooler Middle Triassic climate. These mudstones show a notable dilution of conservative lithogenic elements, i.e., Al, K, Ti, Ga, Rb, Zr, Nb, Cs and Th, coinciding with the early Ladinian maximum flooding of the basin and subsequent sediment starvation on the NBS. Thus, their high preservation potential, intense marine production and low sedimentation rate during deposition ultimately resulted in the formation of the best Triassic source rocks in the region. The upper Blanknuten Mb mudstones (upper Ladinian) in Svalbard show strong enrichment in Mo and U, suggesting intermittently euxinic conditions as the TBO became increasingly shallower. The increased hydrodynamic activity is further supported by an increase in grain size proxies, however the production and preservation of OM were still excellent, eventually resulting in development of dominantly oil prone source rocks. The Carnian Tschermakfjellet Fm mudstones marks the introduction of prodelta muds of the TBO delta system in eastern Svalbard, representing a younger, time-transgressive facies equivalent to the Snadd Fm on the southern NBS. The non-biogenic element assemblage of the Tschermakfjellet Fm indicates a change from a Caledonian provenance to a Uralide provenance, in concert with the cessation of the conditions favoring the formation of highly oil-prone and marine source rocks in the Barents Shelf and Svalbard region of the TBO.

The findings of this study show that the Vikinghøgda–Botneheia Fm boundary, which roughly correlate to the Spathian–Anisian boundary (Krajewski, 2008; Krajewski, 2013), denotes a substantial shift in the benthic redox conditions from intermittent euxinic to oxic–dysoxic, perhaps due to global climate changes. Similarly, euxinic phases have been recorded in Smithian and Spathian marine strata in western Spitsbergen (Wignall et al., 2016), as well in the Sverdrup Basin, Arctic Canada (Grasby et al., 2013). These findings were further linked with the hot global climate of the Early Triassic, which possibly restricted circulation and upwelling within the TBO, inhibiting nutrient supply and marine productivity (Grasby et al., 2016; Grasby et al., 2020). The Spathian–

Anisian Steinkobbe Fm, which shows a prominent TOC decline at the Spathian–Anisian boundary (Mørk and Elvebakk, 1999), could thus have been affected by these potentially regional oceanographic processes. The abundant P-nodules in the Anisian Steinkobbe Fm, as described in Mørk and Elvebakk (1999), resemble the age-equivalent Anisian upper Muen and lower Blanknuten members, both rich in P-nodules. This indicates that high productivity in the TBO was not well established before the Anisian, suggesting that the lower (Spathian) and middle–upper (Anisian) parts of the Steinkobbe Fm, both oil-prone source rock successions, could have been formed during different depositional settings. This study therefore raises questions about the suggested facies-equivalent and diachronous relationship between the Botneheia Fm in Svalbard and the lower Steinkobbe Fm on the southern NBS.

Additionally, this study demonstrates that the identified lithostratigraphic units have elemental assemblages that are geochemically distinct. The supplied elemental chemostratigraphic framework and its proxy capabilities are therefore useful with respect to mapping, correlation and interpretation of the above paleoenvironmental factors and their influence on source rock formation and potential.

3.3 Paper III

Wesenlund, F., Grundvåg, S.-A., Thießen, O., Engelschiøn, V.S., Lerch, B., & Pedersen, J. H. **Organic chemostratigraphy of Triassic black shales in Svalbard: implications for Triassic source facies development, thermal maturity evaluations, and correlations with Barents Sea oils.** *Manuscript in preparation, planned for submission to* Journal of Petroleum Geology.

In Paper III, extracts of the Lower–Upper Triassic mudstones on Edgeøya, eastern Svalbard, were geochemically characterized using gas chromatographic separation techniques (i.e., GC-FID and GC-MS) to identify selected *n*-alkanes, acyclic isoprenoids, aromatic compounds and biomarkers. The TOC, TIC and TS data derived from the Lower–Upper Triassic mudstone units investigated in Papers I and II were included. Parts of the sample set were subjected to Rock-Eval pyrolysis, LECO analysis and visual kerogen composition analysis by APT. Furthermore, previously analyzed oils from the *Alta*, *Gohta*, *Wisting Central* and *Hanssen* discoveries on the southern NBS were included for comparison. The main aim of this paper is to apply the proxy properties of the above compounds to investigate the paleoredox variations, OM input, source rock lithology and their influence on commonly applied biomarker-based maturity parameters. Oil–source correlations were performed to investigate the relationship between the mudstone extracts from eastern Svalbard and the oils retrieved from the

above discoveries, which all likely or possibly have Triassic sources.

The results show that the Vendomdalen Mb extracts (Spathian) exhibit a clay-rich facies deposited in reducing conditions, promoting good preservation of oil-prone marine OM. The lower–middle Muen Mb extracts (lower Anisian) also show a clay-rich facies, however the maceral composition, acyclic isoprenoids and biomarkers witness that these mudstones were deposited during more oxic conditions and have relatively less marine OM. The abrupt organic chemostratigraphic upwards transition into the upper Muen and Lower Blanknuten members (middle–upper Anisian) records a marked increase in absolute and relative marine OM content, resulting in a less clay-rich facies. This is is related to the onset of intense phosphogenesis and OMZ formation due to high marine production, again linked with the increased nutrient supply made available through sustained and efficient upwelling from the Panthalassic Ocean. The middle Blanknuten Mb mudstones exhibits the best kerogen richness (i.e., highest TOC) and quality (i.e., highest Hydrogen Index (HI)). Their extracts show highly asymptotic *n*-alkane envelopes and low Pristane (Pr)/Phytane (Ph) ratios and a clay poor facies (e.g., low 29αβ/30αβ, high C_{24}tet/30αβ). These observations are linked with high marine OM content, benthic oxygen deficiency and sediment starvation, all a consequence of the high primary productivity and highstand conditions during the early Ladinian. The upper Blanknuten Mb mudstones (upper Ladinian) indicate deposition during a lowered redox boundary and greater input of terrestrial OM (e.g., higher Pr/Ph values and terrigenous/aquatic ratio (TAR)). This suggests that marine productivity was still high but with increasing benthic hydrodynamic activity and terrestrial OM input, perhaps caused by the shallowing epicontinental sea. The Tschermakfjellet Fm mudstones (Carnian) exhibit high Pr/Ph ratios, reworked terrestrial OM, and low TOC, a testament to the dominantly oxidizing benthic conditions that took place as the prodelta muds of the TBO reached eastern Svalbard.

The strong facies contrasts of the investigated stratigraphic units are shown to have similar impacts on especially the Ts/(Ts + Tm) ratio and the 29Ts/(29Ts + 29αβ) ratios. Their strong correlation, when plotted in tandem, could therefore simply indicate source facies variations rather than maturity variations. As a consequence, the use of these two maturity parameters in a binary plot may lead to incorrect maturity assessments of Triassic source rock extracts and oils in the region.

The oil–source correlation of the mudstone extracts and the *Alta*, *Gohta*, *Wisting Central* and *Hanssen* oils shows that the clay-rich facies biomarker signature of the Vendomdalen Mb is overall comparable to these oils. Extracts from the phosphatic and partly calcareous lower, middle and upper Blanknuten Mb also show similar biomarker characteristics as the oils, however their biomarker

content indicate lower clay content that render these mudstones less probable facies equivalents. Previous investigations of age-specific biomarkers by Lerch et al. (2018) suggest that the Wisting *Central/Hanssen* discoveries were sourced by the lower Steinkobbe Fm (Spathian) and not its middle–upper part (Anisian). The source signature of the Vendomdalen Mb, as demonstrated in the present study, appears to be similar to the lower Steinkobbe Fm in both organofacies and age, thus challenging the commonly accepted notion that the (entire) Steinkobbe Fm is a facies-equivalent to the Botneheia Fm onshore Svalbard. The *Alta/Gohta* oils show a clay-rich facies signature, supporting previous work that indicate a siliciclastic source rock. It is therefore suggested that these oils were sourced from dominantly siliciclastic source rocks, rather than Upper Paleozoic carbonates or evaporites as previously speculated (Matapour et al., 2019). The present study may suggest some contributions from Lower Triassic source rocks to the *Alta/Gohta* discoveries, however no new evidence that rule out source contributions from the Upper Permian Ørret Fm is provided.

The findings of this study clearly show good agreement between kerogen- and bitumen-based biomarker proxies of the investigated Lower–Upper Triassic mudstone extracts, and that their organic composition and abundance are a direct consequence of their variable and changing depositional environments. As the source-specific parameters agree with the paleoenvironmental interpretations of Papers I and II, the provided biomarker-based data are useful to differentiate between Lower and Middle Triassic source rock contributions on the NBS, potentially reducing exploration risk.

3.4 Author contributions

Although I am the lead author of Papers I–III presented in this dissertation, they are all joint research collaborations between multiple authors. My contributions, as well as the contributions from the various co-authors, are summarized in Table 3.1.

Table 3.1: Author contributions to the included manuscripts according to the Contributor Roles Taxonomy (CRediT) criteria (Brand et al., 2015). The order of the authors represents the degree of involvement. BL = Benedikt Lerch, FW = Fredrik Wesenlund, JHP = Jon Halvard Pedersen, OT = Olaf Thießen, SAG = Sten-Andreas Grundvåg, VSE = Victoria Sjøholt Engelschiøn.

Contribution	Paper I	Paper II	Paper III
Conceptualization	FW, SAG, OT, JHP	FW, SAG, OT, JHP	FW, SAG, OT, JHP
Methodology	FW	FW	FW
Software	FW	FW	FW
Validation	FW, OT	FW	FW, OT
Formal analysis	FW	FW	FW
Investigation	FW, SAG, VSE	FW, SAG, VSE	FW, SAG, VSE
Resources	FW, VSE	FW, VSE	FW, VSE, BL
Data curation	FW, VSE	FW, VSE	FW, VSE
Visualization	FW	FW	FW
Supervision	SAG, OT, JHP	SAG, OT, JHP	SAG, OT, JHP
Project administration	FW, SAG	FW, SAG	FW, SAG
Funding acquisition	SAG, OT, JHP, FW	SAG, OT, JHP	SAG, OT, JHP, FW
Writing - original draft	FW	FW	FW
Writing - review and editing	FW, SAG, VSE, OT, JHP	FW, SAG, VSE, OT, JHP	FW, SAG, OT, VSE, BL, JHP

4

Paper I

Linking facies variations, organic carbon richness and bulk bitumen content – A case study of the organic-rich Middle Triassic shales from eastern Svalbard

*Fredrik Wesenlund[1], Sten-Andreas Grundvåg[1], Victoria Sjøholt Engelschiøn[2], Olaf Thießen[3], Jon Halvard Pedersen[4]

[1]Department of Geosciences, UiT The Arctic University of Norway, Tromsø, Norway

[2]The Natural History Museum, University of Oslo, Norway

[3]Equinor ASA, Harstad, Norway

[4]Lundin Energy Norway, Lysaker, Norway

*Corresponding author. E-mail: `fredrik.wesenlund@uit.no`

Note: The geochemical dataset used in this publication is available through the journal article webpage. The citations included in this paper refer to the reference list of the journal paper and not the reference list in Chapter 8 of this dissertation.

Marine and Petroleum Geology 132 (2021) 105168

Contents lists available at ScienceDirect

Marine and Petroleum Geology

journal homepage: www.elsevier.com/locate/marpetgeo

Linking facies variations, organic carbon richness and bulk bitumen content – A case study of the organic-rich Middle Triassic shales from eastern Svalbard

Fredrik Wesenlund [a,*], Sten-Andreas Grundvåg [a], Victoria Sjøholt Engelschiøn [b], Olaf Thießen [c], Jon Halvard Pedersen [d]

[a] ARCEx – Research Centre for Arctic Petroleum Exploration, Department of Geosciences, UiT–The Arctic University of Norway, Tromsø, Norway
[b] The Natural History Museum, University of Oslo, Oslo, Norway
[c] Equinor ASA, Harstad, Norway
[d] Lundin Energy Norway, Lysaker, Norway

ARTICLE INFO

Keywords:
eastern Svalbard
Middle Triassic
Botneheia Formation
Facies characterization
Total organic carbon
Bulk bitumen composition
Iatroscan TLC-FID
Multivariate analysis

ABSTRACT

The organic-rich shales of the Middle Triassic Botneheia Formation in Svalbard and its correlative units offshore are considered important source rock intervals for oil and gas generation in the Norwegian Barents Shelf region. Detailed investigation of these intervals is essential to better understand the intra source rock variations and thus to improve exploration models. As source rocks are rarely cored during exploration campaigns, outcrop studies of analogue source rocks onshore Svalbard are of great importance for gaining a comprehensive understanding of the Triassic petroleum system offshore. This integrated sedimentological and geochemical study of the Botneheia Formation investigates the intricate relationship between mudstone facies, total sulfur, total organic/inorganic carbon, and the absolute and relative abundance of bulk bitumen content. Both the Muen Member (Anisian) and the overlying Blanknuten Member (mostly Ladinian) of the Botneheia Formation were densely sampled and analyzed from three outcrop localities on Edgeøya, eastern Svalbard. The results show that total sulfur, total organic carbon, bitumen richness, and relative and absolute aromatic hydrocarbon content increase from bioturbated, gray-colored shales in the lower to middle Muen Member upwards into non-bioturbated, phosphogenic black shales in the middle part of the Blanknuten Member. From here, organic carbon and bulk bitumen richness subsequently decrease upwards in concert with the occurrence of bioturbated, calcareous mudstones and impure limestones towards the top of the Blanknuten Member. Optical vitrinite reflectance variations do not suggest significant maturity variations with depth in the sample profiles, highlighting that the total organic carbon and bulk bitumen content are dominantly coupled with the developing source facies. These facies and chemostratigraphic trends mirror the implied marine vs. terrigenous organic matter sedimentation and benthic preservation potential, which were at a maximum in the middle Blanknuten Member. These processes appear to be closely related to the supply of nutritious upwelled waters that are further linked with an evolving pan-Arctic 2nd order Middle Triassic transgressive–regressive sequence. Facies and multivariate analyses of the geochemical data show that the lower to middle Muen Member are comparable to the pro-delta mudstones of the younger Tschermakfjellet Formation (Carnian), and that both units are clearly distinct from the increased source rock potential and richness in the upper part of the Muen Member and the entire Blanknuten Member. This provides evidence of genetically different paleo-depositional environments and source rock properties that are confined to the lower and upper parts of the Middle Triassic Botneheia Formation, and may have wide applications for Triassic source rock assessment in the offshore Norwegian Barents Sea.

* Corresponding author.
E-mail address: fredrik.wesenlund@uit.no (F. Wesenlund).

https://doi.org/10.1016/j.marpetgeo.2021.105168
Received 21 November 2020; Received in revised form 30 April 2021; Accepted 29 May 2021
Available online 3 June 2021

1. Introduction

The Middle Triassic Botneheia Formation (Fm.) in Svalbard is a regionally extensive, organic-rich 'black' shale deposited during the Anisian–Ladinian (Krajewski, 2008; Leith et al., 1992; Mørk and Bjorøy, 1984) (Fig. 1). The unit is well-exposed across the Svalbard Platform, and thins from c. 150 m thickness in western Spitsbergen to c. 80 m on Edgeøya, further to the east (Mørk et al., 1999). On the Barents Shelf, approximately 550 km south of Svalbard, slightly older, lateral facies-equivalent shale-units are represented by the Olenekian–Anisian Steinkobbe Fm. (Fig. 1c) as documented by shallow bore holes in the Svalis Dome-area (Mørk and Elvebakk, 1999; Vigran et al., 1998) and the 7222/1-1 Aurelia exploration well (Fig. 1a) (Norwegian Petroleum Directorate, 2020). In these two offshore localities (c. 44 km apart), the Steinkobbe Fm. is c. 250 m and c. 280 m thick respectively (Mørk and Elvebakk, 1999; Norwegian Petroleum Directorate, 2020). Collectively, these organic-rich Lower–Middle Triassic formations are considered to host regionally important source rocks extending the Norwegian Barents Shelf.

Basin modelling of the Hammerfest Basin indicates that the Middle Triassic source rocks expelled petroleum as early as c. Early Cretaceous time, with total expelled petroleum estimated to be c. 62 Gt (30 Gt of oil and 32 Gt of gas) (Rodrigues Duran et al., 2013b). Geochemical analyses of petroleum from the Goliat Field support a Triassic source contribution to its Triassic reservoirs (Rodrigues Duran et al., 2013a). Basin modelling further north in the Bjarmeland Platform areas surrounding the Wisting/Hanssen oil discoveries (Fig. 1a) suggests that the Upper Jurassic Hekkingen Fm. is immature, while the Steinkobbe Fm. is early oil expulsion to gas mature in the same area (Stueland, 2016). Source–oil biomarker correlations by Lerch et al. (2018) considered the Olenekian part of the Steinkobbe Fm. as the principal oil contributor to the Wisting/Hanssen oil discoveries. This formation is also indicated to source several other technical oil discoveries (Lerch et al., 2016). The Steinkobbe Fm. and facies equivalents may therefore represent important, oil-prone source rocks that could span more than 250 km in the acreage open to petroleum exploration in the Norwegian Barents Sea. Additionally, the recent report by the Norwegian Petroleum Directorate (2017) estimates that the Middle Triassic source rocks are the most important contributors to liquid petroleum accumulations in the northeastern Norwegian Barents Sea. While this region is not yet open for commercial exploration, it appears that potential Lower–Middle Triassic source rocks may occur throughout large parts of the Norwegian Barents shelf.

Source rock intervals are rarely cored during exploration campaigns, and consequently, there is limited core material available for detailed geochemical analyses of such units. Because Svalbard represents the uplifted and exhumed northwestern corner of the Barents Shelf (Fig. 1a), the Botneheia Fm. may thus serve as a valid facies and geochemical analogue for the under-examined, subsurface Triassic source rock-system offshore. Oil–oil correlation of primary migrated oil (not extract) from an oil-filled ammonoid from the thermally mature Upper Anisian–Ladinian part of the Botneheia Fm. in northwestern Edgeøya (Smelror and Sollid, 2007) suggests a good match with oils from the northwestern Bjarmeland Platform (e. g. 7324/8-1 Wisting Central, 7324/7-2 Hanssen), the Loppa High (e. g. 7220/11-1 Alta, 7222/6-1 S Obesum), the Hammerfest Basin (e. g. 7122/7–3 Goliat - Kobbe & Klappmyss fms.) and the Måsøy Fault Complex (e. g. 7125/4-1 Nucula - Kobbe Fm.) (Thießen et al., 2019). This justifies the use of the Botneheia Fm. as an analogue for the facies equivalent Steinkobbe Fm.

There are many previous publications that document source rock properties, organic richness and the generation potential of the Botneheia Fm. in Svalbard (e.g. Abay et al., 2017; Abay et al., 2014; Abay et al., 2018; Abdullah, 1999; Bjorøy et al., 2009; Brekke et al., 2014; Forsberg and Bjorøy, 1983; Hubred, 2006; Krajewski, 2008, 2013; Leith et al., 1992; Mørk and Bjorøy, 1984; Riis et al., 2008; Vigran et al., 2008; Xu et al., 2012). In addition, the bulk bitumen content of the Botneheia Fm. shales was recently investigated in detail by Brekke et al. (2014) and Abay et al. (2017). However, few of the previous studies attempt to integrate the stratigraphic distribution of total organic carbon (TOC), total inorganic carbon (TIC), total sulfur (TS) and especially bitumen content in light of the most recent lithostratigraphic subdivision of the Botneheia Fm. by Krajewski (2008). Thus, it appears that a complete understanding of the stratigraphic development of the bulk bitumen content in the Botneheia Fm. is missing.

The majority of previous investigations have focused on the organic-rich paper shales of the mostly Ladinian-aged Blanknuten Member (Mb.) (sensu Mørk et al., 1982). The underlying, Anisian-aged Muen Mb. (sensu Krajewski, 2008) has received notably less attention, probably due to the inferred lower source rock quality and quantity. The bottom conditions during deposition of the shales in the lower to middle part of the Muen Mb. on Edgeøya are debated, and previous studies suggest either dominantly anoxic conditions with absent bioturbation (Vigran et al., 2014), or oxic conditions, with the oxic–sulfidic boundary located primarily below the sediment surface (Krajewski, 2013). The source rock potential of the Muen Mb. might therefore be incorrectly evaluated depending on the chosen depositional interpretation.

The main objective of this study is therefore to characterize chemostratigraphic variations in TOC, TIC, TS and bulk bitumen content (saturates, aromatics and polars) and to tie their relationship to recognized lithostratigraphic changes in the Botneheia Fm. on Edgeøya, eastern Svalbard. Optical vitrinite reflectance data (R_o) of the Muen and Blanknuten mbs. and the Tschermakfjellet Fm. is included to determine the influence of differential thermal maturity variations in the sample profiles. The second objective is to evaluate the depositional conditions of the Muen Mb. and compare it to the overlying Blanknuten Mb. The third objective is to assess the applicability of multivariate exploratory data analysis as a tool to identify genetically different mudstone facies based on the bulk geochemical data. The Blanknuten and Skrukkefjellet localities on northwestern Edgeøya (Fig. 1b) were chosen for this study, as they provide excellent outcrop exposures with minimal structural influence, and because the most recent lithostratigraphic framework is well-established (Krajewski, 2008, 2013).

2. Geological setting

2.1. Tectonostratigraphic development

The end of the Permian resulted in an intracratonic sag basin that covered wide parts of northwestern Pangaea (Faleide et al., 1984, 2015; Glørstad-Clark et al., 2011). This paleo-basin also made up the Triassic Boreal Sea, which was confined by the North American continent towards west, the Panthalassic Sea towards north, Novaya Zemlya towards east, and the northwestern Eurasian plate towards south (Glørstad-Clark et al., 2011) (Fig. 2). During the Early–Middle Triassic, Svalbard received sediments mostly sourced from the west, corresponding to present-day Greenland (Mørk, 2015). A major shift in provenance and sedimentation direction took place in the Late Triassic, when a large deltaic system, which had prograded since Latest Permian from southeast, eventually became the dominating sedimentary system across the entire Barents Shelf (Mørk, 2015). This deltaic system record sediment influx from the development of the Uralian orogeny, ultimately becoming the dominant sediment source of the region (Lundschien et al., 2014) (Fig. 2), and possibly represents the world's largest palaeo-delta system (Klausen et al., 2019). Palynological studies indicate a humid climate regime at the time when the delta-front reached Svalbard in the Late Triassic (Paterson et al., 2017).

In eastern Svalbard, the Middle Triassic Botneheia Fm. is interpreted to represent a 2nd order transgressive–regressive (TR) cycle, possibly reflecting global eustatic sea-level changes over several millions of years due to lithospheric plate movement (Glørstad-Clark et al., 2010; Mørk et al., 1989). Correlative, organic-rich deposits are seen in the Sverdrup Basin, Arctic Canada (Middle Triassic Murray Harbor and Hoyle Bay

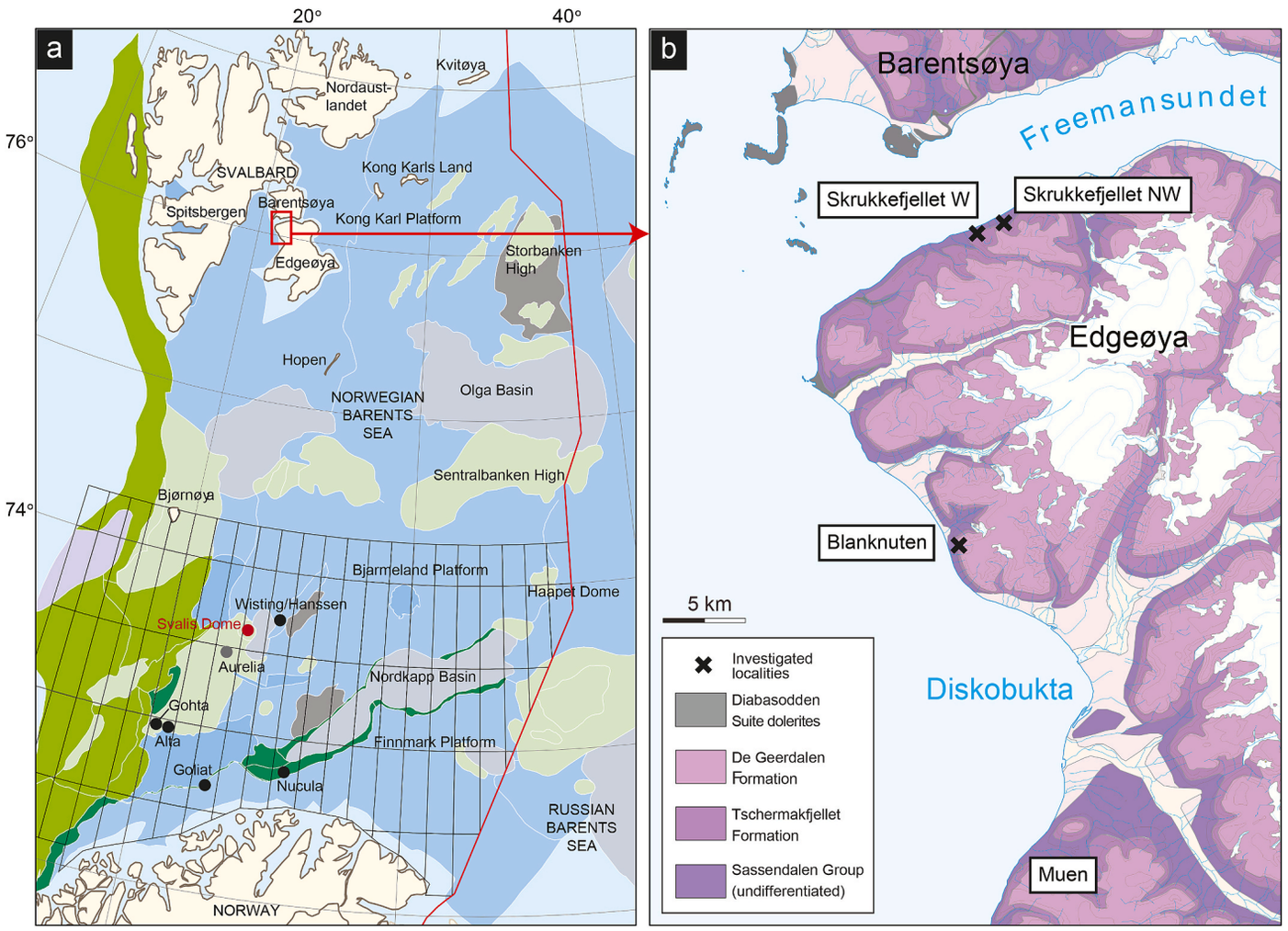

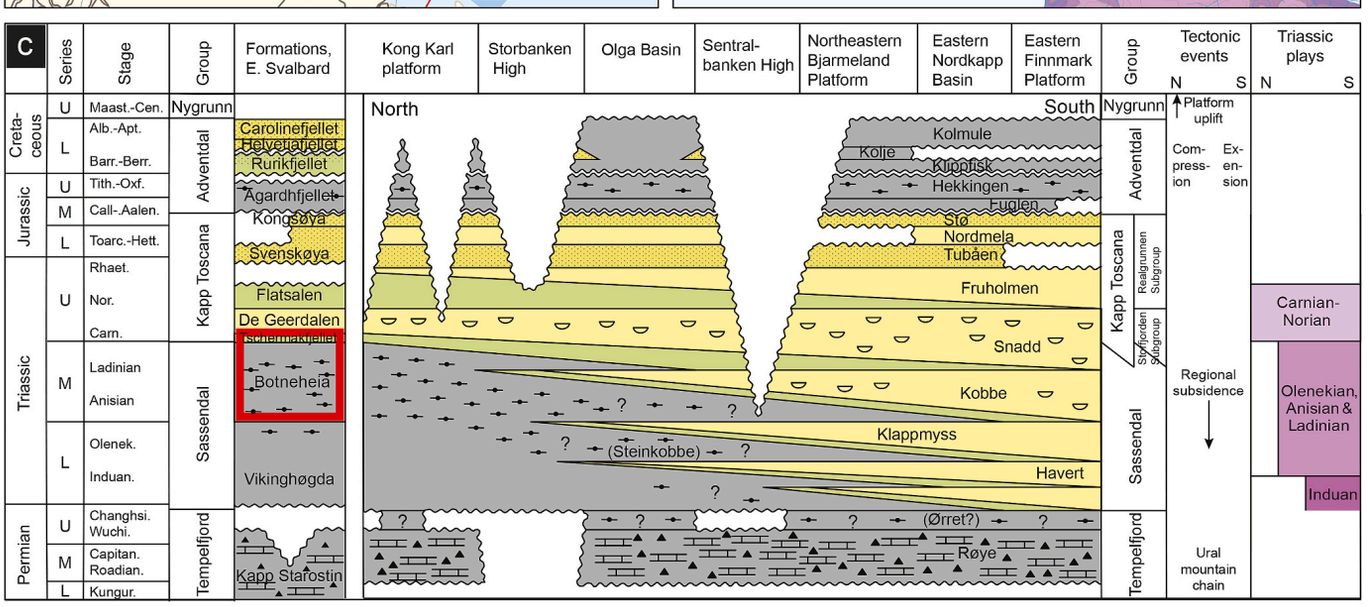

Cretaceous High
Deep Cretaceous High
Palaeozoic High in Platform
Platform
Hydrocarbon field or discovery
pre-Jurassic High in Platform
Shallow Cretaceous Basin in Platform
Terraces and Intra-Basinal Elevations
Volcanics
Steinkobbe Fm. well type section (7323/07)
Uplifted/eroded area
Coastal, deltaic and flood-plain deposits
Shallow-marine deposits, mainly sandstone
Marine deposits, mainly shale
Deep-Marine deposits,mainly shale
Exploration well
Calc. sh., ls, and marl stringers
Spiculite
Sandy intercalations
Source rock
Channels

(caption on next page)

Fig. 1. **(a)** Regional map of the Norwegian Barents Sea, where commercially available exploration blocks in areas opened for petroleum activity are shown in the southern part and the area not opened for exploration in the northern part. Modified from the Norwegian Petroleum Directorate (2017). The legend is located below Fig. 1c. **(b)** Local map of the northwestern part of Edgeøya, showing the Blanknuten locality (77°59′43.1″N, 21°11′44.1″E), the Skrukkefjellet W locality (78°09′42.1″N, 21°12′51.1″E), and the Skrukkefjellet NW locality (78°10′10.3"N, 21°18′01.8"E). Modified from Dallmann and Elvevold (2015). **(c)** Chrono- and lithostratigraphic chart of the Permian–Cretaceous periods comparing the offshore Barents Sea to the onshore eastern Svalbard. Note the time-transgressive relationship between the Lower–Middle Triassic Steinkobbe and Middle Triassic Botneheia fms. from south to north. The mapped Triassic plays are included for reference. Modified from the Norwegian Petroleum Directorate (2017).

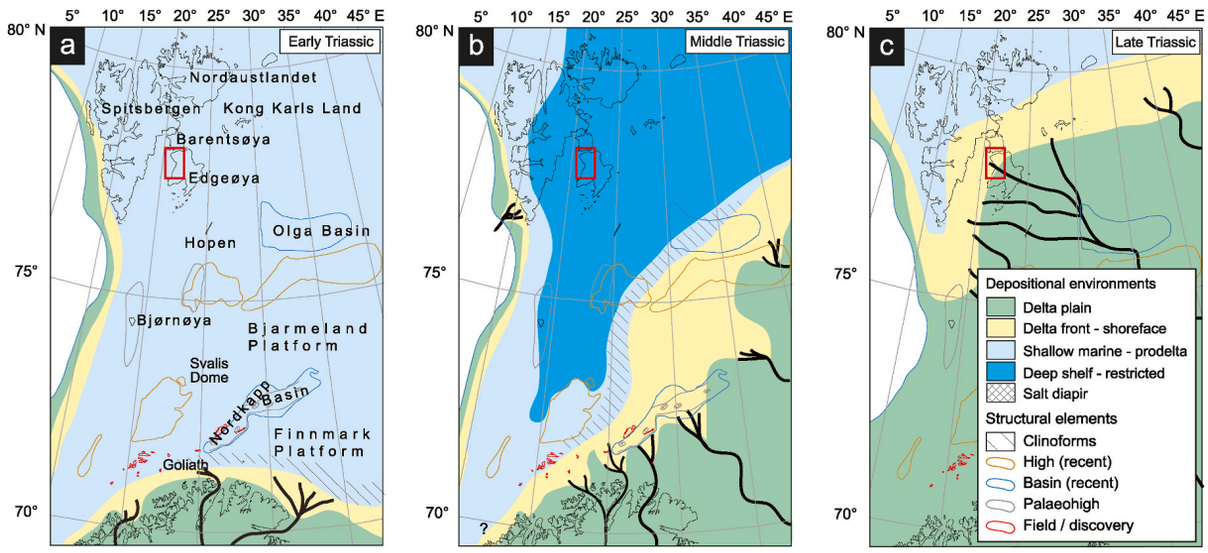

Fig. 2. Early–Late Triassic paleogeography including generalized depositional environments and selected structural elements. The red rectangle marks the study area at Edgeøya. **(a)** Early Triassic. **(b)** Middle Triassic. **(c)** Late Triassic. Modified from Lundschien et al. (2014). (For interpretation of the references to color in this figure legend, the reader is referred to the Web version of this article.)

fms.), and Northern Alaska (Middle–Late Triassic Shublik Fm.) (Leith et al., 1992), as well as in northeastern Greenland in the Wandel Sea Basin (Middle–Late Triassic Israd Fm.) (Alsen et al., 2017; Bjerager et al., 2019). Thus, the Early–Late Triassic Boreal Sea contained widespread organic-rich, fine-grained sediments.

The Triassic period has traditionally been regarded as tectonically quiescent in the northern Barents Shelf (Riis et al., 2008). However, the presence of localized growth faults in the Carnian Tschermakfjellet and De Geerdalen fms. on Edgeøya (Høy and Lundschien, 2011; Smyrak-Sikora et al., 2019) has been linked to a series of deep-rooted normal faults (Anell et al., 2013; Osmundsen et al., 2014). Here, the transition from the shale-dominated Botneheia Fm. to the heterolithic sandstone-bearing Tschermakfjellet Fm. is seen to act as a basal detachment surface for a series of listric faults soling out along the lithological transition (Ogata et al., 2018). Although debated (Klausen, 2013), this could suggest some regional-scale tectonic activity during the Triassic in the northern Barents Shelf (Anell et al., 2013). An angular unconformity between the Upper Triassic and the overlying Lower Jurassic strata in the southern Barents Sea suggests a basin-wide tectonic regime induced by the Novaya Zemlya Fold and Thrust Belt (Muller et al., 2019).

The Barents Shelf records a complex history of differential burial, uplift and erosion through time (Ohm et al., 2008). A regional net erosion estimate of the greater Barents Sea suggest that the southern Barents Shelf was uplifted between 1 and 2 km, increasing monotonically towards northwest, with more than 3 km of uplift and erosion in northwestern Svalbard (Henriksen et al., 2011). However, Marshall et al. (2015) estimate overburden erosion of c. 1.0 km in central Spitsbergen, emphasizing the difficulty of estimating burial depth. In addition, increased magmatic activity during the Early Cretaceous resulted in the High Arctic Large Igneous Province (HALIP) (Ineson et al., 2021; Maher et al., 2004; Senger et al., 2014). In Svalbard, this is manifested by abundant sills and dykes within the sedimentary strata (Mørk and Bjorøy, 1984), often preferentially penetrating the organic-rich Botneheia Fm. (Hubred, 2006). The burial, uplift and erosion coupled with igneous intrusions provide a complex thermal maturation pattern throughout eastern Svalbard, ranging from immature to overmature (Haile et al., 2018).

In the Muen locality on Edgeøya (Fig. 1b), the Botneheia Fm. is late mature, but no igneous intrusions are outcropping (Brekke et al., 2014; Mørk and Bjorøy, 1984). This could indicate the presence of a subsurface igneous body with a sufficient thickness that have thermally affected the Botneheia Fm. in this locality (Brekke et al., 2014; Hubred, 2006; Mørk and Bjorøy, 1984). 20 km northwards in the Blanknuten locality (Fig. 1b), the Botneheia Fm. shows T_{max} ranging from 440 to 447 (°C) (Krajewski, 2013), suggesting a thermally mature outcrop section. This maturation is dominantly caused by progressive burial (Haile et al., 2018), indicating that sills or dykes have insignificant thermal contribution and that the inferred underlying igneous body in the south probably does not affect the Botneheia Fm. this far north. This can also be assumed for mudstones from the Skrukkefjellet locality (Fig. 1b) on northern Edgeøya as they are less mature than those from the Blanknuten locality (Mørk and Bjorøy, 1984; Schou et al., 1984). T_{max} data from the Skarpryttaren locality c. 10 km north of the Skrukkefjellet locality range from 435 to 443 (°C) (Krajewski, 2013), confirming a northwards decreasing maturity trend from the Blanknuten locality.

2.2. *Lithostratigraphic framework and sedimentology of the Middle Triassic, Eastern Svalbard*

The Botneheia Fm. is considered to conformably overlie the Olenekian-aged Vendomdalen Mb. of the Lower Triassic Vikinghøgda Fm. (Brekke et al., 2014; Høy and Lundschien, 2011), although this boundary might also represent a disconformity (Hounslow et al., 2008). In eastern Svalbard, Krajewski (2008) subdivided the Botneheia Fm. into nine informal units based on litho- and chemostratigraphic

characteristics (unit 1 to unit 9). Lithostratigraphically, units 1 to 5 represent the Muen Mb., and units 6 to 9 represent the Blanknuten Mb. In addition, Krajewski (2008) identified two dominant chemostratigraphic units consisting of a lower non-phosphogenic (corresponding to units 1–4) and an upper phosphogenic facies (corresponding to units 5–9). Note that these two chemostratigraphic units do not correspond directly to the formal lithostratigraphic member division.

On Edgeøya, the boundary between the Botneheia Fm. and the overlying Tschermakfjellet Fm. is rather sharp and abrupt (Fig. 3a), suggesting that it might represent a break in deposition or a submarine hiatus developing at the Ladinian–Carnian boundary (Mørk et al., 1989). The Tschermakfjellet Fm. consists of mainly dark gray mudstones (Fig. 3g) enriched in terrestrial organic matter (Mørk and Bjorøy, 1984). In the northern Barents Sea, the Tschermakfjellet Fm. is seen to downlap (in a continuous fashion) onto the top surface of the Botneheia Fm., suggesting a pro-delta (bottomset) origin for these early Carnian deposits (Høy and Lundschien, 2011). A pro-delta origin is supported by its stratigraphic position below the transitionally overlying fluvio-deltaic De Geerdalen Fm., which prograded from the southeast during Carnian times (Lord et al., 2017). *Tasmanites* algae have been recorded in the lowermost part of the Tschermakfjellet Fm. (Vigran et al., 2014).

In the present study, we refer to units 1 to 4 of Krajewski (2008) collectively as the *lower–middle Muen Mb.*, unit 5 as the *upper Muen Mb.*, unit 6 and unit 7 as the *lower* and *middle Blanknuten mbs.*, respectively, and the combined units 8 and 9 as the *upper Blanknuten Mb.* (Table 1).

The non-phosphogenic lower–middle Muen Mb. (Anisian, unit 1 to unit 4; Table 1) consists mostly of gray to dark-gray mudstones and occasional centimeter–decimeter-scale carbonate and siltstone beds (Fig. 3a and b) (Krajewski, 2008), also shown in this study (section 4.1). Although Vigran et al. (2014) and this study report *in situ* phosphate nodules at this stratigraphic level in the studied localities, we apply the term non-phosphogenic as the mudstone matrix from this succession is dominantly phosphate-free (Krajewski, 2008). The upper part (i.e. unit 5) contains black shales (Fig. 3c) with common occurrences of macroscopic phosphate nodules. Krajewski (2008) attributes the non-phosphogenic part of the Muen Mb. (units 1 to 4) to represent deposition under mainly oxic conditions with moderate primary productivity and increased terrestrial runoff, ultimately resulting in varying source rock quality (median HI = 281 ± 52 mg HC/g TOC, 1σ) and richness (median TOC = 2.63 ± 1.08 wt. %, 1σ) (Krajewski, 2013). In contrast, the upper phosphogenic part of the Muen Mb. (unit 5) is interpreted to represent the onset of periods with increased primary productivity, as indicated by the presence of black shale containing pristine, macroscopic phosphate nodules. This chemostratigraphic transition suggest a change from an oxic, early transgressive phase to an oxic–dysoxic, late transgressive phase (Krajewski, 2008).

The overlying, phosphogenic facies-dominated Blanknuten Mb. (mainly Ladinian, unit 6 to unit 9) forms a characteristic black cliff along the coastline of Edgeøya (Fig. 3a). It consists of dominantly black-colored, calcareous, organic-rich mudstones with calcareous siltstone beds and silty limestone beds (Mørk et al., 1982, 1999). These shales contain dominantly kerogen type II, with TOC values ranging from c. 2–11 wt. % (Krajewski, 2013).

The lower part of the Blanknuten Mb. (unit 6 of Krajewski, 2008, Table 1) consists of mostly black, laminated shale with abundant pristine and macroscopic phosphate nodules (Fig. 3d), suggesting deposition under high primary productivity in dysoxic to anoxic conditions (Krajewski, 2013). The middle part of the member (i.e. unit 7 of Krajewski, 2008, Table 1) consists of massive, cliff-forming, paper-laminated shale (Fig. 3e), which marks increased stagnation with subsequent regional anoxia. On northwestern Edgeøya and southern Barentsøya (Fig. 1b), this unit has excellent richness (median TOC = 8.10 ± 1.06 wt. %, 1σ) and oil generation potential (median HI = 538 ± 42 mg HC/g TOC, 1σ), and is considered the best source rock unit within the Botneheia Fm., presumably deposited during a Middle Triassic eustatic sea-level high-stand phase (Krajewski, 2013). A maximum flooding surface is located in the lower part of unit 7 (Krajewski, 2013), which occurred during early Ladinian (Krajewski and Weitschat, 2015). The upper part of the member (units 8 and 9 of Krajewski, 2008, Table 1) consists mainly of fissile mudstones (Fig. 3f) with abundant reworked phosphate nodules and phosphate-filled flattened *Thalassinoides* burrows (Mørk and Bromley, 2008). Siltstone interbeds (interpreted as distal storm deposits) are common, contrasting the underlying massive, cliff-forming shale (Mørk and Bromley, 2008). The facies variability indicates recurrent changes in the benthic environment triggered by a regressive trend with fluctuating oxic to anoxic conditions (Krajewski, 2013; Mørk and Bromley, 2008).

3. Samples and methods

3.1. Field work

A complete vertical section of the Botneheia Fm. (and the lowermost few meters of the overlying Tschermakfjellet Fm.) was logged for sedimentary features and concertedly sampled in the Blanknuten locality (Bernhardsen, 2019). Two stratigraphically incomplete, but partly overlapping sections were sampled at Skrukkefjellet W (exposing the lower part of the formation) and Skrukkefjellet NW (exposing the upper part of the formation; Fig. 1b). These are combined to form a stratigraphically complete, composite sample profile of the Botneheia Fm. at Skrukkefjellet. Although the two sections at Skrukkefjellet are located c. 2 km apart (Fig. 1b for location), the excellent outcrop quality makes physical and visual tracing of the main stratigraphic units possible, ensuring that the composite sample profile represents a complete section through the formation. For all sections, sample pits were dug (average sample interval: < 2 m) in the slope or outcrop whenever possible, and *in situ* rock material was collected to minimize weathering influence and contamination from recent organic matter. Although siltstone/cementstone beds and concretions were partly sampled along-side mudstones, this study pertains to the latter.

3.2. Sample preparation

Prior to geochemical analysis, the outcrop samples were rinsed and scrubbed in temperate, running water. Rock material with weathering skins, contemporary organic matter or abundant calcite veins was discarded. The samples were dried at < 30 °C overnight. Macroscopic phosphate nodules were removed to obtain comparable samples of mudstone matrix composition. Still, abundant phosphate content cannot be ruled out. The samples were crushed to gravel size using an agate mortar and pestle. 1 dl of the crushed sample material was milled using a Retsch PM 100 with agate chamber and agate milling balls set at 450 rpm for 10 min, resulting in a homogenized, fine rock powder.

3.3. LECO combustion

101 samples were quantified for TS, TOC and total carbon (TC) using a LECO™ CS744 carbon/sulfur determinator (Table 1). Prior to analysis, 2.0 g of the pulverized sample material was dried at 105 °C overnight. For TS and TC analysis, between 0.23 and 0.25 g of the dry, heated sample was weighed in a single-use crucible. For TOC analysis, between 0.40 and 0.45 g of dry heated sample was weighed in a single-use fluid-permeable crucible, and subsequently acid treated with 10% HCl and rinsed with water until no reaction between the acid and powder was observed. The acid treated samples were dried at 105 °C overnight. The TOC and TC/TS prepared samples were combusted with accelerators to facilitate combustion, with an instrument run time set at 70 s. TIC was calculated by subtracting TOC from TC.

3.4. Bitumen extraction

Based on the LECO analysis, 57 samples (Table 1) were picked for

Fig. 3. Lithostratigraphic boundaries and facies of the Botneheia Fm. in the Blanknuten locality. **(a)** Overview of the Muen and Blanknuten mbs. Stratigraphic boundaries (dashed lines), phosphogenic facies, and kerogen types adapted from Krajewski (2008, 2013). Note that the entire Blanknuten Mb. is phosphogenic. **(b)** Dark gray, flaky, non-phosphogenic mudstone (F1), lower–middle Muen Mb. **(c)** Flaky to platy, black mudstone (F2) from phosphogenic upper Muen Mb. **(d)** Massive, black, platy mudstone (F2) with defined fissility of the lower Blanknuten Mb. White arrows indicate abundant phosphate nodules. **(e)** Outcrop expression of the fissile mudstone (F3) of the massive middle Blanknuten Mb., yielding platy fragments. Gray weathering skin masks the true black color of the mudstone. **(f)** Platy, highly fissile outcrop expression of the black mudstones (F4) in the upper Blanknuten Mb. Arrows denote flattened phosphate-precipitated burrows. **(g)** Flaky fragmentation and crumbled outcrop expression of the dark gray mudstones (F1) in the lowermost Tschermakfjellet Fm. The marker pen in panels b–e measures 14 cm. Locations are given in Fig. 1b. (For interpretation of the references to color in this figure legend, the reader is referred to the Web version of this article.)

Table 1
Comparison between the amount of analyzed samples and coinciding stratigraphic units from Krajewski (2008) and this study.

Stratigraphic unit, this study	Stratigraphic unit, Krajewski (2008)	Samples analyzed	
		LECO	Iatroscan TLC-FID
lower–middle Muen Mb.	Units 1–4	32	12
upper Muen Mb.	Unit 5	6	4
lower Blanknuten Mb.	Unit 6	15	11
middle Blanknuten Mb.	Unit 7	30	19
upper Blanknuten Mb.	Units 8–9	15	8
Tschermakfjellet Fm.	Tschermakfjellet Fm.	3	3

bitumen extraction using a ST 243 Soxtec™ system. Empty cellulose extraction thimbles were boiled for 10 min and rinsed for 20 min using 100 ml of DCM:MeOH (93:7 vol. %) solvent prior to sample extraction to remove possible contaminants. c. 10 g of powdered sample material was inserted into the pre-extracted thimbles. Elemental copper beads were added to the extraction cups as boiling stones and to remove residual sulfur. The samples were boiled for 60 min and rinsed for 120 min with 100 ml of solvent, later concentrated to 0.5 ml by solvent evaporation in a fume hood. The concentrated extracts were not deasphaltened.

3.5. Iatroscan TLC-FID

An Iatroscan™ MK-5 thin layer chromatography – flame ionization detector (TLC-FID) was used to separate and quantify the absolute and normalized (% by weight) saturate (SAT), aromatic (ARO) and polar (POL; resins + asphaltenes) fractions of the total bitumen extracts (Karlsen and Larter, 1991). 3 μl or 2 μl depending on extract richness of 3.85 vol. % strength of the 0.5 ml extract concentrate was applied onto silica gel-coated rods (type Chromarod IV). Variations in analyte volume were necessary to prevent column overload and subsequent poor peak separation. The silica rods were lowered into containers of cyclohexane for 20 min and toluene for 8 min to elute and separate the SAT and ARO fractions respectively. The POL fraction remained stationary and was thus also separated from the other fractions. The applied rods were dried for 2 min in between each elution and ultimately dried at 40 °C for 40 s to remove solvents prior to analysis. Scan time was set to 30 s, with H_2 and O_2 flow set at 180 ml/min and 2.1 l/min respectively. A blank sample and the Norwegian Geochemical Standard NSO-1 (Weiss et al., 2000) were used for quality checking each run. Analytical precision was 46.5 ± 1.0%, 25.0 ± 1.0%, and 28.6 ± 2.0% (n = 4, 1σ) for the normalized (by weight) SAT, ARO and POL fractions of non-deasphaltened NSO-1 respectively. This yielded a mean SAT/ARO ratio of 1.86 ± 0.03 (1σ), i.e. within the permissible range of c. 1.3–2.0 (Weiss et al., 2000). Response factors for the SAT, ARO and POL fractions were 0.000607249, 0.000564736 and 0.000328987 respectively. The SES-i-ChromStar software were used to analyze and quantify the bitumen fractions by peak area integration of manually interpreted base lines. The absolute extractable organic matter (EOM) was back calculated to original concentration (100% vol. strength) and is reported in mg/g rock.

3.6. Vitrinite reflectance

The vitrinite reflectance analysis was carried out by Applied Petroleum Technology (APT) in Norway. They applied the following methods: The kerogen was isolated using standard palynological procedures, i.e. HCl and HF treatment followed by floating in $ZnBr_2$, subsequently agitated with ultrasonic energy and then centrifuged. A +10 μm fraction of the sieved and floated kerogen was mounted with resin on petrographic slides and polished with water. Reflectance measurements were made with a Zeiss™ Epiplan – Neofluar 40X oil immersion objective in light at a wavelength of 546 nm (green). The measurements were random (R_o) in nominally unpolarized light. Vitrinite phytoclasts were searched for until 55 have been measured or for half an hour, whichever was the sooner. The sample quality was considered good, i.e. the vitrinite type, quality, size or abundance had no effect on the readings.

3.7. Exploratory data analysis

The exploratory data analysis includes principal component analysis (PCA) and hierarchical cluster analysis (HCA), two common techniques for investigating depositional environment, maturity and correlations of source rocks and crude oils (Peters et al., 2005, 2007; Wang et al., 2018). All samples subjected to both LECO and Iatroscan analysis were included, amounting to a 57 samples (rows) by 13 variables (columns) data matrix. Each column of the matrix was scaled to a range of [0, 1] using min–max feature scaling. The analysis was performed using Python (v. 3.8.5) coupled with the sklearn (v. 0.23.2) and seaborn (v. 0.11.0) software libraries for PCA and HCA respectively. The Python script is open access (see section 7). For the HCA, the distance metric was set to “euclidean”, while the linkage method was set to “average”, which apply the unweighted pair group method with arithmetic mean algorithm (UPGMA). The color palette for the stratigraphic units is from Wong (2011).

4. Results

4.1. Stratigraphic units and boundaries

At the Blanknuten locality, all internal lithostratigraphic boundaries of the Botneheia Fm. are easily recognized by contrasting outcrop weathering expressions (Fig. 3a–f), except the boundary from the lower–middle Muen Mb. to the upper Muen Mb. The base Muen Mb. boundary, i.e. the base Botneheia Fm., lies immediately above slightly darker mudstones of the Vikinghøgda Fm. (Fig. 3a). The bulk Muen Mb. displays an upwards increase in dm-scale event beds, useful to distinguish the lower–middle Muen Mb. and the upper Muen Mb. (Fig. 3a). However, the lower–middle to upper Muen Mb. boundary is inferred based on contrasting facies (see section 4.2 for facies description). Also within the Blanknuten Mb., each sub-unit is visually discernible (Fig. 3d–f), as is the transition into the Tschermakfjellet Fm., marking an abrupt change in the weathering expression and shale fragment morphology (Fig. 3a and g). At this locality, the Botneheia Fm. was measured to be c. 75 m thick.

At the Skrukkefjellet W locality (Fig. 4a), it was difficult to determine the boundary between the upper Muen Mb. and the lower Blanknuten Mb., as the slope morphology changes with varying slope gradients. In addition, two normal faults (related to outcrop failure) were recognized within the apparent monotonous shale succession (Fig. 4a). Displacement in the Muen Mb. (corresponding to units 1 to 5 of Krajewski, 2008, Table 1) and the lower Blanknuten Mb. (unit 6 of Krajewski, 2008, Table 1) is in the order of several meters. The boundaries between the Muen Mb. and the overlying lower Blanknuten Mb., as well as between the lower and middle parts of the Blanknuten Mb. appear to be juxtaposed (Fig. 4a). The southern fault is clearly recognized in map view as a south-dipping normal fault with E–W apparent strike (Fig. 4b). Thus, if not carefully considered, logging the section from south to north on the topographic ridge (which is the most natural thing to do) will inevitably result in several meters of repeated strata, and consequently an overestimated formation thickness.

A tub-like discoidal concretion has previously been reported from the Skrukkefjellet W locality (Vigran et al., 2014, their Fig. 49b). This feature is easily recognized and provides an excellent reference point in the outcrop (Fig. 4a, c, d) and map view (Fig. 4b). Based on our field observations and correlation to previous studies (Krajewski, 2008, 2013; Vigran et al., 2014), the base Blanknuten Mb. boundary is placed at the base of this characteristic discoidal concretion. This horizon appears to host several other concretions in the Skrukkefjellet Mountain. The base

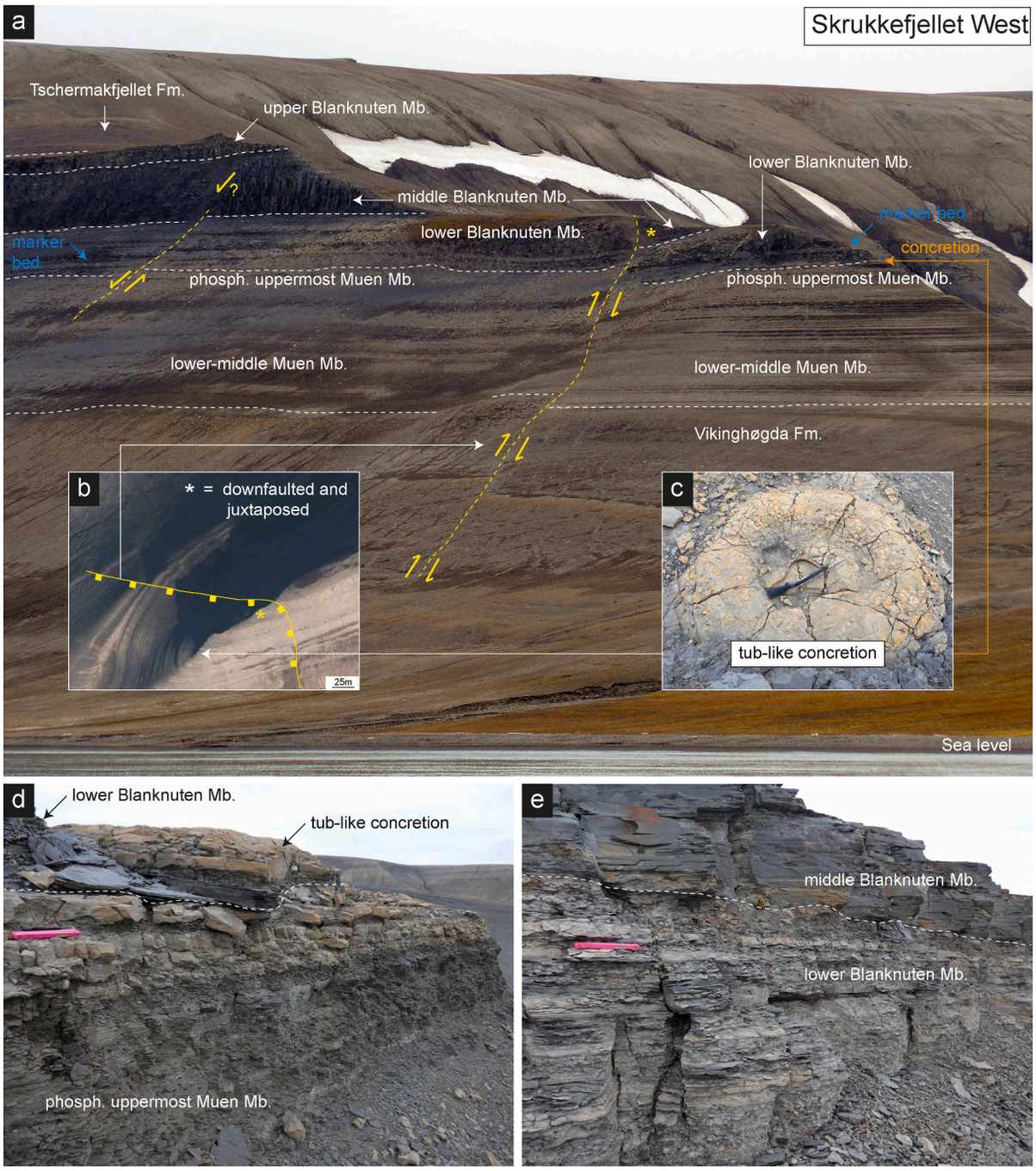

Fig. 4. Overview of the Botneheia Fm. in the Skrukkefjellet W locality with annotated lithostratigraphic and structural boundaries and features. **(a)** Overview photograph with stratigraphic boundaries (white dashed lines) and normal fault planes (dashed yellow lines). Juxtaposition of the lower Blanknuten Mb. and middle Blanknuten Mb. in the footwall is shown in the upper right of the picture, marked with a yellow asterisk (*). The marker bed (blue arrow) potentially marks the correct Blanknuten Mb. lower boundary. **(b)** Map view of the fault plane, roughly indicating an E–W strike with southerly dip. The yellow asterisk (*) marks the same downfaulted part as in panel a. Map retrieved from the Norwegian Polar Institute (2020). **(c)** A characteristic, discoidal tub-like concretion seen at the southern ridge in the locality. The orange and white arrows mark the concretion in panels a and b respectively. Ruger M77 Hawkeye rifle (c. 110 cm) for scale. **(d)** Close-up of the phosphogenic upper Muen Mb. (F2), showing the member boundary just underneath the tub-like concretion. The pink ruler is c. 23 cm. **(e)** outcrop expression of the lower–middle Blanknuten Mb. boundary, showing the characteristic change from dark gray to black mudstones (F2) to black calcite cemented, massive and smooth shales (F3). Pink ruler is c. 23 cm. Locations are given in Fig. 1b. (For interpretation of the references to color in this figure legend, the reader is referred to the Web version of this article.)

of the middle Blanknuten Mb. boundary is arguably the most recognizable sub-unit boundary within the Botneheia Fm. as it marks an abrupt transition from nodule-rich to nodule-free mudstones (Fig. 4e). In contrast, the boundary between the middle to uppermost Muen Mb. was not pinpointed in the field but is inferred based on facies variations (see section 4.2 for facies descriptions).

Owing to the faulted strata in the Skrukkefjellet W locality, the top lower Blanknuten Mb. and the entire middle and upper Blanknuten Mb. and the lowermost Tschermakfjellet Fm. were sampled at the Skrukkefjellet NW locality (Fig. 5). While all the main stratigraphic units may be recognized at the Skrukkefjellet NW locality, scree hindered detailed observations of the entire Muen Mb. and the lower Blanknuten Mb. (Fig. 5a and b). Intra-Blanknuten Mb. stratigraphic boundaries are easily recognized (Fig. 5c and d). The lower–middle Blanknuten Mb. boundary

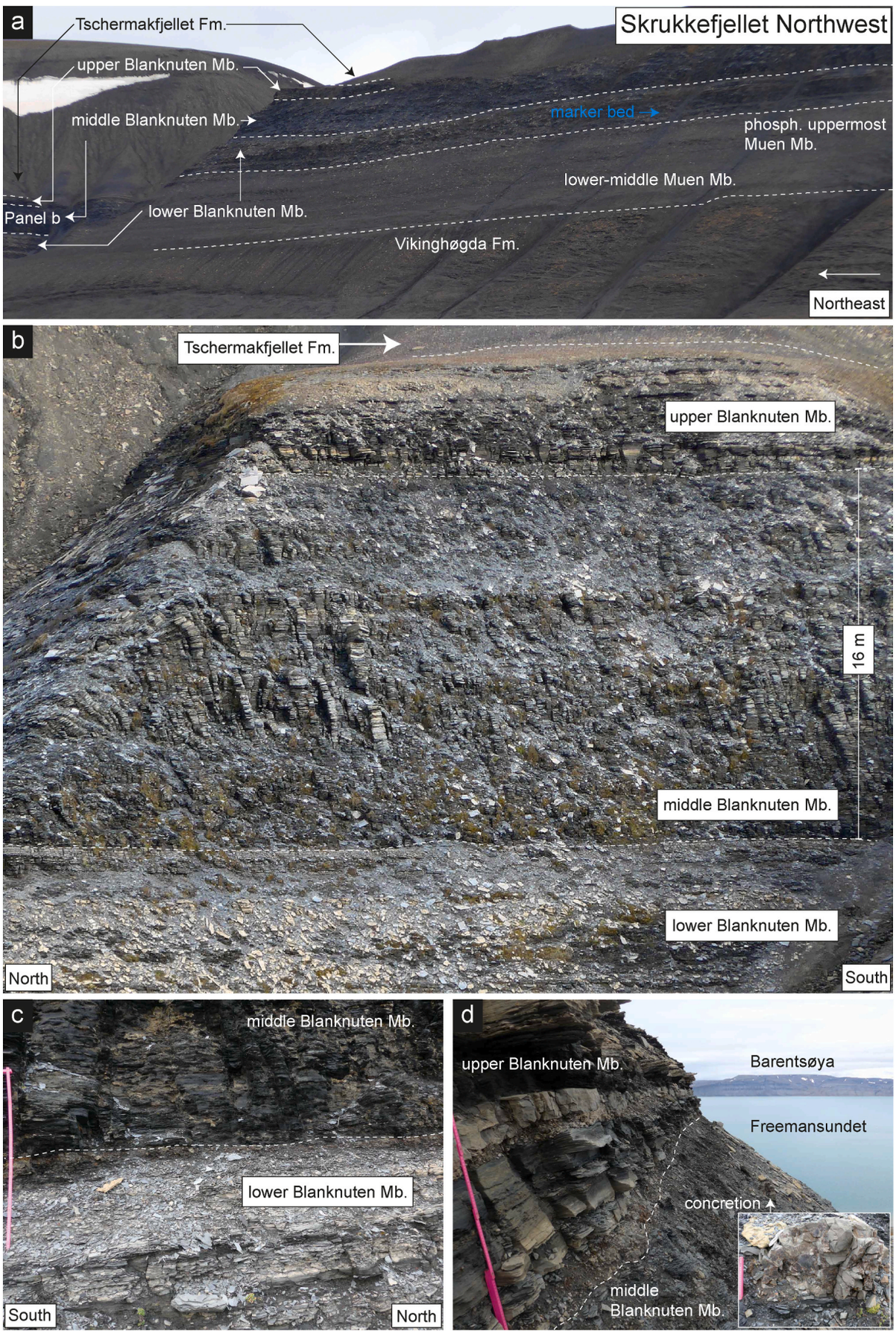

(caption on next page)

Fig. 5. Outcrop expression of the Botneheia Fm. in the Skrukkefjellet NW locality with annotated stratigraphic units and boundaries. **(a)** Overview photograph with stratigraphic boundaries. Here, the bulk Muen Mb. and much of the lower Blanknuten Mb. is covered by scree. No faulting is observed. The marker bed in blue possibly indicates the base Blanknuten Mb., see section 5.1 for discussion. **(b)** Overview photograph showing the weathering expression of the lower Blanknuten Mb. upwards into the Tschermakfjellet Fm. The middle Blanknuten Mb. shows characteristic weathering-formed columnar stacks of F3 mudstones. Note that this photograph represents the eastern side (78°10′08.9″N, 21°18′57.6"E) of an N–S trending unnamed valley in the Skrukkefjellet NW locality. The samples from this locality were collected c. 350 m directly west from this cliff face (78°10′10.3"N, 21°18′01.8"E). **(c)** Close-up of the lower–middle Blanknuten Mb. boundary (dashed line), displaying a sharp color contrast between these units. Pink ruler measures 1 m. **(d)** Close-up of the middle–upper Blanknuten Mb. boundary (dashed line), looking N–NW towards Barentsøya. The base is defined by the change from fissile shales (F3) below and the occurrence of yellowish gray siltstone/cementstone interbedding the F4 mudstones. Pink ruler measures c. 65 cm in the photograph. Locations are given in Fig. 1b. (For interpretation of the references to color in this figure legend, the reader is referred to the Web version of this article.)

marks the transition from brighter, weathered rock fragments, sharply changing into black, fissile, cliff-forming shales making up the base of the Blanknuten Mb. cliff in this locality (Fig. 5c). The boundary between the middle and upper parts of the Blanknuten Mb. is characterized by a change from cemented and massive, fissile mudstones into more yellowish fissile mudstones with abundant macroscopic phosphate nodules and interbeds of cemented siltstones (Fig. 5d).

A laterally extensive carbonate-cemented siltstone bed forms the base of dense, cliff-forming, black mudstones in the coastal exposures of Skrukkefjellet (highlighted with blue text and arrow; Figs. 4a, 5a and 6a, 6b). The significance of this bed is discussed in Section 5.2. Selected features from the Blanknuten Mb. are included in Fig. 7 and will be tied to the facies description below.

4.2. Facies description

The facies division presented here is based on distinct visual and textural differences observed in various mudstone types seen in the

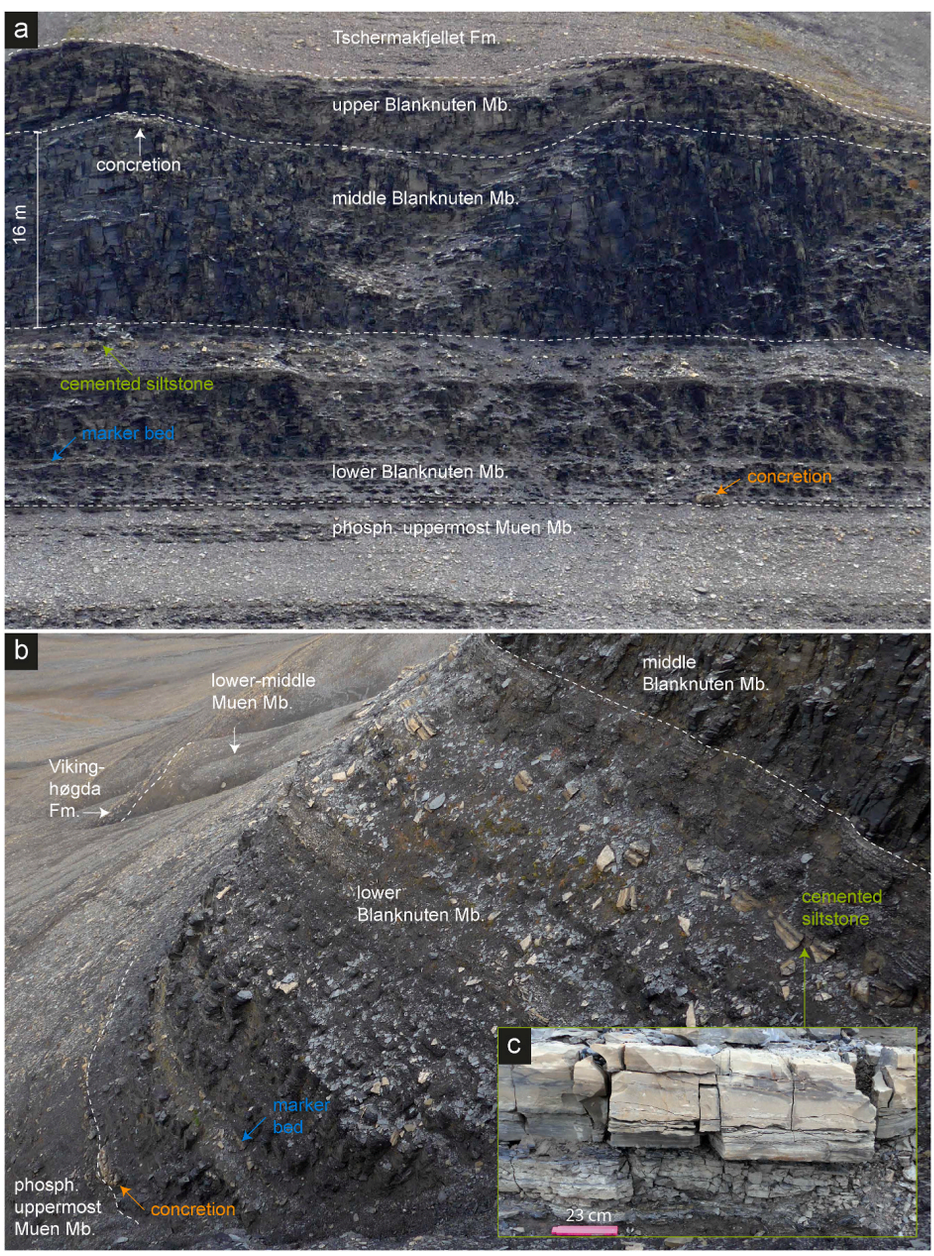

Fig. 6. Outcrop expression of the Blanknuten Mb. in the north face of the Skrukkefjellet Mountain. **(a)** Lithostratigraphic division, highlighting a concretion (orange arrow) at the same stratigraphic level as the concretion shown in Fig. 4c. A continuous marker bed (blue arrow) marks the onset of cliff-forming black shales in certain gentler-sloping areas of Skrukkefjellet. The upper concretion (white arrow) marks the uppermost part of the middle Blanknuten Mb. and is c. at the same stratigraphic level as the concretion in Fig. 5d. A c. 0.5 m siltstone bed (green arrow) is highlighted for reference. **(b)** Overview of the lower Blanknuten Mb., showing its lower cliff-forming part (F2), and the more scree covered upper part. The colored arrows refer to equivalent beds and concretion at the same stratigraphic height as explained in panel a. The thickness of the lower Blanknuten Mb. is c. 16 m. **(c)** A continuous carbonate cemented siltstone bed, acting as a marker in the upper part of the lower Blanknuten Mb. Folded meter stick (23 cm) for scale. (For interpretation of the references to color in this figure legend, the reader is referred to the Web version of this article.)

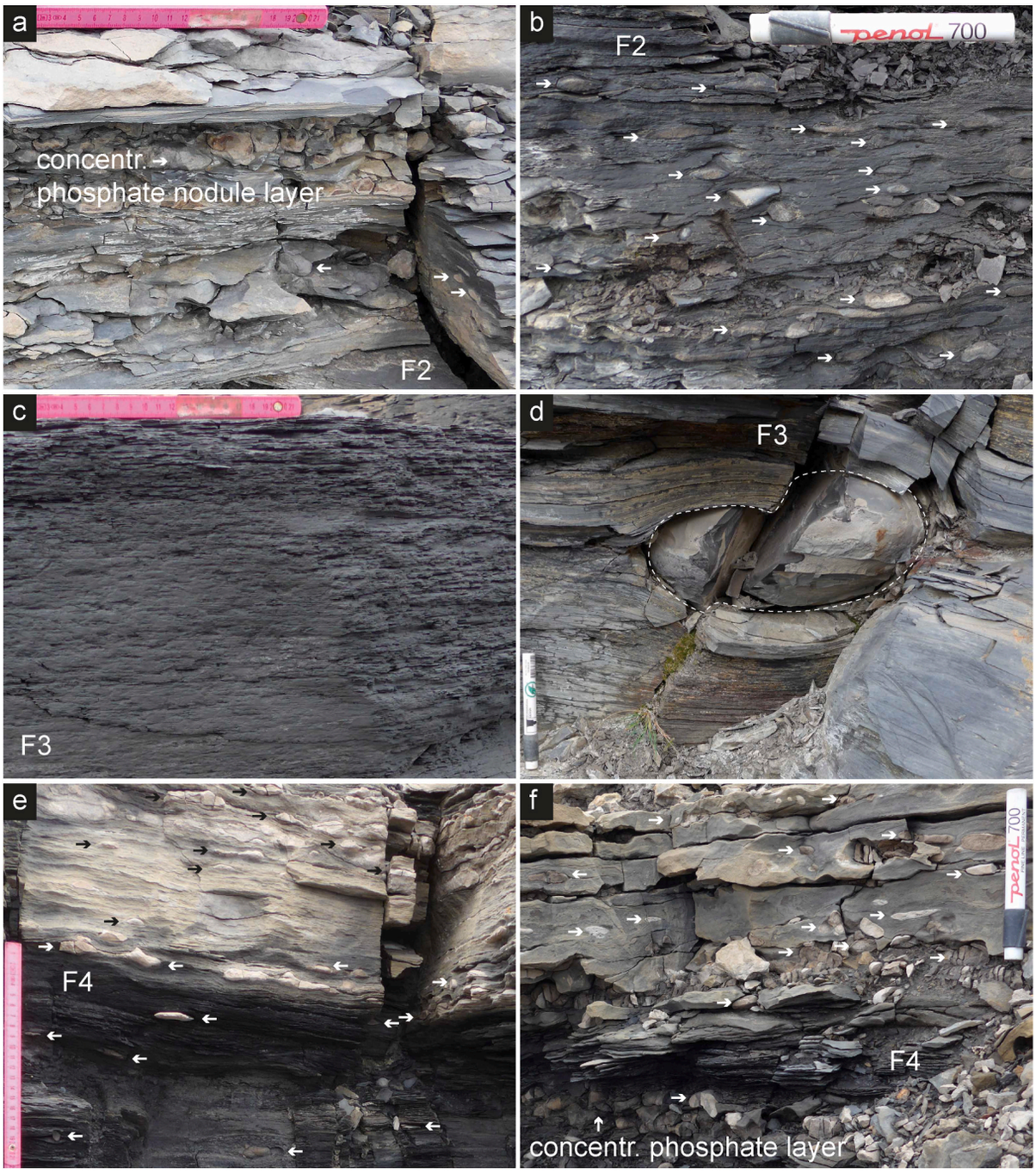

Fig. 7. Outcrop expression of identified facies in the Blanknuten Mb. **(a)** Phosphate grainstone beds and interbeds of phosphatic mudstones (F2) containing phosphate nodules. lower Blanknuten Mb., Skrukkefjellet W. **(b)** Massive, black mudstones (F2) with abundant phosphate nodules. lower Blanknuten Mb., Blanknuten type locality. **(c)** Massive and fissile black shales (F3) with no apparent bioturbation. middle Blanknuten Mb., Skrukkefjellet W. **(d)** Massive, fissile shales (F3) with a dark gray, authigenic calcite concretion. Note the deformed shales around the concretion. middle Blanknuten Mb., Blanknuten. **(e)** Black and yellow weathering fissile mudstones (F4) with ovoidal to irregular authigenic phosphate nodules. upper Blanknuten Mb., Skrukkefjellet NW **(f)** Cemented siltstone bed with reworked phosphate nodules, interbedded with mudstones (F4). upper Blanknuten Mb., Skrukkefjellet NW. Arrows denote phosphate nodules. Locations are given in Fig. 1. (For interpretation of the references to color in this figure legend, the reader is referred to the Web version of this article.)

Muen and Blanknuten members, and Tschermakfjellet Fm. (Fig. 8). This method is commonly applied in the description of core cuttings during well-site operations (Whittaker and Morton-Thompson, 1992). A brief description of the four types of visually discernible mudstone facies is provided below. Note that the mudstone facies recognized in this study partly correspond to those of Krajewski (2008).

Facies 1 (F1). This facies (Fig. 8a) occurs in the lower and middle parts of the Muen Mb. (Fig. 3b). and in the lowermost Tschermakfjellet Fm. (Fig. 3g). It consists of gray to dark gray mudstone and shows variable fissility. Fragmentation is both concoidal and platy, but is generally seen to yield flaky fragments, commonly associated with non-laminated fabric. The bedding surface of fragments lacking fissility may be rough, depending on degree of bioturbation. Cleavage surfaces do not necessarily follow bedding surfaces. Bioturbation in both localities is mainly seen as scattered, gently curved, mm-scale burrows (Fig. 8b). The burrows are darker than the mudstone matrix, possibly due to pyritization. Two samples

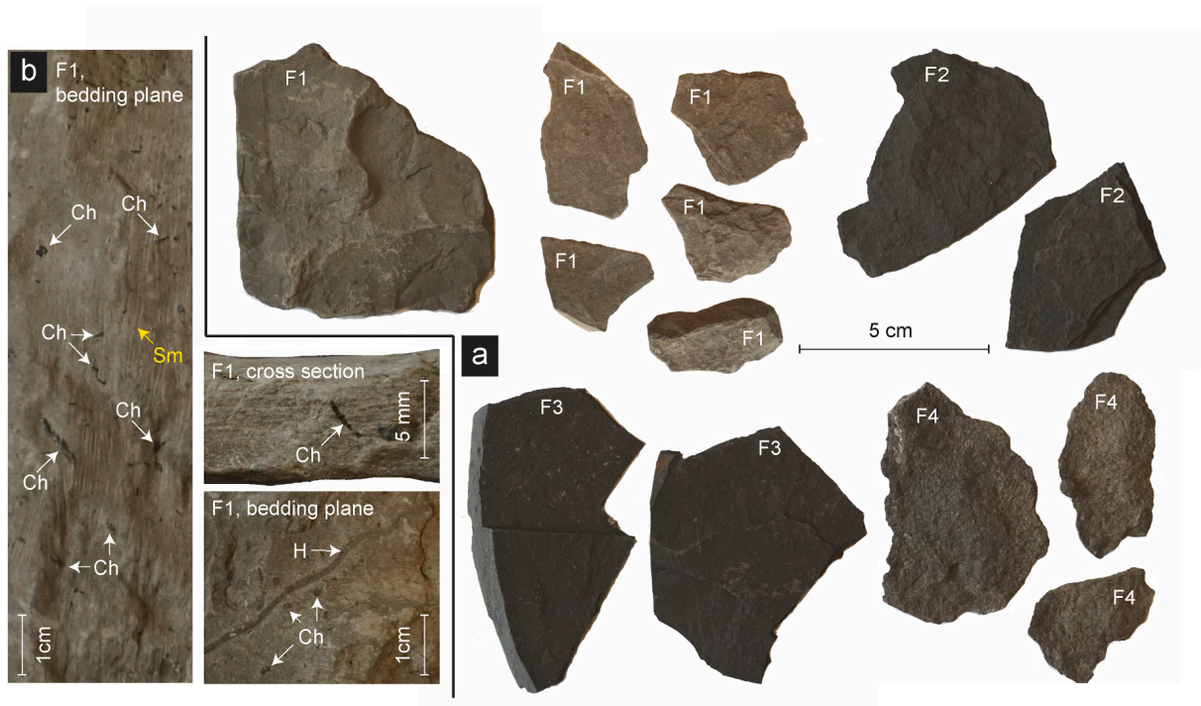

Fig. 8. **(a)** Images of dried shale fragments of facies F1–F4 shot at constant ISO, aperture, shutter speed and white balance settings, allowing for direct comparison of color and brightness. The large F1 fragment represents the lower–middle Muen Mb., while the smaller F1 fragments represents the Tschermakfjellet Fm. The F2, F3 and F4 fragments represent the upper Muen Mb., middle Blanknuten Mb., and upper Blanknuten Mb. respectively. **(b)** Images of F1 mudstone with traces of interpreted *Chondrites* (Ch) and *Helminthopsis* (H), see sections 4.1 for description and 5.2 for interpretation. Scratch marks (Sm) are recent and not related to geological processes. (For interpretation of the references to color in this figure legend, the reader is referred to the Web version of this article.)

at levels 28 and 30 m in the Skrukkefjellet W section show unbranched, mm wide, cylindrical and smooth horizontal trails with winding pattern (Fig. 8b). This facies corresponds to sediment type A and B of Krajewski (2008).

Facies 2 (F2). This facies (Fig. 8a) is seen in the upper Muen Mb. (Fig. 3c), and in the lower and upper parts of the Blanknuten Mb. (Figs. 3d, 7a and 7b). It consists of laminated, black-colored mudstones and has mostly fissile weathering. Upon forced breakage, the fragments may appear both platy and flaky, but are typically harder and more brittle when compared to F1. The lamination planes are typically smooth, straight and parallel. Undulating laminae around phosphate nodules within this facies are common (Figs. 3d, 7a and 7b). These nodules partly represent phosphate-precipitated, filled burrows that are unlined, branched, and parallel to the bedding. This facies corresponds to sediment type C and E of Krajewski (2008).

Facies 3 (F3). This facies (Fig. 8a) occurs in the middle Blanknuten Mb. exclusively, and consists of finely laminated, black shales (Figs. 3e, 7c and 7d). Weathered sections are characterized by columnar, weather-resistant shale stacks in the outcrop face (Figs. 3a, 5b and 6b), forming the steepest cliff faces along outcrops of the Botneheia Fm., exemplifying the greatest weathering resistance among the mudstone facies (Figs. 4a and 5b). The lamination planes are mostly smooth, sharp, and parallel (Fig. 8a). Bioturbation and macroscopic phosphate nodules are virtually absent. This facies corresponds to sediment type D of Krajewski (2008), assigned to the phosphogenic succession (Fig. 3a).

Facies (F4). This facies occurs in the upper Blanknuten Mb. It is slightly brighter in color compared to F3 (Fig. 8a). Fragments may be highly fissile, but also calcareous and competent, resembling marlstone or limestone. Forced splitting of well-laminated samples generally reveals less mechanical competence and internal cohesion between laminae compared to F2 and F3. The plane texture between laminae is typically rougher than F2 and F3 (Fig. 8a). Mm-sized shell fragments are scattered throughout the matrix. Like F2, undulating laminae due to phosphate nodule precipitation are common. Filled, unlined, branched phosphate-precipitated burrows occur parallel to the bedding (Fig. 7e). Based on changes in hardness, lamination, color, texture and reaction to hydrochloric acid, this facies appears to contain significant internal variations in carbonate content, ranging from calcareous shales to impure limestones. The broad variations in detrital siliciclastic and calcite content denote this facies to represent varying combinations of sediment type C and G of Krajewski (2008).

4.3. Bulk elements

The lower–middle Muen Mb. consists of relatively low TOC values (median 1.42 ± 0.64 wt. %; Table 2) that are mostly stable throughout this part of the Botneheia Fm. (Fig. 9). All but one sample of the upper Muen Mb. show TOC of 4 wt. % or more (median 4.93 ± 1.75 wt. %) and marks the onset of a prominent positive TOC excursion that strongly contrasts the underlying strata (Fig. 9). An upwards increasing TOC trend is seen through the lower Blanknuten Mb. (median 5.36 ± 2.42 wt. %) until the middle Blanknuten Mb. (median 8.41 ± 1.93 wt. %) is reached (Fig. 9). From here, TOC decreases from the base upper Blanknuten Mb. (median 6.10 ± 2.30 wt. %) and upwards until the top formation boundary is encountered (Fig. 9). The TOC values for the Tschermakfjellet Fm. (median 1.76 ± 0.70 wt. %) are very similar to the lower–middle Muen Mb., both consisting of F1 mudstones (Fig. 8a; Table 2). These trends are valid for both the Blanknuten and Skrukkefjellet localities (Fig. 9).

The TIC content slightly increases from the lowermost Muen Mb. (median 1.36 ± 0.24 wt. %) and upwards until the top of the middle Blanknuten Mb. (median 2.30 ± 0.71) (Fig. 9). The upper Blanknuten Mb. shows a correlative, positive excursion in both localities, and the highest TIC content among the stratigraphic units (median 3.73 ± 1.61 wt. %). As with TOC, the TIC content in the Tschermakfjellet Fm. (median 1.43 ± 0.94 wt. %) is comparable to the lower–middle Muen Mb. (both F1 mudstones).

Table 2
Descriptive statistics of parameters derived from LECO and Iatroscan TLC-FID analyses for the defined stratigraphic units and facies, combining both localities. min = minimum, max = maximum, std = standard deviation (±1σ).

		Stratigraphic unit						Facies			
		lower-middle Muen Mb.	upper Muen Mb.	lower Blanknuten Mb.	middle Blanknuten Mb.	upper Blanknuten Mb.	Tschermakfjellet Fm.	F1	F2	F3	F4
	count	32	6	15	30	15	3	35	22	30	14
TOC (wt. %)	min	0.55	2.49	3.66	4.70	2.18	1.18	0.55	2.49	4.70	2.18
	median	1.42	4.93	5.36	8.41	6.10	1.76	1.44	5.16	8.41	6.04
	std	0.64	1.75	2.42	1.93	2.30	0.70	0.64	2.23	1.93	2.36
	max	3.92	7.78	12.03	11.61	11.84	2.58	3.92	12.03	11.61	11.84
TIC (wt. %)	min	0.87	0.99	1.12	0.76	1.94	0.11	0.11	0.99	0.76	1.94
	median	1.36	1.42	1.73	2.30	3.73	1.43	1.36	1.63	2.30	3.78
	std	0.24	0.31	0.46	0.71	1.61	0.94	0.33	0.47	0.71	1.60
	max	1.92	1.80	2.78	3.63	7.45	1.92	1.92	2.78	3.63	7.45
TS (wt. %)	min	0.35	0.75	0.66	0.53	0.38	0.04	0.04	0.66	0.53	0.38
	median	0.83	0.99	1.09	1.43	1.11	0.77	0.80	1.11	1.43	1.09
	std	0.27	0.34	0.30	0.67	0.60	0.57	0.30	0.43	0.67	0.46
	max	1.30	1.63	1.72	3.53	2.61	1.17	1.30	2.61	3.53	1.78
TOC/TS	min	0.78	3.17	2.75	1.98	1.71	2.21	0.78	2.75	1.98	1.71
	median	1.61	4.52	4.56	5.76	5.80	2.30	1.78	4.41	5.76	6.10
	std	1.00	1.57	3.08	2.44	4.56	17.66	5.31	2.71	2.44	4.58
	max	5.19	7.32	12.64	11.99	18.16	32.84	32.84	12.64	11.99	18.16
	Count	12	4	12	19	7	3	15	17	19	6
SAT (mg/g rock)	min	0.21	1.51	0.30	0.73	0.33	0.06	0.06	0.30	0.73	0.60
	median	0.75	2.44	1.62	1.64	0.80	0.22	0.52	1.63	1.64	0.87
	std	0.44	1.15	0.88	0.43	0.28	0.22	0.46	1.04	0.43	0.21
	max	1.70	4.05	3.33	2.20	1.18	0.50	1.70	4.05	2.20	1.18
ARO (mg/g rock)	min	0.03	0.91	0.27	0.64	0.11	0.04	0.03	0.27	0.64	0.11
	median	0.10	1.97	0.89	2.00	0.28	0.04	0.10	0.91	2.00	0.32
	std	0.08	0.61	0.97	2.18	0.21	0.07	0.08	0.92	2.18	0.23
	max	0.27	2.30	3.44	7.97	0.68	0.17	0.27	3.44	7.97	0.68
POL (mg/g rock)	min	1.05	4.88	4.39	6.02	4.14	1.91	1.05	4.39	6.02	4.14
	median	2.12	8.85	5.71	8.58	5.26	2.12	2.12	5.72	8.58	5.30
	std	1.00	2.93	1.96	2.20	1.34	0.72	0.93	2.34	2.20	1.40
	max	4.56	11.67	10.43	12.70	7.49	3.26	4.56	11.67	12.70	7.49
EOM (mg/g rock)	min	1.29	7.29	4.97	7.90	5.13	2.01	1.29	4.97	7.90	5.37
	median	3.02	13.26	8.77	12.84	6.25	2.39	2.76	8.96	12.84	6.30
	std	1.46	4.60	3.47	4.18	1.43	1.01	1.37	4.03	4.18	1.40
	max	6.45	18.02	17.20	21.71	8.76	3.92	6.45	18.02	21.71	8.76
EOM/TOC	min	0.17	0.15	0.07	0.10	0.07	0.14	0.14	0.07	0.10	0.08
	median	0.21	0.23	0.17	0.15	0.10	0.15	0.20	0.18	0.15	0.12
	std	0.03	0.05	0.07	0.04	0.07	0.02	0.04	0.07	0.04	0.07
	max	0.26	0.27	0.29	0.23	0.27	0.17	0.26	0.29	0.23	0.27
SAT (%)	min	16.07	16.43	6.11	7.05	6.36	3.05	3.05	6.11	7.05	8.08
	median	24.77	20.28	17.91	11.63	11.13	9.31	21.69	19.01	11.63	11.96
	std	4.54	2.55	6.17	3.20	4.59	4.90	7.72	6.04	3.20	4.20
	max	29.91	22.50	27.92	18.22	20.32	12.70	29.91	27.92	18.22	20.32
ARO (%)	min	2.08	12.47	5.48	6.75	1.83	1.74	1.74	5.39	6.75	1.83
	median	4.12	13.22	12.17	16.55	5.39	1.84	3.66	12.63	16.55	5.04
	std	2.06	1.81	5.06	9.54	2.98	1.45	2.03	4.68	9.54	3.26
	max	8.26	16.43	22.14	37.64	8.39	4.30	8.26	22.14	37.64	8.39
POL (%)	min	64.55	64.76	56.74	50.13	71.28	83.00	64.55	56.74	50.13	71.28
	median	72.29	66.64	69.47	71.22	82.91	88.86	73.66	67.11	71.22	82.03
	std	4.85	1.07	8.82	8.49	6.08	6.10	8.55	8.83	8.49	6.11
	max	81.48	67.15	88.41	84.00	89.57	95.21	95.21	88.41	84.00	89.57
SAT/ARO	min	3.14	1.00	0.52	0.19	1.18	1.75	1.75	0.52	0.19	1.37
	median	5.56	1.55	1.40	0.70	2.42	2.96	4.67	1.45	0.70	2.93
	std	3.78	0.34	0.68	0.60	2.45	1.68	3.73	0.59	0.60	2.48
	max	12.85	1.77	2.88	2.70	7.00	5.07	12.85	2.88	2.70	7.00

Except for a few excursions, the TS curve shows a similar trend as the TOC curves (Fig. 9), however with an overall lower range (0.04–3.53 wt. % in all samples; Table 2).

TS vs. TOC plots are commonly used to infer paleo-depositional environments focusing on benthic redox conditions (Alsenz et al., 2015; Berner and Raiswell, 1983; Smolarek et al., 2017). While this study does not distinguish pyritic versus kerogen sulfur, the results are comparable with the C/S systematics of Krajewski (2013, his Fig. 23). The inferred depositional environments denote oxic–suboxic benthic conditions for the lower–middle Muen Mb. and the Tschermakfjellet Fm. (both F1 mudstones) (Fig. 10). This greatly contrasts the upper Muen Mb. and the entire Blanknuten Mb. (consisting of F2, F3 and F4 mudstones) that generally plot below the normal marine line (Fig. 10).

4.4. Bulk bitumen distribution

Source rock extracts are often characterized using relative and absolute abundancy of saturates, aromatics, resins and asphaltenes (Tissot and Welte, 1984). Bitumen abundance or composition may be visually evaluated by variations in extract color (e.g., Abay et al., 2014; Matapour et al., 2019). The lower–middle Muen Mb. to the upper Muen Mb. boundary displays a strong change in extract hue from transparent cognac-like to opaque dark brown to black (Fig. 11) which imply richer extracts and/or more polar compounds above the F1–F2 boundary in the

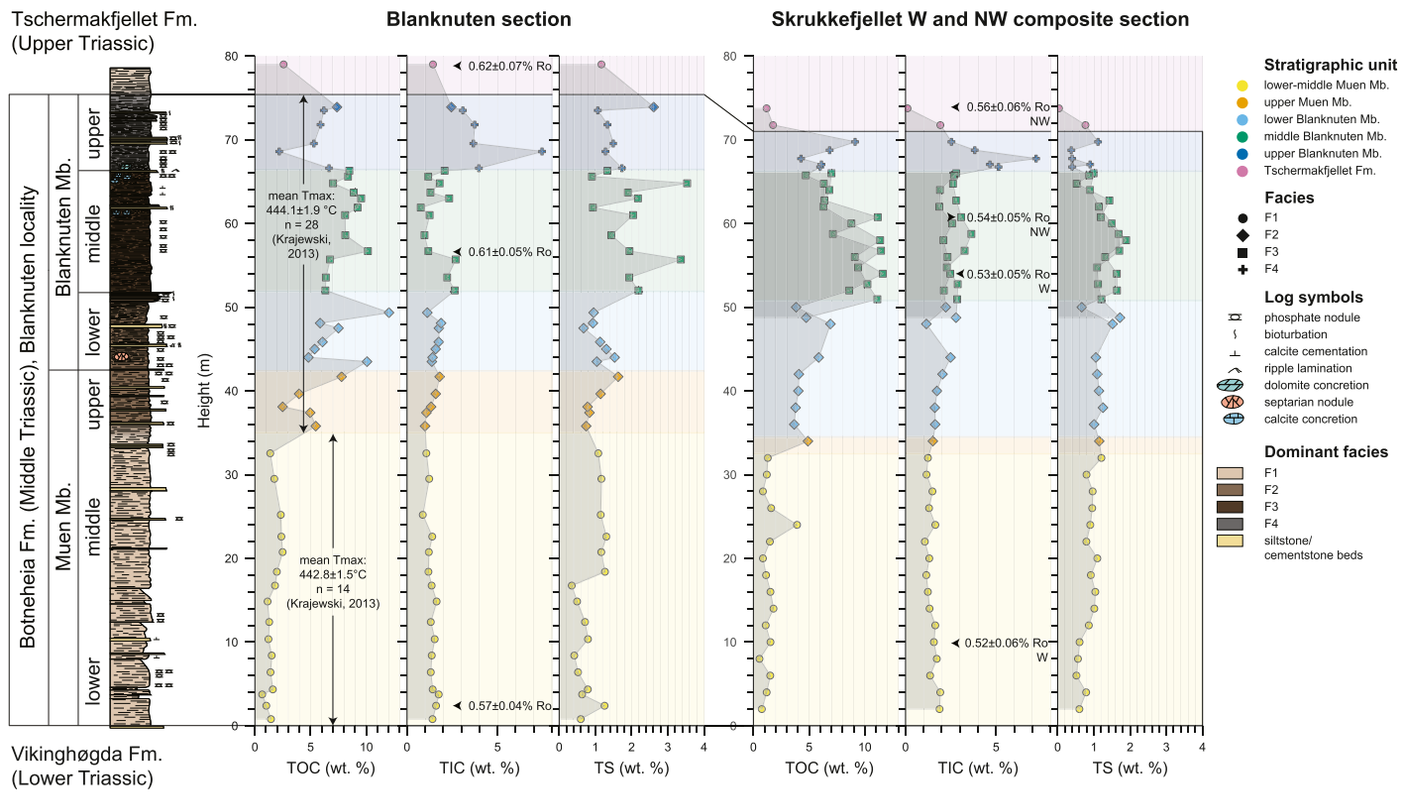

Fig. 9. Lithostratigraphic log from Blanknuten compared with LECO data (TOC, TIC, TS) and vitrinite reflectance from the Blanknuten section and Skrukkefjellet composite section. The lower and upper part of the two Skrukkefjellet logs are combined from the W and NW localities, resulting in overlap at level 49–66 m marked by darker shade of gray. The T_{max} values are taken from Krajewski (2013, his Appendix A) and represents samples from units 2–4 and units 5–8 in the in the Blanknuten locality respectively. (For interpretation of the references to color in this figure legend, the reader is referred to the Web version of this article.)

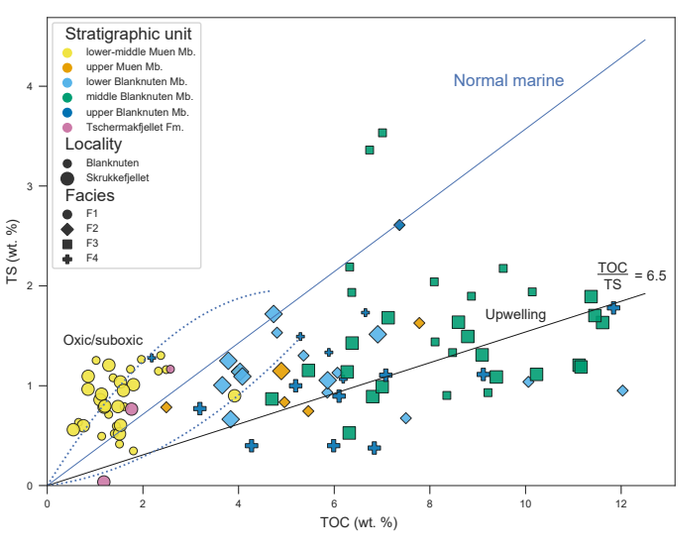

Fig. 10. Cross plot showing the relationship between TOC and TS. The blue line reflects the normal marine trend (Berner and Raiswell, 1983), while the dotted compartment shows typical distribution of normal marine samples (Berner and Raiswell, 1983; Leventhal, 1995). Areas indicating oxic/suboxic conditions and upwelling are retrieved from Ghassal et al. (2018) and Smolarek et al. (2017) respectively. (For interpretation of the references to color in this figure legend, the reader is referred to the Web version of this article.)

Muen Mb. The lower Blanknuten Mb. is not discernible from the upper Muen Mb. in agreement with both units consisting of F2 mudrocks. In contrast, all the extracts from the middle Blanknuten Mb. (F3) are black. The dark brown–black extracts from the upper Blanknuten Mb. samples are slightly brighter and comparable to the upper Muen Mb. and the lower Blanknuten Mb. The Tschermakfjellet Fm. in the Skrukkefjellet locality shows comparable brightness to the lower–middle Muen Mb. (both F1 mudstones), however the uppermost Tschermakfjellet Fm. sample from the Blanknuten locality is clearly darker. These visual properties generally match the quantitative TLC-FID chromatograms (Fig. 12).

The stratigraphic distribution of the total EOM in both study localities clearly shows relatively low but stable values in the lower–middle Muen Mb. that suddenly increase at the onset of the upper Muen Mb., in adherence to the F1–F2 facies boundary within this member (Fig. 13). A varying upwards EOM increase is seen within the upper Muen Mb. and the lower Blanknuten Mb., where these two units show maximum absolute SAT content in the Blanknuten (4.05 mg/g rock) and Skrukkefjellet (3.33 mg/g rock) localities respectively. Maximum EOM and absolute ARO values are encountered in the middle Blanknuten Mb. in both localities (Fig. 13). From here, the EOM content progressively decreases upwards into the upper Blanknuten Mb. and the Tschermakfjellet Fm., where the latter unit is comparable to the lower–middle Muen Mb. (both F1 mudstones). These trends correlate well with the TOC curve (Fig. 9).

The normalized SAT (%), ARO (%) and POL (%) fractions (Fig. 14) show that all samples are dominated by the POL (%) fraction, a common trait for source rock extracts (Le Tran and Philippe, 1993). The lower–middle Muen Mb. shows a dominance of SAT (%) content that progressively decreases through the upper Muen Mb. and the lower Blanknuten Mb., ultimately resulting in the lowest SAT (%) in the middle Blanknuten Mb. This distribution is mainly caused by a relative increase in aromatic hydrocarbons (HCs) rather than decreasing polar compounds (Table 2; Fig. 12). The upper Blanknuten Mb. and Tschermakfjellet Fm. show lowered SAT (%) and ARO (%), concurrently resulting in a dominating POL (%) fraction (Fig. 14).

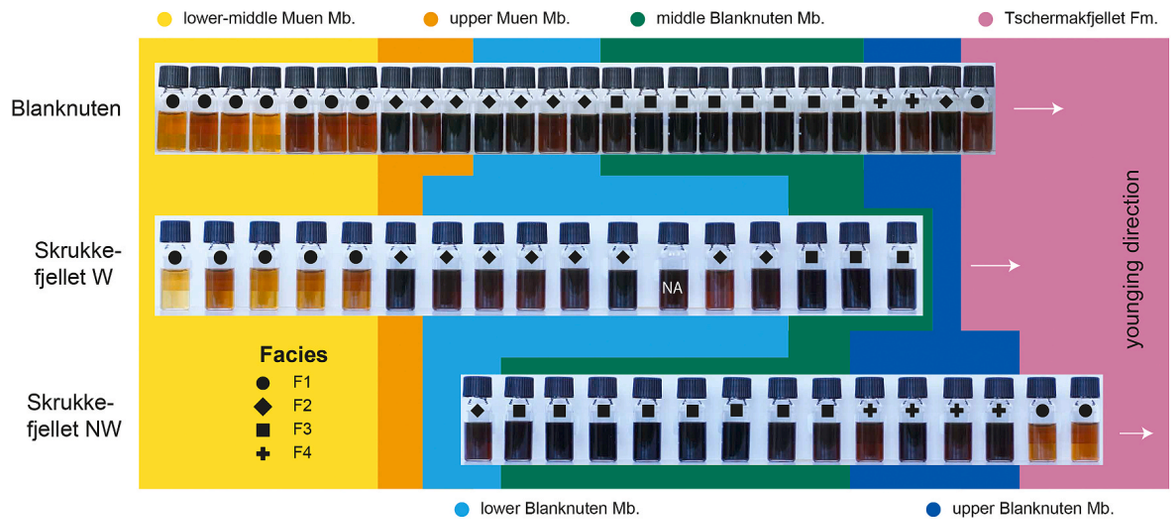

Fig. 11. Comparison of 2 ml vials containing extracts at equal dilution (3.85 vol % of original strength) against stratigraphic units. The sample labeled NA is not included in this study.

4.5. Thermal maturity and source facies

The vitrinite reflectivity data (Fig. 9) indicates that the Botneheia Fm. in the Blanknuten locality (mean R_o = 0.60%) and in the Skrukkefjellet composite section (mean R_o = 0.54%) are dominantly early mature and immature respectively (cf. Peters and Cassa, 1994). The Skrukkefjellet W and NW localities show virtually identical maturities. The vitrinite values in each of the Blanknuten and Skrukkefjellet localities overlap regardless of sample elevation (Fig. 9) inferring a negligible maturity gradient with depth for each locality but a lateral maturity contrast between these localities.

The SAT/ARO and EOM/TOC ratios of source rock extracts are expected to increase with increasing thermal maturation (Law, 1999; Peters and Cassa, 1994). This is because kerogen and bitumen are cracked into saturate HCs rather than aromatic HCs with increasing maturity, resulting in the relative decrease of aromatic compounds respective to saturates and thus increasing the ratio. However, the SAT/ARO ratio is also affected by organofacies (Waples and Curiale, 1999) and weathering effects (Forsberg and Bjorøy, 1983), which might overprint any maturity signature. Similarly, the EOM/TOC ratio is expected to increase with increasing maturity, as kerogen crack into bitumen with increasing maturity (Peters and Cassa, 1994), but is similarly affected by organofacies and weathering.

The lower–middle Muen Mb. shows the highest SAT/ARO ratios (max 12.85), which may decrease up to an order of magnitude into the upper Muen Mb. (min 1.00) (Fig. 15; Table 2). These contrasting values form a chemostratigraphic boundary that conforms to the F1–F2 boundary in the Muen Mb. SAT/ARO ratios further decrease upward through the lower Blanknuten Mb. and into the middle Blanknuten Mb. The latter unit shows the minimum SAT/ARO ratios in both localities, which concurrently increases upwards into the upper Blanknuten Mb. and the Tschermakfjellet Fm. These two units show comparable SAT/ARO ratios (Fig. 15; Table 2). As there is no clear shift in SAT/ARO ratios comparing the Blanknuten and Skrukkefjellet localities with each other, it is not possible to apply this ratio as a maturity parameter to distinguish the proven maturity difference between these localities.

The EOM/TOC logs do not follow the same trends as the SAT/ARO logs (Fig. 15). This is shown by the highly variable and overlapping EOM/TOC values between all the stratigraphic units and associated facies for both sections (Fig. 15). Still, the lower–middle Muen Mb. shows overall higher EOM/TOC ratios compared to the middle Blanknuten Mb. in the Blanknuten section (median 0.21 ± 0.03 vs. median 0.13 ± 0.05) and the Skrukkefjellet composite section (median 0.20 ± 0.02 vs. median 0.17 ± 0.03). These EOM/TOC ratios alone give the impression that the middle Blanknuten Mb. in the Skrukkefjellet locality is more mature compared to the same unit in the Blanknuten locality, which is clearly false (Fig. 9). This parameter is therefore not reliable as a maturity indicator.

TOC content alone is not sufficient to determine source rock potential (Dembicki, 2009), but combined with EOM content, it is possible to evaluate gas-prone vs. oil-prone hydrocarbon generation potential (Fig. 16) (Dembicki, 2017; Le Tran and Philippe, 1993). The lower–middle Muen Mb. shows considerable variation and includes samples with the lowest oil potential in the sample set (Fig. 16). The upper Muen Mb. marks a prominent increase and plots similarly as the lower Blanknuten Mb., while the middle Blanknuten Mb. appears to reflect the most oil-prone unit (Fig. 16). The upper Blanknuten Mb. shows comparable oil potential as the lower Blanknuten Mb. The three Tschermakfjellet Fm. samples (i.e. strongly limited dataset) show EOM content >2 mg/g rock and TOC content >2 wt. % (Fig. 16), which is considered very good petroleum potential for immature source rocks (Peters and Cassa, 1994).

4.6. Exploratory data analysis

The principal component analysis (PCA) shows that 74.4% of the variance can be explained by principal components (PCs) 1 and 2 (Fig. 17). The lower–middle Muen Mb. correlates the most with elevated SAT/ARO ratio and SAT (%) content, and least with TOC, TS, and absolute ARO and POL content. The upper Muen Mb. shows grouping tendencies with the lower Blanknuten Mb. due to elevated absolute SAT concentrations, although the latter unit displays prominent scatter for both PCs. The middle Blanknuten Mb. (F3) correlates best with absolute ARO, POL, EOM and TOC content, and shows the greatest contrast to the lower–Middle Muen Mb. The upper Blanknuten Mb. is distinguished by relatively high content in polars, and overall low EOM/TOC. The samples from the Tschermakfjellet Fm. do not overlap with the other samples, but group between the lower–Middle Muen Mb. and the upper Blanknuten Mb.

From the hierarchical cluster analysis (HCA), five clusters (C1–C5) were identified (Fig. 18).

Cluster 1 (C1). This cluster consists of a single Tschermakfjellet Fm. F1 sample in the top Skrukkefjellet composite log (Fig. 9). This sample shows the greatest cluster distance and thus the least similarity with the remaining sample set (Fig. 18). This distinction is based on relatively low abundance in almost all the geochemical variables and especially the ARO (%) fraction (1.74%), resulting in a

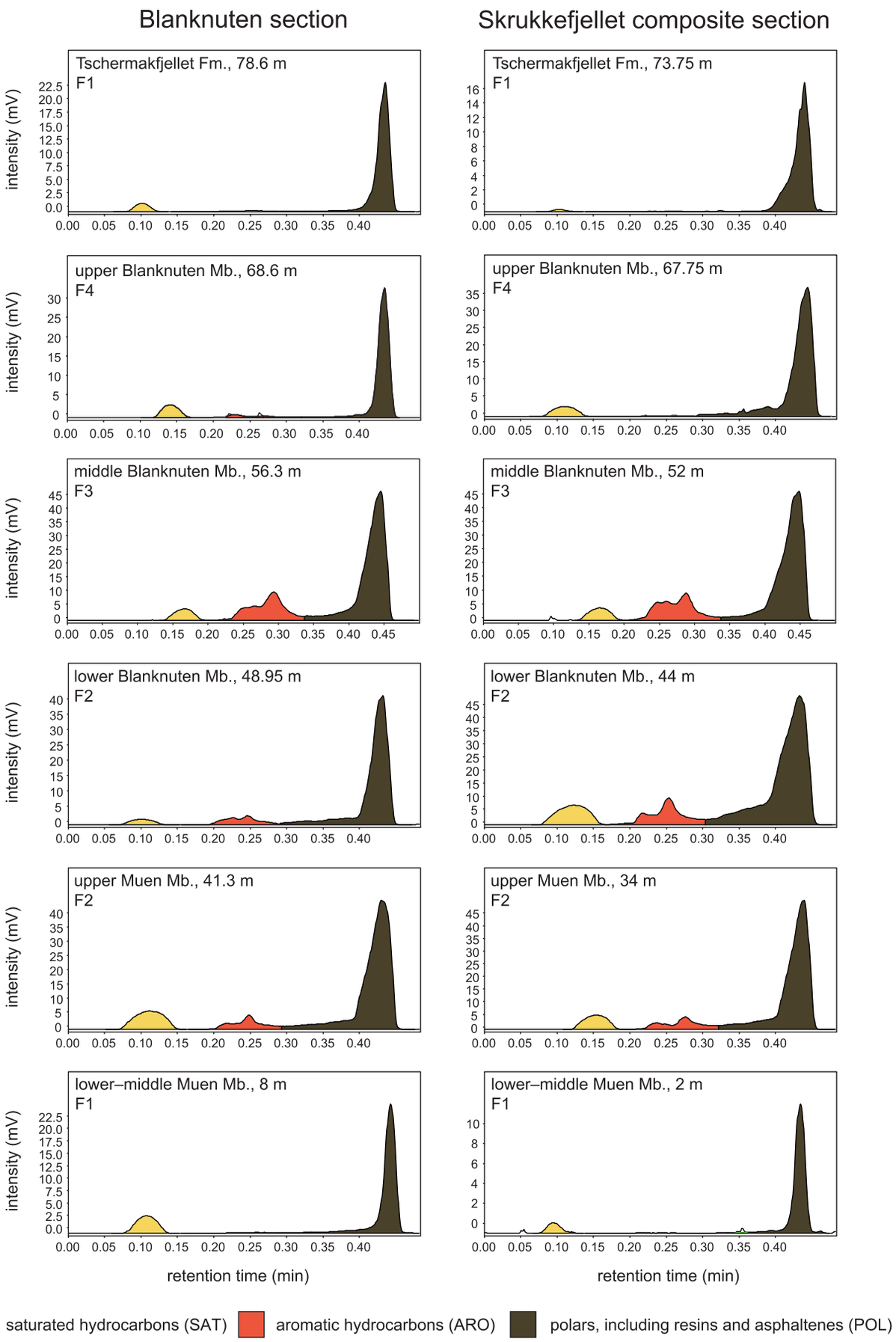

Fig. 12. Iatroscan chromatograms from each stratigraphic unit in both the Blanknuten and Skrukkefjellet localities. Note the overall absence of aromatic HCs in the lower–middle Muen Mb. and the Tschermakfjellet Fm. (both F1 mudstones).

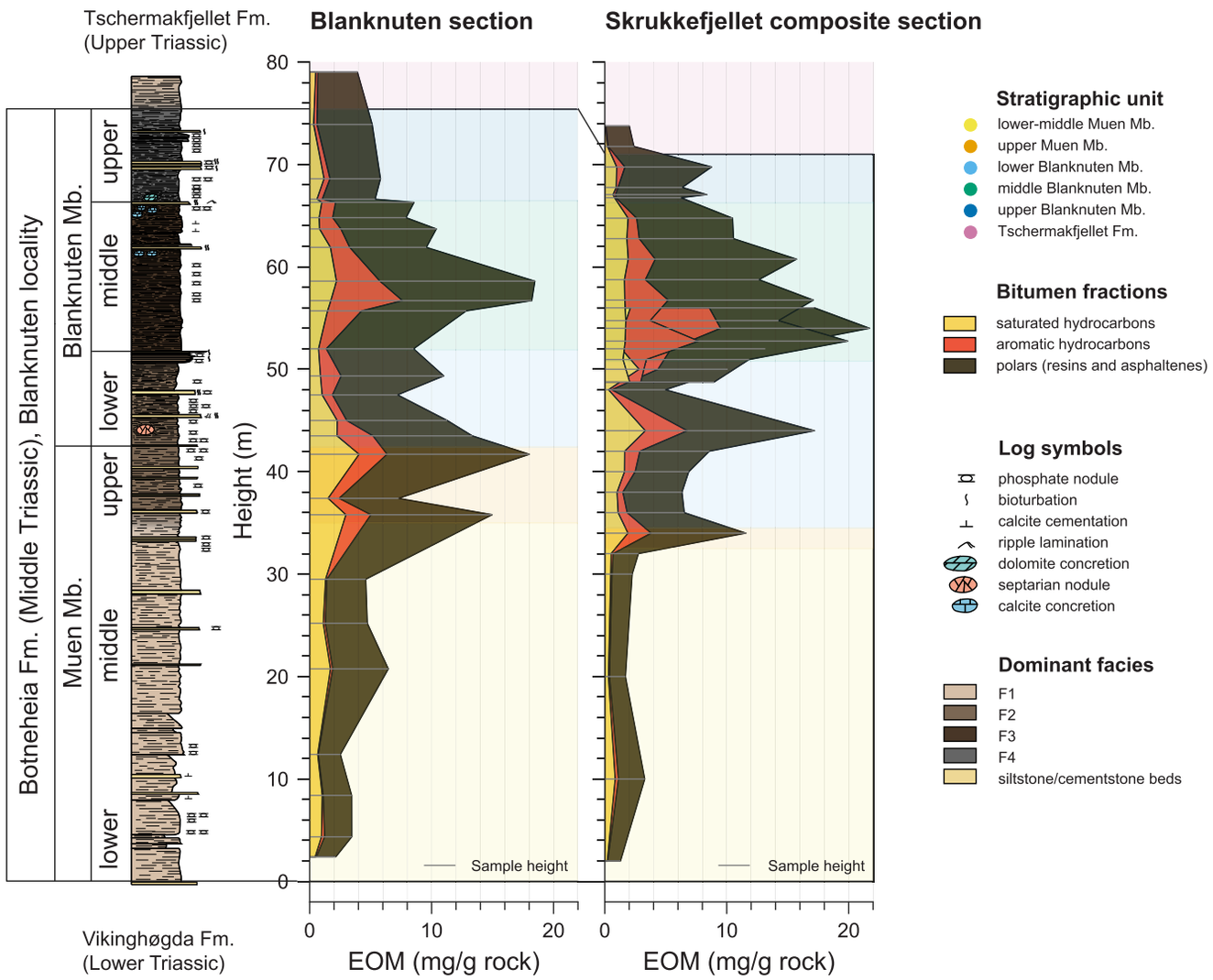

Fig. 13. Lithostratigraphic log from the Blanknuten locality compared with Iatroscan-derived EOM logs of the Blanknuten section and Skrukkefjellet composite section. The EOM content between the sample positions, as denoted by horizontal lines in the EOM logs, is linearly interpolated.

high POL (%) fraction (95.21%). TOC/TS is extremely high (32.84), and deviates substantially off the median (1.78) for F1 mudstones.

Cluster 2 (C2). This cluster contains nine samples representing F2 mudstones from the upper Muen Mb. and the lower Blanknuten Mb, but dominantly middle Blanknuten Mb. F3 mudstones (Fig. 18). C2 is recognized by high contents of TOC (5.46–11.61, median 8.60 wt. %), absolute POL (7.73–12.70, median 10.60 mg/g rock), ARO (2.06–7.97, median 4.08 mg/g rock) and EOM (13.16–21.71, median 18.02 mg/g rock). ARO (%) and POL (%) are relatively high (12.74–37.64, median 30.30%) and low to intermediate (50.13–68.78, median 60.67%) respectively (Fig. 14).

Cluster 3 (C3). This cluster represents 14 samples consisting of F1 mudstones only (i.e. the lower–middle Muen Mb. and Tschermakfjellet Fm.). It is characterized by low TOC (0.75–2.58, median 1.52 wt. %), TOC/TS (0.78–3.63, median 1.91), POL (1.05–4.56, median 2.14 mg/g rock), and EOM (1.29–6.45, median 3.02 mg/g rock). SAT (%) (9.31–29.91, median 22.64%) and POL (%) (64.55–88.86, median 73.21%) are both relatively high. This results in the highest SAT/ARO ratios (2.96–12.85, median 4.87) among all the clusters (Fig. 18).

Cluster 4 (C4). This cluster contains 29 samples including the upper Muen Mb. (F2) and the lower, upper and middle Blanknuten Mb. (F2–F4). C4 exhibits a complex relationship between all variables, leading to difficulties towards finding general geochemical systematics. However within the cluster, the two upper Muen Mb. samples (F2) clearly group with the five lower Blanknuten Mb. samples. These seven samples are stratigraphically close (Fig. 9) and of the same F2 mudstones (Fig. 18).

Cluster 5 (C5). This cluster contains four samples from the upper Blanknuten Mb. only. It is recognized by high TIC (4.66–7.45, median 6.17 wt. %) (Fig. 9), high POL (%) (71.28–89.57, median 84.15%), and high SAT/ARO ratios (2.42–7.00, median 4.94).

5. Discussion

The presented geochemical log panels of the Blanknuten and Skrukkefjellet localities are the first attempt at stratigraphically correlating and comparing carbon, sulfur and bulk bitumen content to described mudstone facies of the Botneheia Fm. and correlate these parameters against the regional Middle Triassic lithostratigraphic framework provided by Krajewski (2008). Given the significance and regional distribution of Early–Late Triassic organic rich deposits, the presented geochemical logs and correlations provide new insights in how the elemental and bitumen composition is tied to mudstone facies and stratigraphic units of the Botneheia (Anisian–Ladinian) and Tschermakfjellet (Carnian) fms. in Svalbard.

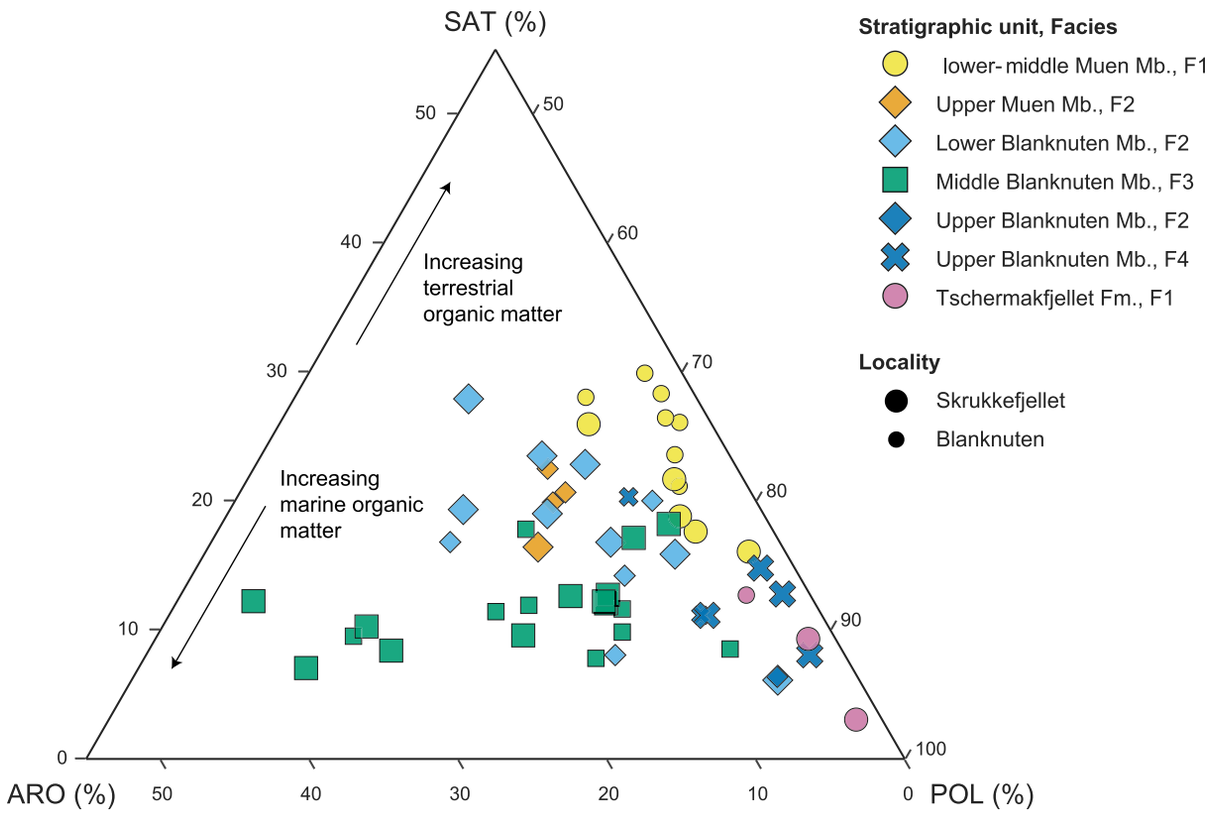

Fig. 14. Ternary plot of the bulk SAT (%), ARO (%) and POL (%) fractions (including resins and asphaltenes) normalized to 100% by weight. A greater content of SAT (%) in respect to ARO (%) indicates increased content of terrestrial relative to marine organic matter and vice versa (Tissot and Welte, 1984).

5.1. Challenges in estimating formation thickness and correlating lithostratigraphic sub-units

In this study, the basal boundary of the middle Blanknuten Mb. is placed at level c. 51–52 m in each study locality (Fig. 9). According to Mørk et al. (1999) and Vigran et al. (2008), the base of the Blanknuten Mb. is placed at c. 53 and 55 m height in the same localities. Thus, their base Blanknuten Mb. boundary can only correspond with the base of the middle Blanknuten Mb. of Krajewski (2008) and this study. The lower boundary of the Blanknuten Mb. was initially defined as the base of a calcareous, cliff-forming siltstone unit occurring within the upper part of Botneheia Fm. (Mørk et al., 1999). Later work by Krajewski (2008) identified the lower boundary of the Blanknuten Mb. at the base of cliff–forming mudstones and shales in the upper part of the Botneheia Fm. However, this definition may be too ambiguous. For instance, in steeper outcrops, the base of the lower Blanknuten Mb. acts as the onset of the so-called "Blanknuten Mb. cliff" (Fig. 3a), while in outcrops with gentler slope gradients, the base of the "Blanknuten Mb. cliff" starts at the base of the middle Blanknuten Mb., i.e. a younger stratigraphic level than in steeper sections (Figs. 4a and 5b). Thus, we emphasize that the *earliest* occurrence of F2 mudstones that show a remarkable increase in cliff-forming capability (Fig. 3a) should be considered as the base Blanknuten Mb., adhering to the boundary as defined by Krajewski (2008, his Fig. 4).

Source rock thickness is required to determine the source potential index (Demaison and Huizinga, 1991) and is therefore a crucial parameter for determining petroleum expulsion from source rocks. In central Spitsbergen, the formation thickness may be difficult to measure due to structural thickening (e.g. Haremo et al., 1990). Such effects are negligible on Edgeøya. Mørk et al. (1982) and Krajewski (2008) report a Botneheia Fm. thickness of c. 75 m and 101 m in the Blanknuten locality respectively. Krajewski (2008) reports a thinning of the Botneheia Fm. from the Blanknuten locality to the Skrukkefjellet locality, a distance of c. 20 km (Fig. 1b), while Vigran et al. (2008) report a formation thickness of c. 84 m in the Skrukkefjellet locality, i.e. a slight thickening of the Botneheia Fm. along the same trajectory. This study demonstrates that the formation thickness is generally the same in both localities (Fig. 9). The thickness difference of c. 5 m between the study localities might simply be due to the nature of the meter stick measurements, where a ±5 m error margin is realistic. If the measured thicknesses represent the true thicknesses, the thinning trend from south to north is in agreement with Krajewski (2008), however, the thickness estimates (Fig. 9) correspond much better with Mørk et al. (1982) and Vigran et al. (2008). A Botneheia Fm. thickness substantially above c. 85 m therefore appears unlikely on Edgeøya, in disagreement with Krajewski (2008, 2013). Thickness measurements retrieved from structure-from-motion drone surveys (e.g. Buckley et al., 2019) could provide a more accurate answer.

The facies change from lower–middle Muen Mb. F1 mudstones to upper Muen Mb. F2 mudstones occurs at level c. 33 m in both the Blanknuten and Skrukkefjellet sections (Fig. 9). Two tightly spaced siltstone layers at level 33 m in the Blanknuten section (Fig. 9) also occur at level 32 m in the Skrukkefjellet W section (not shown). Thus, the tub-like concretion in the Skrukkefjellet W section (Fig. 4c), which currently is assigned to the lower Blanknuten Mb. (Krajewski, 2008; Vigran et al., 2014), may instead belong to the phosphogenic F2 mudstones of the upper Muen Mb. We find it curious that the combined thickness of the upper Muen Mb. and the lower Blanknuten Mb. in the Blanknuten locality (c. 17 m; Fig. 9) and the Skrukkefjellet locality (c. 18 m; Fig. 9) is almost identical in both localities. Still, lateral facies variations should be expected (Krajewski, 2013).

A laterally extensive marker bed (highlighted blue text and arrow) marks the base of continuously competent F2 mudstones in the lower Blanknuten Mb. (Figs. 4a, 5a and 6a). This marker bed occurs c. 10 m above the currently defined base of the lower Blanknuten Mb. in the Skrukkefjellet locality (Fig. 9). If the base lower Blanknuten Mb. boundary was placed at the top of this bed, a good match in the Muen Mb. thickness and geochemical parameters between the localities would

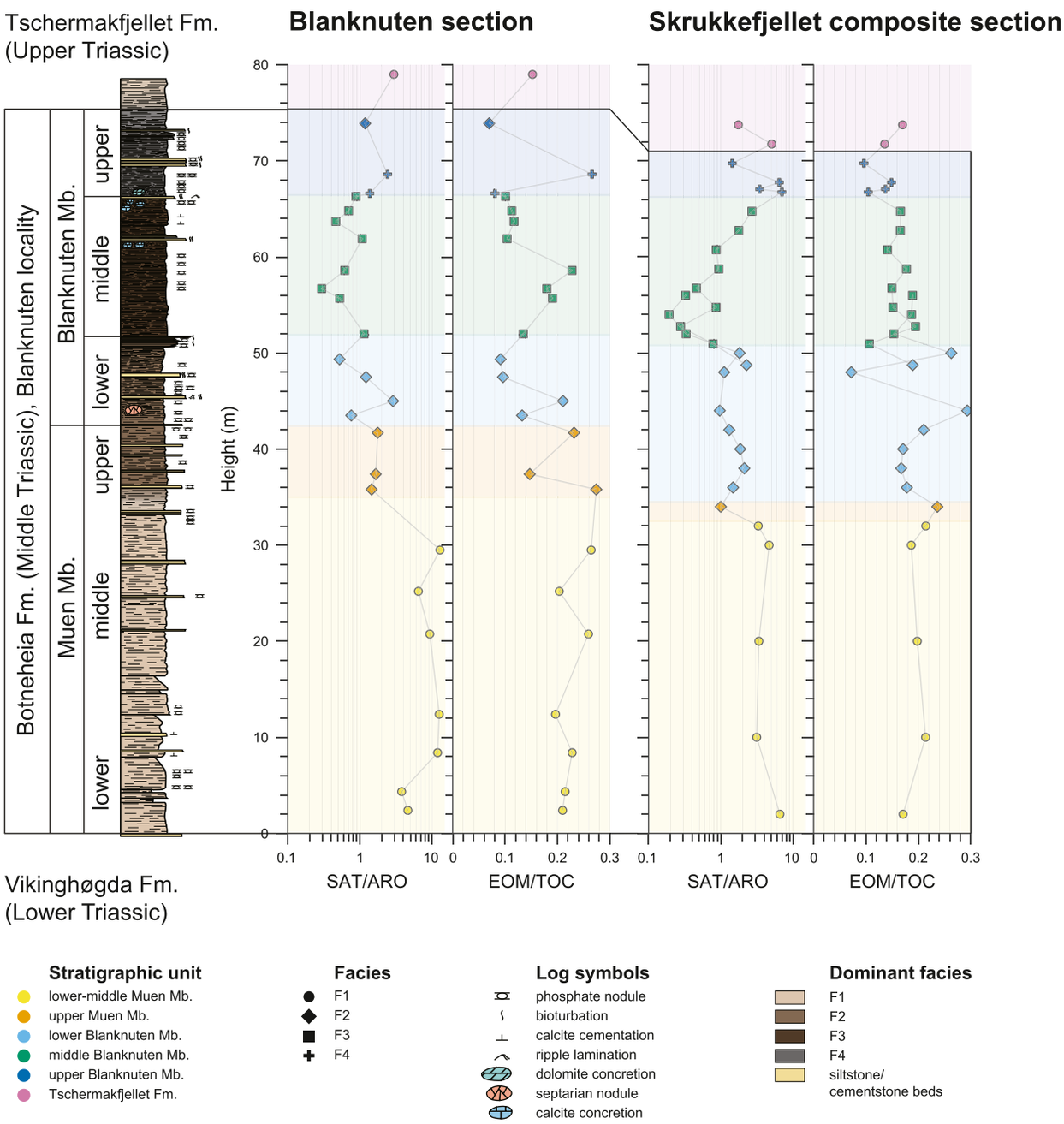

Fig. 15. Lithostratigraphic log from the Blanknuten locality compared with LECO and Iatroscan-derived geochemical logs from the Blanknuten and Skrukkefjellet localities.

be met (Figs. 9, 13 and 15). Still, as the upper Muen Mb. and the lower Blanknuten Mb. both consist of F2 mudstones and display comparable bulk geochemical assemblages (Figs. 17 and 18), their lithostratigraphic distinction appears less important for source rock characterization.

5.2. *Relating mudstone facies to depositional conditions*

Vigran et al. (2014) reported the entire Muen Mb. on Edgeøya to represent deposition during dominantly anoxic conditions based on pelagic fossil content and lack of bioturbation. However, the gray color and the presence of trace fossils within the lower–middle Muen Mb. F1 mudstones (Fig. 8) suggest that burrowing occured after deposition. The flaky weathering of these F1 mudstones (Fig. 3b) indicates a lack of laminae (cf. Potter et al., 2005) that may represent thorough matrix homogenization by biogenic reworking (Byers, 1974). Alternatively, the homogeneous matrix may reflect rapid deposition by low-density, mud-rich turbidity currents (Traykovski et al., 2000), fluid mud migration (Ruttenberg and Goni, 1997), or fallout from hypopycnal plumes (Schieber, 2016; Wilson and Schieber, 2014).

The mm-scale, sub-vertical burrows in the lower–middle Muen Mb. F1 mudstones are interpreted to be small-scale *Chondrites* trace fossils (Fig. 8b). These appear to be monogeneric and may indicate anoxic or possibly dysoxic benthic conditions (Bromley and Ekdale, 1984). However, a study on the Kimmeridge Clay Fm. reports *Chondrites* trace fossils in upper dysaerobic facies and not in the anaerobic facies (Wignall, 1991). *Chondrites* might also represent opportunistic exploitation of deeper, anoxic beds with oxygenated sea floor conditions (cf. Vossler and Pemberton, 1988). Consequently, these trace fossils are not clearly indicative of anoxic bottom conditions.

The unbranched, winding trails are interpreted to be *Helminthopsis* trace fossils (Fig. 8b) and provide evidence of a habitable sea floor. The co-occurrence of *Chondrites* and *Helminthopsis* trace fossils and the gray

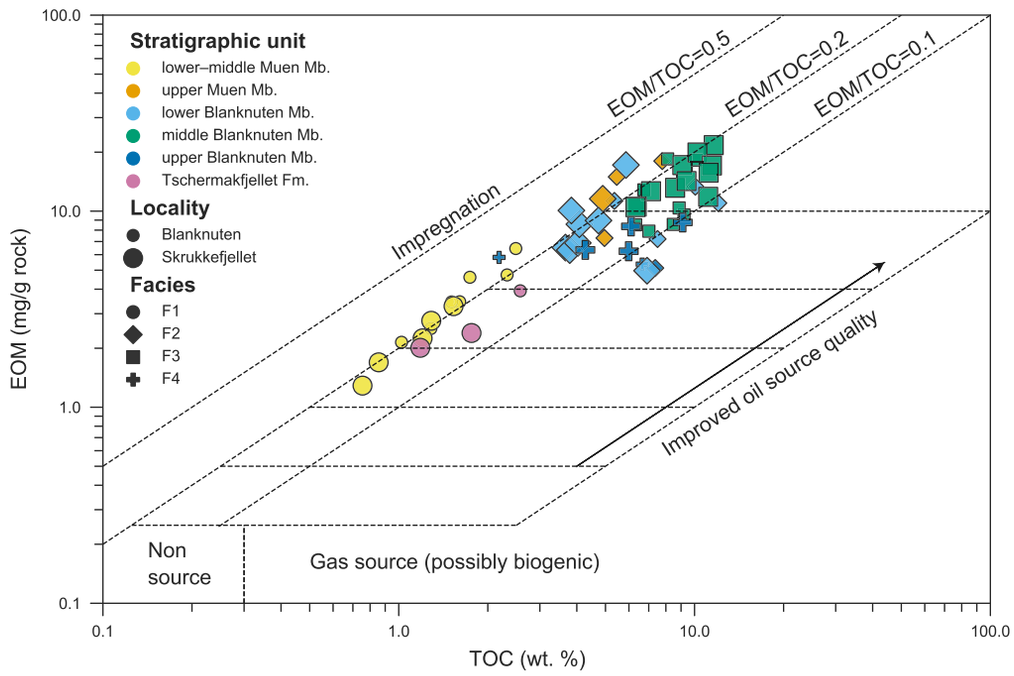

Fig. 16. Cross plot of TOC (wt. %) versus total EOM (mg/g rock). The inferred zones are adapted from Le Tran and Philippe (1993).

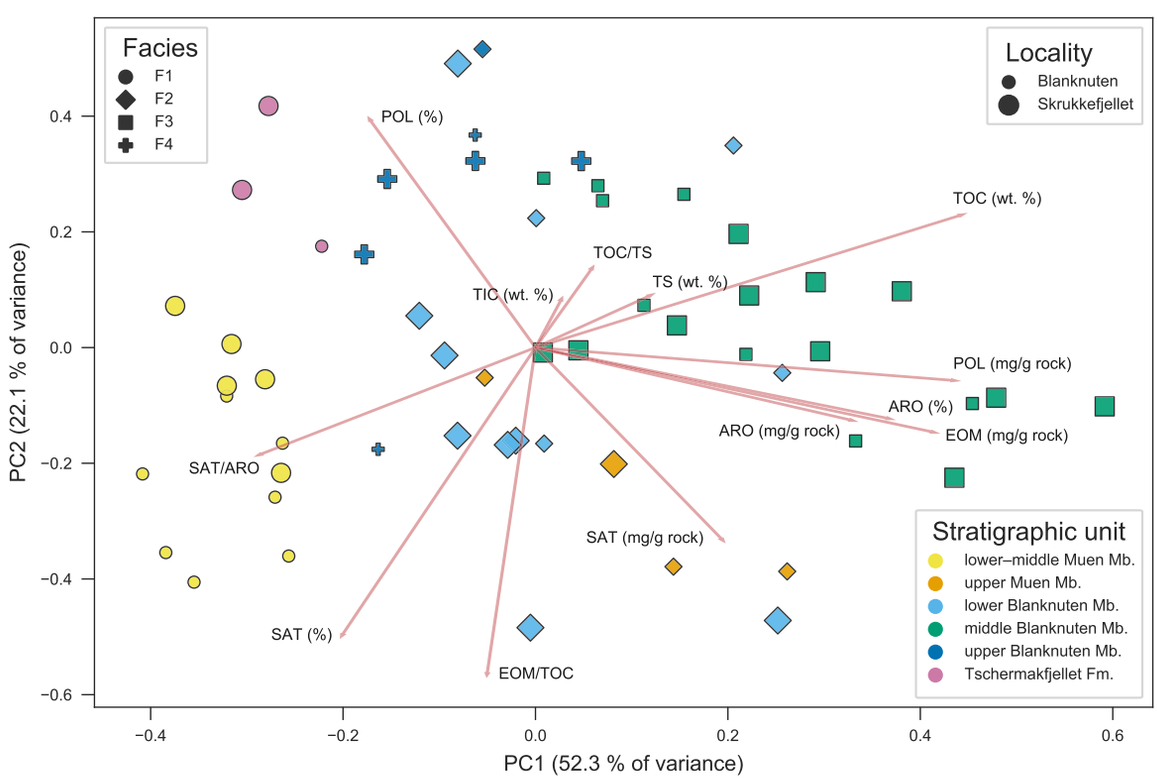

Fig. 17. Combined PCA score plot and loading plot of 13 variables derived from 57 samples. The loadings (red arrows) are normalized by the largest range in each PC. (For interpretation of the references to color in this figure legend, the reader is referred to the Web version of this article.)

color of the lower–middle Muen Mb. F1 mudstones indicates oxic–dysoxic bottom conditions (MacEachern et al., 2009). The low abundance of macroscopic trace fossils might indicate benthic soup-ground conditions during deposition as such conditions are biased against the preservation of soft biogenic structures (MacEachern et al., 2009). However, microscopic investigations by Krajewski (2013) show that the lower–middle Muen Mb. is bioturbated as a rule and suggest that the benthic conditions were dominantly oxic.

Recent work on the Tschermakfjellet Fm. on Edgeøya (i.e. F1 mudstones in this study) report on *Helminthopsis* trails within the mudstones facies of this unit and interpreted this facies to represent low-energy, offshore to distal pro-delta suspended load deposits (Anell et al., 2020). Similarly, Krajewski (2013) denotes the F1 mudstones in the lower–middle Muen Mb. to represent pro-deltaic to open shelf deposits.

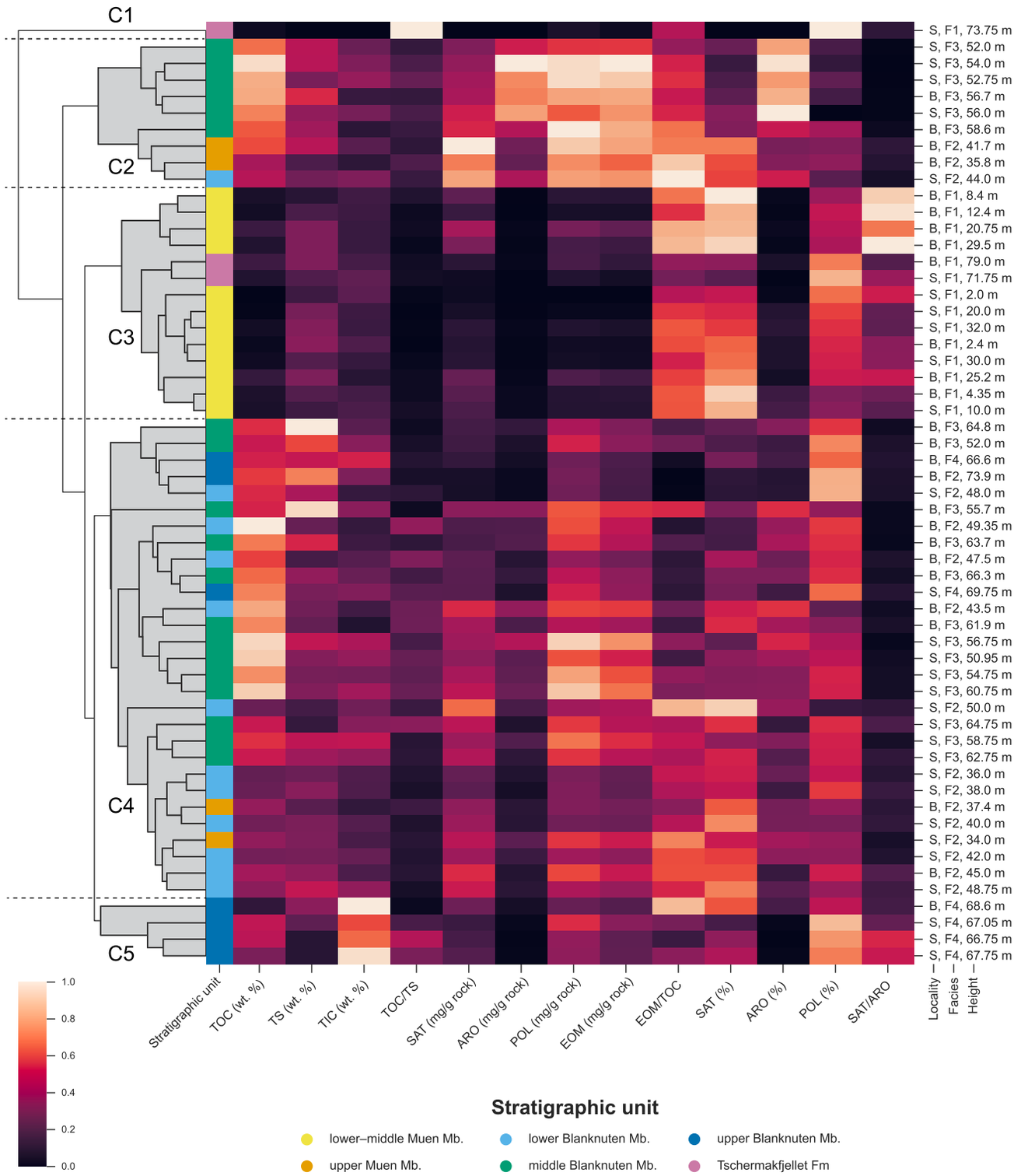

Fig. 18. Combined HCA dendrogram and heatmap of 13 variables (columns) derived from 57 samples (rows) from the Blanknuten and Skrukkefjellet localities. The heatmap and associated color map represents the rescaled [0, 1] values of each variable. B and S represents Blanknuten and Skrukkefjellet localities, respectively. (For interpretation of the references to color in this figure legend, the reader is referred to the Web version of this article.)

This correlation between the F1 mudstones from the lower–middle Muen Mb. and the Tschermakfjellet Fm. suggests that these stratigraphic units were deposited in similar depositional settings. A dominantly deep, restricted and anoxic shelf setting for the lower–middle Muen Mb. F1 mudstones as suggested by Lundschien et al. (2014, their Fig. 7) and Vigran et al. (2014) therefore seems questionable.

The oxygenated conditions in the lower–middle Muen Mb. might be related to the distal regressive phase conforming to the Anisian–Ladinian TR-cycle seen in the time-equivalent Bravaisberget Fm. in western Spitsbergen (Mørk et al., 1989). This could explain the relative abundance of carbonate cemented siltstone beds in the upper Muen Mb. compared to its lower part (Figs. 3a and 9). The base Anisian transgression could also have flooded the Svalbard Platform and created hydrodynamic configurations that allowed benthic ventilation and

oxygenation. This mechanism was initially suggested as an explanation for the well-ventilated conditions that followed the base Carnian transgression (Høy and Lundschien, 2011).

The well preserved laminae, increased brittleness and dark color of F2 mudstones (Figs. 3c and d, 7a–b, 8a) are interpreted to represent less or no bioturbation due to decreased oxygen levels, thus favoring organic matter preservation (Demaison and Moore, 1980). In addition, phosphogenesis in marine sediments, as evidenced by phosphate nodules (Figs. 3d, 7a–b), is commonly associated with a continental shelf to slope environment with high organic productivity induced by upwelling, low detrital input, and periodic winnowing and reworking (Arthur and Sageman, 1994; Demaison and Moore, 1980; Filippelli, 2011). The increased brittleness is likely to represent the sudden increase in both TOC and TIC content (Fig. 9), as both kerogen and calcite cement may act as binders causing brittle shales (Krajewski, 2008; Potter et al., 2005). The burrows (Fig. 9) indicate occasionally hospitable benthic conditions. The first occurrence of this facies may represent the earliest phosphogenic mudstones in eastern Svalbard (Krajewski, 2008). However, the F1–F2 boundary at level 35 m (Fig. 9) in the Blanknuten locality does not directly correspond to the non-phosphogenic–phosphogenic boundary within the Muen Mb. as defined by Krajewski (2008, 2013). Using Fig. 9 in this study as a height reference, Krajewski (2008, his Fig. 3a; 2013, his Fig. 3b, d) defined the non-phosphogenic–phosphogenic boundary in the Blanknuten locality to be at level c. 29 m and 25 m respectively. These inconsistencies make it challenging to determine the true stratigraphic level of the non-phosphogenic–phosphogenic boundary in the Muen Mb.

The F3 mudstones (Fig. 7c and d) are characterized by the best-preserved laminae among all the facies, absent bioturbation, darkest color (Fig. 8a), highest TOC (median 8.41 wt. %) and greatest brittleness. F3 is interpreted to be deposited during oxygen-depleted conditions with absent macroscopic bioturbation, contrasting the underlying F1 and F2 mudstones. The elevated brittleness is likely a result of the increased TOC and TIC cementation (Fig. 9). The F3 mudstones are exclusive to the middle Blanknuten Mb. (Fig. 3a), and this unit probably reflects the most stable depositional conditions among the described facies as it displays only two high-energy, macroscopic event beds and shows an overall homogenous sedimentary log (Fig. 9). However, Vigran et al. (2008) reported abundant *Daonella* bivalves in the middle Blanknuten Mb. in the Skrukkefjellet locality, indicating that the sea floor was occasionally inhabited, i.e. not permanently anoxic (Schatz, 2005). Similar observations were made by Alsen et al. (2017) for the equivalent Israd Fm. in the Wandel Sea Basin, northeastern Greenland. Krajewski (2013) shows frequent microscopic packstone layers within F3 mudstones in the middle Blanknuten Mb., reflecting that bottom waters cannot have been permanently stagnant, in agreement with the two macroscopic event beds (Fig. 9). This suggests that high primary productivity rather than water mass restriction introduced by bathymetric relief was the main driver for oxygen depletion and subsequent benthic preservation potential (cf. Ghadeer and Macquaker, 2012). Krajewski (2013) argues that a submarine swell c. 50 km N–NE of the Blanknuten locality contributed to water mass restriction during the deposition of F3 mudstones, as he did not observe this facies there. Based on the paleogeographic setting, Høy and Lundschien (2011) conclude that a halocline triggered by abundant fresh water and nutrient supply from the southwestern delta system with subsequent primary production was more important than bathymetric relief for organic matter preservation in the bulk Botneheia Fm.

Based on the dark color and high TOC (median 6.10 wt. %), the F4 mudstones (exclusive to the upper Blanknuten Mb.) are interpreted to be deposited during mainly oxygen-depleted conditions caused by high primary productivity. However, abundant macroscopic, coarser-grained event beds and phosphate-filled burrows (Figs. 3f, 5d, 7e–f) indicate high-energy deposits and oxygenation episodes. The sudden increase in TIC also demarcates this facies from the underlying F3 mudstones (Fig. 9). The TIC content is linked to the abundance of shell fragments in the F4 mudstones, increasing in concert with its mechanical competency. This is expressed in the Skrukkefjellet locality, where the base of the upper Blanknuten Mb. is more cliff-forming than the underlying top middle Blanknuten Mb. (Fig. 5d). The TIC excursion therefore acts as a marker horizon in delineating the underlying F3 dominated source rock unit and the above F4 dominated source rock (Fig. 9). These observations and descriptions support the observations of Krajewski (2008) and Mørk and Bromley (2008), who interpreted the F4 mudstones to represent regional regressive deposits, with interchanging hospitable–unhospitable benthic conditions.

Three factors have been extensively debated in terms of their significance in forming organic-rich sedimentary successions, i. e. (i) organic productivity (Pedersen and Calvert, 1990); (ii) organic-matter preservation (Demaison and Moore, 1980); and (iii) sedimentation rate (Creaney and Passey, 1993). From the discussion above, it appears that oxygen depletion due to high primary productivity coupled with condensation caused by increased relative sea level are important factors contributing to the organic richness in the Botneheia Fm. in eastern Svalbard. Water mass restriction as a result of paleobathymetric configuration seems less important, given the implied oxic conditions during the Anisian (F1 mudstones, lower–middle Muen Mb.).

5.3. Defining normal marine vs. upwelling conditions by TOC/TS systematics

TOC/TS ratios are higher in sediments deposited in upwelling zones than those deposited under normal marine settings (Morse and Emeis, 1990). The relatively low TOC/TS ratios in the lower–middle Muen Mb. (median 1.61) and the Tschermakfjellet Fm. (median 2.30) (both F1 mudstones) are representative of normal marine conditions with oxic to slightly dysoxic bottom waters (Fig. 10) (cf. Ghassal et al., 2018). In contrast, the TOC/TS ratios in the upper Muen Mb. (median 4.52) and the lower, middle and upper Blanknuten Mb. (median 4.56, 5.76 and 5.80 respectively) indicate conditions that are consistent with high primary productivity and possibly upwelling (Fig. 10). Greater TOC/TS ratios might reflect regularly ventilated seafloor conditions (Smolarek et al., 2017), as pyrite is oxidized more rapidly than organic matter (Marynowski et al., 2011). The reported oxygenation events during deposition of the Blanknuten Mb. could deplete sulfur more readily than organic carbon and thus preserve organic matter. The very low TS in the uppermost Tschermakfjellet Fm. sample in the Skrukkefjellet locality (minimum 0.04 wt. %) (Fig. 9) could indicate intense TS depletion caused by a well-ventilated and oxic depositional environment.

Alsenz et al. (2015) assigned a TOC/TS ratio of 6.5 in the Maastrichtian Ghareb Fm. (Negev, Israel) to upwelling conditions, which overlaps with the entire Blanknuten Mb. but mostly its middle and upper part (Fig. 10). Alsenz et al. (2015) concluded that low iron availability promoted sulfur incorporation into the organic matter, preserving the-organic matter against microbial degradation. The iron content has previously been reported to be lower for the Blanknuten Mb. compared to the Muen Mb. (Krajewski, 2013). The distal parts of the Triassic Boreal Sea were sediment starved during the Ladinian transgression (Klausen et al., 2015) and the distal shelf setting likely received less detrital iron and perhaps fluvial-sourced nutrients. In Svalbard, Anisian sedimentation rates were higher than Ladinian (Hounslow et al., 2008). Thus, Svalbard most likely received more detrital iron content during the Anisian than in the Ladinian.

5.4. Main influences on bitumen quantity and composition

Bitumen represents a continuum of compounds, from simple, straight *n*-alkanes to large and complex asphaltenes (Redelius and Soenen, 2015). It is therefore challenging to deconvolute the influence of organofacies, thermal maturity, and biodegradation, which are the most important factors affecting the composition of petroleum fluids (England and Mackenzie, 1989). Outcrop samples are also prone to weathering,

which can severely alter the organic composition (Clayton and Swetland, 1978). It is therefore crucial to assess these factors given the nature of the samples in this study.

Aromatic HCs may constitute 25–60% of oils derived from marine organic matter, but only around 10–30% of oils from non-marine organic matter (Tissot and Welte, 1984). The Botneheia Fm. ranges from kerogen type III/II in the lower Muen Mb. F1 mudstones to dominantly kerogen type II in the middle Blanknuten Mb. F3 mudstones (Krajewski, 2013). These two sub-units show the largest contrast in kerogen type (Fig. 3) and richness (Fig. 9), implying that they should also record a strong contrast in SAT/ARO ratios. Indeed, this is consistent for both the Blanknuten and Skrukkefjellet localities in this study (Figs. 14 and 15), suggesting that the source facies variations are the most important influences on the relative bitumen composition in the studied sections.

The R_o data from this study and T_{max} data from Krajewski (2013) (Fig. 9) suggest that no significant maturity contrast exists within each sample profile (Fig. 9). This is consistent with Haile et al. (2018), who concluded that the thermal maturity of the Blanknuten and Skrukkefjellet localities constrains the regional burial history without any obvious influence from nearby sill intrusions. Both of the sampled sections are less than 100 m (Fig. 9), and a difference greater than c. 4 °C from bottom to top appears unreasonable based on previously determined geothermal gradients in the region, i.e. c. 40 °C/km (Braathen et al., 2012). Thus, differential thermal maturation is considered a minor or insignificant influence on the relative bitumen content or composition throughout the study localities.

Previously published gas chromatography (FID) data of the Botneheia Fm. shales in the Blanknuten locality suggests incipient to mild biodegradation (Abay et al., 2014), indicating that biodegradation is unlikely to have caused major compositional changes to the studied bitumen in both localities.

Forsberg and Bjorøy (1983) found that the total EOM content in weathered shales from the Botneheia Fm. was reduced by an average of 10% compared to non-weathered shales from shallow, meter-deep boreholes. In addition, SAT/ARO ratios were generally higher in the cores than in the outcrop samples (up to 54% greater), showing a preferential loss of aromatic HCs vs. saturated HCs in weathered vs. "non-weathered" shale. These losses are considerably less than the variations observed in this study (Figs. 13 and 15).

From the discussion above, we interpret the kerogen richness and quality to be the dominating factors that influence the SAT/ARO ratio and the absolute and relative bulk bitumen fractions. However, we cannot rule out the possibility that minor influences of thermal maturation, weathering and biodegradation affect the facies differentially throughout the formation.

5.5. Relating bitumen content to source rock quality and richness

Studies of thin-sections (Krajewski, 2013) show that the lower–middle Muen Mb. F1 mudstones contain mostly marine macerals (lamalignite and telalginite) but elevated content of terrestrial macerals (vitrodetrinite, collinite, hebamorphinite and inertodetrinite). In contrast, the middle Blanknuten Mb. F3 mudstones contain dominantly amorphous organic matter, lamalginite and telalginite that show low degree of reworking and only negligible amounts of vitrinite (mostly telinite and vitrodetrinite) (Krajewski, 2013). These stratigraphic units therefore reflect organic petrological end-members in the Botneheia Fm. in terms of organic matter type. The upper Muen Mb. (F2) and the lower and upper Blanknuten Mb. (F2 and F4) show an intermediate composition (Krajewski, 2013). The SAT/ARO ratios are highest in the lower–middle Muen Mb. F1 mudstones (median 5.56), and lowest in the middle Blanknuten Mb. F3 mudstones (median 0.70), with the remaining stratigraphic units generally showing intermediate values (Fig. 15). It therefore appears that the total EOM (Fig. 13) and the SAT/ARO trends (Fig. 15) directly reflect the inferred relative content of terrestrial vs. marine maceral types throughout the Botneheia Fm. The highstand conditions and the resulting Early Ladinian maximum flooding surface appear to have favored abundant preservation and accumulation of marine organic matter, in accordance with Krajewski and Weitschat (2015).

The bitumen and TOC content of immature shales typically indicates their petroleum generation potential: the higher, the better (Peters and Cassa, 1994). EOM may correlate strongly with the S_1 parameter from Rock-Eval pyrolysis (Bhullar et al., 2000; Othman, 2004), since both parameters quantify free hydrocarbons within the mudstones. The relative EOM vs. TOC distribution of all the stratigraphic units in the Botneheia Fm. (Fig. 16) is consistent with the reported maceral composition and source rock richness and quality as determined by Rock-Eval (Krajewski, 2013). Still, it appears that the EOM vs. TOC plot overestimates the source potential for the Tschermakfjellet Fm. F1 mudstones as this formation is considered gas-prone only (Abay et al., 2018; Krajewski, 2013; Mueller et al., 2014; Mørk and Bjorøy, 1984). However, Krajewski (2013) describes the lowermost Tschermakfjellet Fm. samples as black shales and reports two immature samples with TOC values of 1.99 and 1.61 wt. % and HI values of 201 and 195 mg HC/g TOC respectively, indicating borderline oil potential. Some liquid petroleum might therefore have been generated (but not expelled) in the lowermost few meters of the Tschermakfjellet Fm. in the Blanknuten locality, although this is speculative and would not amount to any significant HC volumes.

EOM/TOC ratios of all samples from the Skrukkefjellet (0.07–0.29, median 0.19) and Blanknuten (0.07–0.27, median 0.19) localities indicate that the Botneheia Fm. has generated petroleum in both localities (Peters and Cassa, 1994), in agreement with T_{max} and biomarker parameters from Schou et al. (1984). Bitumen in Botneheia Fm. mudstones from the Blanknuten locality is *in situ* (Abay et al., 2017), and is probably the same in the Skrukkefjellet locality. There is clear evidence of hydrocarbon generation and primary migration in the Blanknuten Mb. in the Blanknuten locality by the intriguing discovery of a late Anisian–Ladinian ammonoid (*Aristoptychites trochleaeformis*) with oil-filled, hollow chambers (Smelror and Sollid, 2007; Thieβen et al., 2019). This evidently illustrates that the Blanknuten Mb. has sufficient source rock quality and richness for primary migrated oil to occur. While such a discovery is inherently rare and has not been encountered in the Skrukkefjellet locality, the similar EOM/TOC ratios compared to the Blanknuten locality (Fig. 15) could be a result of generated petroleum that is retained within the mudstone facies.

5.6. Towards a chemostratigraphic framework through multivariate analysis

The lithology and geochemistry of sediments are genetically related to the depositional environment. Therefore, multivariate analysis of facies-dependent inorganic and/or organic geochemical parameters by principal component analysis (PCA) and hierarchical cluster analysis (HCA) are useful tools in identifying properties (or groups of properties) reflecting depositional environment of lithified sediments, rock extracts, or oils (Garcia et al., 2020; Lerch et al., 2017; Yurchenko et al., 2018). Such chemostratigraphic analyses are typically done using biomarker parameters that are resistant to e.g. thermal maturation and biodegradation (Peters et al., 2007). The presented chemostratigraphic and multivariate analyses in this study therefore differs in the way that it tests whether the qualitative and macroscopically identified mudstone facies F1–F4 can be distinguished based solely on their bulk geochemical assemblages or not.

The chemostratigraphic correlation between the lower–middle Muen Mb. F1 mudstones and the two F1 mudstones from the lower Tschermakfjellet Fm. (Fig. 18, cluster C3) justifies the grouping of these two units into a common facies F1. This supports a similar depositional environment for these samples. Oxygenated conditions are known to preferentially preserve less labile terrestrial organic matter compared to

marine, lipid-rich organic matter (Demaison and Moore, 1980), which could have resulted in the high SAT/ARO ratios. Another explanation could be an overall elevated supply of terrestrial organic matter relative to the other facies types (i.e. F2, F3 or F4).

The single F1 sample in cluster C1 deviates significantly from the other F1 samples mudstones from the Tschermakfjellet Fm. and the lower–middle Muen Mb. (Fig. 18). Similar to the Blanknuten locality, Riis et al. (2008) report dark shales in the lowermost Carnian succession on the shelf east of Edgeøya. These lowermost Carnian shales show upwards decreasing source quality and richness (Xu et al., 2014), likely related to the upwards grading into the deltaic sandstones of the De Geerdalen Fm&tnqh_x02025 The base part of the Tschermakfjellet Fm. in eastern Svalbard and the shelf east of Edgeøya might reflect gradually less reworked upper Botneheia Fm. sediments or continuous sedimentation across the Ladinian–Carnian boundary. The latter was proposed by Høy and Lundschien (2011) to occur in the offshore Northern Norwegian Barents Sea. The Tschermakfjellet Fm. F1 sample of cluster C1 (Fig. 18) might therefore represent a more ventilated and proximal facies that better represents the entire Tschermakfjellet Fm.

The F2 mudstones from the upper Muen Mb. and the lower and upper Blanknuten Mb. are split between the clusters C2 and C4, indicating that the geochemical assemblages of these samples vary considerably (Figs. 17 and 18). However, the matching between the F2 mudstones from the upper Muen Mb. and the lower Blanknuten Mb. indicates that they were deposited during the same late transgressive phase, and that they therefore are genetically related (Krajewski, 2013). Macroscopic allochthonous phosphate nodule layers (Fig. 7a) shows that the F2 mudstones were deposited during hydrodynamically active bottom conditions, and varying compositional variations of these F2 mudstones should be expected (Krajewski, 2008). The correlation with absolute SAT and normalized SAT (%) for the dominant part of the F2 mudstones (Fig. 17) might indicate fairly well-preserved terrestrial organic matter that was provided before and after the deposition of F3 mudstones, which on the other hand show very low contributions of terrestrial organic matter (Krajewski, 2013).

The massive and well-laminated middle Blanknuten Mb. F3 mudstones and their strongly positive PC1 scores (Fig. 17) reflect the greatest absolute bitumen content and TOC among the analyzed facies (Table 2). These geochemical properties demarcate a distinct F3 mudstone group from the remaining sample set (Fig. 17) and provide overall good chemostratigraphic criteria to distinguish this facies. Still, it is evident that geochemical overlap between F2, F3 and F4 takes place as shown in cluster C2 and C4 (Fig. 18). This could be due to episodes of weak oxygenation and hydrodynamic reworking that caused source rock heterogeneity within the F3 mudstones (Krajewski, 2013). However, the organic matter composition is dominantly marine and highly oil prone (Krajewski, 2013), resulting in the specific distribution of normalized bulk bitumen fractions and very low SAT/ARO ratios that are unique for the F3 mudstones (Figs. 14 and 17; Table 2).

Four out of six F4 mudstone samples form a recognizable group based on the PCA (Fig. 17), correlating to the cluster C5 in the HCA (Fig. 18). This distinction from the lower and middle Blanknuten Mb. indicates a change in depositional environment that corresponds to the onset of a regressive phase with increased content of terrestrial organic matter and TIC from bivalve shell fragments (Krajewski, 2013; Mørk and Bromley, 2008). Currently we have no explanation for the elevated normalized polar fraction of the F4 mudstones (Fig. 17), but it may be due to increased sulfurization of saturated and unsaturated hydrocarbons (Tissot and Welte, 1984), which is more common in carbonates compared to siliciclastic mudstones (Jones, 1984). Although not specified in detail, Høy and Lundschien (2011) noted an abrupt change in the chemical conditions in this part of the Botneheia Fm., which could be partly captured by the HCA as cluster C5 (Fig. 18). The TIC content (Figs. 9 and 18) and normalized polar fraction (Figs. 14 and 17) provide the best bulk parameters to distinguish the regressive, calcareous F4 mudstones from F2 and F3 in the lower and middle Blanknuten Mb. respectively.

From the analysis above, the non-phosphogenic (lower–middle Muen Mb.) F1 mudstones and the phosphogenic (upper Muen Mb. to upper Blanknuten Mb.) F2–F4 mudstones are clearly distinguished without detailed analyses of the phosphate content or microfacies descriptions. This is important, because these two successions form principally different source rocks of dominantly kerogen type III/II and II respectively (Krajewski, 2013). In cases with highly fragmented sample material, e.g. when analyzing drill cuttings, textural and structural facies descriptions of mudstones are challenging. The coupling between facies and multivariate analysis may contribute to a lithostratigraphic and chemostratigraphic framework with use in the regional northern Norwegian Barents Shelf.

6. Conclusions

The Middle Triassic Botneheia Fm. in Svalbard represents the onshore counterpart to potentially important regional oil-prone source rocks in the Norwegian part of the Barents Shelf. Despite being one of the most attractive play models, the many disappointing exploration campaigns demonstrate that the Triassic petroleum system is not fully understood. The presence, distribution, richness and quality of the Lower–Middle Triassic organic-rich shales are among the risk factors. Because of the limited amount of core data available for detailed geochemical studies, outcrop investigations of analogue source rock units onshore Svalbard are very important for gaining a comprehensive understanding of their facies development on the Barents Shelf.

The presented investigation of organic-rich mudstone facies of the Botneheia Fm. in eastern Svalbard coupled with high-resolution chemostratigraphy sheds new light on the stratigraphic distribution of TS, TOC, TIC and bulk bitumen content in relation to the changing paleodepositional environments and benthic oxygen conditions. The mudstone facies-transitions forth and back from dark gray (F1) to black (F2 or F4), bioturbated mudstones via black, paper-laminated shale (F3) appears to be closely tied to the relative and absolute abundance of terrestrial vs. marine organic matter. This ratio, as inferred from the TOC and bulk bitumen content, is at a maximum in the Anisian and Carnian F1 mudstones, intermediate in the upper Anisian F2 and upper Ladinian F2 and F4 mudstones, and minimum in the lower Ladinian F3 mudstones. The high marine organic matter content in the F3 mudstones was probably a result of deeper, upwelled and nutrient rich waters that promoted high primary productivity in the photic zone which was subsequently exported to the sediment surface during early Ladinian time. The deposited necromass caused extensive phosphate precipitation within the mudstone matrix and concurrently the development of bottom water oxygen deficiency and TS enrichment. This resulted in less efficient organic matter degradation and therefore preservation of oil-prone kerogen. At this time, terrestrial organic matter and detrital input were at a minimum. The documented facies and chemostratigraphic trends, where the early Ladinian marks a defining turning point, may thus reflect the development of a pan-Arctic Middle Triassic transgressive–regressive sequence identified by previous studies.

This study shows that the non-phosphogenic lower–middle Muen Mb. differs substantially in facies and geochemistry from the phosphogenic mudstones of the upper Muen Mb. and the Blanknuten Mb. The former succession was likely deposited in a ventilated and oxygenated pro-deltaic to open shelf environment, while the latter succession was deposited in a deeper, more restricted dysoxic/anoxic shelf setting. The lack of high productivity and the low preservation potential in the non-phosphogenic lower–middle Muen Mb. are the main factors that promote the clear difference in TOC and bitumen content compared to the phosphogenic upper Muen and entire Blanknuten mbs. The suggested chemostratigraphic approach combined with the mudstone facies analysis could therefore be applied during exploration campaigns when only sidewall cores or cuttings are available to identify these principally different non-phosphogenic and phosphogenic source rock units

respectively.

The exploratory data analyses presented in this study partly distinguish the genetic differences between mudstones that may reflect separable sequence stratigraphic phases within the Middle Triassic Botneheia Fm. We therefore consider the exploratory data analysis as an applicable approach to link the geochemical content and the facies development of the Botneheia Fm. However, it is evident that the presented bulk geochemistry of the phosphogenic F2, F3, and F4 mudstones and their associated lithostratigraphic subunits within this formation overlap, and that the chemostratigraphic framework lacks sufficient resolution to clearly separate these units or facies.

7. Computer code availability

- Name of code: Wesenlund_et_al_2021_MPG.py
- Developer: Fredrik Wesenlund
- Contact details: Fredrik Wesenlund, Department of Geosciences, UiT–The Arctic University of Norway, Tromsø, Norway; email: Fredrik.wesenlund@uit.no; Year first available: 2021
- Hardware used: The Python script was developed and run on a notebook PC with a quad core CPU @ 1.60–2.11 GHz and 16 GB RAM
- Software used and required: The Python script was developed with the Anaconda 2020.11 Python distribution platform using Spyder 4.1.5 and needs the pandas, matplotlib, seaborn, scikit-learn, numpy and plotly (including express and orca) packages
- Program language: the code is written in Python 3.8.5
- Total size of script: c. 30 KB
- Details on how to access the source code: the source file can be downloaded from GitHub: https://github.com/fredrwes/Publications.

Declaration of competing interest

The authors declare that they have no known competing financial interests or personal relationships that could have appeared to influence the work reported in this paper.

Acknowledgments

This study forms part of the ARCEx consortium (Research Centre for Arctic Petroleum Exploration) which is funded by the Research Council of Norway (grant number 228107) and ARCEx partners. We are grateful for additional economic support from Lundin Energy Norway and the Norwegian Petroleum Directorate for the field expedition to Edgeøya. Atle Mørk is thanked for field expedition planning, logistics and great companionship, and the crew at research vessel SS Youexplore by The Dale Oen Experience for safe execution. Sofie Bernhardsen is acknowledged for field assistance and scientific contributions. Trine Dahl, Ingvild Hald and Karina Monsen are thanked for help and discussions in the geology lab at UiT–The Arctic University of Norway. Kristian Backer-Owe and Dag Arild Karlsen are appreciated for permission to use the organic geochemical lab at the University of Oslo, and the Petroleum Research School of Norway (NFiP) are thanked for covering travel expenses. Comments and suggestions by Associate Editor Richard Patience and the anonymous reviewers that helped to improve the manuscript are gratefully acknowledged.

Appendix A. Supplementary data

Supplementary data to this article can be found online at https://doi.org/10.1016/j.marpetgeo.2021.105168.

Credit author statement

Fredrik Wesenlund: Conceptualization, Methodology, Software, Validation, Formal analysis, Investigation, Data Curation, Writing – original draft, Visualization. Sten-Andreas Grundvåg: Investigation, Writing - Review & Editing, Supervision, Project administration, Funding acquisition. Victoria Sjøholt Engelschiøn: Investigation, Data Curation, Validation, Writing - Review & Editing. Olaf Thieβen: Conceptualization, Writing - Review & Editing, Supervision. Jon Halvard Pedersen: Conceptualization, Writing - Review & Editing, Supervision.

References

Abay, T.B., Karlsen, D.A., Pedersen, J.H., 2014. Source rocks at Svalbard: an overview of Jurassic and Triassic formations and comparison with offshore Barents Sea time equivalent source rock formations. AAPG Datapages Search and Discovery, 30372. https://www.searchanddiscovery.com/documents/2014/30372abay/ndx_abay.pdf.

Abay, T.B., Karlsen, D.A., Lerch, B., Olaussen, S., Pedersen, J.H., Backer-Owe, K., 2017. Migrated petroleum in outcropping Mesozoic sedimentary rocks in Spitsbergen: organic geochemical characterization and implications for regional exploration. J. Petrol. Geol. 40, 5–36.

Abay, T.B., Karlsen, D.A., Pedersen, J.H., Olaussen, S., Backer-Owe, K., 2018. Thermal maturity, hydrocarbon potential and kerogen type of some Triassic–Lower Cretaceous sediments from the SW Barents Sea and Svalbard. Petrol. Geosci. 24, 349–373.

Abdullah, W.H., 1999. Organic facies variations in the Triassic shallow marine and deep marine shales of central Spitsbergen, Svalbard. Mar. Petrol. Geol. 16, 467–481.

Alsen, P., McRoberts, C., Svennevig, K., Bojesen-Koefoed, J., Hovikoski, J., Piasecki, S., 2017. The Isrand Formation: a Middle Triassic Daonella-bearing, black shale unit in Kilen, North Greenland (with a note on the Triassic in Amdrup Land). Newsl. Stratigr. 50, 31–46.

Alsenz, H., Illner, P., Ashckenazi-Polivoda, S., Meilijson, A., Abramovich, S., Feinstein, S., Almogi-Labin, A., Berner, Z., Püttmann, W., 2015. Geochemical evidence for the link between sulfate reduction, sulfide oxidation and phosphate accumulation in a Late Cretaceous upwelling system. Geochem. Trans. 16, 13.

Anell, I., Braathen, A., Olaussen, S., Osmundsen, P.T., 2013. Evidence of faulting contradicts a quiescent northern Barents Shelf during the Triassic. First Break 31, 67–76.

Anell, I., Zuchuat, V., Röhnert, A.D., Smyrak-Sikora, A., Buckley, S., Lord, G., Maher, H., Midtkandal, I., Ogata, K., Olaussen, S., Osmundsen, P.T., Braathen, A., 2020. Tidal amplification and along-strike process variability in a mixed-energy paralic system prograding onto a low accommodation shelf, Edgeøya, Svalbard. Basin Res. 33, 478–512.

Arthur, M.A., Sageman, B.B., 1994. Marine black shales - depositional mechanisms and environments of ancient deposits. Annu. Rev. Earth Planet Sci. 22, 499–551.

Berner, R.A., Raiswell, R., 1983. Burial of organic-carbon and pyrite sulfur in sediments over phanerozoic time - a new theory. Geochem. Cosmochim. Acta 47, 855–862.

Bernhardsen, S., 2019. A sedimentological study of the organic-rich Botneheia Formation (Middle Triassic) with emphasis on the ichnogenus Thalassinoides, Edgeøya, Svalbard. MSc thesis. Norwegian University of Science and Technology (NTNU), Trondheim, Norway, p. 142.

Bhullar, A.G., Karlsen, D.A., Backer-Owe, K., Le Tran, K., Skalnes, E., Berchelmann, H.H., Kittelsen, J.E., 2000. Reservoir characterization by a combined micro-extraction - micro thin-layer chromatography (Iatroscan) method: a calibration study with examples from the Norwegian North Sea. J. Petrol. Geol. 23, 221–244.

Bjerager, M., Alsen, P., Hovikoski, J., Lindstrom, S., Pilgaard, A., Stemmerik, L., Therkelsen, J., 2019. Triassic lithostratigraphy of the Wandel Sea Basin, North Greenland. Bull. Geol. Soc. Den. 67, 83–105.

Bjorøy, M., Hall, P.B., Ferriday, I.L., Mørk, A., 2009. Triassic Source Rocks of the Barents Sea and Svalbard. AAPG Datapages Search and Discovery, 10219. https://www.searchanddiscovery.com/documents/2009/10219bjoroy/ndx_bjoroy.pdf.

Brekke, T., Krajewski, K.P., Hubred, J.H., 2014. Organic geochemistry and petrography of thermally altered sections of the Middle Triassic Botneheia Formation on south-western Edgeøya, Svalbard. Norwegian Petroleum Directorate Bulletin 11, 111–128.

Bromley, R.G., Ekdale, A.A., 1984. *Chondrites*: a trace fossil indicator of anoxia in sediments. Science 224, 872–874.

Braathen, A., Baelum, K., Christiansen, H.H., Dahl, T., Eiken, O., Elvebakk, H., Hansen, F., Hanssen, T.H., Jochmann, M., Johansen, T.A., Johnsen, H., Larsen, L., Lie, T., Mertes, J., Mørk, A., Mørk, M.B., Nemec, W., Olaussen, S., Oye, V., Rod, K., Titlestad, G.O., Tveranger, J., Vagle, K., 2012. The Longyearbyen CO2 Lab of Svalbard, Norway-initial assessment of the geological conditions for CO2 sequestration. Norw. J. Geol. 92, 353–376.

Buckley, S.J., Ringdal, K., Naumann, N., Dolva, B., Kurz, T.H., Howell, J.A., Dewez, T.J. B., 2019. LIME: software for 3-D visualization, interpretation, and communication of virtual geoscience models. Geosphere 15, 222–235.

Byers, C.W., 1974. Shale fissility - relation to bioturbation. Sedimentology 21, 479–484.

Clayton, J.L., Swetland, P.J., 1978. Subaerial weathering of sedimentary organic-matter. Geochem. Cosmochim. Acta 42, 305–312.

Creaney, S., Passey, Q.R., 1993. Recurring patterns of total organic carbon and source rock quality within a sequence stratigraphic framework. AAPG (Am. Assoc. Pet. Geol.) Bull. 77, 386–401.

Dallmann, W.K., Elvevold, S., 2015. Bedrock geology. In: Dallmann, W. (Ed.), Geoscience Atlas of Svalbard. Norwegian Polar Institute.

Demaison, G.J., Moore, G.T., 1980. Anoxic environments and oil source bed genesis. AAPG (Am. Assoc. Pet. Geol.) Bull. 64, 1179–1209.

Demaison, G.J., Huizinga, B.J., 1991. Genetic classification of petroleum systems. AAPG (Am. Assoc. Pet. Geol.) Bull. 75, 1626–1643.
Dembicki, J.H., 2009. Three common source rock evaluation errors made by geologists during prospect or play appraisals. AAPG (Am. Assoc. Pet. Geol.) Bull. 93, 341–356.
Dembicki, J.H., 2017. Source rock evaluation. In: Dembicki, J.H. (Ed.), Practical Petroleum Geochemistry for Exploration and Production. Elsevier, pp. 61–133.
England, W.A., Mackenzie, A.S., 1989. Some aspects of the organic geochemistry of petroleum fluids. Geol. Rundsch. 78, 291–303.
Faleide, J.I., Gudlaugsson, S.T., Jacquart, G., 1984. Evolution of the western Barents Sea. Mar. Petrol. Geol. 1, 123–150.
Faleide, J.I., Bjørlykke, K., Gabrielsen, R.H., 2015. Geology of the Norwegian continental shelf. In: Bjørlykke, K. (Ed.), Petroleum Geoscience: from Sedimentary Environments to Rock Physics. Springer Berlin Heidelberg, Berlin, Heidelberg, pp. 603–637.
Filippelli, G.M., 2011. Phosphate rock formation and marine phosphorus geochemistry: the deep time perspective. Chemosphere 84, 759–766.
Forsberg, A., Bjorøy, M., 1983. A sedimentological and organic geochemical study of the Botneheia Formation, Svalbard, with special emphasis on the effects of weathering on the organic matter in shales. In: Bjorøy, M., Albrecht, P., Cornford, C., others (Eds.), Advances in Organic Geochemistry 1981. Wiley, Chichester, pp. 60–68.
Garcia, R.J.L., da Silva, J.B., Abreu, I.M., Soares, S.A.R., Araujo, R.G.O., de Souza, E.S., Ribeiro, H.J.S., Hadlich, G.M., Queiroz, A.F.D., 2020. Application of PCA and HCA in geochemical parameters to distinguish depositional paleoenvironments from source rocks. J. S. Am. Earth Sci. 103.
Ghadeer, S.G., Macquaker, J.H.S., 2012. The role of event beds in the preservation of organic carbon in fine-grained sediments: analyses of the sedimentological processes operating during deposition of the Whitby Mudstone Formation (Toarcian, Lower Jurassic) preserved in northeast England. Mar. Petrol. Geol. 35, 309–320.
Ghassal, B.I., Littke, R., El Atfy, H., Sindern, S., Scholtysik, G., El Beialy, S., El Khoriby, E., 2018. Source rock potential and depositional environment of Upper Cretaceous sedimentary rocks, Abu Gharadig Basin, Western Desert, Egypt: an integrated palynological, organic and inorganic geochemical study. Int. J. Coal Geol. 186, 14–40.
Glørstad-Clark, E., Faleide, J.I., Lundschien, B.A., Nystuen, J.P., 2010. Triassic seismic sequence stratigraphy and paleogeography of the western Barents Sea area. Mar. Petrol. Geol. 27, 1448–1475.
Glørstad-Clark, E., Birkeland, E.P., Nystuen, J.P., Faleide, J.I., Midtkandal, I., 2011. Triassic platform-margin deltas in the western Barents Sea. Mar. Petrol. Geol. 28, 1294–1314.
Haile, B.G., Klausen, T.G., Jahren, J., Braathen, A., Hellevang, H., 2018. Thermal history of a Triassic sedimentary sequence verified by a multi-method approach: Edgeøya, Svalbard, Norway. Basin Res. 30, 1075–1097.
Haremo, P., Andresen, A., Dypvik, H., Nagy, J., Elverhøi, A., Eikeland, T.A., Johansen, H., 1990. Structural development along the Billefjorden Fault Zone in the area between Kjellströmdalen and Adventdalen/Sassendalen, central Spitsbergen. Polar Res. 8, 195–216.
Henriksen, E., Bjørnseth, H.M., Hals, T.K., Heide, T., Kiryukhina, T., Kløvjan, O.S., Larssen, G.B., Ryseth, A.E., Rønning, K., Sollid, K., Stoupakova, A., 2011. Uplift and erosion of the greater Barents Sea: impact on prospectivity and petroleum systems. In: Spencer, A.M., Embry, A.F., Gautier, D.L., Stoupakova, A.V., Sørensen, K. (Eds.), Arctic Petroleum Geology. The Geological Society of London, pp. 271–281.
Hounslow, M.W., Hu, M.Y., Mørk, A., Weitschat, W., Vigran, J.O., Karloukovski, V., Orchard, M.J., 2008. Intercalibration of Boreal and Tethyan time scales: the magnetobiostratigraphy of the Middle Triassic and the latest Early Triassic from Spitsbergen, Arctic Norway. Polar Res. 27, 469–490.
Hubred, J.H., 2006. Thermal effects of basaltic sill emplacement in source rocks on maturation and hydrocarbon generation. Department of Geosciences, University of Oslo, Oslo, Norway. Cand. Scient. thesis.
Høy, T., Lundschien, B.A., 2011. Triassic deltaic sequences in the northern Barents Sea. In: Spencer, A.M., Embry, A.F., Gautier, D.L., Stoupakova, A.V., Sørensen, K. (Eds.), Arctic Petroleum Geology. The Geological Society of London, pp. 249–260.
Ineson, J.R., Hovikoski, J., Sheldon, E., Piasecki, S., Alsen, P., Fyhn, M.B.W., Bjerager, M., Dybkjaer, K., Guarnieri, P., Lauridsen, B.W., Nohr-Hansen, H., Pedersen, G.K., Svennevig, K., Therkelsen, J., Weibel, R., Bojesen-Koefoed, J.A., 2021. Regional impact of Early Cretaceous tectono-magmatic uplift in the Arctic: implications of new data from eastern North Greenland, 33. Terra Nova, pp. 284–292.
Jones, R.W., 1984. Comparison of carbonate and shale source rocks. In: Palacas, J.G. (Ed.), Petroleum Geochemistry and Source Rock Potential of Carbonate Rocks. American Association of Petroleum Geologists.
Karlsen, D.A., Larter, S.R., 1991. Analysis of petroleum fractions by TLC-FID - applications to petroleum reservoir description. Org. Geochem. 17, 603–617.
Klausen, T.G., 2013. Does evidence of faulting contradict a quiescent northern Barents Shelf during the Triassic? First Break 31, 69–72.
Klausen, T.G., Ryseth, A.E., Helland-Hansen, W., Gawthorpe, R., Laursen, I., 2015. Regional development and sequence stratigraphy of the Middle to Late Triassic Snadd Formation, Norwegian Barents Sea. Mar. Petrol. Geol. 62, 102–122.
Klausen, T.G., Nyberg, B., Helland-Hansen, W., 2019. The largest delta plain in Earth's history. Geology 47, 470–474.
Krajewski, K.P., 2008. The Botneheia Formation (Middle Triassic) in Edgeøya and Barentsøya, Svalbard: lithostratigraphy, facies, phosphogenesis, paleoenvironment. Pol. Polar Res. 29, 319–364.
Krajewski, K.P., 2013. Organic matter–apatite–pyrite relationships in the Botneheia Formation (Middle Triassic) of eastern Svalbard: relevance to the formation of petroleum source rocks in the NW Barents Sea shelf. Mar. Petrol. Geol. 45, 69–105.
Krajewski, K.P., Weitschat, W., 2015. Depositional history of the youngest strata of the Sassendalen Group (Bravaisberget Formation, Middle Triassic–Carnian) in southern Spitsbergen, Svalbard. Ann. Soc. Geol. Pol. 85, 151–175.
Law, C.A., 1999. Evaluating source rocks. In: Beaumont, E.A., Foster, N.H. (Eds.), Exploring for Oil and Gas Traps, 1 ed. AAPG, pp. 1–41.
Le Tran, K., Philippe, B., 1993. Oil and rock extract analysis. In: Bordenave, M.L. (Ed.), Applied Petroleum Geochemistry. Editions Technip, pp. 376–394.
Leith, T.L., Weiss, H.M., Mørk, A., Århus, N., Elvebakk, G., Embry, A.F., Brooks, P.W., Stewart, K.R., Pchelina, T.M., Bro, E.G., Verba, M.L., Danyushevskaya, A., Borisov, A.V., 1992. Mesozoic hydrocarbon source rocks of the Arctic region. In: Vorren, T.O., Bergsager, E., Dahl-Stamnes, A., Holter, E., Johansen, Å., Lie, Å., Lund, T.B. (Eds.), Arctic Geology and Petroleum Potential. Elsevier, Amsterdam, pp. 1–25.
Lerch, B., Karlsen, D.A., Abay, T.B., Duggan, D., Seland, R., Backer-Owe, K., 2016. Regional petroleum alteration trends in Barents Sea oils and condensates as a clue to migration regimes and processes. AAPG (Am. Assoc. Pet. Geol.) Bull. 100, 165–190.
Lerch, B., Karlsen, D.A., Seland, R., Backer-Owe, K., 2017. Depositional environment and age determination of oils and condensates from the Barents Sea. Petrol. Geosci. 23, 190–209.
Lerch, B., Karlsen, D.A., Thiessen, O., Abay, T.B., van Soelen, E.E., Kurschner, W.M., Planke, S., Backer-Owe, K., 2018. Investigations on the use of triaromatic dimethylcholesteroids as age-specific biomarkers in bitumens and oils from Arctic Norway. Org. Geochem. 122, 1–16.
Leventhal, J.S., 1995. Carbon-sulfur plots to show diagenetic and epigenetic sulfidation in sediments. Geochem. Cosmochim. Acta 59, 1207–1211.
Lord, G.S., Johansen, S.K., Støen, S.J., Mørk, A., 2017. Facies development of the Upper Triassic succession on Barentsøya, Wilhelmøya and NE Spitsbergen, Svalbard. Norw. J. Geol. 97, 33–62.
Lundschien, B.A., Høy, T., Mørk, A., 2014. Triassic hydrocarbon potential in the Northern Barents Sea; integrating Svalbard and stratigraphic core data. Norwegian Petroleum Directorate Bulletin 11, 3–20.
MacEachern, J.A., Pemberton, S.G., Bann, K.L., Gingras, M.K., 2009. Departures from the archetypal ichnofacies: effective recognition of physico-chemical stresses in the rock record. In: MacEachern, J.A., Bann, K.L., Gingras, M.K., Pemberton, S.G. (Eds.), Applied Ichnology. SEPM Society for Sedimentary Geology, Tulsa, Oklahoma, USA, pp. 64–94.
Maher, H.D., Hays, T., Shuster, R., Mutrux, J., 2004. Petrography of Lower Cretaceous sandstones on Spitsbergen. Polar Res. 23, 147–165.
Marshall, C., Uguna, J., Large, D.J., Meredith, W., Jochmann, M., Friis, B., Vane, C., Spiro, B.F., Snape, C.E., Orheim, A., 2015. Geochemistry and petrology of Palaeocene coals from Spitzbergen — Part 2: Maturity variations and implications for local and regional burial models. Int. J. Coal Geol. 143, 1–10.
Marynowski, L., Kurkiewicz, S., Rakocinski, M., Simoneit, B.R.T., 2011. Effects of weathering on organic matter: I. Changes in molecular composition of extractable organic compounds caused by paleoweathering of a Lower Carboniferous (Tournaisian) marine black shale. Chem. Geol. 285, 144–156.
Matapour, Z., Karlsen, D.A., Lerch, B., Backer-Owe, K., 2019. Petroleum occurrences in the carbonate lithologies of the Gohta and Alta discoveries in the Barents Sea, Arctic Norway. Petrol. Geosci. 25, 50–70.
Morse, J.W., Emeis, K.C., 1990. Controls on C/S ratios in hemipelagic upwelling sediments. Am. J. Sci. 290, 1117–1135.
Mueller, S., Veld, H., Nagy, J., Kürschner, W.M., 2014. Depositional history of the Upper Triassic Kapp Toscana Group on Svalbard, Norway, inferred from palynofacies analysis and organic geochemistry. Sediment. Geol. 310, 16–29.
Muller, R., Klausen, T.G., Faleide, J.I., Olaussen, S., Eide, C.H., Suslova, A., 2019. Linking regional unconformities in the Barents Sea to compression-induced forebulge uplift at the Triassic-Jurassic transition. Tectonophysics 765, 35–51.
Mørk, A., Knarud, R., Worsley, D., 1982. Depositional and diagenetic environments of the Triassic and Lower Jurassic succession of Svalbard. In: Embry, A.F., Balkwill, H.R. (Eds.), Arctic Geology and Geophysics: Proceedings of the Third International Symposium on Arctic Geology, vol. 8. Canadian Society of Petroleum Geologists Memoir, pp. 371–398.
Mørk, A., Bjorøy, M., 1984. Mesozoic source rocks on Svalbard. In: Spencer, A.M. (Ed.), Proceedings of the North European Margin Symposium (NEMS '83), Organized by the Norwegian Petroleum Society and Held at the Norwegian Institute of Technology (NTH) in Trondheim 9–11 May. Springer Netherlands, pp. 371–382.
Mørk, A., Embry, A., Weitschat, W., 1989. Triassic transgressive-regressive cycles in the Sverdrup Basin, Svalbard and the Barents shelf. In: Collinson, J. (Ed.), Correlation in Hydrocarbon Exploration. Graham and Trotman, Bergen, Norway, pp. 113–130.
Mørk, A., Dallmann, W.K., Dypvik, H., Johannessen, E.P., Larssen, G.B., Nagy, J., Nøttvedt, A., Olaussen, S., Pčelina, T.M., Worsley, D., 1999. Mesozoic lithostratigraphy. In: Dallmann, W.K. (Ed.), Lithostratigraphic Lexicon of Svalbard. Norwegian Polar Institute, pp. 127–214.
Mørk, A., Elvebakk, G., 1999. Lithological description of subcropping Lower and Middle Triassic rocks from the Svalis Dome, Barents Sea. Polar Res. 18, 83–104.
Mørk, A., Bromley, R.G., 2008. Ichnology of a marine regressive systems tract: the Middle Triassic of Svalbard. Polar Res. 27, 339–359.
Mørk, A., 2015. Historical geology. In: Dallmann, W. (Ed.), Geoscience Atlas of Svalbard. Norwegian Polar Institute.
Norwegian Petroleum Directorate, 2017. Geological assessment of petroleum resources in eastern parts of Barents Sea north 2017. Norwegian Petroleum Directorate.
Norwegian Petroleum Directorate, 2020. Factpages. Norwegian Petroleum Directorate. http://factpages.npd.no/factpages/. (Accessed 20 November 2020).
Norwegian Polar Institute, 2020. Map view of Skrukkefjellet. Norwegian Polar Institute. https://toposvalbard.npolar.no/. (Accessed 20 November 2020).

Ogata, K., Mulrooney, M.J., Braathen, A., Maher, H., Osmundsen, P.T., Anell, I., Smyrak-Sikora, A.A., Balsamo, F., 2018. Architecture, deformation style and petrophysical properties of growth fault systems: the Late Triassic deltaic succession of southern Edgeøya (East Svalbard). Basin Res. 30, 1042–1073.

Ohm, S.E., Karlsen, D.A., Austin, T.J.F., 2008. Geochemically driven exploration models in uplifted areas: examples from the Norwegian Barents Sea. AAPG (Am. Assoc. Pet. Geol.) Bull. 92, 1191–1223.

Osmundsen, P.T., Braathen, A., Rød, R.S., Hynne, I.B., 2014. Styles of normal faulting and fault-controlled sedimentation in the Triassic deposits of Eastern Svalbard. Norwegian Petroleum Directorate Bulletin 11, 61–79.

Othman, R.S., 2004. Relationships between Rock-Eval S1 and extractable organic matter for selected source rock samples from New South Wales. 21th Annual Meeting of the Society for Organic Petrology, Sydney, New South Wales, Australia. https://archives.datapages.com/data/tsop/TSOPv21_2004/othman02.pdf.

Paterson, N.W., Mangerud, G., Mørk, A., 2017. Late Triassic (early Carnian) palynology of shallow stratigraphical core 7830/5-U-1, offshore Kong Karls Land. Norwegian Arctic. Palynology 41, 230–254.

Pedersen, T.F., Calvert, S.E., 1990. Anoxia vs productivity - what controls the formation of organic-carbon-rich sediments and sedimentary-rocks. AAPG (Am. Assoc. Pet. Geol.) Bull. 74, 454–466.

Peters, K.E., Cassa, M.R., 1994. Applied source rock geochemistry. In: Magoon, L.B., Dow, W.G. (Eds.), The Petroleum System - from Source to Trap. AAPG, pp. 93–120.

Peters, K.E., Walters, C.C., Moldowan, J.M., 2005. Biomarkers and Isotopes in Petroleum Systems and Earth History, the Biomarker Guide, 2 ed. Cambridge University Press.

Peters, K.E., Ramos, L.S., Zumberge, J.E., Valin, Z.C., Scotese, C.R., Gautier, D.L., 2007. Circum-Arctic petroleum systems identified using decision-tree chemometrics. AAPG (Am. Assoc. Pet. Geol.) Bull. 91, 877–913.

Potter, P.E., Maynard, J.B., Depetris, P.J., 2005. Mud and Mudstones. Springer-Verlag Berlin Heidelberg.

Redelius, P., Soenen, H., 2015. Relation between bitumen chemistry and performance. Fuel 140, 34–43.

Riis, F., Lundschien, B.A., Høy, T., Mørk, A., Mørk, M.B.E., 2008. Evolution of the Triassic shelf in the northern Barents Sea region. Polar Res. 27, 318–338.

Rodrigues Duran, E., di Primio, R., Anka, Z., Stoddart, D., Horsfield, B., 2013a. Petroleum system analysis of the Hammerfest Basin (southwestern Barents Sea): comparison of basin modelling and geochemical data. Org. Geochem. 63, 105–121.

Rodrigues Duran, E., di Primio, R., Anka, Z., Stoddart, D., Horsfield, B., 2013b. 3D-basin modelling of the Hammerfest Basin (southwestern Barents Sea): a quantitative assessment of petroleum generation, migration and leakage. Mar. Petrol. Geol. 45, 281–303.

Ruttenberg, K.C., Goni, M.A., 1997. Phosphorus distribution, C:N:P ratios, and $\delta^{13}C$(oc) in arctic, temperate, and tropical coastal sediments: tools for characterizing bulk sedimentary organic matter. Mar. Geol. 139, 123–145.

Schatz, W., 2005. Palaeoecology of the Triassic black shale bivalve Daonella—new insights into an old controversy. Palaeogeogr. Palaeoclimatol. Palaeoecol. 216, 189–201.

Schieber, J., 2016. Mud re-distribution in epicontinental basins - exploring likely processes. Mar. Petrol. Geol. 71, 119–133.

Schou, L., Mørk, A., Bjorøy, M., 1984. Correlation of source rocks and migrated hydrocarbons by GC-MS in the Middle Triassic of Svalbard. Org. Geochem. 6, 513–520.

Senger, K., Tveranger, J., Ogata, K., Braathen, A., Planke, S., 2014. Late mesozoic magmatism in svalbard: a review. Earth Sci. Rev. 139, 123–144.

Smelror, M., Sollid, K., 2007. Blekkspruter fulle av olje. GEO 2, 28–29.

Smolarek, J., Marynowski, L., Trela, W., Kujawski, P., Simoneit, B.R.T., 2017. Redox conditions and marine microbial community changes during the end-Ordovician mass extinction event. Global Planet. Change 149, 105–122.

Smyrak-Sikora, A., Osmundsen, P.T., Braathen, A., Ogata, K., Anell, I., Mulrooney, M.J., Zuchuat, V., 2019. Architecture of growth basins in a tidally influenced, prodelta to delta-front setting: the Triassic succession of Kvalpynten, East Svalbard. Basin Res. 32, 949–978.

Stueland, E., 2016. Wisting – shallow reservoir. Possibilities and challenges. FORCE Underexplored Plays II, Stavanger, Norway. https://www.npd.no/globalassets/2-force/2019/documents/archive-2010-2018/underexplored-plays–part-ii/wisting—force-edited_underexplored-plays-ii-omv_v2_eirikstueland.pdf.

Thießen, O., Weiss, H.M., Smelror, M., Sollid, K., 2019. Triassic oil from the Botneheia Formation of Svalbard and oil-oil Correlation with recent Norwegian Barents Sea discoveries, 29th International Meeting on Organic Geochemistry. European Association of Organic Geochemists, Gothenburg, Sweden.

Tissot, B.P., Welte, D.H., 1984. Geological Control of Petroleum Type, Petroleum Formation and Occurrence, 2 ed. Springer-Verlag, Berlin, Germany, p. 699.

Traykovski, P., Geyer, W.R., Irish, J.D., Lynch, J.F., 2000. The role of wave-induced density-driven fluid mud flows for cross-shelf transport on the Eel River continental shelf. Continent. Shelf Res. 20, 2113–2140.

Vigran, J.O., Mangerud, G., Mørk, A., Bugge, T., Weitschat, W., 1998. Biostratigraphy and sequence stratigraphy of the Lower and Middle Triassic deposits from the Svalis Dome, central Barents Sea, Norway. Palynology 22, 89–141.

Vigran, J.O., Mørk, A., Forsberg, A.W., Weiss, H.M., Weitschat, W., 2008. Tasmanites algae—contributors to the Middle Triassic hydrocarbon source rocks of Svalbard and the Barents shelf. Polar Res. 27, 360–371.

Vigran, J.O., Mangerud, G., Mørk, A., Worsley, D., Hochuli, P.A., 2014. Palynology and geology of the Triassic succession of Svalbard and the Barents Sea. Geological Survey of Norway Special Publication 14.

Vossler, S.M., Pemberton, S.G., 1988. *Skolithos* in the Upper Cretaceous Cardium Formation: an ichnofossil example of opportunistic ecology. Lethaia 21, 351–362.

Wang, Y.-P., Zou, Y.-R., Shi, J.-T., Shi, J., 2018. Review of the chemometrics application in oil-oil and oil-source rock correlations. Journal of Natural Gas Geoscience 3, 217–232.

Waples, D.W., Curiale, J.A., 1999. Oil–oil and oil–source rock correlations. In: Beaumont, E.A., Foster, N.H. (Eds.), Exploring for Oil and Gas Traps. AAPG.

Weiss, H.M., Wilhelms, A., Mills, N., Scotchmer, J., Hall, P.B., Lind, K., Brekke, T., 2000. NIGOGA - The Norwegian Industry Guide to Organic Geochemical Analyses, 4th. Norsk Hydro, Statoil, Geolab Nor, SINTEF Petroleum Research and the Norwegian Petroleum Directorate.

Whittaker, A., Morton-Thompson, D., 1992. Mudlogging: drill cuttings analysis. In: Morton-Thompson, D., Woods, A.M. (Eds.), Development Geology Reference Manual. AAPG, Tulsa, Oklahoma, USA, pp. 104–105.

Wignall, P.B., 1991. Dysaerobic trace fossils and ichnofabrics in the Upper Jurassic Kimmeridge Clay of southern England. Palaios 6, 264–270.

Wilson, R.D., Schieber, J., 2014. Muddy prodeltaic hyperpycnites in the Lower Genesee Group of central New York, USA: implications for mud transport in epicontinental seas. J. Sediment. Res. 84, 866–874.

Wong, B., 2011. Color blindness. Nat. Methods 8, 441.

Xu, G.P., Hannah, J.L., Bingen, B., Georgiev, S., Stein, H.J., 2012. Digestion methods for trace element measurements in shales: paleoredox proxies examined. Chem. Geol. 324, 132–147.

Xu, G., Hannah, J.L., Stein, H.J., Mørk, A., Vigran, J.O., Bingen, B., Schutt, D.L., Lundschien, B.A., 2014. Cause of Upper Triassic climate crisis revealed by Re–Os geochemistry of Boreal black shales. Palaeogeogr. Palaeoclimatol. Palaeoecol. 395, 222–232.

Yurchenko, I.A., Moldowan, J.M., Peters, K.E., Magoon, L.B., Graham, S.A., 2018. The role of calcareous and shaly source rocks in the composition of petroleum expelled from the Triassic Shublik Formation, Alaska North Slope. Org. Geochem. 122, 52–67.

5

Paper II

Multi-elemental chemostratigraphy of Triassic mudstones in eastern Svalbard: implications for source rock formation in front of the World's largest delta plain

*Fredrik Wesenlund[1], Sten-Andreas Grundvåg[1], Victoria Sjøholt Engelschiøn[2], Olaf Thießen[3], Jon Halvard Pedersen[4]

[1]Department of Geosciences, UiT The Arctic University of Norway, Tromsø, Norway

[2]The Natural History Museum, University of Oslo, Norway

[3]Equinor ASA, Harstad, Norway

[4]Lundin Energy Norway, Lysaker, Norway

*Corresponding author. E-mail: `fredrik.wesenlund@uit.no`

Note: The manuscript below is the accepted version of the paper now currently undergoing copyediting in *The Depositional Record*. Appendix A is provided in this manuscript, while Appendices B and C consisting of tabulated data will be available on the article webpage after publication. The accepted manuscript is formatted to the LaTeX style of this dissertation. The full references to the included citations are available in the reference list (Chapter 8).

Abstract

The Triassic Boreal Ocean was a shallow epicontinental basin and the sink of the World's largest delta plain known to date. Nutrient and freshwater supply from this delta plain have been considered as important causes for high marine productivity and water mass stratification, forming Middle Triassic oil-prone source rocks. Recent studies of these source rocks attribute marine upwelling and a productivity-induced oxygen minimum zone as important factors. A multi-elemental chemostratigraphic study of a Spathian–Carnian marine mudstone succession exposed on Edgeøya, eastern Svalbard was performed to investigate their formation. This includes 89 samples from three localities. In total, 34 elements ranging from carbon to uranium were acquired using combustion and X-ray fluorescence analyses. The goal is to provide a correlation framework and infer the role of primary productivity, benthic redox and water mass restriction on organic matter accumulation and source rock formation. The Spathian Vendomdalen Member suggests deposition during intermittent euxinic bottom waters and low productivity, corresponding with a reported deep thermocline in the Triassic Boreal Ocean that obstructed upwelling and nutrient supply. The lower Anisian lower–middle Muen Member shows negligible enrichment in redox-sensitive elements but in situ phosphate-nodules, consistent with a change towards enhanced upwelling and moderate primary productivity. High productivity and intense phosphogenesis took place first in the middle Anisian upper Muen Member and are linked with basin-wide upwelling. Productivity, phosphate, and redox proxies are strongly elevated and correlated in the overlying upper Anisian–Ladinian Blanknuten Member. In the southern Barents Sea, the pro-deltaic environment of the emerging Triassic Boreal Ocean delta system (Ladinian–Carnian Snadd Formation) had terminated these conditions. The regressive upper Ladinian upper Blanknuten Member returned to intermittent benthic euxinia due to the shallowing sea level. The Carnian Tschermakfjellet Formation (Snadd Formation facies equivalent) exemplifies the dominance of the prograding Triassic Boreal Ocean delta system, terminating the conditions for oil-prone source rock formation in the Svalbard area.

5.1 Introduction

To identify organic-rich mudstones with source rock potential and elucidate their constituent organic facies types is a principal task in any petroleum system analysis (Magoon and Dow, 1994). The depositional environment is considered a primary control on organic facies type and abundance, and thus ultimately influences the organic composition of source rocks and their resulting generation potential (England and Mackenzie, 1989; Tissot and Welte, 1984;

Tyson, 1995). Elevated primary productivity (e.g., Pedersen and Calvert, 1990), oxygen depletion and organic matter (OM) preservation (e.g., Demaison and Moore, 1980), and sedimentation rate affecting OM concentration by dilution or condensation (e.g., Creaney and Passey, 1993) are considered the most influential on OM accumulation and source rock formation (Bohacs et al., 2005; Katz, 2005). These processes form complex feedback loops, and it is challenging to determine if oxygen deficiency was caused by intense primary productivity demanding the available oxygen in the water mass, or whether the physiographic conditions in the basin resulted in water mass restriction and limited bottom water oxygenation (Katz, 2005).

Marine mudstones are commonly enriched in elements that change oxidation state and solubility depending on the benthic palaeoredox conditions (Calvert and Pedersen, 2007; Jones and Manning, 1994; Morford and Emerson, 1999; Tribovillard et al., 2006). Some elements may also precipitate in the sediments by decaying necromass and provide nutrients (Goldberg and Arrhenius, 1958; Schoepfer et al., 2015; Zhao et al., 2016). Marine mudstones may therefore represent element sinks that reflect palaeoredox and palaeoproductivity conditions in a basin (Ferriday and Montenari, 2016). The recognition of unique elemental assemblages and the application of elemental chemostratigraphy have proven useful to characterise mudstone successions and discern internal boundaries (Eisenberg and Harris, 1995; Qin et al., 1985). The technique has successfully been applied to investigate climate fluctuations (e.g., Grabowski et al., 2021), weathering and erosion rates (e.g., Ramirez-Montoya et al., 2021), changing palaeoredox conditions (e.g., Hammer et al., 2019), primary palaeoproductivity (e.g., Borchers et al., 2005), ancient water-mass chemistry (e.g., Algeo and Maynard, 2008), and sequence stratigraphic development of fine-grained successions (e.g., LaGrange et al., 2020; Thöle et al., 2019).

The fine granularity of mudstones often hampers sedimentological characterisation in outcrops (Potter et al., 2005). Thin sections or high-quality cores provide the best opportunities to investigate mudstones and to recognise both sedimentary and organic facies variations (Percy and Pedersen, 2020; Zuchuat et al., 2020). However, mudstone successions are rarely cored during wellsite operations and source rock studies are thus commonly based on drill cuttings (e.g., Mansour et al., 2020; Rosenberg et al., 2021; Silva et al., 2017). While drilling mud contamination may pose a serious issue for organic geochemical characterisation of cuttings (Sanei et al., 2020), its influence on the elemental assemblage is generally negligible (Craigie, 2018). Elemental studies of drill cuttings have been shown to be highly useful in mapping chemostratigraphic zones (Craigie, 2015; Wright et al., 2010) and for multilateral well steering of shale plays (Hildred et al., 2011; Hildred, 2012; Zhang et al., 2019).

Elemental chemostratigraphy is not without limitations. For instance, it has

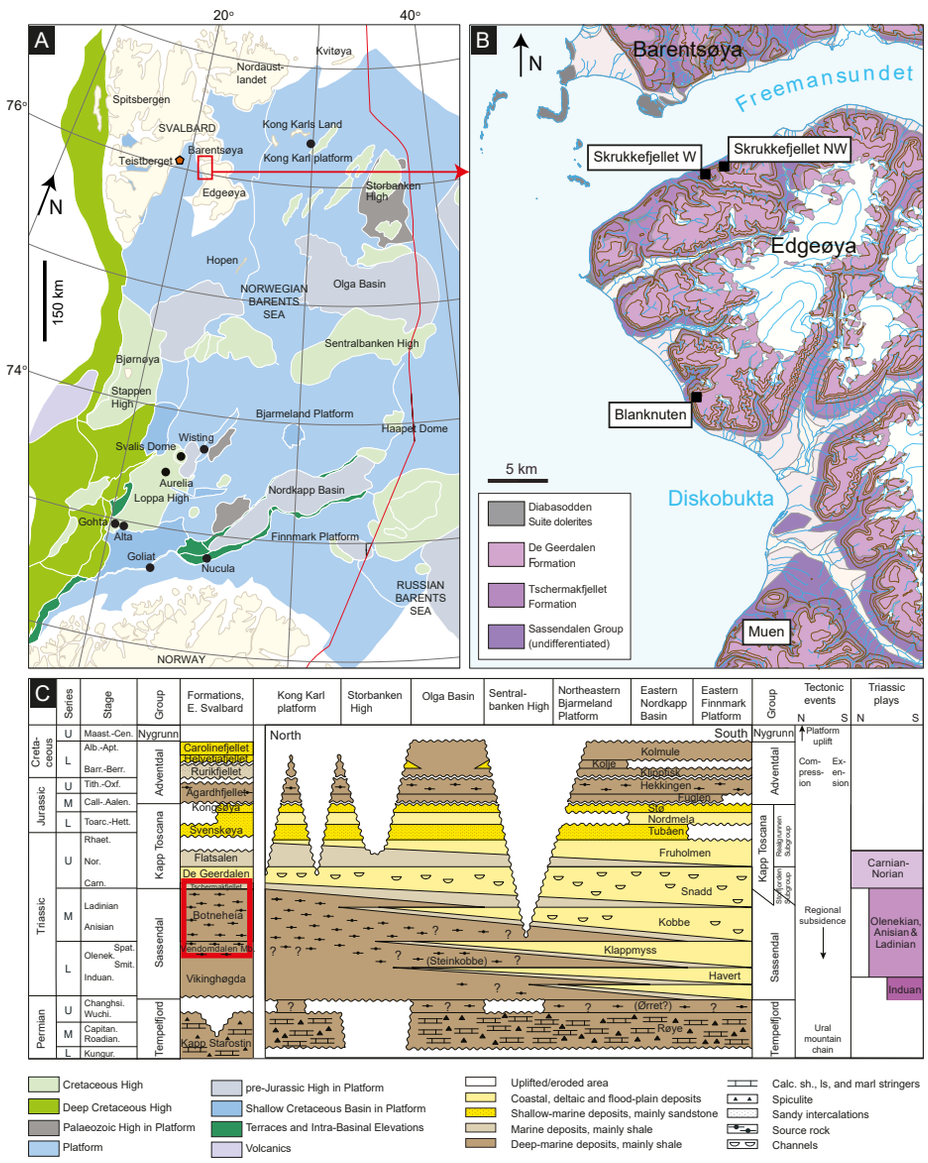

Figure 5.1: (A) Regional map of the Norwegian Barents Sea. The red rectangle marks the study area. The black circles denote fields, discoveries or localities described in the main text. The red pentagon marks the Teistberget locality from which the NGS SR-1 geochemical standard was sampled. Modified from the NPD (2017). **(B)** Geological map showing the NW part of Edgeøya with the Blanknuten (UTM: 35X E365439 N8664519), Skrukkefjellet W (UTM: 35X E367689 N8682947) and Skrukkefjellet NW (UTM: 35X E369750 N8683650) localities marked. Modified from Dallmann and Elvevold (2015). **(C)** Regional correlation panel of the Upper Permian to Lower Cretaceous succession from the Finnmark Platform in the south to the eastern islands of Svalbard in the north. Note the diachronous, lateral facies relationship between the Lower–Middle Triassic Steinkobbe Formation and Middle Triassic Botneheia Formation, younging from south to north. Modified from the NPD (2017).

been shown that Mo–TOC (total organic carbon) correlations decrease with increasing maturity (Ardakani et al., 2016). Elements originally hosted by source rocks are found in migrated oils (Lewan, 1984). Furthermore, whole rock analysis do not separate between authigenic and detrital elements, which can cause unreliable data for assessing palaeoenvironmental processes (Xu et al., 2012). Hydrothermal sources and post-depositional dissolution resulting in remigration of trace elements should also be considered (Tribovillard et al., 2006). Consequently, elemental chemostratigraphic studies should ideally be combined with sedimentological, petrographic, biostratigraphic and organic geochemical data when available, and further anchored to the lithostratigraphic framework of the particular study area (Craigie, 2018).

This paper presents a high-resolution, multi-elemental and multivariate chemostratigraphic study of a Triassic (Spathian–Carnian) composite mudstone succession exposed in eastern Svalbard, Arctic Norway (Fig. 5.1). Previous studies have demonstrated that the succession has highly variable source rock potential, containing both organic-lean, gas-prone source rocks (dominated by kerogen type III) and organic-rich, oil-prone source rocks (dominated by kerogen type II) (Abay et al., 2018; Krajewski, 2013; Lutz et al., 2021; Mørk et al., 1999b; Mørk and Bjorøy, 1984). The succession includes the organic-rich mudstones of the renowned Botneheia Formation (Anisian–Ladinian), which is considered a diachronous onshore counterpart to the Steinkobbe Formation (Spathian–Anisian) in the offshore basins south of Svalbard (Lundschien et al., 2014). These genetically related and organic-rich mudstones are considered important source rock units throughout the Norwegian Barents Shelf (Abay et al., 2018; Krajewski, 2013; Lerch et al., 2016a; Lerch et al., 2016b; Lerch et al., 2017; Lerch et al., 2018; NPD, 2017). Collectively, these two formations accumulated in a basin floor setting in front of a large north-westward prograding delta, here termed the Triassic Boreal Ocean (TBO) delta system (Fig. 5.2). These formations thus exhibit a diachronous relationship, younging from the south-east to the north-west across the Barents Shelf. Recent studies have suggested that the associated delta plain may have been the World's largest (Klausen et al., 2019), causing a large influx of fresh water and terrestrial OM into the marine basin (Paterson et al., 2017; Paterson et al., 2016).

At least three models have been discussed for the depositional conditions of the Botneheia Formation. Leith et al. (1993) argue that a potential land mass termed Crockerland north of Arctic Canada (Embry, 1993) could form an enclosed basin setting that promoted benthic water mass restriction, allowing marine OM to be preserved during moderate productivity. Høy and Lundschien (2011) and Vigran et al. (2008) considered water mass stratification and high surface productivity promoted by river-supplied, nutrient-rich fresh water as the primary mechanisms for elevated OM production and anoxic–dysoxic benthic conditions. Krajewski (2008) and Krajewski (2013) suggested organic

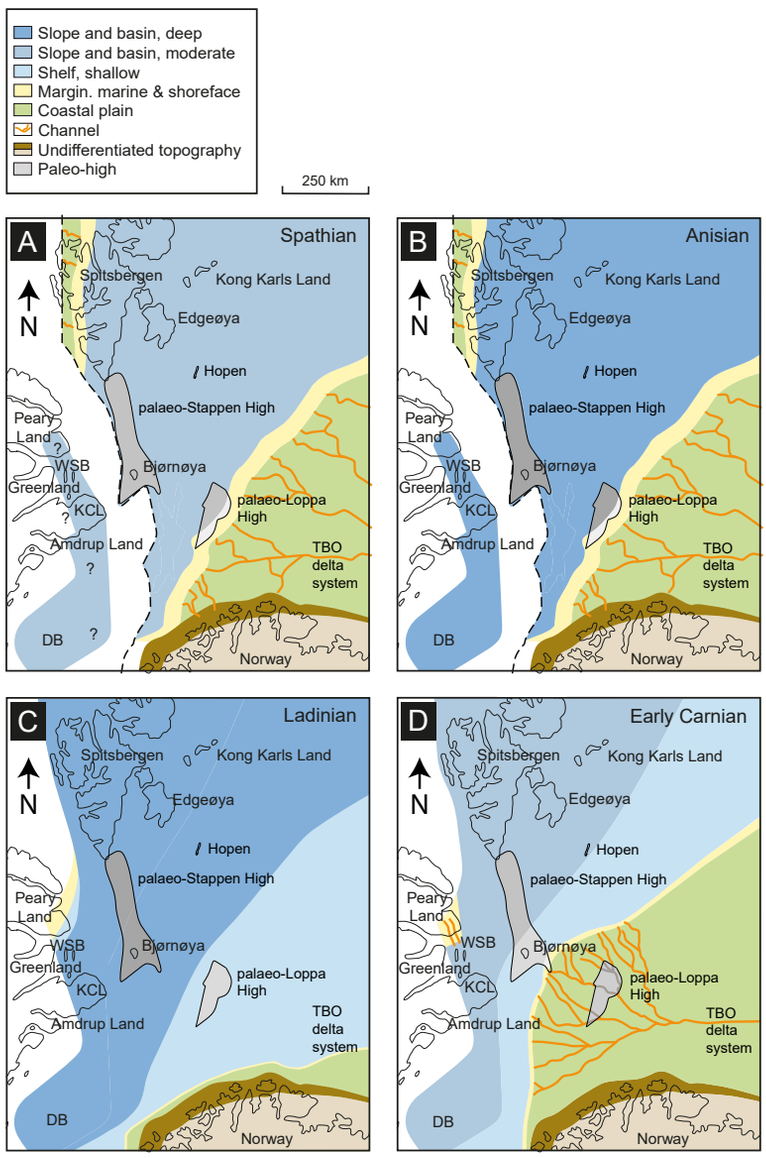

Figure 5.2: Spathian–Early Carnian Triassic palaeogeography of the Barents Shelf including generalised facies distributions. DB: Danmarkshavn Basin. KCL: Kronprins Christian Land. WSB: Wandel Sea Basin. TBO: Triassic Boreal Ocean. **(A)** During the Spathian, eastern Svalbard was dominated by distal muds, testifying to a basinal setting and deposition of the organic-rich and silty Vendomdalen member mudstones, whereas north-eastern Greenland acted as a source area for deltaic sandstone wedges along the western basin margin. **(B)** The Early Anisian saw shelf conditions that resulted in deposition of the lower–middle Muen Member in Svalbard. The middle–late Anisian demarcates the onset of basin-wide upwelling and phosphogenesis (not shown). **(C)** The Ladinian records a maximum flooding event, resulting in further deepening of the basin and widespread deposition of organic-rich mud in northern Barents Sea. In the south, pro-deltaic deposits of the Snadd Formation (Tschermakfjellet Formation facies-equivalent) had reached the Svalis Dome (Fig. 5.1A). **(D)** The Early Carnian shows further progradation of the TBO delta system. The pro-deltaic Tschermakfjellet Formation muds of the TBO delta system eventually blanket the underlying Botneheia Formation in Svalbard. Palaeodepositional maps modified from Bjerager et al. (2019), based on Eide et al. (2018), Glørstad-Clark et al. (2011), Glørstad-Clark et al. (2010), Klausen et al. (2015), Krajewski (2013), Lundschien et al. (2014), Riis et al. (2008), and Wesenlund et al. (2021).

productivity and oxygen depletion to be a product of intense upwelling caused by favourable atmospheric circulation (Parrish and Curtis, 1982), resulting in widespread phosphogenesis and the development of an oxygen minimum zone (OMZ). Clearly, a complete understanding of the processes that controlled the fluctuating redox conditions and primary production intensities in the basin are still lacking. By integrating whole-rock X-ray fluorescence (XRF) data with TOC, total inorganic carbon (TIC) and total sulphur (TS) geochemistry, as well as sedimentological descriptions, this study provides a novel approach to investigate changes in these depositional conditions in front of the TBO delta system.

The main objectives of this paper are thus to:

1. Characterise the chemostratigraphic development of the Spathian to Carnian mudstone-dominated succession in eastern Svalbard using major, minor and trace elements.

2. Test whether the recognised chemostratigraphic units reflect the previously assigned lithostratigraphic sub-division of the succession (cf. Krajewski, 2008; Krajewski, 2013; Wesenlund et al., 2021).

3. Apply and compare elemental proxies to understand fluctuations in palaeoproductivity and palaeoredox conditions, variations in water mass restriction and non-biogenic vs. biogenic sedimentation and evaluate their influence on regional source rock quality, richness and distribution.

5.2 Geological setting

This study focusses on a Lower–Upper Triassic organic-rich mudstone succession in eastern Svalbard and includes the Vendomdalen Member (Spathian) of the Vikinghøgda Formation (Lower Triassic), the Botneheia Formation (Anisian–Ladinian), and the lower part of the Tschermakfjellet Formation (Carnian) (Fig. 5.1). The succession accumulated in an epicontinental embayment on the north-western margin of Pangea here referred to as the TBO (Fig. 5.2). The embayment faced the deep Panthalassic Ocean to the north and landmasses to the east–southeast (i.e. Novaya Zemlya and the northern margin of the Baltic Shield) and to the west–northwest (i.e. Greenland) (Glørstad-Clark et al., 2010; Mørk et al., 1982; Sømme et al., 2018). The northern Barents shelf, including Svalbard, was part of a platform representing the central part of the embayment, acting as a site for mud deposition throughout major parts of the Triassic (Eide et al., 2018; Klausen et al., 2015; Riis et al., 2008). Despite the fact that there is evidence of local fault activity and structurally controlled prove-

nance shifts (Anell et al., 2013; Anell et al., 2016; Gilmullina et al., 2021; Muller et al., 2019; Ogata et al., 2018), the platform was overall tectonically stable throughout the Triassic (Faleide et al., 1984; Riis et al., 2008). Following the Uralian orogeny, the south-eastern region of the Barents Shelf saw the arrival of the large, north-westward-prograding TBO delta system in Early Triassic times (Fig. 5.2), eventually prograding across Svalbard during the Late Triassic (Glørstad-Clark et al., 2010; Klausen et al., 2019; Riis et al., 2008).

The mudstones of the Lower Triassic Vikinghøgda Formation were deposited in storm-influenced, shallow marine to shelf conditions and locally intercalate with deltaic sandstone wedges that built eastward into the basin across a gently sloping ramp (Fig. 5.2) (Mørk et al., 1999b; Wignall et al., 2016). This study pertains only to the Spathian Vendomdalen Member of this formation, which consists of dark, organic-rich silty mudstones deposited in a moderately deep and distal shelf setting below wave base (Mørk et al., 1999b). The benthic conditions were suboxic to euxinic (Hammer et al., 2019; Hansen et al., 2018; Mørk et al., 1999b; Vigran et al., 2014; Wignall et al., 2016; Xu et al., 2012). The Vendomdalen Member shows mainly kerogen type II/III and TOC up to 6 wt. % (Bjorøy et al., 2009; Krajewski, 2013; Mørk et al., 1999b). An *in situ* oil-filled hollow-chambered ammonoid (*Svalbardiceras spitzbergensis*) outcropping in this member in Central Spitsbergen proves its oil generation potential (Pedersen et al., 2020). The age-equivalent lower Steinkobbe Formation (Spathian) in the southern Barents Sea is considered the principal source rock for the Wisting discovery (Lerch et al., 2018), displaying kerogen types II and II/III with TOC up to 9 wt. % in the immature shallow stratigraphic well cores in the Svalis Dome area (Abay et al., 2018; Mørk and Elvebakk, 1999).

A circum-Arctic flooding event of early Anisian age marks the base of the overlying Middle Triassic Botneheia Formation (Gilmullina et al., 2021; Mørk et al., 1989). The Botneheia Formation consists of the Muen Member (Anisian) in its lower part, and the Blanknuten Member (Anisian–Ladinian) in its upper part. The upper part of the Muen Member indicates the onset of regional phosphogenesis and abundant matrix-filled phosphatic mudstones that continue into the overlying and characteristic cliff-forming Blanknuten Member (Krajewski, 2008). These phosphate-bearing mudstones are by far the richest source rock units of the region, dominated by kerogen type II and TOC up to 12 % wt. (Krajewski, 2013; Mørk and Bjorøy, 1984; Wesenlund et al., 2021). These mudstones were deposited in a deep shelf environment influenced by upwelling of nutrient-rich water from the Panthalassic Ocean during a transgressive to highstand phase (Fig. 5.2B) (Krajewski, 2013). Fluvial runoff from the TBO delta system is also considered a significant nutrient source and driver for organic-rich shale formation (Høy and Lundschien, 2011; Vigran et al., 2008). The oil generation potential of these source rocks is shown by interbedded bitumen-stained siltstones (Schou et al., 1984), and the discovery of yet an-

other *in situ* oil filled hollow-chambered Ladinian ammonoid (*Aristoptychites trochleaeformis*) (Smelror and Sollid, 2007).

The boundary between the Blanknuten Member (Botneheia Formation) and the overlying Tschermakfjellet Formation represents the onset of an early Carnian regional flooding event (Vigran et al., 2014). The Tschermakfjellet Formation exhibits a large-scale coarsening and shallowing upward trend and thus represents the pro-deltaic, lateral distal part of the overlying delta front to delta plain succession of the Late Triassic De Geerdalen (Svalbard) and Snadd (Barents Sea) formations (Klausen et al., 2015; Lord et al., 2017; Mørk et al., 1982). Collectively, these units are part of the large TBO delta system that prograded from the Uralides across the Barents Shelf eventually reaching Svalbard in Late Triassic times (Klausen et al., 2019). The Tschermakfjellet Formation mudstones show dominantly gas-prone (type III) kerogen and TOC = 1–3 wt. % (Abay et al., 2018; Krajewski, 2013; Mørk and Bjorøy, 1984; Mueller et al., 2014).

5.3 Materials and methods

5.3.1 Field work

The Blanknuten, Skrukkefjellet W and Skrukkefjellet NW localities (Fig. 5.1B) were previously investigated by (Wesenlund et al., 2021, their fig. 1b) in the coastal exposures of north-western Edgeøya and forms the basis of the lithostratigraphic logs, facies classification and sample set used in this study. In the Blanknuten locality, a ca 120 m thick vertical section was logged and sampled, covering the upper ca 40 m of the Vendomdalen Member (Vikinghøgda Formation), the entire Botneheia Formation and the lowermost few metres of the overlying Tschermakfjellet Formation. See Table 5.1 for an overview of the sample set. At the Skrukkefjellet W locality, only the upper part of the Blanknuten Member (Botneheia Formation) and the lower ca 20 m of the Tschermakfjellet Formation were logged and sampled. At the Skrukkefjellet NW locality, the sample profile starts immediately below the base of the middle Blanknuten Member and terminates within the first few metres of the Tschermakfjellet Formation. Collectively, the three sections form a stratigraphically complete composite profile that sufficiently covers the Spathian to lower Carnian succession (i.e. the Vendomdalen Member of the Vikinghøgda Formation, the entire Botneheia Formation, and the lower part of the Tschermakfjellet Formation). The lithostratigraphic units and their respective boundaries are recognised at all the investigated localities and are thus correlated with high confidence (Fig. 5.3). At each logged section, bed thickness, lithology, sedimentary structures, fabric, trace fossils and diagenetic features (e.g. phosphate nodules)

were noted. During sampling, several decimetre-deep pits were dug to acquire in situ rock material and minimise contamination from weathering or recent OM. Additional photographs of the investigated localities including the defined lithostratigraphic units and their boundaries are provided in (Wesenlund et al., 2021).

Table 5.1: The investigated localities and number of samples for each stratigraphic unit. The study localities are shown in Figure 5.1B. See the supplementary material for the samples deriving from Wesenlund et al. (2021).

	Locality		
Stratigraphic unit	Blanknuten	Skrukkefjellet W	Skrukkefjellet NW
Vendomdalen Mb	20	0	0
lower-middle Muen Mb	16	0	0
upper Muen Mb	5	0	0
lower Blanknuten Mb	7	0	1
middle Blanknuten Mb	12	0	9
upper Blanknuten Mb	6	1	5
Tschermakfjellet Fm	1	4	2
Sum:	**67**	**5**	**17**

5.3.2 Sample set and preparation

Of the 89 samples included in this study, 64 samples with TOC–TIC–TS data acquired from LECO analysis were collected from Wesenlund et al. (2021). The remaining 25 samples were introduced in this study and includes the Vendomdalen Member (Vikinghøgda Formation, Blanknuten locality, 20 samples), the upper Blanknuten Member (Botneheia Formation, Skrukkefjellet W locality, one sample), and the Tschermakfjellet Formation (Skrukkefjellet W locality, four samples). These samples were subjected to LECO analysis to determine TOC, TIC and TS content using the same procedures described in Wesenlund et al. (2021). Note that the samples from the Skrukkefjellet W in Wesenlund et al. (2021) were not included in this study. A complete overview of the geochemical data introduced in this study and those obtained from Wesenlund et al. (2021) is available in Appendix B. Wesenlund et al. (2021) describe the following sample preparation procedures: the samples were rinsed and scrubbed in temperate, running water. Weathering skin, contemporary organic matter and/or abundant calcite veins were removed from the samples. The samples were dried at <30°C overnight. An effort was made to remove macroscopic phosphate nodules to promote comparable samples of mainly mudstone matrix composition. An agate mortar and pestle were used to crush the mudstone fragments to gravel size. Then 1 dl of the remaining gravel-sized sample material was milled using a Retsch PM 100 with agate chamber and agate milling balls set at 450 rpm for 10 min, resulting in a homogenised, fine rock powder.

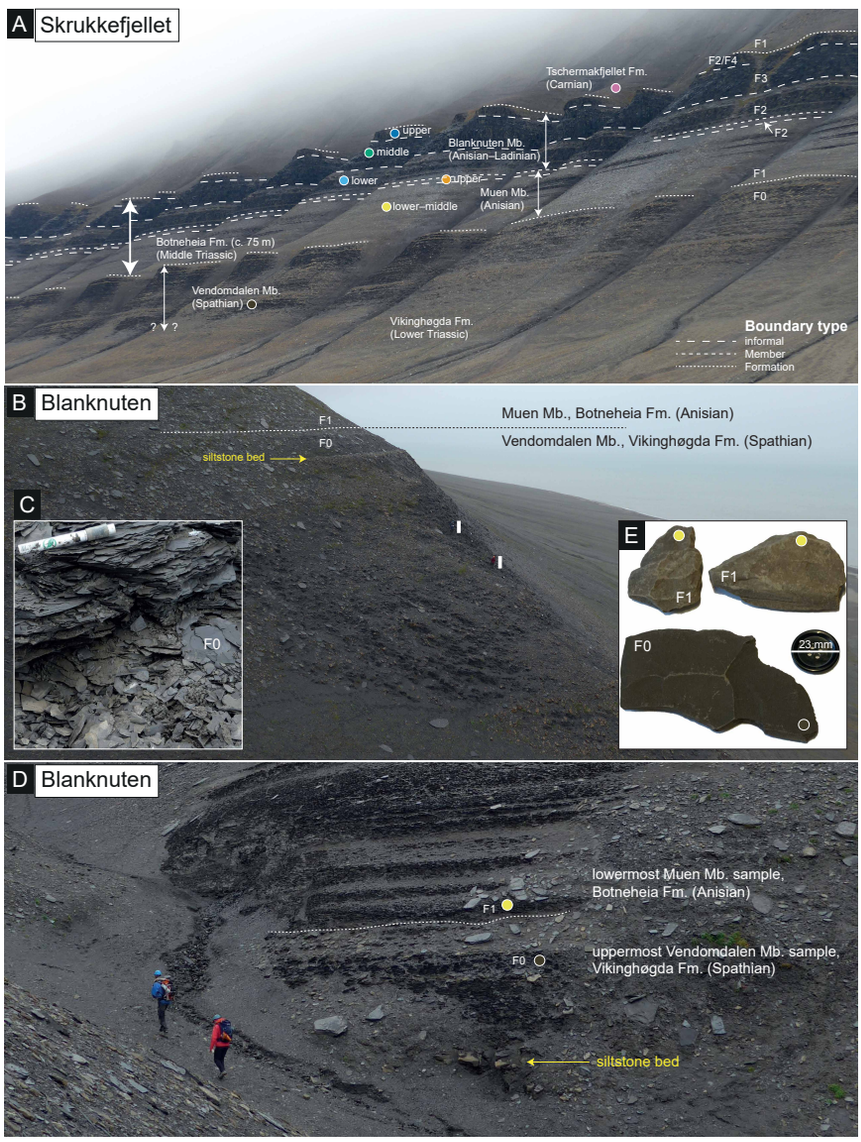

Figure 5.3: **(A)** Overview of the investigated lithostratigraphic units in outcrop view. Photograph taken from Freemansundet (see Fig. 5.1B) looking south into the coastal exposure of the Skrukkefjellet mountain. Note the slightly more reddish hue in the Vendomdalen Member (Vikinghøgda Formation) compared to the Blanknuten Member (Botneheia Formation). The coloured circles are used to distinguish the stratigraphic units in this paper. **(B)** Overview of the boundary between the Vendomdalen and Muen members in the Blanknuten locality (UTM: 35X E365275 N8664356), corresponding to the VenMb–MueMb boundary in the text. Note the change in slope dip directly at the siltstone bed (yellow arrow) within the uppermost Vendomdalen Member. Two persons are highlighted with white boxes for scale. **(C)** Close-up photograph showing the weathering expression of the Vendomdalen Member mudstones. The marker pen is 14 cm. **(D)** Overview of the sample site of the uppermost Vendomdalen Member and lowermost Muen Member samples, with the VenMb–MueMb boundary marked with dashed white line (UTM: 35X E365354 N8664442). The siltstone bed is the same as the one highlighted in (B). **(E)** Single exposure indoor photograph of dry mudstone samples retrieved from the sample sites shown in (D). Note the distinct change in shale brightness from darker to lighter comparing the Vendomdalen Member (below) with the Muen Member (above).

5.3.3 X-ray fluorescence (XRF)

The XRF analyses in this study were performed on the same pulverised and homogenised sample set originally prepared by Wesenlund et al. (2021). The pressed pellets used for the XRF analyses were prepared in the following way: 2.4 ± 0.005 g of Fluxana Cereox binder was inserted into a sample glass. Then 9.6 ± 0.005 g pulverised rock sample was added. The binder and sample were mixed and homogenised using a Heidolph Reax top vortex mixer for 2 minutes at 1750 rpm, later transferred and evenly distributed into a Vaneox 40 mm pressing die, then pressed at 20 ton using a Vaneox 25-ton automatic press, yielding a press pellet ready for analysis.

The major, minor and trace element measurements were analysed using a Bruker S8 Tiger wavelength dispersive X-ray fluorescence (WDXRF) spectrometer in vacuum mode utilising four crystals (XS-55, PET, LiF200 and LiF220) and an OEG95LT rhodium X-ray tube. The collimator was set at 0.23 degrees, and the sample mask diameter was 34 mm. The energy calibration for the major elements Si, Al, K, Ca, Mg, Na, P and Se was done by the standard-less semi-quantitative Bruker Spectraplus software (Quant Express) package using the "best detection" method with run duration of ca 18 min/sample. The energy calibration for the major, minor and trace elements Sc, Ti, V, Cr, Mn, Fe, Co, Ni, Cu, Zn, Ga, As, Rb, Sr, Y, Zr, Nb, Mo, Sn, Sb, Cs, Ba, La, Ce, Pb, Th and U was done by the quantitative Bruker Spectraplus software (Geo Quant T) package using a run time of ca 38 min/sample and automatic matrix correction.

To check for analytical accuracy, the Norwegian Geochemical Standard Svalbard Rock – 1 (NGS SR-1), a mudstone standard maintained by the Norwegian Petroleum Directorate (NPD) and described by Dahlgren et al. (1998), was analysed and compared with its original data sheet (Table 5.2). Additionally, the TOC–TIC–TS values for the NGS SR-1 used in this study were collected from Dahlgren et al. (1998). No shale standards were utilised in the XRF energy calibration. The XRF results in this study should thus be regarded as specific to the methods above and semi-quantitative. However, the analytical precision was considered good and sufficient for chemostratigraphic purposes, as TS from LECO analysis and S from XRF analysis yielded a very strong linear correlation for the entire sample set (least squares linear regression without intercept: $S = 0.4905 \times TS$, $R^2 = 97.5$ %).

The detection of the elements Sn and Sb, both with a typical lower limit of detection = 2 ppm, was unsatisfactory and are not included in this study. Semi-quantitative determination of Se was considered unreliable, however Se was detected in 26 of 89 samples, where 25 of these 26 samples represent the Blanknuten Member. Certain samples yielded unquantifiable U (one sample), Th (one sample), Mo (five samples), and Co (13 samples). To create a complete

Table 5.2: Comparison of major, minor and trace element concentrations of the NGS SR-1 from XRF analyses in this study and Dahlgren et al. (1998). LLD = lower limit of detection, n = number of samples analyzed, SD = standard deviation.

		NGS SR-1, this study				NGS SR-1, Dahlgren et al. (1998)					
Element	Unit	Value	Stat. error (%)	LLD (ppm)	n	Min	Max	Mean	Median	SD	n
SiO_2	%	49,67	18,3	132,7	1	53,03	54,01	53,5	53,5	0,466	5
Al_2O_3	%	13,03	0,32	133,1	1	13,91	14,3	14,07	14	0,18	5
CaO	%	5,17	0,31	67	1	4,6	4,92	4,8	4,82	0,123	5
K_2O	%	3,59	0,34	39,3	1	3,05	3,39	3,29	3,35	0,138	5
MgO	%	2,44	0,71	229,7	1	3,28	3,78	3,43	3,36	0,204	5
Na_2O	%	0,5	2,78	288,4	1	0,66	0,78	0,75	0,78	0,051	5
P_2O_5	%	0,18	3,48	95,6	1	0,18	0,19	0,18	0,18	0,006	5
Sc	ppm	14	9,1	2,4	1	12,8	17	14,5	14,1	1,846	4
TiO_2	%	0,78	0,29	7,9	1	0,73	0,77	0,74	0,73	0,018	5
V	ppm	533	0,31	2	1	425	647	574	588	83,221	6
Cr	ppm	62	2,36	4,4	1	80	114	89	86	12,438	6
MnO	%	0,06	1,09	7,3	1	0,06	0,06	0,06	0,06	0,002	5
Fe_2O_3	%	5,48	0,17	81,2	1	5,8	6,19	5,93	5,85	0,169	5
Co	ppm	8	1,04	1,7	1	15	20	18	18	2,136	6
Ni	ppm	77	1,63	2,5	1	68	80	73	71	4,708	6
Cu	ppm	46	2,27	2,3	1	47	57	52	51	5,033	3
Zn	ppm	139	0,79	1,7	1	146	162	152	151	5,619	6
Ga	ppm	17	1,96	0,7	1	18	19	18	18	0,812	4
As	ppm	22	16,4	2	1	14	19	17	17	3,536	2
Rb	ppm	131	0,35	0,8	1	137	154	147	148	7,028	6
Sr	ppm	113	0,37	0,7	1	112	131	119	118	6,566	6
Y	ppm	30	0,69	1	1	27	36	31	31	3,183	6
Zr	ppm	163	0,24	0,8	1	123	182	167	175	22,258	6
Nb	ppm	14	1,69	0,5	1	10	16	15	16	2,544	6
Mo	ppm	45	0,89	0,7	1	41	48	43	41	4,157	3
Ba	ppm	448	0,67	6	1	505	559	531	528	27,099	3
La	ppm	33	7,98	5,8	1	40	41	41	41	0,99	2
Ce	ppm	79	2,46	7	1	68	77	71	68	5,225	3
Pb	ppm	15	1,65	1,1	1	19	24	20	20	2,283	4
Th	ppm	6	4,51	0,9	1	11	20	15	14	4,583	3
U	ppm	5	15,1	0,9	1	8	12	9	8	2,2	4

data matrix for multivariate analysis, the unquantified U, Th, Mo, and Co values for these samples were set to 0 ppm as the lower limit of detection was typically 1–2 ppm for all these elements. Oxide–element conversions were carried out using a multiplication factor—i.e., the molecular weight ratio of element/oxide—for the raw data initially presented as oxides by the Spectraplus software solution.

5.3.4 Enrichment factors (EFs)

All element enrichment factors (EFs) in this study were calculated using the following equation: $X_{EF} = (X_{sample}/Al_{sample})/(X_{standard}/Al_{standard})$, where "X" is the element of interest, and "standard" is a representative reference material

(Tribovillard et al., 2006). In this study, the EFs for all elements except As were calculated using the post-Archean Australian shale (PAAS) (Taylor and McLennan, 1985) as the standard. The EF for As was calculated using the As value from the "average shale" from Wedepohl (2004) and the Al value from the PAAS since As was not determined for the PAAS in Taylor and McLennan (1985). The above normalisation equation using an average shale standard is a common approach to compare elemental proxies related to depositional processes of mudstones and ideally corrects for dilution by e.g. biogenic carbonates, silica, or organic carbon (e.g., Algeo and Li, 2020; Tribovillard et al., 2006). Correlations between EFs could occur due to the normalisation process itself (Van der Weijden, 2002), however, strongly correlated EFs are considered here to dominantly represent associated depositional processes (see Section 5.5 for discussion).

5.3.5 Degree of pyritisation using total Fe

Degree of pyritisation using total Fe (DOP_T) is a palaeoredox proxy and was calculated using the following equation (Algeo and Li, 2020, , their equation 2): $DOP_T = TS \times (55.85/64.12)/Fe$, where "TS" and "Fe" represents total sulphur from LECO analysis and total iron from XRF analysis respectively, while the coefficient 55.85/64.12 is the molecular weight ratio of Fe/TS in pyrite (FeS_2). This is opposed to distinguishing pyritic Fe and acid soluble Fe that is necessary to determine "true" DOP (Raiswell et al., 1988). Thus, DOP_T may include minor non-pyrite sulphur and/or silicate-bound Fe, and it is necessary to calibrate DOP_T to DOP on a formation-specific basis if DOP_T is used as a proxy for DOP (Algeo and Li, 2020). However, as DOP_T and DOP correlate strongly, the variations in DOP_T still provide robust criteria to evaluate palaeoredox fluctuations (Algeo and Liu, 2020; Algeo and Maynard, 2004).

5.3.6 Multivariate analysis

This study applies Pearson correlation coefficients (PCCs), PCA (principal component analysis) and HCA (hierarchical cluster analysis) for the multivariate analyses. Three samples (BLA2-18-49, BLA2-18-65, and SKØ2-18-11, see Appendix B) were anomalously rich in TIC or P, and were discarded prior to the PCC, PCA and HCA analyses, but were otherwise included in this study. The PCC analysis, PCA and HCA preprocessing and settings were thus carried out on an 87 (samples) by 35 (variables) data matrix (including the NGS SR-1). Prior to the HCA and PCA, the parameters were rescaled in between [0,1] using min–max normalisation. The statistical analysis was performed using PYTHON and the open-source SCIKIT-LEARN, PANDAS, SEABORN, NUMPY and MATPLOTLIB software libraries bundled with the Anaconda Data Science Platform

(Anaconda Inc., 2021). Details on script availability are given in Section 5.7, and the script contains all the statistical methods used in this study.

5.4 Results

5.4.1 Facies descriptions and stratigraphic distribution

Based on the physical appearance of the studied mudstones, Wesenlund et al. (2021) recognised and defined four dominant mudstone facies in the Botneheia Formation and the lowermost Tschermakfjellet Formation (facies F1–F4, summarised in Table 5.3). This study introduces a fifth facies (here referred to as F0; Table 5.3), restricted to the underlying Spathian Vendomdalen Member. Some of the facies are recurrent and occur in multiple stratigraphic units, whereas others are unique to specific stratigraphic units (see Table 5.3 and Figs 5.3A,B and 5.4). A brief facies description for F0 is given below.

Facies 0 (F0). This facies consists of cliff-forming, laminated, dark brown silty mudstones (Figs 5.3E and 5.4A) and is exclusive to the Vendomdalen Member in the upper part of the Vikinghøgda Formation. Lamination planes are smooth, straight, and parallel to sub-parallel, whereas fragments are brittle and angular, and appear both flaky and platy in outcrop exposures. Burrows were not observed in the investigated section. F0 has a reddish weathering hue and exhibits clear fissility parallel to the bedding plane (Fig. 5.3A,C). Macroscopic weathered pyrite nodules were observed. Phosphate-nodules were recorded in only one horizon.

While facies transitions within mudstones may generally be difficult to discern in outcrops, the investigated succession exhibits some abrupt and clearly visible vertical facies transitions, which demarcate regional lithostratigraphic boundaries (Fig. 5.3). The transition from the cliff-forming facies F0 (unique to the Vendomdalen Member) upwards into F1 (characterised by gentle slopes), represent the regional boundary between the Vendomdalen Member of the Vikinghøgda Formation and the lower–middle Muen Member of the Botneheia Formation (referred to as the "VenMb-MueMb" boundary throughout this paper). In addition, the vertical transition from the cliff-forming facies F4 (unique to the upper Blanknuten Member) abruptly back to F1 marks the regional boundary between the Botneheia and Tschermakfjellet formations (referred to as the "BlaMb-TschFm" boundary).

Table 5.3: Summary of mudstone facies of non-weathered samples. Fo is from this study, while F1 to F4 are from Wesenlund et al. (2021). *The upper Muen Member and lower Blanknuten Member (both F2 mudstones) are not cliff-forming and cliff-forming respectively.

Facies	Stratigraphic unit	Description	Color	Bedding plane	Cliff-forming	Burrows	P-nodules	Benthic oxygen regime	Productivity	Interpretation
Fo	Vendomdalen Member	Brittle, flaky to platy dark brown mudstone. The bedding plane is smooth, straight and parallel.	Dark brown	Smooth, straight, and parallel	Yes	Not observed	Only observed in one horizon	Oxic? to euxinic	Low	Deposition from suspension fallout below wave base interrupted by rare event beds in a weakly restricted benthic setting
F1	lower–middle Muen Member, Tschermakfjellet Formation	Soft to brittle, mostly flaky grey-dark grey mudstone. The bedding plane is smooth or rough depending on degree of bioturbation.	Grey to dark grey	Smooth and rough depending on degree of bioturbation, and not always evident	No	*Chondrites* and *Helminthopsis*	Only observed in the Botneheia Formation	Oxic to dysoxic	Moderate	Deposition from suspension in a deep shelf setting interrupted by bioturbation and common event beds. More ventilated than Fo mudstones
F2	upper Muen Member, lower and upper Blanknuten Member	Brittle and flaky to platy dark grey-black mudstone. The bedding plane is smooth, straight and parallel. Laminae are deformed around P-nodules.	Dark grey to black	Smooth, straight, and parallel, but commonly deformed around P-nodules	Partly*	*Thalassinoides*	Yes, abundant	Dysoxic to anoxic	High	Deposition from suspension fallout interrupted by winnowing, bioturbation and abundant event beds. Deeper and less ventilated than F1 mudstones
F3	middle Blanknuten Member	Brittle and platy black mudstone. The bedding plane is smooth, straight, and highly parallel.	Black	Smooth, straight, and highly parallel	Yes	Not observed	Not observed	Anoxic to euxinic	High	Deposition from suspension fallout interrupted by winnowing/reworking and rare event beds. Deeper and less ventilated than F2 mudstones
F4	upper Blanknuten Member	Soft to brittle, platy to flaky dark grey-black calcareous mudstone to impure limestone. The bedding plane is straight and parallel, but rough as a rule. Laminae are deformed around P-nodules	Dark grey to black	Straight, parallel, and dominantly rough. Deformed around P-nodules	Yes	*Thalassinoides*	Yes, abundant	Dysoxic to euxinic	High	Deposition from suspension fallout interrupted by bioturbation and rare event beds. Shallower and more ventilated than F3 mudstones

5.4.2 Elemental chemostratigraphy

Appendix A shows the geochemical logs of the weight concentrations and EFs for all elements in this study, highlighting the defined facies and associated lithostratigraphic units (Fig. 5.3, Table 5.3). This lithostratigraphic subdivision is supported by recent organic geochemical investigations (Wesenlund et al., 2021) and linked with the Middle Triassic informal stratigraphic units from Krajewski (2008) and Krajewski (2013). Appendices B and C provide the tabulated data and descriptive statistics (minimum, mean, standard deviation [SD] and maximum), respectively, for each parameter grouped by stratigraphic unit.

Pearson correlation coefficient (PCC)

The Pearson correlation coefficient (PCC) matrix provides a full overview of the linear correlations between all weight concentrations (Fig. 5.5A) and element EFs (Fig. 5.5B). Aluminium (%) correlates strongly with the weight concentrations of the conservative lithogenic elements Ga, K, Ti, Rb, Zr, Nb and Th (PCC > 79 %, Fig. 5.5A). Calcium, Sr, Ba, TIC and P correlate positively with each other and up to 90 % PCC, but negatively with Al, indicating that Al (%) is dominantly hosted within the non-biogenic mineral fraction.

Hierarchical cluster analysis (HCA)

The hierarchical cluster analysis (HCA) of the TOC, TIC, TS, DOP_T and all EFs are presented in Figure 5.6. The analysis resulted in three main elemental EF clusters (EFCs) (Table 5.4) and seven main stratigraphic clusters (SCs) (Table 5.5). Surprisingly, The NGS SR-1 correlates best with the Vendomdalen Member and not the currently assigned Botneheia Formation.

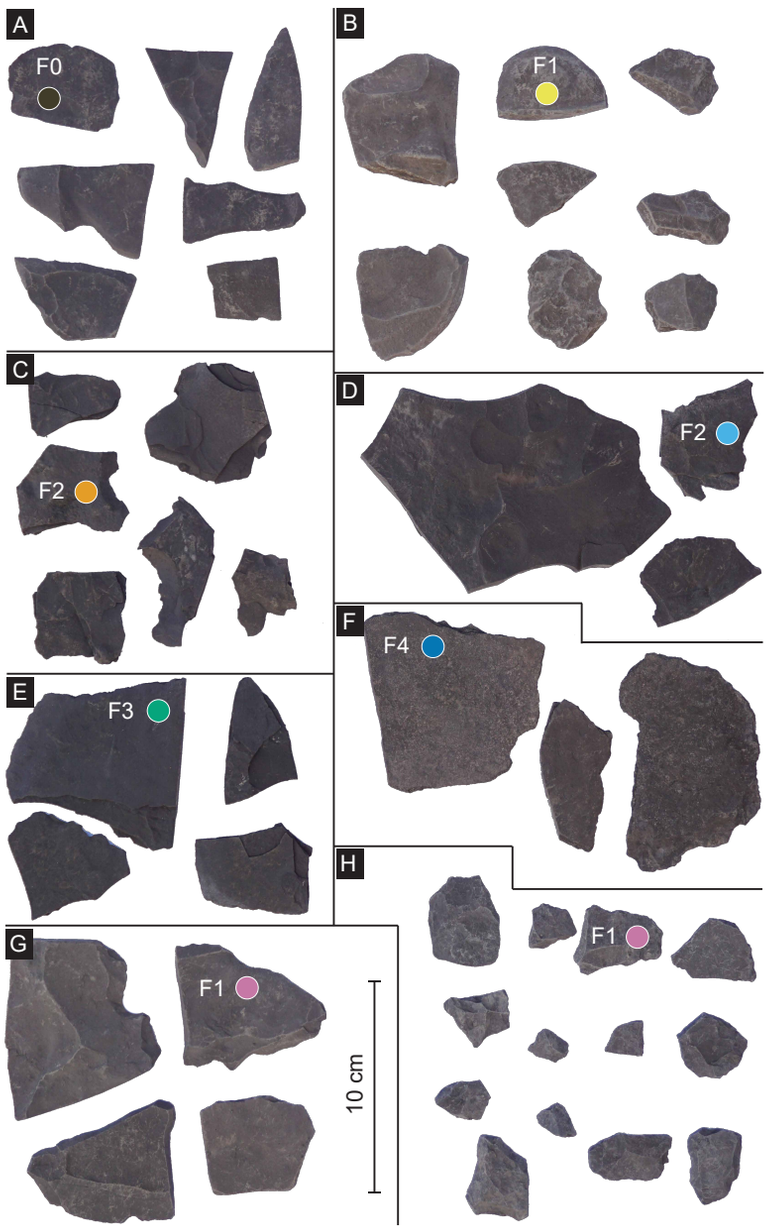

Figure 5.4: Single exposure outdoor photograph of dry mudstone fragments representing the recognized mudstone facies within the various lithostratigraphic units (characteristics summarized in Table 5.3). The colour-coding is the same as in Fig. Fig. 5.3A. **(A)** F0, Vendomdalen Member. **(B)** F1, lower–middle Muen Member. **(C)** F2, upper Muen Member. **(D)** F2, lower Blanknuten Member. **(E)** F3, middle Blanknuten Member. **(F)** F4, upper Blanknuten Member. **(G)** F1, Tschermakfjellet Formation. **(H)** F1, Tschermakfjellet Formation. Note the contrasts in brightness, clast angularity and lamination. (4A through H) and (4F) are from the Blanknuten and Skrukkefjellet W localities respectively.

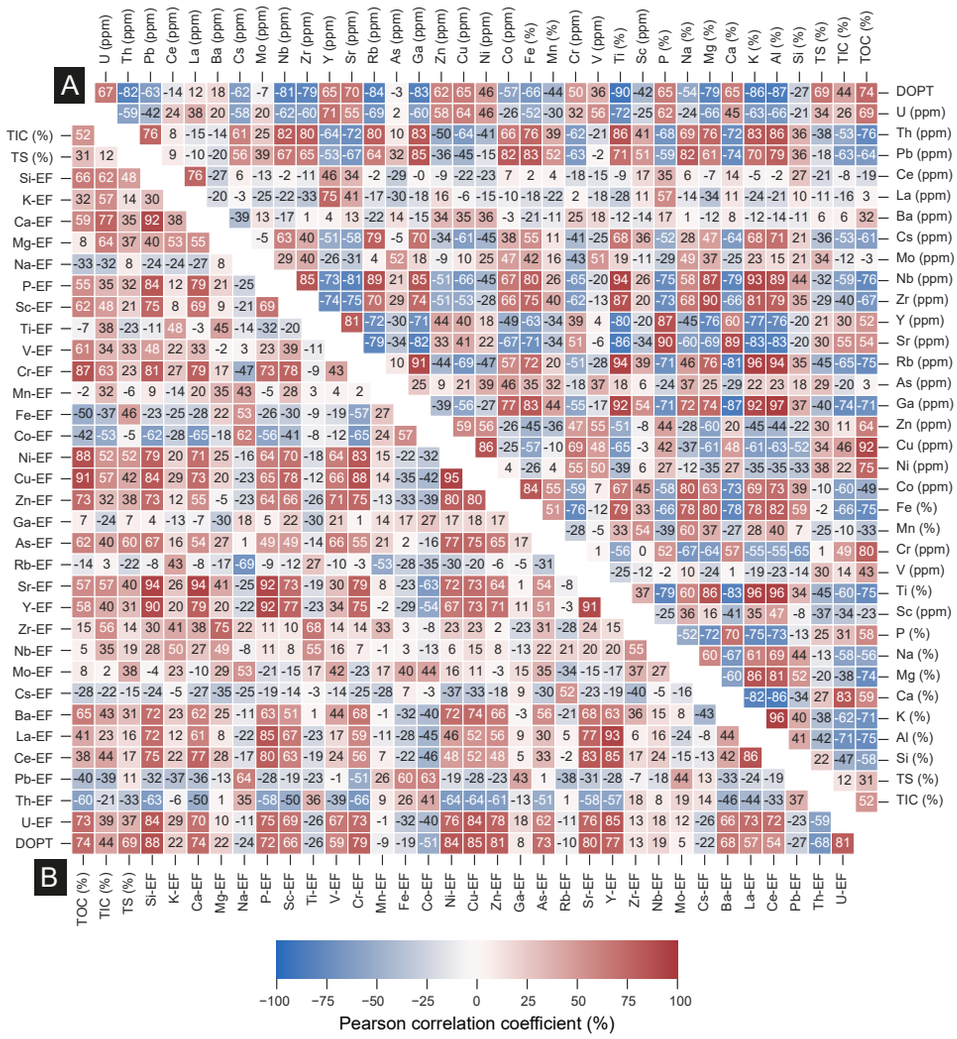

Figure 5.5: Pearson correlation coefficient (PCC) matrix, showing the linear correlation between all the variables used in this study. Three samples with anomalous TIC or P content were not included in this analysis (see Section 5.3.6). **(A)** PCCs for non-normalised concentrations and DOP_T. **(B)** PCCs for TOC, TIC, TS, DOP_T and element EFs.

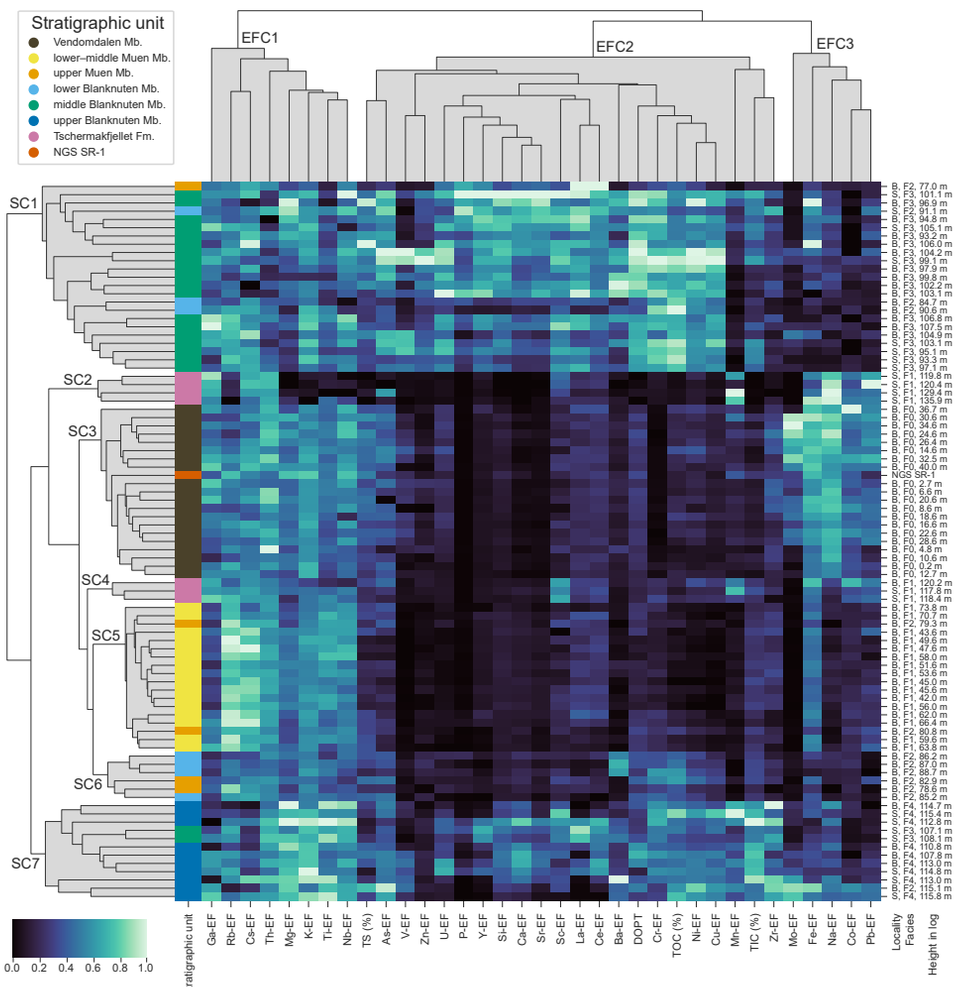

Figure 5.6: Hierarchical cluster analysis (HCA) of TOC, TIC, TS, DOP_T and element EFs. Columns and rows represent variables and observations respectively, and each column is scaled to [0,1]. The element EF clusters 1 to 3 (EFC1–EFC3) and stratigraphic clusters 1 to 7 (SC1–SC7) are described in Tables 5.4 and 5.5, respectively. Three samples with anomalous TIC or P content were not included in this analysis (see Section 5.3.6).

Table 5.4: Defined enrichment factor clusters based on correlating parameters.

Enrichment factor cluster	Parameters
EFC1	Ga-EF, Rb-EF, Cs-EF, Th-EF, Mg-EF, K-EF, Ti-EF, and Nb-EF
EFC2	TOC, TIC, TS, DOP_T, As-EF, V-EF, Zn-EF, U-EF, P-EF, Y-EF, Si-EF, Ca-EF, Sr-EF, Sc-EF, La-EF, Ce-EF, Ba-EF, Cr-EF, Ni-EF, Cu-EF, Mn-EF and Zr-EF
EFC3	Mo-EF, Fe-EF, Na-EF, Co-EF, and Pb-EF

Table 5.5: Defined stratigraphic clusters based on recognisable criteria that separate the elemental assemblages and their sample assemblage.

Stratigraphic cluster	Vendomdalen Member samples	lower–middle Muen Member samples	upper Muen Member samples	lower Blanknuten Member samples	middle Blanknuten Member samples	upper Blanknuten Member samples	Tschermakfjellet Formation samples	Relative abundance of element EFs or EFCs
SC1	0	0	1	3	19	0	0	High EFC_2 (except Mn-EF), low EFC_3
SC2	0	0	0	0	0	0	4	Low EFs of Mg, K, Ti and Nb in EFC_1
SC3	20	0	0	0	0	0	0	Low EFC_2, high EFC_3
SC4	0	0	0	0	0	0	3	Low EFC_2 (except EFs of Sc and Mn), variable EFC_3
SC5	0	16	2	0	0	0	0	Low EFC_1 and EFC_2
SC6	0	0	2	4	0	0	0	Low EFC_1 and EFC_3, variable EFC_2
SC7	0	0	0	0	2	10	0	Variable EFC_1 (but high EFs of Mg, K, Ti, Nb), variable EFC_2 and EFC_3 (but high TIC)

Principal component analysis (PCA)

A biplot of PC1 (principal component 1) vs PC2 (principal component 2) is shown in Figure 5.7. PC1 and PC2 account for 59.78 % of the total variance and clearly demonstrate that the assigned stratigraphic units form groups that correlate well with the stratigraphic clusters from the HCA (compare Figs 5.6 and 5.7). Likewise, EFs of Na, Mo, Fe, Pb and Co group together and are captured by the PC2, which correlates with EFC_3 (Fig. 5.6, Table 5.4). Correlations between the loadings on PC1 and EFC_2 are also evident (compare Figs 5.6 and 5.7). The Tschermakfjellet Formation in the PCA displays a bipartite grouping as expressed by SC_2 and SC_4 in the HCA (compare Figs 5.6 and 5.7). As with the HCA, the PCA shows that the NGS SR-1 correlates best with the Fo mudstones of the Vendomdalen Member (Figs 5.6 and 5.7).

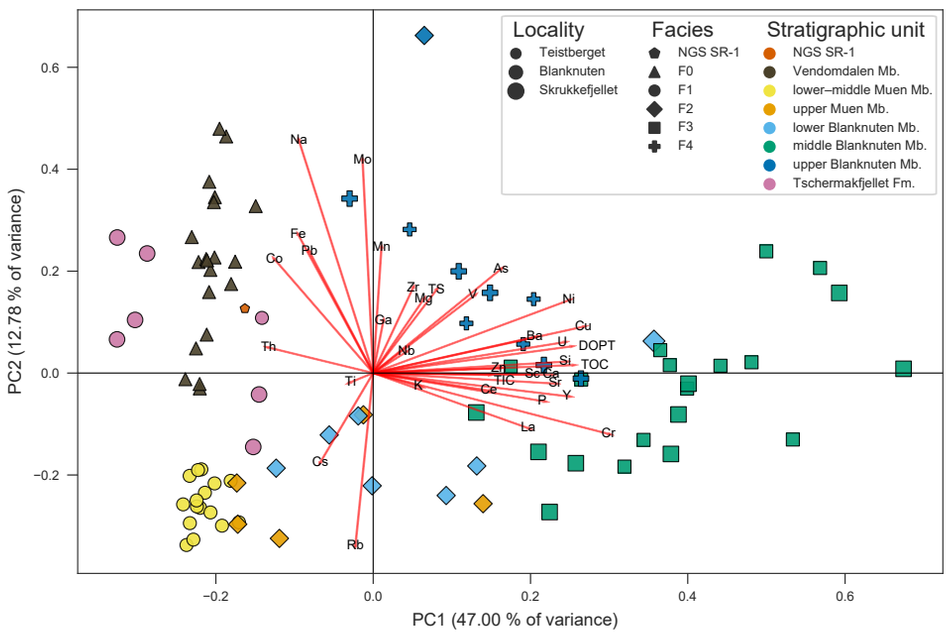

Figure 5.7: Biplot of the principal components 1 (PC1) and 2 (PC2) derived from PCA analysis of TOC, TIC, TS, DOP_T and element EFs. The axes represent the values for the loadings, while the scores are scaled by the largest range in each PC. Three samples with anomalous TIC or P content were not included in this analysis (see Section 5.3.6).

The stratigraphic distribution of the PC1, PC2 and PC3 (principal component 3) scores and the loadings are shown in Figure 5.8. In PC1, all samples from the Vendomdalen and lower–middle Muen members show similar, negative scores. The onset of the upper Muen Member from level ca 75 m (Fig. 5.8) up to the BlaMb–TschFm boundary mark a prominent positive "bow-shaped" excursion with maximum PC1 scores in the middle Blanknuten Member. A steep, negative trend across the BlaMb–TschFm boundary results in negative PC1 scores for all Tschermakfjellet Formation samples. PC2 scores show a positive incline within the Vendomdalen Member but is abruptly terminated at the VenMb–MueMb boundary. This marks the onset of a second positive incline arguably interrupted at the BlaMb–TschFm boundary. PC3 shows a small, positive excursion across the VenMb–MueMb boundary, while the BlaMb–TschFm boundary denotes a steep negative incline and a prominent geochemical transition with positive loadings for EFs of Nb, Zr, Ti and Mg (Fig. 5.8).

Summarised chemostratigraphic log panel

A chemostratigraphic log panel including 10 features with substantial loadings on PC1, PC2 or PC3 is included (Fig. 5.9). Chemostratigraphic logs of TS, TIC,

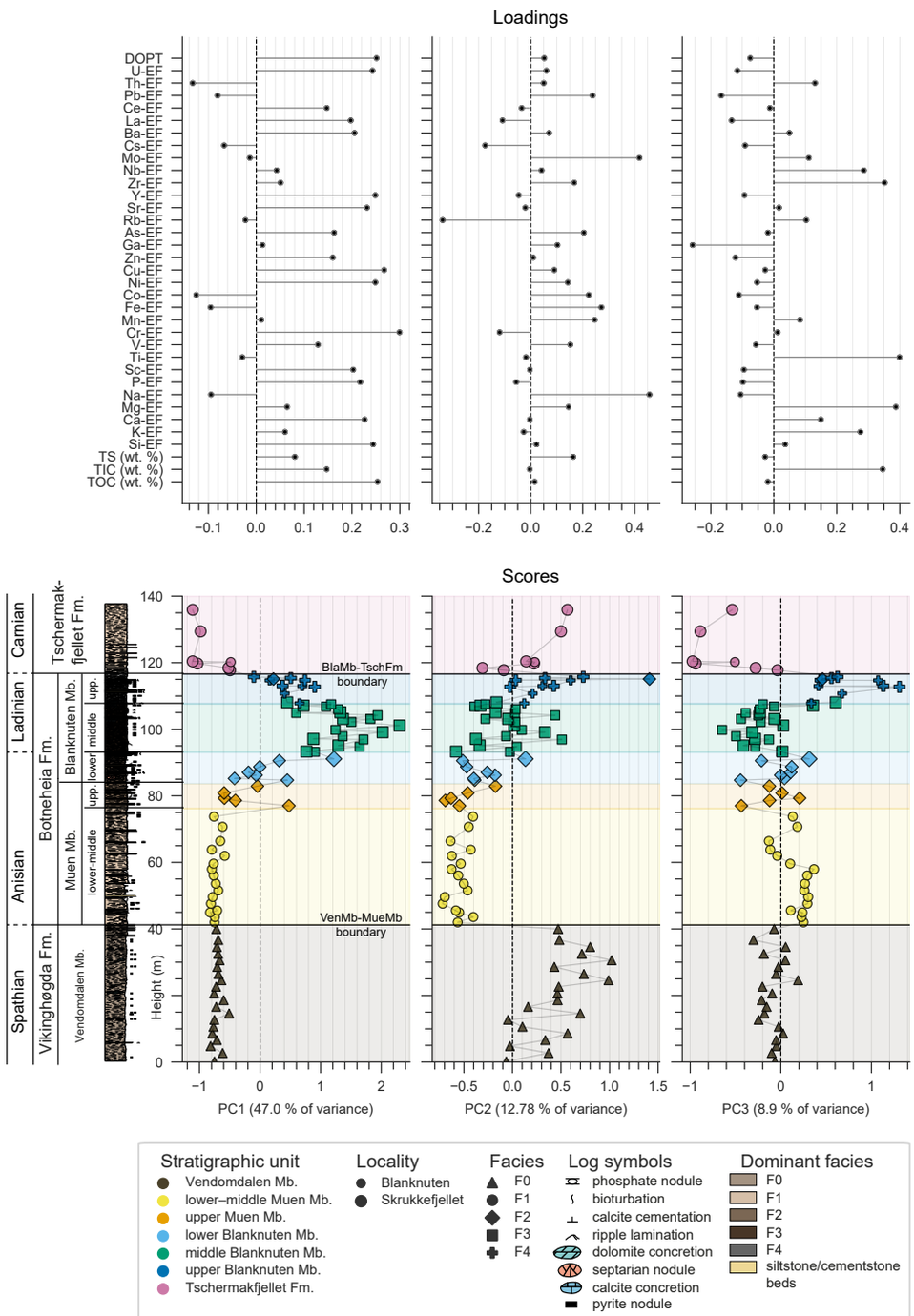

Figure 5.8: Sedimentary log and combined plots showing the PC1, PC2 and PC3 loadings on top and the corresponding stratigraphic distribution of PC1, PC2 and PC3 scores below. Note the positive bow-shape in the Botneheia Formation (PC1) and the prominent discontinuities at the VenMb–MueMb boundary (PC2), and the BlaMb–TschFm boundary (PC3). Three samples with anomalous TIC or P content were not included in this analysis (see Section 5.3.6).

DOP_T and the remaining element EFs are available in Appendix A. The EFs of Si, Ba and P show log trends equivalent to the PC1 log (compare Figs 5.8 and 5.9). These EFs show no enrichment in either the Spathian Vendomdalen Member (Vikinghøgda Formation, facies F0), the Anisian lower–middle Muen Member (Botneheia Formation, facies F1), or the Carnian Tschermakfjellet Formation (facies F1), but capture a "bow trend" in the phosphogenic upper Muen and the entire Blanknuten members (Botneheia Formation) with consistently high values in its middle part (Fig. 5.8). The TOC and Cr-EF trends are strongly coupled with each other and the variables above (Figs 5.5, 5.6, 5.7 and 5.9) but display a negative and positive excursion across the VenMb–MueMb boundary, respectively. The U-EF shows strong positive loadings for PC1 and slight positive loadings for PC2 (Fig. 5.8). In contrast, Mo-EF has the strongest loading on PC2 and a slight negative loading on PC1 (Fig. 5.8).

The Mo-EF log clearly records the negative geochemical discontinuity at the VenMb–MueMb and BlaMb–TschFm boundaries (Fig. 5.9) and an overall positive incline within the Botneheia Formation, consistent with the PC2 log (Fig. 5.8). The Co-EF log resembles that of the Mo-EF, but in contrast, it shows a positive excursion across the BlaMb–TschFm boundary with equivalent values in the Vendomdalen Member (Facies F0) and Tschermakfjellet Formation (facies F1; Fig. 5.9). The Na-EF log demonstrates a clear negative excursion directly at the VenMb–MueMb boundary and is generally constant through all the stratigraphic units in the Botneheia Formation except the upper Blanknuten Member (F2/F4 mudstones). The BlaMb–TschFm boundary marks a Na-EF reversal into the lowermost Tschermakfjellet Formation (Fig. 5.9). Three samples in the lowermost part of this unit show an elemental assemblage comparable to the Botneheia Formation (SC4, Fig. 5.6), contrasting its younger samples (SC2, Fig. 5.6). These two SCs show a bipartite division in the PCA analysis (Fig. 5.7). The Ti-EF log records the strongest loading on PC3 (Fig. 5.8) and shows a minor positive excursion at the VenMb–MueMb boundary and a slight negative bow shape in the Botneheia Formation with maximum values in the upper Blanknuten Member (Facies F4). A negative Ti-EF incline takes place across the BlaMb–TschFm boundary (Fig. 5.9), as confirmed in the PC3 log (Fig. 5.8).

5.5 Discussion

5.5.1 Chemostratigraphic rationale

The unsupervised multivariate analyses of the elemental EFs clearly demonstrate that the various mudstone facies and their associated stratigraphic units are recognised via distinct HCA clusters and PCA groups (Figs 5.6, 5.7 and

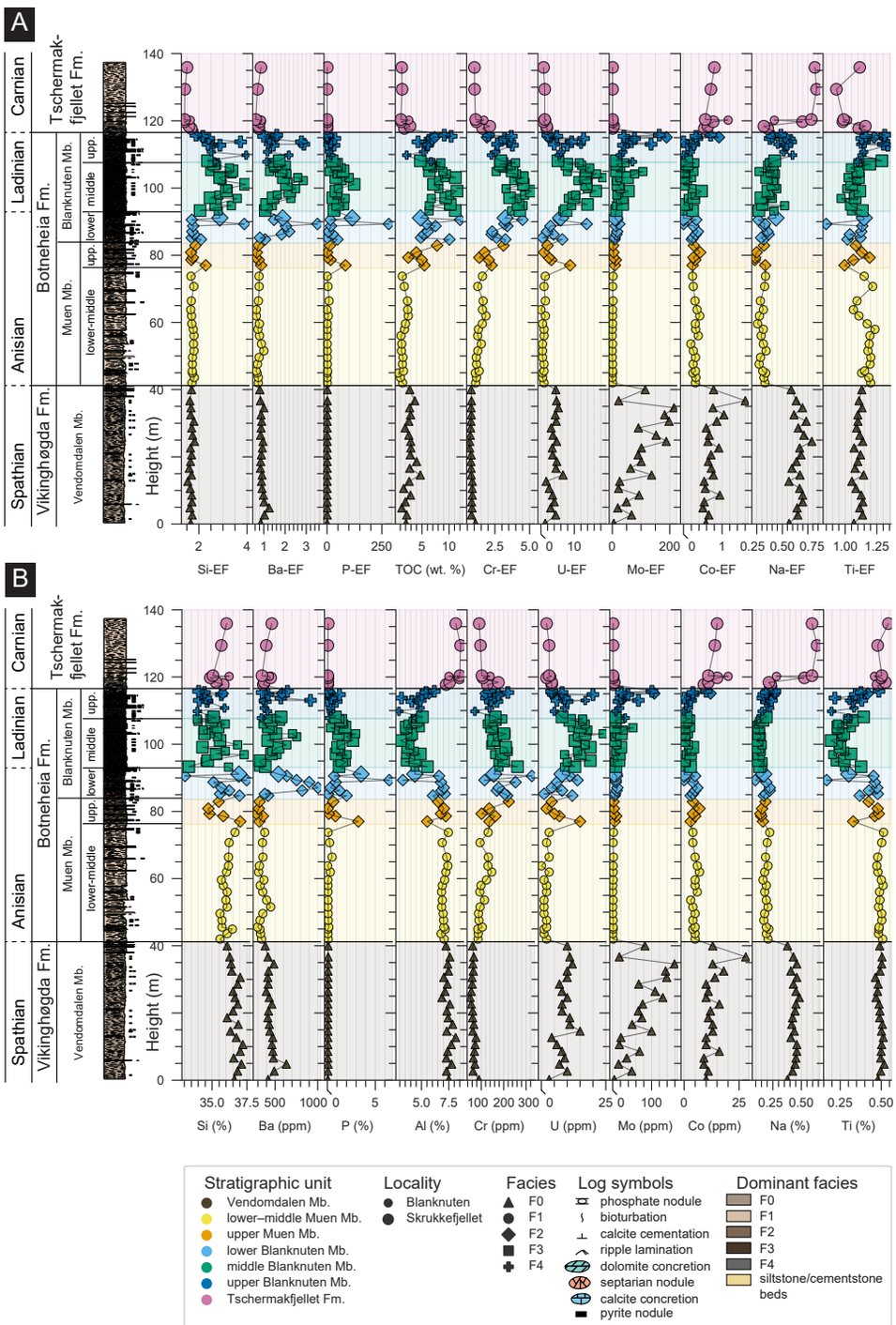

Figure 5.9: Representative log panel of selected geochemical variables (TOC, element EFs and DOP_T) with strong loadings (Fig. 5.8) showing the geochemical development throughout the Spathian–Carnian mudstone succession.

5.8). Wesenlund et al. (2021) reported that the various (informal) sub-units of the Botneheia Formation (i.e. at intra-member scale) show discernable TOC, TIC, TS and bitumen variations related to facies variations and kerogen quality and richness, which further agree with previously published geochemical and Rock-Eval data (Krajewski, 2008; Krajewski, 2013). This indicates that the bulk of the element EFs are genetically related to inferred palaeodepositional processes that affect organic composition and hence source rock formation. Furthermore, most geochemical logs (Fig. 5.8 and Appendix A) clearly record the vertical facies transitions that marks the VenMb–MueMb and BlaMb–TschFm stratigraphic boundaries, demonstrating that they also represent regional geochemical boundaries. Previous studies have assigned these surfaces to the early Anisian and early Carnian flooding events, respectively, and have shown that they delimit a circum-Arctic Middle Triassic 2nd order transgressive–regressive sequence (Mørk et al., 1989). The included parameters and their excursions are therefore highly relevant as palaeoenvironmental proxies and are useful to identify regional sequence stratigraphic boundaries. It is evident that the lower–middle Muen Member F1 and the Vendomdalen Member F0 mudstones are geochemically dissimilar (Figs 5.6 , 5.7 and 5.8).

The NGS SR-1 (Dahlgren et al., 1998), typically assigned to the Anisian Muen Member of the Botneheia Formation (Brekke et al., 2014; Lutz et al., 2021) and its strong correlation with the Spathian Vendomdalen Member F0 mudstones (Figs 5.6 and 5.7) is unfitting and must be investigated. No biostratigraphic age has been assigned to the NGS SR-1 as it was unsuitable for palynological studies (Dahlgren et al., 1998). Isolated kerogen from the NGS SR-1 shows $\delta^{13}C$ = -33.0 ‰ (Dahlgren et al., 1998), very similar to $\delta^{13}C$ values of TOC from the upper Vendomdalen Member mudstones in central Spitsbergen (min. $\delta^{13}C$ = -32.9 ‰) (Hammer et al., 2019, their fig. 4). In both western Spitsbergen and the Sverdrup Basin, $\delta^{13}C$ of TOC from Spathian mudstones are commonly lower than Anisian mudstones and the latter are never lower than -32.0 ‰ (Grasby et al., 2016; Grasby et al., 2020). It was specifically noted that phosphate-nodules were not observed in the sample locality of the NGS SR-1 (Dahlgren et al., 1998). Phosphate-nodules are generally absent in the Vendomdalen Member but common in the Muen Member throughout Svalbard (Vigran et al., 2014). Consequently, it is suggested that the NGS SR-1 was in fact sampled from the Vendomdalen Member, implying that cluster SC3 (which includes the NGS SR-1) only represents this stratigraphic unit (Fig. 5.6).

5.5.2 Primary productivity

The rate of primary productivity in the water column during time of deposition is a fundamental factor controlling the organic richness of mudstones (Bohacs et al., 2005; Katz, 2005). The degree of palaeoproductivity may be assessed

using detrital-corrected P, Si and Ba (e.g. EFs) as proxies (Algeo et al., 2011; Eggimann et al., 1980). Biogenic carbonate enrichment is also a commonly used proxy and may be indirectly estimated using the TIC content and detrital-corrected Ca and Sr (Niebuhr, 2005; Song et al., 2014). In addition, EFs or concentrations of Cu and Ni are useful proxies for the organic matter flux or productivity, assuming sufficiently reducing conditions (Tribovillard et al., 2006). However, as Cu and Ni may also be concentrated in clay minerals, heavy minerals and carbonates (Craigie, 2018), their enrichment may have variable detrital influence. The TIC content and EFs of P, Si, Ba, Ca and Sr are overall low within the Vendomdalen Member F0 mudstones (Figs 5.8 and 5.9, Appendix A), indicating limited primary productivity in eastern Svalbard during the Spathian. A prolonged Early Triassic period with regional nutrient limitation caused by a lowered nutricline may have occurred along the northern margin of Pangea and within the Triassic Boreal Ocean (Grasby et al., 2016; Grasby et al., 2020). The depressed nutricline and limited P could be a result of high ocean temperatures caused by global hothouse conditions during the Early Triassic (Grasby et al., 2016; Sun et al., 2012).

The transition from the Vendomdalen Member F0 mudstones to the lower–middle Muen Member F1 mudstones and the associated negative geochemical excursion correspond roughly to the Spathian–Anisian boundary (Krajewski, 2008; Weitschat and Lehmann, 1983), although this formation boundary is erosional and diachronous throughout Svalbard (Hounslow et al., 2008a; Hounslow et al., 2008b). The phosphate-nodules within these F1 mudstones indicate elevated primary productivity and phosphorite formation due to upwelling of nutrient rich marine waters (Filippelli, 2011), although not sufficient to substantially increase the phosphate cement in the mudstone matrix (Fig. 5.9) or to form an OMZ (Krajewski, 2008; Krajewski, 2013). This coincides with deposition during cooler, more nutrient-rich waters that initiated increased productivity during Middle Triassic times (Grasby et al., 2016; Grasby et al., 2020). The small increase in TIC but limited Si-, P- and Ba-EFs directly above the VenMb–MueMb boundary suggest that the carbonate cement (i.e. TIC) primarily formed in concert with elevated bicarbonate alkalinity in the sediments due to increased microbial oxidation (Taylor and Macquaker, 2014).

The facies change upwards into the upper Muen/lower Blanknuten Member F2 mudstones (Fig. 5.4) marks an abrupt increase in element EFs associated with PC1 and includes the productivity proxies TIC and EFs of Si, P, Ba, Ni and Cu (Figs 5.8 and 5.9). These F2 mudstones therefore mark the onset and development of matrix-supported phosphogenesis, reflecting enhanced upwelling of nutritious deep marine water and elevated phosphogenesis (Krajewski, 2008; Krajewski, 2013). The productivity proxies above provide valid criteria to chemostratigraphically distinguish these F2 mudstones from the underlying F1 mudstones (Figs 5.6 through 5.9).

The persistently high enrichment in TIC, TOC and EFs of Si, Ba, P, Ni and Cu in the middle Blanknuten Member F3 mudstones indicates deposition during periods with the most intense and prolonged primary productivity of all the studied facies types. The increased enrichment in the geochemical nutrient trinity Si-EF, P-EF and TOC is common for major marine phosphorite deposits (Kolodny, 2009). The elevated Si-EF in these F3 mudstones probably reflects the abundant radiolarian moulds reported in these mudstones (Bernhardsen, 2019; Krajewski, 2013). Conversely, the overall depleted Al (%) and Ti (%) (Fig. 5.9B) and the conservative lithogenic elements K, Ga, Rb, Nb, Th (Appendix A) in these F3 mudstones (Fig. 5.9B) indicate low detrital input during the early Ladinian. These proxies thus coincide with former work that considered the F3 mudstones to represent deposition during a highstand phase, including the maximum flooding surface of the Middle Triassic 2nd order TR-sequence (Krajewski, 2008; Krajewski, 2013).

The relative decrease in all the EFs above except TIC in the upper Blanknuten Formation F2/F4 mudstones suggests that primary productivity generally decreased with the onset of the regressive phase in the late Ladinian. The serrated nature of the TOC, Si-EF and Ba-EF logs in these F2/F4 mudstones may correspond with short bursts of intense productivity related to algal blooms (Krajewski, 2013; Vigran et al., 2008). The TIC likely represents the abundant micro-coquina shell deposits previously reported within this unit (Mørk and Bromley, 2008). However, due to the possibly reworked nature of this stratigraphic unit and reported mass mortality events of juvenile bivalves (Krajewski, 2008; Krajewski, 2013; Mørk and Bromley, 2008), the TIC content does not necessarily reflect the productivity rate. The strong correlation between the EFs of the rare earth elements (REEs) Sc, Y, La and Ce with P-EF (Figs 5.4 through 5.8) shows that the P-rich mudstones (F2–F4) are the most important hosts for REEs. Indeed, REEs are typically scavenged from the sea water during authigenic phosphate formation (Tribovillard et al., 2006). Furthermore, carbonate fluorapatite is by far the dominant phosphate mineral in the Botneheia Formation (Krajewski, 2008). As the mineral lattice of carbonate fluorapatite is compatible with REEs (Jarvis et al., 1994), it appears that the enrichment in REEs is directly tied to the abundance of carbonate fluorapatite.

The Tschermakfjellet Formation F1 mudstones record a termination of all the productivity proxies above. This demarcates that upwelling-induced nutrient supply and phosphogenesis ceased in the early Carnian in eastern Svalbard.

5.5.3 Palaeoredox regimes

Degradation of organic matter by scavengers and bacteria in aerobic conditions is relatively quick and efficient, resulting in oxidised and less lipid-rich OM (Demaison and Moore, 1980). In contrast, decomposition under anaerobic conditions, which is mostly due to bacterial activity, is less efficient and typically results in increasingly reduced (i.e. more C-H bonds) and lipid-rich OM with increased oil potential (Demaison and Moore, 1980). The benthic redox conditions are therefore closely tied to the preservation potential of reactive OM. In this study, the palaeoredox conditions for the defined mudstone facies (Fo–F4) are reconstructed using TOC, TS, DOP_T, and EFs of the redox-sensitive elements V, Cr, Fe, Co, Zn, As, Mo, Pb and U (Algeo and Li, 2020; Algeo and Liu, 2020; Algeo and Maynard, 2004; Tribovillard et al., 2006).

The planar lamination, weathered pyrite nodules and lack of bioturbation suggest impeded benthic oxygen supply as the Vendomdalen Member Fo mudstones were deposited. These mudstones show an affinity for sulphide-related redox-proxies (EFs of Co, Fe, Mo, Pb, As) as demonstrated by the EFC3 (Fig. 5.6 and PC2 (Figs 5.7 and 5.8), indicating that they were deposited during sulphate-reducing conditions. The Mo content for these Fo mudstones (mean 71 ± 46 ppm, SD) in combination with DOP values of the Vendomdalen Member (mean 0.43 ± 0.07, SD) from Krajewski (2013) further indicate frequent and intermittent euxinia (Scott and Lyons, 2012). This corroborates with Spathian euxinia reported in western and central Spitsbergen (Grasby et al., 2020; Hammer et al., 2019; Wignall et al., 2016; Xu et al., 2012), and Arctic Canada (Grasby et al., 2013; Grasby et al., 2016). Late Olenekian—presumably Spathian—mudstones on the New Siberian Islands are similar to the mudstones of the Spathian Vikinghøgda Formation in eastern Svalbard (Pčelina and Korčinskaja, 2008), further supporting a synchronous, regional Spathian anoxic event along the northern Pangea margin. As discussed by Grasby et al. (2016), this was possibly triggered by high ocean temperatures caused by the Early Triassic hothouse setting (Sun et al., 2012). On Edgeøya, this resulted in prolonged periods with depleted oxygen conditions favourable for extensive OM preservation (Fig. 5.9).

The abrupt decline in the redox-sensitive element EFs (V, Fe, Co, Ni, Cu, As, Mo, Pb and U), TOC and TS in the Anisian lower–middle Muen Member F1 mudstones strongly indicates that the Spathian benthic euxinia on Edgeøya did not continue into the Anisian (Fig. 5.8). Previously reported *Chondrites* and *Helminthopsis* trace fossils and OM–apatite–pyrite relationships in these F1 mudstones suggest oxygenated and hospitable sea floor conditions as they were deposited (Krajewski, 2013; Wesenlund et al., 2021). This contrasts Lundschien et al. (2014) and Vigran et al. (2014), who considered the entire Muen Member on Edgeøya to represent mudstones deposited during restricted and

dominantly benthic anoxic conditions. The Cr-EF remains the only redox-sensitive proxy with a positive excursion across the VenMb–MueMb boundary (Fig. 5.9). Interestingly, Algeo and Maynard (2004, their fig. 6a) show that euxinic conditions likely result in Cr depletion relative to anoxic (non-sulphidic) conditions at equal TOC values. Thus, the positive Cr-EF excursion directly above the VenMb–MueMb boundary is consistent with a change from euxinic to oxic/dysoxic benthic conditions. However, Cr enrichment is reported to be strongly affected by the land-derived clastic fraction and/or be enriched in carbonate fluorapatite (Tribovillard et al., 2006). The observed Cr-EF excursion could thus be unrelated to palaeoredox variations (Fig. 5.9).

The upper Muen Member F2 mudstones up to the middle Blanknuten Member F3 mudstones mark a strong positive trend in EFs of Cr, Zn, V, As, U, but also TOC, TS and DOP_T (Figs 5.6 through 5.9). This is also captured convincingly by PC1 (Fig. 5.8) and the DOP curve from Krajewski (2013, , their fig. 21). This indicates that the F2 mudstones of the upper Muen/lower Blanknuten members were deposited in less oxic (dysoxic) conditions compared to the underlying F1 mudstones of the lower–middle Muen Member. The overall high enrichment in the redox-sensitive elements in the middle Blanknuten Member F3 mudstones above thus implies that this facies was deposited during greater oxygen depletion, likely triggered by excessive benthic oxygen demand. This agrees well with Krajewski (2008) and Krajewski (2013), who interpreted the facies development within the lower–middle Muen Member to the middle Blanknuten Member interval to indicate deposition under progressively increasing primary productivity, OM sedimentation, ultimately forming a widespread OMZ.

The transition into the upper Blanknuten Member F2/F4 mudstones shows variable but overall decreasing concentrations in TOC, TS and EFs of U, Cr, V, indicating deposition during more oxic conditions relative to the underlying F3 mudstones. Abundant *Thalassinoides* burrows within these mudstones show that the O_2–H_2S boundary must have been frequently below the sediment–water interface during deposition (Krajewski, 2013; Mørk and Bromley, 2008). However, this does not explain the increase in Mo-EF in these F2/F4 mudstones, which in fact suggests euxinic conditions (Fig. 5.9). This contrasts with Krajewski (2013), who only considered the middle Blanknuten Member to display benthic euxinia within the entire Botneheia Formation.

The cessation of the EFs of U and Mo (and TOC) across the BlaMb–TschFm boundary marks the onset of the well-ventilated, oxic Tschermakfjellet Formation F1 mudstones. This formation is overall poor in pyrite but is enriched in siderite cement and siderite nodules (Krajewski, 2013; Mørk et al., 1982). The elevated Co-EF (Fig. 5.9) appears thus to reflect the siderophile properties of this element rather than reduced oxygen conditions.

5.5.4 Water mass restriction

The relationship between U, Mo and TOC (Fig. 5.9) enrichment in mudstones and the ratios Mo/U and Mo/TOC (Figs 5.10 and 5.11) are used to evaluate restricted vs. unrestricted benthic water masses in modern and ancient basins (Algeo and Lyons, 2006; Algeo and Maynard, 2008; Algeo and Rowe, 2012; Algeo and Tribovillard, 2009; Tribovillard et al., 2012). Uranium is primarily enriched under suboxic or less oxygen-rich conditions (i.e. in reducing conditions without the requirement of free H_2S) and is only scavenged within the sediment (Algeo and Maynard, 2004; Algeo and Tribovillard, 2009). However in non-sulphidic anoxic conditions, U strongly correlates with TOC, exemplifying that U enrichment is not necessarily proportional to redox potential (Algeo and Maynard, 2004).

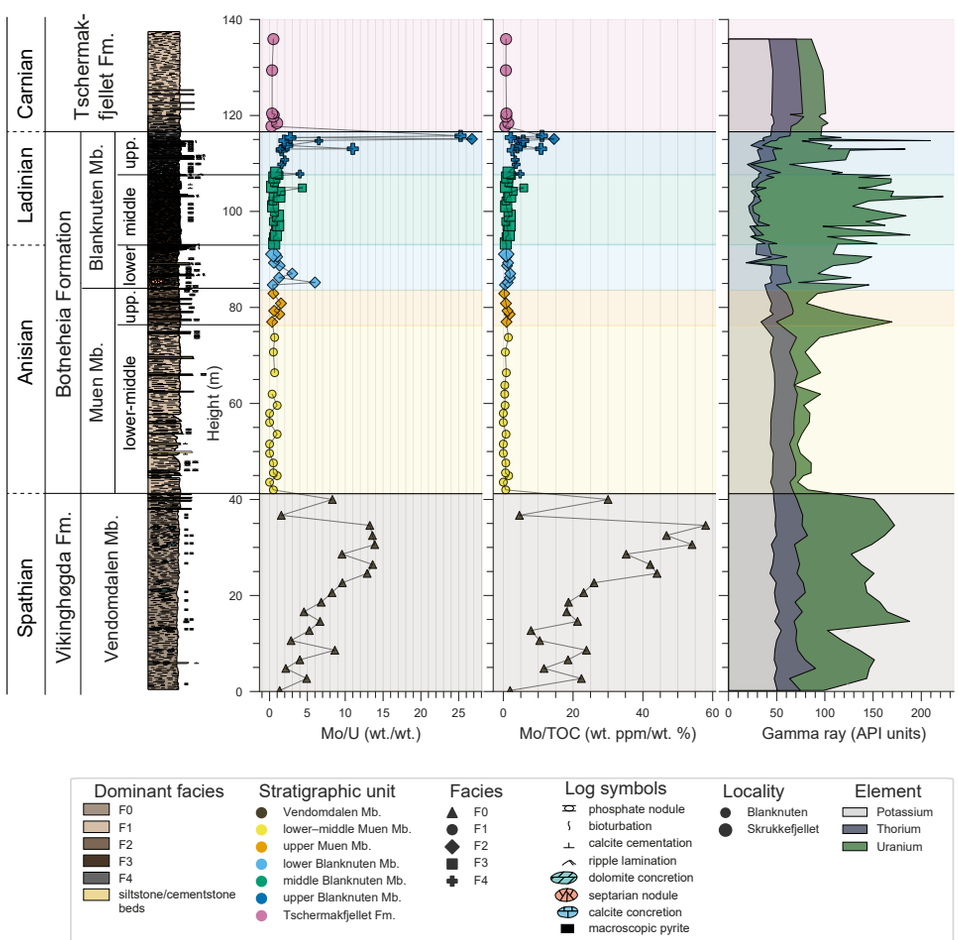

Figure 5.10: Logs of Mo/TOC, Mo/U and synthetic spectral gamma ray response calculated from K, Th and U compared with the lithostratigraphic division.

Similarly, Mo can be scavenged at or below the sea floor but requires the presence of H_2S (Helz et al., 2011; Helz et al., 1996). Strong Mo enrichment relative to U (i.e. 3–10 times greater than seawater Mo/U weight/weight concentrations) relies on active Mn-Fe redox cycling that effectively "pumps" Mo into the sediments, and is most efficient when the O_2–H_2S boundary frequently fluctuates above and within the sediment–water interface (Tribovillard et al., 2012). Furthermore, while the Mo/TOC ratio is a commonly used water mass restriction proxy, it cannot be applied to unrestricted upwelling systems as oxygen depletion in such settings may be controlled by variable primary productivity rather than hydrogeographic effects (Algeo and Rowe, 2012).

The variable U enrichment (Figs 5.8 and 5.9) will affect the gamma ray (GR) expression of the studied mudstone section. A synthetic GR log is included (Fig. 5.10) for interpretation and correlation to offshore Lower–Middle Triassic mudstone equivalents (i.e. the Steinkobbe Formation; see Section 5.5.6). The GR log was calculated from U, Th and K (Ellis and Singer, 2007, their equation 11.1): $GR_{API} = 8U + 4Th + 16K$, where GR is given in API units, and U, Th and K are given in ppm, ppm and % respectively. The geochemical logs of U (ppm), Th (ppm) and K (%) are available in Appendix A.

The Mo/TOC ratios of the Vendomdalen Member Fo mudstones are mostly comparable to Mo/TOC trend of the modern-day Saanich Inlet in western Canada (Fig. 5.11), which is a seasonally euxinic basin (Algeo and Lyons, 2006; Francois, 1988). The Mo vs. TOC plot (Fig. 5.11) and the Mo-EF vs. U-EF (Fig. 5.12) plot of the Vendomdalen Member Fo mudstones also correlate to the latest Albian–earliest Campanian La Luna Formation source rock (Maracaibo Basin, Venezuela) that was deposited in a basin bounded by shallow sills and during the Cenomanian–Turonian OAE-2 and the Coniacian–Santonian OAE-3 (Mongenot et al., 1996; Tribovillard et al., 2012). Overall, this suggests that Mn-Fe redox cycling was highly effective and caused Mo-enriched muds during deposition of these Fo mudstones. Similarly, Chen et al. (2019) report active Mn–Fe redox cycling constrained to a mid-Spathian section (Chaohu, east China) deposited in the Early Triassic eastern palaeo-Tethys Ocean. Zhang et al. (2018) suggest that global benthic anoxia was particularly evident at the Spathian–Anisian transition, termed the C4 event. It may thus be speculated that the strong and upwards increasing Mo enrichment in the Spathian Vendomdalen Member Fo mudstones (Fig. 5.9) formed due to global ocean stratification that promoted worldwide intermittent benthic euxinia.

However, the observed euxinia and interpreted weak water mass restriction during deposition of the Vendomdalen Member Fo mudstones could be due to local relief related to inherited bathymetry caused by underlying Upper Palaeozoic fault blocks (Anell et al., 2016; Steel and Worsley, 1984). At a regional scale, a structurally controlled bedrock sill located between the Alaska-

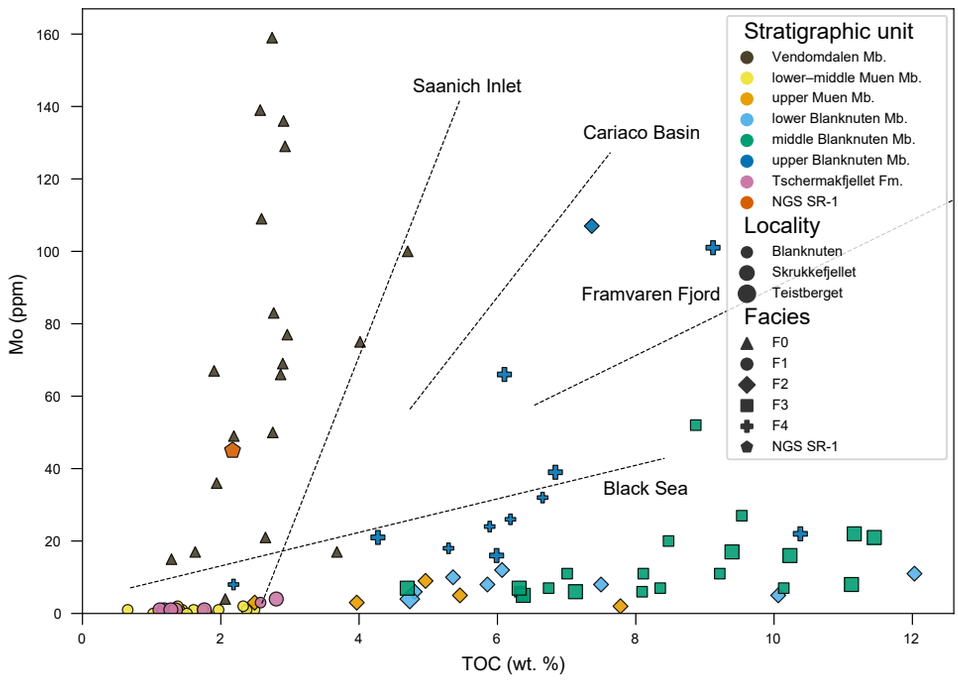

Figure 5.11: Cross plot of TOC (%) vs Mo (ppm). The dashed lines are collected from Algeo and Lyons (2006) and represent linear regression trends of TOC and Mo content in modern basins with variable water mass restriction, where the Saanich Inlet is the least restricted, and the Black Sea the most restricted. The bulk data from the Blanknuten Member mudstones correlate with a Black Sea water mass restriction type but see Section 5.5.4 for discussion on possible misinterpretation.

Chukotka microcontinent (also known as Crockerland; see Embry, 1993) and Arctic Canada could hypothetically enable a silled or restricted basin setting for the entire TBO (Leith et al., 1993; Sømme et al., 2018). The Bosporus Strait, which serves as a narrow connection between the restricted Black Sea and the less restricted Mediterranean Sea, is a modern example of such a silled basin setting (Demaison and Moore, 1980). However, the high Mo/U and Mo/TOC ratios (Figs 5.10 and 5.11) and Mo-EF vs U-EF (Fig. 5.12) recorded in this study do not suggest such an extreme restriction compared to that of the Black Sea, which has significantly lower Mo/U and Mo/TOC ratios (cf. Algeo and Lyons, 2006; Algeo and Tribovillard, 2009).

The Mo-EF, U-EF, TOC, Mo/U and Mo/TOC ratios abruptly decrease above the VenMb–MueMb boundary (Figs 5.9, 5.10 and 5.11), indicating that the Anisian lower–middle Muen Member F1 mudstones were deposited in oxygenated and ventilated waters relative to the Vendomdalen Member F0 mudstones. The VenMb–MueMb boundary denotes a regional early Anisian flooding event (Mørk et al., 1989) and represents the onset of rising sea level that likely

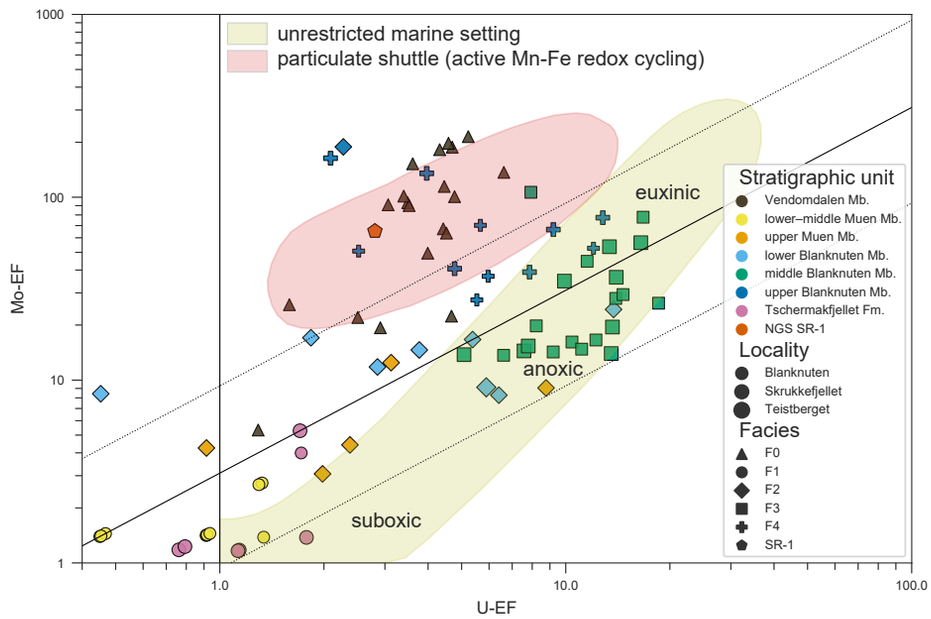

Figure 5.12: Cross plot of U-EF vs Mo-EF. The particulate shuttle field, unrestricted marine field and the diagonal solid line representing modern day seawater U/Mo ratio = 3.1 (wt./wt.) are taken from Tribovillard et al. (2012) and based on Algeo and Tribovillard (2009). The dotted diagonal lines represent multiples of 0.3 and 3.

enhanced the physical connection between the Boreal Sea and the deep Panthalassic Ocean during the early Anisian, promoting mixing of shelf waters with nutritious upwelling water masses (Krajewski, 2008; Krajewski, 2013). A cooling climate during the Middle Triassic probably raised the thermocline to a substantially shallower position, also resulting in improved oxygen conditions in the basin (Grasby et al., 2016; Grasby et al., 2020).

The Mo-EF and U-EF relationship in the Anisian upper Muen Member mudstones (F2) and Anisian–Ladinian lower–middle Blanknuten Member mudstones (F2–F3) indicates a hydrodynamically unrestricted marine setting (Fig. 5.12). The observed coupling between redox and productivity proxies (Figs 5.6 through 5.9), strongly suggests that the recorded oxygen depletion was promoted by a growing primary production, organic sedimentation and benthic oxygen consumption, likely caused by high nutrient availability due to the increasing influx of deep marine water from the Panthalassic Ocean. The Mo-EF and U-EF trends of these F2 and F3 mudstones directly overlap with those of the Upper Jurassic Kashpir oil shales of the Russian Platform (Riboulleau et al., 2003; Tribovillard et al., 2012). The Kashpir oil shales were deposited in an epicontinental unrestricted marine environment characterised by high primary productivity and frequently fluctuating oxic to anoxic conditions (Riboulleau

et al., 2003). High concentrations of redox-sensitive elements and TOC within the intensively burrowed but oil-prone Kashpir mudstones show that the redox boundary was close to the sediment-water interface and frequently within the sediment during deposition. A similar depositional setting has also been suggested for the mudstones of the upper Muen and the lower Blanknuten members (Krajewski, 2008; Krajewski, 2013).

The Ladinian middle Blanknuten Member F3 mudstones indicate deposition during maximum primary productivity and in euxinic bottom waters (Figs 5.8, 5.9 and 5.12), suggesting that benthic OM degradation stalled as oxygen demand exceeded the supply. Neither this study or that of Wesenlund et al. (2021) documented bioturbation in these F3 mudstones. However thin, but common, peloidal packstone layers provide evidence of hydrodynamic activity in this unit (Krajewski, 2013). Vigran et al. (2014) reported abundant *Daonella* bivalves in the middle Blanknuten Member mudstones. *Daonella* bivalves probably lived on top of the soft sediment as "snowshoe" strategists (Schatz, 2005), indicating short, recurrent periods of habitable benthic bottom waters despite the prevailing oxygen deficient environment. The inefficient or even inactive Fe–Mn redox cycling as indicated by the Mo-EF vs U-EF ratio (Fig. 5.12) also supports that the redox boundary was fluctuating at the sediment–water interface and above, but rarely (or never) within the sediment, in agreement with Krajewski (2013).

The late Ladinian upper Blanknuten Member F2/F4 mudstones mark the reintroduction of efficient Mn-Fe redox cycling and Mo enrichment comparable to the Vendomdalen Member mudstones (Fig. 5.12), indicating that the upper Blanknuten Member F4 mudstones were largely deposited during intermittent benthic euxinia. This contrasts with the findings of Krajewski (2013), who interpreted true euxinic conditions to have only occurred during deposition of the middle Blanknuten Member F3 mudstones. The upper Blanknuten Member F2/F4 mudstones were likely deposited in a gradually shallowing environment, which experienced a stepwise change from euxinic to dysoxic conditions due to water mass stirring and ventilation caused by the shoaling of the basin (Krajewski, 2008; Krajewski, 2013). This could have initiated a weakly restricted silled basin setting, possibly enhanced by undulating bottom morphology if present. The regressive development and the relative position to the approaching TBO delta system or Greenland to the west probably increased the influx of fresh water and riverine nutrients as indicated by common terrestrial organic matter within this unit (Krajewski, 2013). The influx of riverine water and nutrients could have triggered algal blooms of *Tasmanites* and resulted in brackish waters and formation of halocline/thermocline stratification (Høy and Lundschien, 2011; Vigran et al., 2008), promoting water mass restriction in the basin without the aid of underlying bathymetry.

The lowermost Tschermakfjellet Formation F1 mudstones denote an abrupt termination of elevated Mo/TOC and Mo/U ratios (Figs 5.11 and 5.12). The onset of oxygenated conditions that prevailed in the early Carnian during deposition of these F1 mudstones may have been caused by oceanographic reconfiguration that lowered the preservation potential following the base Carnian flooding (Høy and Lundschien, 2011).

5.5.5 Influences on the non-biogenic mineral fraction

The EFC1 from the HCA (Fig. 5.6; Table 5.4) and the dominant element EFs with positive loadings on PC3 (Fig. 5.8) contain several elements (Ga, Rb, Cs, Th, K, Ti, Nb) that are commonly associated with non-carbonate minerals (cf. Craigie, 2015; Craigie, 2018). Variations in EFC1 and PC3 (except for TIC and Mg) appear therefore to be influenced by changes in the non-biogenic mineral fraction. The variations in EFC1 and PC3 could therefore provide important information on the resulting rock composition due to, e.g., varying detrital grain size, switching provenance area, palaeoweathering or authigenic mineral precipitation (Boës et al., 2011; Craigie, 2015; Craigie, 2018; Craigie et al., 2016; Rothwell and Croudace, 2015).

Both Ga and Cs are typically correlated with clay minerals and feldspars, and Nb and Th with heavy minerals (Craigie, 2018). Aluminium, K and Rb are principally associated with aluminosilicate minerals (i.e., clays) (Calvert and Pedersen, 2007), but K is also hosted by K feldspar (Craigie, 2018). Titanium is often assigned to represent silt-sized Fe-rich clastic mineral particles (Rothwell and Croudace, 2015). Zirconium is almost exclusive to zircons (Craigie, 2018), and the Zr/Al ratio (Zr-EF in this study) is useful as a grain size proxy as zircons commonly show grain sizes coarser than clays (Atar et al., 2019; Liang et al., 2013; Pang et al., 2018). Sodium is linked with smectite, plagioclase or halite (Craigie, 2018), however, halite is a very unlikely mineral to occur within the studied mudstone succession as the depositional environment in eastern Svalbard was a shallow–open marine shelf during the Lower–Middle Triassic (Fig. 5.2). Consequently, the stratigraphic variations in EFC1 (Fig. 5.6) and PC3 (Figs 5.7 and 5.8)–including Zr-EF and Na-EF but excluding TIC and Mg–appear to mainly record compositional changes between clay minerals, feldspars and heavy minerals. The significant vertical changes in the EFs of Na, K, Ti, Ga, Rb, Zr, Nb, Cs and Th across the regionally extensive VenMb–MueMb or BlaMb–TschFm lithostratigraphic boundaries therefore confirm the chemostratigraphic significance of these elements (Figs 5.8 and 5.9; Appendix A).

The negative shifts in Na-EF and Zr-EF but positive shifts in Rb-EF and Cs-EF across the VenMb–MueMb boundary (Figs 5.8 and 5.9; Appendix A) corre-

spond to the transition from coarser-grained (F0) to finer-grained (F1) mudstones seen on Edgeøya (Krajewski, 2008; Vigran et al., 2014, This study). This chemostratigraphic boundary thus correlates to the previously reported earliest Anisian flooding event and associated relative decrease in grain size and sedimentation rate (Mørk et al., 1994; Vigran et al., 2014). Spathian–early Anisian sedimentation rates in Svalbard were both relatively higher compared to the late Anisian–Ladinian (Hounslow et al., 2008a). Consequently, these variations do not appear to reflect a change in provenance area, as the muds that eventually formed the Vikinghøgda and Botneheia formations on Edgeøya were both dominantly sourced from the west, i.e. Greenland (Gilmullina et al., 2021; Mørk et al., 1982).

The significant decrease in the Ti-, Nb-, Rb- and Zr-EFs across the BlaMb–TschFm boundary also points to a decrease in relative grain size. As PC3 increases upwards within the Botneheia Formation (Fig. 5.8), the upper Blanknuten Member F2/F4 mudstones appear to record the coarsest mudstones within this formation. This may reflect increased sediment influx during the regressive phase of the Middle Triassic TR-sequence following the Ladinian highstand phase (F3 mudstones) or increased hydrodynamic reworking and winnowing related to shallower water depths (Krajewski, 2013; Mørk et al., 1982; Mørk et al., 1989). The relative increase and decrease in Na-EF and K-EF above this boundary could suggest that plagioclase (Na-rich) became more abundant relative to K-feldspar (K-rich) (Fig. 5.8). However, dedicated mineralogical analyses are necessary to confirm the proposed element:mineral links as authigenic mineral precipitation may overprint the detrital mineral signature (Craigie, 2018). Still, Uralian-sourced sands from Anisian and Carnian deposits on the southern Barents Shelf host abundant plagioclase (Fleming et al., 2016; Line et al., 2018), while age-equivalent Caledonian-derived sands typically comprise less feldspars, although with relatively more K-feldspar (Fleming et al., 2016). This could indicate that the Tschermakfjellet Formation F1 mudstone samples in SC4 (low Na-EF, high K-EF; Fig. 5.6) are still dominantly Caledonian (from NW–W), while the overlying SC2 F1 mudstone samples from the same formation (High Na-EF, low K-EF; Fig. 5.6) are dominantly Uralian-sourced (from E–SE) (cf. Fleming et al., 2016; Line et al., 2018). The lowermost Tschermakfjellet Formation F1 mudstones could therefore have been deposited during a gradually increasing influx of Uralian sediments that eventually became the dominant provenance in eastern Svalbard during the Early Carnian (Bue and Andresen, 2014; Gilmullina et al., 2021).

5.5.6 Source rock potential and regional correlation

A flowchart of important variations in source rock-forming processes (discussed in Sections 5.5.2 to 5.5.5) is proposed for each stratigraphic unit and their

resulting source potential (Fig. 5.13) (based on Katz, 2005, their fig. 1). From the proxies discussed above and the flowchart, a conceptual depositional model is presented for the Lower to Middle Triassic succession in eastern Svalbard (Fig. 5.14). The relative source rock potential between the Vendomdalen, lower–middle Muen and the upper Muen/entire Blanknuten members (Fig. 5.14) fits well with replotted TOC-S2 and HI data from Bjorøy et al. (2009) (Fig. 5.15). This shows that immature and oil-prone mudstones within these stratigraphic units have intermediate, lower and higher oil generation potential respectively.

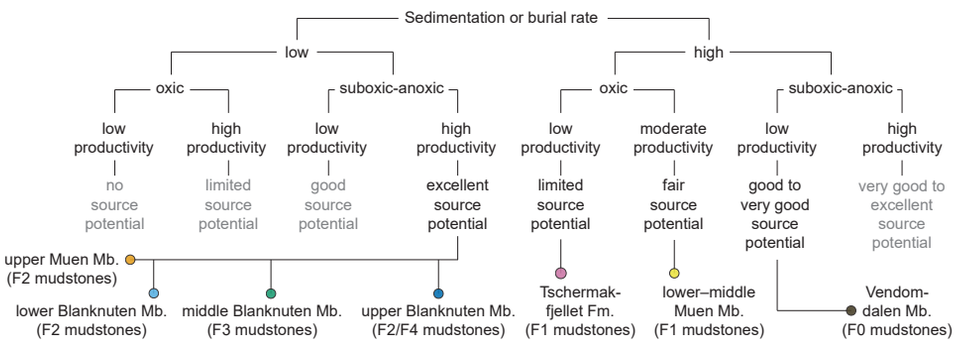

Figure 5.13: Flowchart of the three primary factors controlling source rock development and their relative influence on the Spathian–Carnian source rock potential in Svalbard. Grey text represents combinations that are generally not met by the studied units. Feedback loops are not considered. Based on Isaksen and Bohacs (1995) and Katz (2005, their fig. 1).

According to Lundschien et al. (2014), the mudstones of the Spathian–Anisian Steinkobbe Formation in the Svalis Dome, southern Barents Sea (Fig. 5.1) are facies-equivalent (i.e. of the same palaeodepositional environment but time-transgressive) to those from the Anisian–Ladinian Botneheia Formation in Svalbard. The Spathian Vendomdalen Member of the underlying Vikinghøgda Formation in Svalbard is typically excluded in all these types of comparisons (Lundschien et al., 2014; Lutz et al., 2021; NPD, 2017; Riis et al., 2008). A discussion on the correlation, source potential and regional distribution of the onshore and offshore Spathian to Ladinian (and Carnian) successions follows below.

Immature Spathian Vendomdalen Member Fo mudstones in eastern Svalbard show liquid hydrocarbon generation potential (Fig. 5.15) (mean HI = 346 ± 73 mg HC/g TOC, SD). This is almost identical to the Spathian lower Steinkobbe Formation in the Svalis Dome (core 7323/07-U-04; mean HI = 346 ± 116 mg HC/g TOC, SD) (Abay et al., 2018). Both units are largely unbioturbated (Table 5.3; see also Mørk and Elvebakk, 1999). In the Blanknuten locality, the upper part of the Vendomdalen Member Fo mudstones probably encompass the Late Spathian *Jerseyiaspora punctispinosa* palynozone, although the

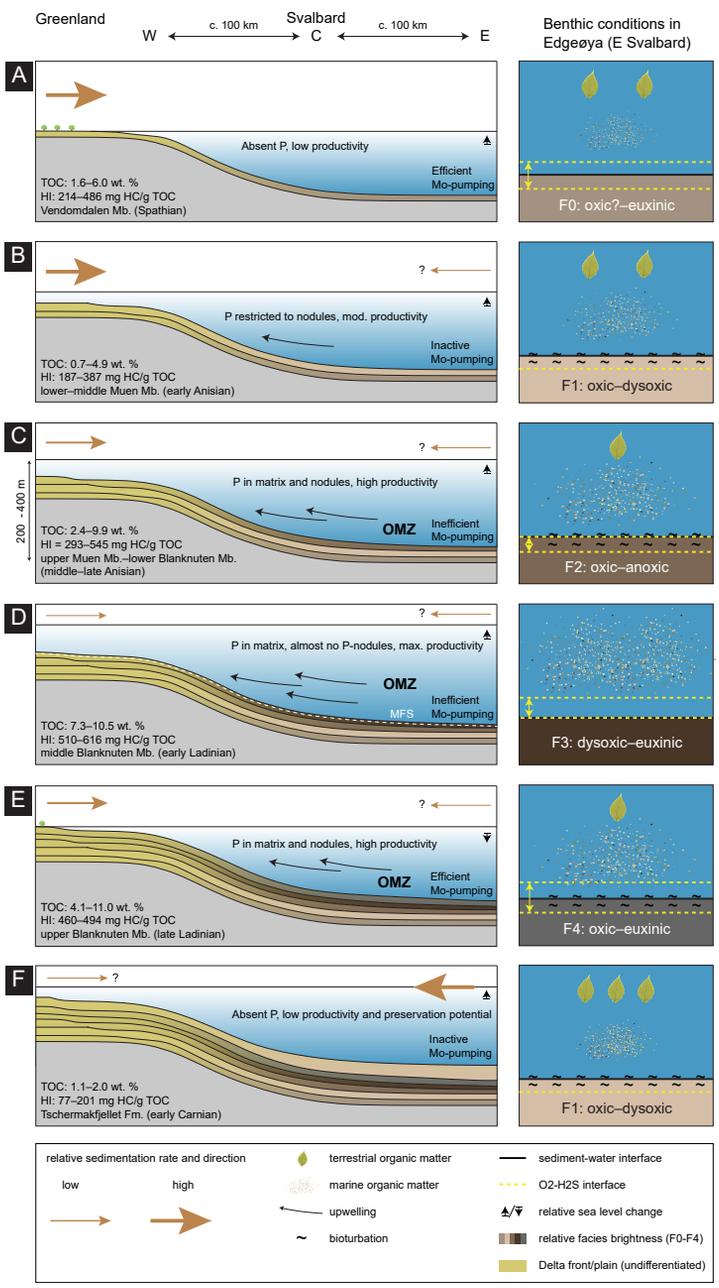

Figure 5.14: Simplified conceptual depositional model of the Spathian–Carnian (A through F; details are discussed in Section 5.5.6) mudstone succession in W (western), C (central) and E (eastern) Svalbard demonstrating how fluctuations in primary productivity, benthic redox and terrigenous flux influenced source rock richness and quality. TOC and HI are based on immature, oil-prone samples of the Vendomdalen Member in eastern Svalbard collected from Bjorøy et al. (2009) (see Fig. 5.15 for explanation), while the TOC and HI data for the subunits of the Botneheia Formation and the Tschermakfjellet Formation are from immature to early mature samples on western and northern Edgeøya collected from Krajewski (2013). Note the similar relative change in TOC compared to Figure 5.10. The position of the delta top and delta front in the west is based on Bjerager et al. (2019), Glørstad-Clark et al. (2010), Klausen et al. (2015), Lundschien et al. (2014), and Riis et al. (2008). Relative sea-level changes and occurrence of an oxygen minimum zone (OMZ) are based on Krajewski (2008) and Krajewski (2013). Ages of the Botneheia and Steinkobbe formations are collected from Hounslow et al. (2008a), Krajewski and Weitschat (2015), Vigran et al. (1998), and Vigran et al. (2014). The correlated lithostratigraphy and chronostratigraphy should be considered approximate and relative as the informal sub-units of the Botneheia Formation and their respective boundaries exhibit a variable degree of diachronicity (Krajewski, 2008). The implied benthic palaeoredox conditions are only covered for the Edgeøya region where the data coverage is sufficient.

lower Fo mudstones may include the Early Spathian *Pechorosporites disertus* palynozone (Vigran et al., 2014). In the Svalis Dome, the lower (but not lowermost) Steinkobbe Formation is also assigned to the *J. punctispinosa* palynozone (Vigran et al., 2014). Thus, the Spathian period may have seen elevated preservation potential that was fairly synchronised throughout the TBO. This could have been triggered by sluggish water mass circulation causing benthic euxinia (Fig. 5.15A) due to the Early Triassic hothouse conditions (Grasby et al., 2016; Grasby et al., 2020) rather than nutrient-driven productivity (upwelling or fluvial) and oxygen demand. This would explain why the uppermost Spathian mudstones of the lower Steinkobbe Formation (core 7323/07-U-04) host far less phosphate-nodules compared to the Anisian mudstones of the upper Steinkobbe Formation (core 7323/07-U-01 and 7323/07-U-09) (Mørk and Elvebakk, 1999, their fig. 10).

Immature and oil-prone lower–middle Muen Member F1 mudstones in eastern Svalbard (implied mode HI ca 320–340 mg HC/g TOC) (Fig. 5.15) and the lowermost Anisian mudstones in the Steinkobbe Formation (core 7323/07-U-04) are assigned to the Early Anisian *Anapiculatisporites spiniger* palynozone (Vigran et al., 2014). While the lower Anisian F1 mudstones in Svalbard are OM-rich and record the onset of increased productivity from the underlying Fo mudstones (Figs 5.13 and 5.14), they still show relatively lower oil generation potential than the Fo mudstones, perhaps due to increased marine OM degradation and preferential preservation of terrestrial OM (Fig. 5.14) (Wesenlund et al., 2021). Interestingly, the lower Steinkobbe Formation also shows a prominent decrease in TOC and GR response (Mørk and Elvebakk, 1999, their fig. 3) at the Spathian–Anisian boundary (compare with Fig. 5.10), suggesting that early Anisian benthic oxygenation was regional in the TBO. In fact, Krajewski (2008), Krajewski (2013), and Wesenlund et al. (2021) considered these lowermost Anisian F1 mudstones to have been deposited during well-ventilated shelf conditions. This would explain the lower organic richness in these mudstones (mean TOC = 1.58 ± 0.51 wt. %, SD) compared to the underlying Fo mudstones (mean TOC = 2.70 ± 0.79 wt. %, SD) (Fig. 5.9). The latter also exhibit a max. HI = 486 mg HC/g TOC which is not expected to be more than ca 400 mg HC/g TOC for the Anisian F1 mudstones (Krajewski, 2013). Lower Anisian F1 mudstones are therefore probably less oil-prone than the underlying upper Spathian mudstones throughout large parts of the Norwegian Barents Sea.

The phosphatic, oil-prone and bioturbated F2 mudstones of the upper Muen and most of the lower Blanknuten members in eastern Svalbard (Fig. 5.14) are assigned to the middle Anisian *Triadispora obscura* palynozone (Vigran et al., 2014). In the same area, the F2 mudstones of the uppermost lower Blanknuten Member are assigned to the late Anisian *Protodiploxypinus decus* palynozone (Vigran et al., 2014). These F2 mudstones are therefore facies-

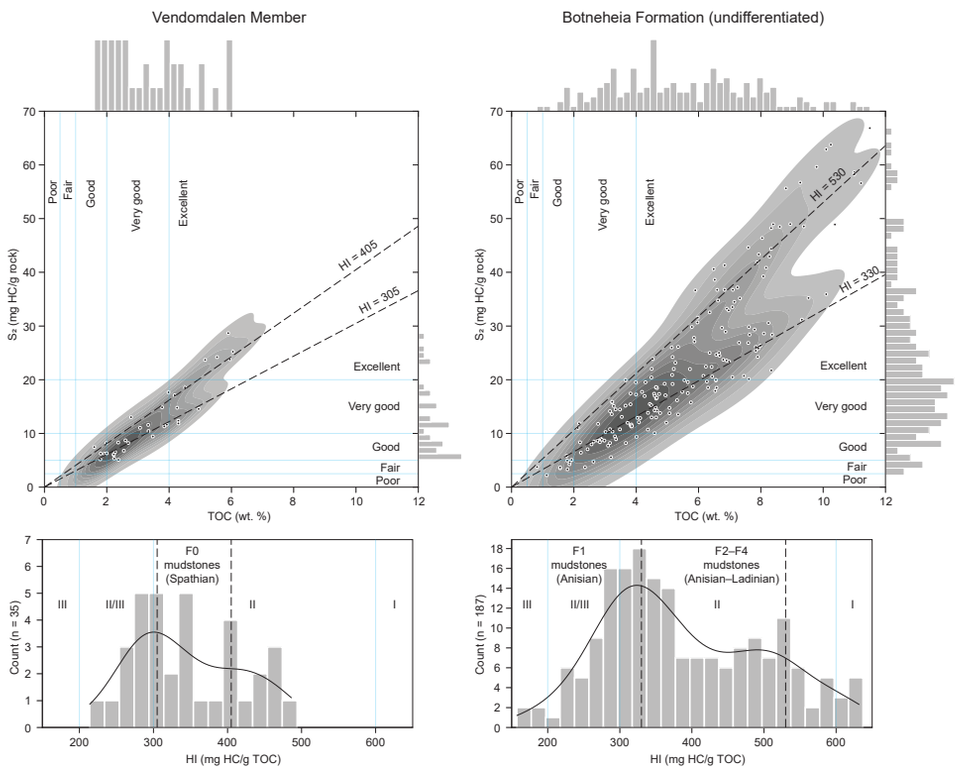

Figure 5.15: Scatter plots, histograms and kernel density estimates of TOC, S_2 and HI (Rock-Eval 6) of immature and oil-prone samples from the Vikinghøgda (n = 35) and Botneheia (n = 187) formations. The data was collected from Bjorøy et al. (2009, their fig. 3a) using the WebPlotDigitizer data extraction software (Rohatgi, 2021). Bjorøy et al. (2009) did not differentiate the data based on members or facies. As only the Vendomdalen Member of the Vikinghøgda Formation is considered oil prone (kerogen type II/III) (Mørk et al., 1999b), it is assumed that all the plotted Vikinghøgda Formation samples are from this member. The HI isolines = 305 and 405 mg HC/g TOC highlight the positively skewed HI distribution. The lower–middle Muen Member F1 mudstones are considered kerogen type II/III mudstones, while the mudstones of the upper Muen–Blanknuten members (F2–F4) are kerogen type II (Krajewski, 2013). The bimodal HI distribution for the Botneheia Formation and the two HI isolines at 330 and 530 mg HC/g TOC most likely reflect representative, typical HI values for immature and oil-prone non-phosphogenic (F1) and phosphogenic (F2–F4) mudstone facies respectively.

and age-equivalent to the organic-rich, phospate-nodule rich and bioturbated mudstones in core 7323/07-U-01 (*T. obscura* palynozone) and 7323/07-U-09 (*P. decus* palynozone) of the middle–upper Steinkobbe Formation (Vigran et al., 1998). The onset of intense middle Anisian phosphogenesis appears thus to be synchronous in the TBO, perhaps triggered by the heightened water column and unrestricted waters that promoted upwelling and marine nutrient supply (Figs 5.13 and 5.14), ultimately forming an OMZ (Grasby et al., 2016; Grasby et al., 2020; Krajewski, 2013). The middle–upper Anisian phosphogenic mudstones in the Svalis Dome are less oil-prone than their Svalbard counterparts (Abay et al., 2018), suggesting that middle–upper Anisian source rock potential increases northwards from the southern Barents Sea. This agrees with the common expectation of higher source rock potential towards the more distal parts of the TBO delta system clinoforms (Lutz et al., 2021).

The middle Blanknuten Member F3 mudstones in eastern Svalbard are assigned to the Ladinian *Echinitosporites iliacoides* palynozone (Vigran et al., 2014). These are highly oil-prone and were deposited during maximum drowning and maximum primary productivity, forming an extensive OMZ (Fig. 5.14) (Krajewski, 2013). These F3 mudstones are age-equivalent to the deltaic and more proximal lower Snadd Formation (Tschermakfjellet Formation facies-equivalent) in the Svalis Dome (cores 7323/07-U-10, 7323/07-U-05, 7323/07-U-02) (Vigran et al., 1998). Ladinian F3-type mudstones appear thus to be restricted to the northern Barents Sea, as the deep shelf conditions necessary for OM accumulation had ceased in the south-eastern Barents Sea at that time (Fig. 5.2) (Klausen et al., 2015). Still, the lateral distribution of the F3 mudstones is not known. Mapping their extent would provide important knowledge of their significance as source rocks in the areas open for commercial exploration in the Norwegian Barents Sea.

The oil-prone upper Blanknuten Member F2/F4 mudstones belong to the same palynozone as the F3 mudstones (Ladinian) and record the regressive phase of the Middle Triassic TR-sequence (Fig. 5.14) (Krajewski, 2013; Vigran et al., 2014). According to Fleming et al. (2016, their fig. 1), these upper Ladinian mudstones indicate less south-eastward extent relative to the underlying F3 mudstones, possibly due to the gradually approaching TBO delta system (Fig. 5.2). East of Kong Karls Land (Fig. 5.1), immature upper Ladinian mudstones (core 7831/02-U-02) show excellent oil generation potential (mean HI = 537 ± 34 mg HC/g TOC, SD), several phosphate-nodules and relatively high and variable Mo/TOC ratios (1.34–28.13, mean 9.38 wt. ppm/wt. %) (Xu et al., 2014). These Mo/TOC ratios can only correspond with the upper Blanknuten Member in Edgeøya (Fig. 5.10). Thus, the upper Ladinian F2/F4 mudstones and the benthic intermittent euxinia (Fig. 5.14) may cover a 250 km SW–NE transect in the northern Barents Sea (Fig. 5.2), suggesting that these late Ladinian palaeodepositional conditions were regional.

The progradation of the TBO delta system during the early Carnian (Fig. 5.14) (Tschermakfjellet Formation F1 mudstones) effectively terminated the conditions to form organic-rich phosphatic mudstones in eastern Svalbard, in agreement with Lundschien et al. (2014). However, upwelling and primary productivity were still highly active towards the west in the North Slope Basin, northern Alaska, eventually forming the organic-rich and phosphatic mudstones of the Middle (not Lower) to Upper Triassic Shublik Formation (Parrish et al., 2001). The lack of Late Triassic oil-prone phosphatic source rocks in the northern Norwegian Barents Sea is therefore linked with changes in depositional environment rather than climate-induced ocean reconfigurations as Late Triassic phosphatic mudstones exist elsewhere in the TBO.

5.6 Conclusion

This study combines sedimentological observations with a hitherto unexplored whole-rock multi-elemental chemostratigraphic framework of an excellently exposed Lower–Upper Triassic mudstone succession in eastern Svalbard, Arctic Norway. The contrasting elemental assemblages of the assigned lithostratigraphic units and their associated mudstone facies prove that whole-rock elemental chemostratigraphy is an effective tool to recognise principally different organic-rich Triassic mudstones with similar source potential. Abrupt elemental chemostratigraphic excursions at the tops of the circum-Arctic Lower and Middle Triassic 2nd order TR–sequences provide excellent criteria to map these important sequence stratigraphic boundaries in the northern Norwegian Barents Sea.

The mudstones of the studied Spathian–Carnian succession were deposited in an epicontinental basin in front of the developing TBO delta system, where the combined and complex interplay between primary productivity, benthic redox conditions, water mass restriction and sedimentation rate resulted in overall organic-rich mudstones, but of varying source rock quality and richness. The redox and productivity sensitive elemental chemostratigraphy were most importantly affected by (i) a deepened thermocline causing weak water mass restriction that lowered nutrient supply and productivity, but introduced intermittent benthic euxinia without observed bioturbation during Spathian hothouse conditions; (ii) introduction of well-ventilated, oxic/dysoxic, bioturbated benthic conditions with lowered preservation potential, but still an increase in upwelled nutrient supply that promoted moderate productivity and phosphate-nodule formation following the regional earliest Anisian transgression; (iii) a gradual relative sea-level rise and developing upwelling and productivity causing increased oxygen consumption, matrix-wide phosphogenesis and subsequent suboxia/anoxia during the middle–late Anisian, although still with

abundant tunnel burrows; (iv) sea-level high stand with intense primary productivity in the early Ladinian due to high nutrient supply from unrestricted upwelled waters, triggering maximum oxygen consumption and dominantly benthic euxinia without observed bioturbation; (v) regression and shallowing waters during the late Ladinian, resulting in weakly restricted water masses and frequent lowering of the O_2–H_2S interface below the sediment surface, thus reintroducing tunnel burrows, and; (vi) the base Carnian transgression, which mostly eliminated preservation of oil prone organic matter as bottom waters became ventilated and oxic.

This study suggests that the Triassic upwelling-induced productivity and widespread phosphogenesis in front of the TBO delta system were not firmly established before the Anisian. The Spathian lower Steinkobbe Formation in the Barents Sea seems therefore genetically unrelated to the Middle Triassic Botneheia Formation in Svalbard. Further work on ocean circulation, nutrient supply, primary productivity and climate change across the Spathian–Anisian boundary in the Barents Sea may provide answers on the importance of climate change and delta development on Triassic source rock formation.

5.7 Computer code availability

- Name of code: `Wesenlund_et_al_2021_TDR.py`
- Developer: Fredrik Wesenlund
- Contact details: Fredrik Wesenlund, Department of Geosciences, UiT The Arctic University of Norway, Norway; email: `Fredrik.wesenlund@uit.no`; Year first available: 2021
- Hardware used: The Python script was developed and run on a notebook PC with a quad core CPU @ 1.60–2.11 GHz and 16 GB RAM
- Software used and required: The Python script was developed with the Anaconda 2020.11 Python distribution platform (Anaconda Inc., 2021) using Spyder 4.1.5 and needs the pandas, matplotlib, seaborn, scikit-learn and numpy packages
- Program language: the code is written in Python 3.8.7
- Total size of script: ca 11 KB
- Access: available on GitHub (`https://github.com/fredrwes/Publications`)

5.8 Declaration of competing interests

The authors declare that they have no known competing financial interests or personal relationships that could have appeared to influence the work reported in this paper.

5.9 Acknowledgements

This study forms part of the ARCEx consortium (Research Centre for Arctic Petroleum Exploration) which is funded by the Research Council of Norway (grant number 228107) and ARCEx partners. We are grateful for additional economic support from Lundin Energy Norway and the Norwegian Petroleum Directorate for the field expedition to Edgeøya. Atle Mørk is thanked for field expedition planning, logistics, helpful discussions and great companionship, and the crew at research vessel SS Youexplore by The Dale Oen Experience for safe execution. Sofie Bernhardsen is acknowledged for field assistance and scientific contributions. Trine Dahl, Ingvild Hald and Karina Monsen are thanked for help and discussions in the geology lab at UiT–The Arctic University of Norway.

5.10 Supplementary material

Appendix A: Geochemical log panel of all parameters (wt. and EFs) included in this study. TOC, TIC and TS of the Blanknuten and Skrukkefjellet localities are partially collected from Wesenlund et al. (2021) as described in Section 5.3.

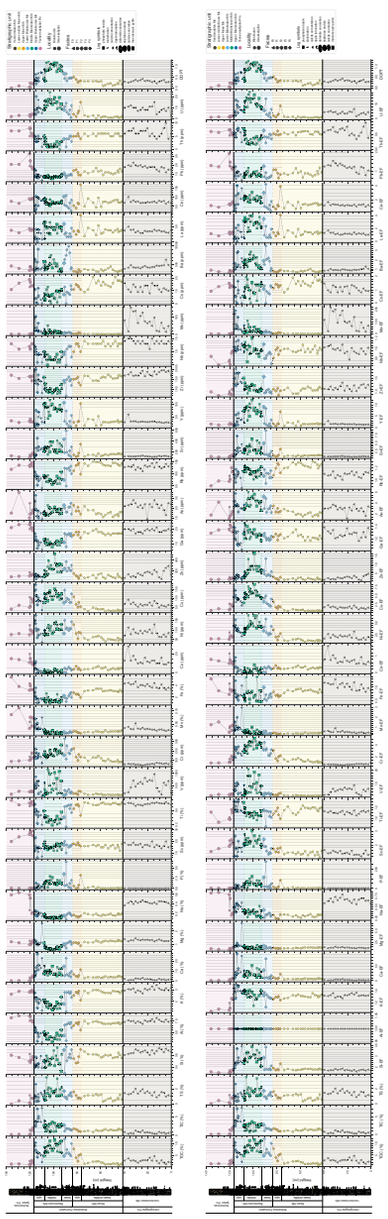

6

Paper III

Organic chemostratigraphy of Triassic black shales in Svalbard: implications for Triassic source facies development, thermal maturity evaluations, and correlations with Barents Sea oils

*Fredrik Wesenlund[1], Sten-Andreas Grundvåg[1], Olaf Thießen[2], Victoria Sjøholt Engelschiøn[3], Benedikt Lerch[4], Jon-Halvard Pedersen[5]

[1]Department of Geosciences, UiT The Arctic University of Norway, Tromsø, Norway

[2]Equinor ASA, Harstad, Norway

[3]The Natural History Museum, University of Oslo, Norway

[4]Aker BP ASA, Oslo, Norway

[5]Lundin Energy Norway, Lysaker, Norway

*Corresponding author. Email: `fredrik.wesenlund@uit.no`

Note: The manuscript is planned for submission to *Journal of Petroleum Geology*. The tabulated geochemical data and raw GC chromatograms used in this study will be open access pending publication. The full references to the included citations are available in the reference list (Chapter 8).

Abstract

This study characterizes selected aliphatic, aromatic and biomarker compounds of Lower–Upper Triassic organic-rich mudstone extracts from eastern Svalbard and oils from the 7220/11-1 *Alta*, 7120/1-3 *Gohta*, 7324/8-1 *Wisting Central* and 7324/7-2 *Hanssen* discoveries on the Norwegian Barents Shelf. The aim is to apply their proxy properties to (i) investigate paleoenvironmental variations in paleoredox, organic matter input and lithofacies, (ii) assess their thermal maturity using commonly applied maturity parameters, and (iii) to perform source–oil and oil–oil correlations. The mudstones are analogous to the oil-prone and effective source rocks of the Steinkobbe Formation (Lower–Middle Triassic) in the southern Norwegian Barents shelf. The investigated source facies parameters of the mudstone extracts generally agree with recent lithostratigraphic facies descriptions and their paleoenvironmental interpretations. The thermal maturity parameters are shown to be highly influenced by source facies. The Vendomdalen Member (Spathian) exhibits a clay-rich facies signature compared to the biogenically diluted and phosphate-rich upper Muen (Anisian) and Blanknuten (Anisian–Ladinian) members. The *Wisting Central/Hanssen* oils, reported to have been sourced from the lower Steinkobbe Formation (Spathian) mudstones, also exhibit a clay-rich source facies. Combined with other biomarker parameters, they indicate that Spathian source rocks from Svalbard and the southern Barents Shelf are organic facies equivalents. Recent work in the study area suggests that regional Triassic phosphogenesis was not firmly established before the Anisian, inferring that the oil-prone Botneheia Formation (Anisian–Ladinian) is not an organic facies equivalent to the lower Steinkobbe Formation (Spathian). This is linked to global climate change at the Lower–Middle Triassic boundary, changing from hot oceans with sluggish circulation and low nutrient supply, to cooler, upwelled waters that resulted in high nutrient supply and primary production. The *Alta/Gohta* oils also show a clay-rich source facies but abundant gammacerane that has not been proven in this or former studies of Lower Triassic extracts in the region. The previously suggested Upper Paleozoic Ørret Formation is therefore not disregarded as a probable hydrocarbon contributor for these discoveries. Overall, these findings have implications on the spatiotemporal development and correlation of the Triassic oil-prone source rocks on the Norwegian Barents Shelf that should be considered when performing petroleum systems analysis in the region.

6.1 Introduction

Sufficient kerogen richness, kerogen quality and thermal maturation are necessary criteria to form effective petroleum source rocks: the basis for conventional petroleum accumulations (Peters and Cassa, 1994). An essential objective during the initial petroleum exploration phase is therefore to identify and map organic-rich sequences and evaluate their thermal exposure (Magoon and Dow, 1994).

Multiple potential source rock units, ranging from Paleozoic to Cenozoic in time, have been identified on the Barents Shelf and the Svalbard archipelago (Abay et al., 2017; Abay et al., 2014; Abay et al., 2018; Abdullah, 1999; Henriksen et al., 2011b; Koeverden et al., 2011; Koeverden et al., 2010; Leith et al., 1993; Lerch et al., 2016a; Lerch et al., 2016b; Lerch et al., 2017; Lerch et al., 2018; Matapour and Karlsen, 2018; Matapour et al., 2019; Mørk and Bjorøy, 1984; Nicolaisen et al., 2019; Ohm et al., 2008). Additional complexity is provided as they may span a range of lithologies, including evaporates, carbonates, siliciclastic mudstones and coals. Few of these source rock units have been cored during exploration and scientific drilling campaigns on the southern NBS detailed source rock analyses. Thus, the time-equivalent successions exposed on Svalbard provide an excellent laboratory for detailed source rock studies.

The Norwegian Barents Shelf (NBS) experienced significant burial and subsequent Cenozoic uplift and erosion, which have, to various degrees, affected source rock parameters as richness, generation potential and maturity, but may have also changed hydrocarbon phase and/or migration history through time (Henriksen et al., 2011a; Ohm et al., 2008). Thus, in many occasions, the source rock units are or have been deeply buried and may have altered their geochemical signature for source-petroleum correlations due to thermal stress (Lerch et al., 2016a). Furthermore, drilling additives used during exploration well drilling may obscure their organic geochemical composition (Sanei et al., 2020). The exposed source rock intervals on Svalbard may therefore provide excellent conditions to evaluate relevant intervals in detail.

One of the most important oil-prone source rock units on the NBS are the organic-rich mudstones of the Lower–Middle Triassic Steinkobbe Formation (Isaksen and Bohacs, 1995; Mørk and Elvebakk, 1999). On the Svalis Dome, the mudstone-dominated Steinkobbe Formation (Spathian–Anisian) reach a thickness of approximately 250 m of which 110 m were cored in a scientific drilling program (Bugge and Fanavoll, 1995; Mørk and Elvebakk, 1999; Vigran et al., 1998). Previous studies of the Steinkobbe Formation have documented a systematic contrast in production index (PI) and $\delta^{13}C$ isotopic values at equally low maturation levels between the lower (Spathian) and the upper P-nodule-rich (Anisian) parts of the unit (Abay et al., 2018; Isaksen and Bohacs, 1995),

perhaps indicating age-related facies differences within this unit.

The Steinkobbe Formation has likely provided liquid hydrocarbons to the Triassic reservoirs of the Goliat Field (Bjorøy et al., 2009; Lundschien et al., 2014), the 7324/8-1 *Wisting Central* and 7324/7-2 *Hanssen* discoveries (Lerch et al., 2018) and possibly to the 7220/11-1 *Alta* and 7120/1-3 *Gohta* discoveries (Matapour et al., 2019), as well as to numerous minor discoveries (Lerch et al., 2016a; Lerch et al., 2016b). This indicates that the Steinkobbe Formation could have regional significance throughout the NBS.

Lerch et al. (2018) used the abundance of the age-specific triaromatic dimethylcholesteroids (TA-DMCs) biomarkers to identify the Spathian part of the lower Steinkobbe Formation as the main precursor for the *Wisting Central* and *Hanssen* discoveries. Matapour et al. (2019) suggest a contribution from lowermost Triassic and/or Upper Paleozoic source rocks to the *Alta* and *Gohta* discoveries. These interpretations are based on the observed lack of TA-DMCs in these oils.

High quality source rock samples from exploration drilling in the southern Norwegian Barents Sea for petroleum-source correlations are sparse, but time equivalent exposed source rock intervals on Svalbard may close this gap. Organic-rich mudstones occur in the Lower to Upper Triassic succession onshore Svalbard, i. e., in the Vikinghøgda Formation (Smithian–Spathian), the Botneheia Formation (Anisian–Ladinian) and the Tschermakfjellet Formation (Carnian) (Leith et al., 1993; Mørk et al., 1999a; Mørk and Bjorøy, 1984; Vigran et al., 2014). These units were deposited under varying productivity and redox conditions, and contain both marine and terrestrial organic matter resulting in mudstones that exhibit a wide range of organic and inorganic facies compositions (Mørk and Bjorøy, 1984; Wesenlund et al., 2022; Wesenlund et al., 2021). As a result of the different paleodepositional environments also their kerogen quality (HI: <200–600< mg hydrocarbon (HC)/g TOC) and richness (total organic carbon, TOC: <1–12< wt. %) varies significantly (Krajewski, 2013; Wesenlund et al., 2021). The phosphate-bearing Middle Triassic Botneheia Formation is widely known as the most important source rock unit of the region and is commonly considered a diachronous lateral facies equivalent to the Steinkobbe Formation of the southern Barents shelf (Abay et al., 2018; Krajewski, 2013; Lundschien et al., 2014; Lutz et al., 2021; Mørk and Bjorøy, 1984; NPD, 2017; Wesenlund et al., 2021).

Recent work considered the intense phosphogenesis and deposition of the phosphatic mudstones on the Barents Shelf, including Svalbard, to be fairly synchronous during the Middle Triassic (Wesenlund et al., 2022). Mudstones in the Spathian part of the Steinkobbe Formation may thus have accumulated under principally different source rock depositional environments than in

its Anisian part and in the Anisian–Ladinian of the Botneheia Formation in Svalbard (Wesenlund et al., 2022). Detailed biomarker investigations of the Lower–Middle Triassic mudstone units in Svalbard could therefore provide important insights with respect to source rock depositional environments of the Lower–Middle Triassic succession on the Barents Shelf.

In this paper, we investigate the *n*-alkane, acyclic isoprenoid, and biomarker compositions of Lower–Upper Triassic organic-rich mudstones in two different sections from Edgeøya, eastern Svalbard. Wesenlund et al. (2021) document insignificant vertical maturity gradients within each of the two locations, Blanknuten and Skrukkefjellet respectively, but a clear, although low maturity difference (ΔRo c. 0.06 %) between them. Moreover, as both locations have reached early oil window maturity, the study area provides ideal conditions to investigate how source facies and thermal maturity contrasts affect common and well-founded *n*-alkane, acyclic isoprenoid and biomarker-based source and maturity parameters. In order to compare onshore and offshore biomarker data, and further elucidate the evolution of well-known Triassic source rock units on both the northern and southern NBS, this study also includes crude oils from the *Alta*, *Gohta*, *Wisting Central* and *Hanssen* discoveries in the sample set. This allows direct comparison between Lower–Upper Triassic mudstone extracts from Svalbard with inferred Lower Triassic (or potentially Upper Paleozoic)-sourced crude oils from the main exploration area on the NBS.

The specific objectives of this paper are thus to:

- Characterize various biomarker-based source facies parameters and link these proxies to previously observed facies variations and paleoenvironmental interpretations in the studied Lower–Upper Triassic succession.

- Evaluate the thermal maturity of the mudstones and oil samples using biomarker-based thermal maturity parameters and investigate their source specificity.

- Perform an oil–source rock and oil–oil correlation between the investigated outcrop sections in eastern Svalbard and the oils from the 7220/11-1 *Alta*, 7120/1-3 *Gohta*, 7324/8-1 *Wisting Central* and 7324/7-2 *Hanssen* discoveries.

6.2 Geological setting

The high-Arctic Svalbard archipelago represents the uplifted and exhumed northwestern corner of the Barents Shelf, and exposes an Upper Paleozoic through Mesozoic to Cenozoic sedimentary succession (Dallmann, 1999). The shelf is bounded by a sheared margin to the west, and a rifted, but now passive continental margin to the north (Faleide et al., 1984; Faleide et al., 2008). The Baltic Shield and Novaya Zemlya defines its southern and southeastern boundaries, respectively (Glørstad-Clark et al., 2010). Although the shelf has undergone multiple tectonic events following the Caledonian orogeny, the present-day structural setting with several basins and highs largely record Late Jurassic to Early Cretaceous rifting and rift-related faulting (Faleide et al., 1984; Faleide et al., 2008) (Fig. 6.1a).

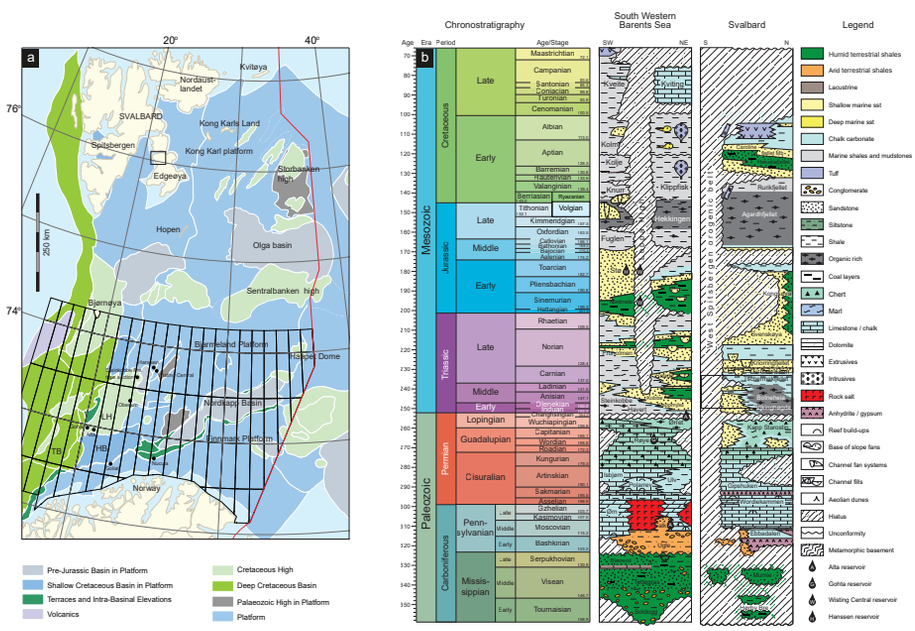

Figure 6.1: (a) Map showing the NBS, displaying the commercially available exploration blocks, selected discoveries, and the Steinkobbe Formation type section in its southern part, and the acreage not opened for commercial exploration in its northern part. The study area on Svalbard is highlighted by the rectangle. HB = Hammerfest Basin, LH = Loppa High, TB = Tromsø Basin. Modified from the NPD (2017). **(b)** Chronostratigraphic charts of the southwestern Norwegian Barents Shelf and Svalbard. The investigated Lower, Middle and Upper Triassic mudstones (Vikinghøgda, Botneheia and Tschermakfjellet formations respectively) are highlighted by the rectangle. Modified from the Norlex Project (2012).

A chrono- and lithostratigraphic summary is given in Figure 6.1b. Continental red-bed deposition occurred in the late Carboniferous (Early Pennsylvanian; Ugle Formation) and suggests an arid to semi-arid depositional environment in the Barents Sea area which was subsequently flooded from Middle Pennsylvanian times (Larssen et al., 2002). High frequency and high amplitude sea-level fluctuations led to variable sedimentation of shallow marine carbonates in high-stand situations and dolomitic mudstones, anhydrates and halites during lowstands (Falk and Ørn formations) (Larssen et al., 2002; Stemmerik and Worsley, 2005). Variable shallow water carbonates prevail into the early Permian (Sakmarian–Artinskian; Polarrev and Ulv formations) associated with a significant shift in the depositional environment to cool-water carbonates (Larssen et al., 2002). Following a major transgression in the Artinskian, cool-water carbonates were deposited in an inner shelf environment (Isbjørn Formation) (Larssen et al., 2002; Stemmerik and Worsley, 2005). Sedimentation on a low relief carbonate platform prevailed during Kungurian to Wuchiapingian times in large parts of the Barents Sea, but distal marine to deep shelf deposits are also present (Røye and Ørret formations) (Larssen et al., 2002).

A dramatic shift in sedimentation occurred across the Permian-Triassic boundary resulting in the onset of a Mesozoic siliciclastic platform (Mørk et al., 1982). Throughout the Triassic, the Barents Shelf, including Svalbard, was part of an intracratonic basin covered by a shallow sea, here referred to as the Triassic Boreal Ocean (TBO) (Klausen et al., 2019) (Fig. 6.2). The TBO formed a large embayment at the northwestern margin of Pangea and faced the deep Panthalassa Ocean to the northwest (Parrish and Curtis, 1982; Sømme et al., 2018). During the Triassic, the TBO saw the arrival of a large delta system that prograded northwestward from the Urals, eventually reaching the western Barents shelf in the Ladinian (Snadd Formation) and Svalbard by the Late Triassic (Eide et al., 2018; Mørk et al., 1982; Vigran et al., 2014). However, marine siliciclastic deposition prevailed during the Early Triassic in the western part of the Barents Sea (Bjerager et al., 2019). In seismic data, onlaps are documented at the eastern flank of the palaeo-Loppa High, suggesting that it acted as a depositional barrier throughout the Early and Middle Triassic (Glørstad-Clark et al., 2011; Glørstad-Clark et al., 2010). The Lower to Middle Triassic succession, including the organic-rich mudstones of the Steinkobbe Formation (Spathian–Anisian), were deposited in a pro-delta to open marine setting in front of the TBO delta system (Glørstad-Clark et al., 2010; Lundschien et al., 2014; Riis et al., 2008).

During the Middle Triassic (Anisian), intensified upwelling and nutrient supply from the Panthalassa Ocean resulted in increased primary productivity and enhanced preservation potential of organic material, thus promoting the deposition of organic-rich mudstones with abundant phosphate cement and/or P-nodules throughout the Arctic basins (Bjerager et al., 2019; Grasby et al., 2016;

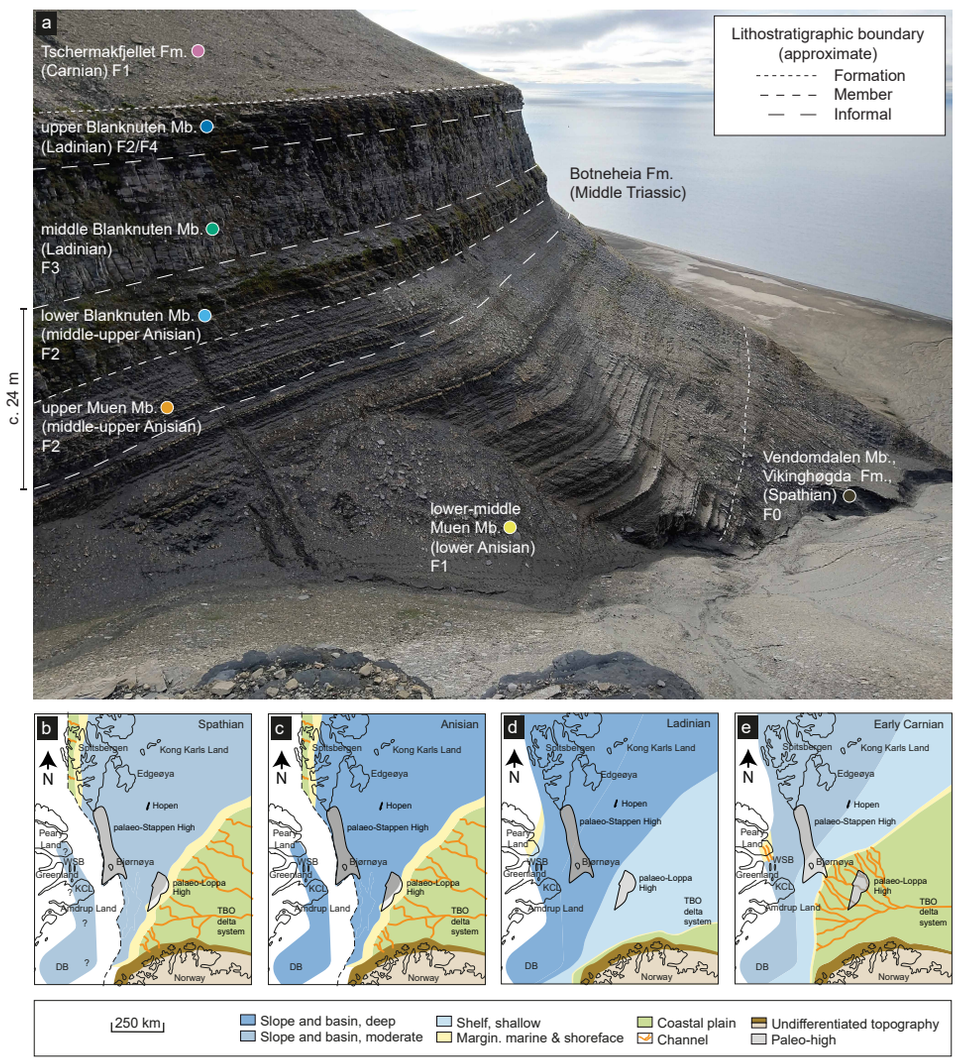

Figure 6.2: (a) Lithostratigraphic outcrop overview of the Blanknuten locality, showing the investigated Lower–Upper Triassic (Spathian–Carnian) mudstones of the Vikinghøgda, Botneheia and Tschermakfjellet formations. The color coding of the identified lithostratigraphic units is applied throughout this study. Ages should be considered approximate and are based on lithostratigraphic correlation of palynozones from the Skrukkefjellet locality, adapted from Vigran et al. (2014). The lithostratigraphic division is adapted from Wesenlund et al. (2022) and Wesenlund et al. (2021), originally based on Krajewski (2008). **(b)** Spathian, **(c)** Anisian, **(d)** Ladinian, and **(e)** Early Carnian paleogeographical development, showing the transition from a moderate marine to deep marine to pro-deltaic marine setting in Svalbard. Modified from Wesenlund et al. (2022), originally based on Bjerager et al. (2019), Eide et al. (2018), Glørstad-Clark et al. (2010), and Klausen et al. (2015).

Krajewski, 2008; Krajewski, 2013; Parrish et al., 2001; Parrish and Curtis, 1982). These deposits are represented by the upper Muen Member and the lower Blanknuten Member of the Botneheia Formation in eastern Svalbard, and by the middle–upper Steinkobbe Formation on the southern NBS (Krajewski, 2008; Krajewski, 2013; Mørk and Elvebakk, 1999; Vigran et al., 2014; Wesenlund et al., 2021). During the early Ladinian, Svalbard continued to experience intense upwelling and increased primary productivity in combination with sediment starvation, resulting in biogenic dilution (Klausen et al., 2015; Krajewski, 2013; Krajewski and Weitschat, 2015). The mudstones deposited during this period are assigned to the middle Blanknuten Member, which by far have the best source rock quality and richness among all the Triassic mudstone deposits on the northern Barents Shelf (Krajewski, 2008; Krajewski, 2013; Wesenlund et al., 2021).

A lowered potential for source rock formation is apparent for the Upper Triassic (i.e. the Tschermakfjellet Formation in Svalbard and the Snadd Formation on the Barents Shelf), reflecting well-ventilated conditions and widespread prodelta to delta plain deposition across the entire region (Abay et al., 2018; Lundschien et al., 2014; Mørk and Elvebakk, 1999; Mørk and Bjorøy, 1984).

The offshore oils analyzed in this study derive from four exploration wells located in the southern part of the Norwegian Barents Shelf (Fig. 6.1). Two of the wells (*Alta* and *Gohta*) are located at the southern margin of the Loppa High, and the other two (*Hanssen* and *Wisting Central*) are located further to the north within the Hoop Fault Complex on the Bjarmeland Platform (Fig. 6.1). Whereas the wells on the Loppa High targeted Upper Carboniferous to Upper Permian karstified carbonates (of the Gipsdalen and Tempelfjorden groups), the latter two targeted Upper Triassic to Middle Jurassic sandstones (of the Kapp Toscana Group and Realgrunnen Subgroup) (NPD, 2021a).

6.3 Samples and methods

The mudstone samples analyzed in this study were stratigraphically collected at the Blanknuten (a c. 120 m thick section) and Skrukkefjellet (two sections spanning a c. 90 m thick composite section) localities on northern Edgeøya (Fig. 6.1). The sample set includes the Vendomdalen Member (Spathian) of the Lower Triassic Vikinghøgda Formation (which is synchronous to the lower Steinkobbe Formation offshore), the Muen (Anisian) and Blanknuten (Anisian–Ladinian) members of the Middle Triassic Botneheia Formation (partly synchronous and facies equivalent to the middle–upper Steinkobbe Formation offshore), and the lowermost part of the Upper Triassic Tschermakfjellet Formation (facies equivalent to the lower Snadd Formation offshore).

This study incorporates the TOC and total inorganic carbon (TIC) dataset of Wesenlund et al. (2022) and Wesenlund et al. (2021), and this study is based on the same samples applied in their work. This study also applies the same mudstone facies subdivision (F0 to F4; see Table 6.1) and chemostratigraphic zonation as presented in Wesenlund et al. (2022) and Wesenlund et al. (2021), allowing direct comparison of the results presented here and the parameters from these studies. The lithostratigraphic division of the Botneheia Formation used in this study and Wesenlund et al. (2022) and Wesenlund et al. (2021) conforms to the Middle Triassic lithostratigraphic classification initially established by Krajewski (2008). The Muen Member is thus subdivided into a *lower–middle* and an *upper* part, whereas the overlying Blanknuten Member is subdivided into a *lower*, a *middle* and an *upper* part.

Table 6.1: Overview of the various mudstone facies applied in this study, their stratigraphic distribution, and main characteristics. The facies divisions and descriptions derive from Wesenlund et al. (2022) and Wesenlund et al. (2021).

Facies	Stratigraphic occurrence	Description	TOC mean ± SD (wt. %)	Kerogen type	Macroscopic trace fossils
F0	Vendomdalen Mb	Dark brown, silty and brittle, laminated mudstone	2.70 ± 0.79	II–III	Not observed
F1	lower-middle Muen Mb, Tschermakfjellet Fm	Gray–dark gray, mostly soft, non-laminated to laminated mudstone	1.53 ± 0.65	III to III–II	*Chondrites* and *Helminthopsis*
F2	upper Muen Mb, lower Blanknuten Mb, upper Blanknuten Mb	Black, phosphate-bearing and brittle, laminated mudstone	5.70 ± 2.23	II	*Thalassinoides*
F3	middle Blanknuten Mb	Black, phosphate-bearing and brittle, well-laminated mudstone	8.34 ± 1.93	II	Not observed
F4	upper Blanknuten Mb	Black, phosphate-bearing, soft and brittle, laminated calcareous mudstones to impure limestones	6.41 ± 2.53	II	*Thalassinoides*

Additional TOC and Rock-Eval analyses were performed by Applied Petroleum Technology (APT) in Oslo, Norway. The resulting TOC values were used to quantify hydrogen index (HI) and Oxygen Index (OI) values rather than the TOC dataset from UiT to promote interlaboratory consistency. For the TOC analysis at APT, a LECO™ SC-632 instrument was used. Diluted hydrochloric acid was added to the crushed rock samples to remove carbonate. The samples were then dried and introduced into the LECO combustion. The amount of carbon in the sample is measured as carbon dioxide by an infrared detector. For Rock-Eval analysis, a HAWK™ instrument was used. The Norwegian Geochemical Standard Jet Rock - 1 (JR-1) was run as every tenth sample and checked for analytical consistency. All Rock-Eval procedures follow the Norwegian Industry Guide to Organic Geochemical Analyses (NIGOGA) (Weiss et al., 2000), and pyrolysis results are within the acceptable range given in NIGOGA. A Pearson correlation coefficient of 99.6 % for the TOC data from UiT and APT show that these parameters are highly correlated and thus represent the same stratigraphic trends.

The source potential index (SPI) (*sensu* Demaison and Huizinga, 1991) was calculated as follows: $SPI = (h \times PP \times \rho)/1000$, where SPI represents the maximum amount of hydrocarbons that can be generated within a column of source rock per m² of surface area (Mg HC/m²), h is source rock thickness (m), PP is the production potential, i.e. S_1 (mg HC/g rock) + S_2 (mg HC/g rock) derived from Rock-Eval pyrolysis, and ρ is the source rock density, assumed to be constant at 2.5 g/cm³. Note that the source rock thicknesses applied in this study have not been corrected for the presence of coarser-grained event beds within the mudstones. However, these are relatively few in both sections and should thus have a negligible influence on the overall SPI.

Visual inspection of the kerogen content and the spore coloration index (SCI) of four representative samples of the Vendomdalen, Muen and Blanknuten members and the Tschermakfjellet Formation—i.e., a sample for each of the formal stratigraphic units investigated in this study—were carried out by APT. They used the following procedures: The slides used to estimate the SCI and relative abundance of fluoramorphinite, algal, herbaceous, woody and coaly organic matter were prepared using standard palynological techniques (hydrochloric and hydrofluoric acids) although without any oxidative stages. The kerogen was floated in zinc bromide and agitated with ultrasonic energy to disaggregate the kerogen components prior to centrifuging. The SCI was determined using dual mounts of sieved un-oxidized kerogen strew-mounted with cover slips for a total kerogen and a plus 10 micron sieved kerogen evaluation.

The extraction procedures, GC-FID and GC-MS analyses were performed at the organic geochemical laboratories at the Department of Geosciences, University

of Oslo. Bitumen was extracted using a ST 243 Soxtec™ system as outlined in Wesenlund et al. (2021). For GC-FID bulk extract characterization, a Varian™ CP-3800 GC system equipped with a 60 m long Agilent DB-1MS UI column which had 0.25 mm inner diameter and a film thickness of 0.25 μm was used. The temperature program was as follows: Initial column temperature was set at 80°C with a hold time of 1 min. The temperature gradient was 4.5°C/min until it reached 320°C. Here, the temperature was held for 35 min. Total runtime was 90 minutes per sample.

Prior to GC-MS analysis, the bulk extracts were added to an organophilic molecular sieve (HiSiv™ 3000) in cyclohexane solution to remove *n*-alkanes and polar compounds. The sieved extract was thereafter analyzed by a Thermo Scientific™ Trace™ 1310 gas chromatograph coupled with a Thermo Scientific™ TSQ™ 8000 Triple Quadrupole MS utilizing a 60 m long Thermo Scientific™ TG-XLBMS fused silica column with inner diameter of 0.25 mm and film thickness of 0.25 μm. The temperature program was as follows: The initial column temperature was 40°C with a hold time of 1 min. The temperature gradient was 20°C/min until 180°C was reached, followed by 1.7°C/min until the final temperature of 310°C, which was held for 40 min. Total runtime was 125 minutes per sample. Ions were recorded in selected ion monitoring (SIM)-mode with m/z of 142, 156, 170, 177, 178, 184, 191, 192, 198, 205, 206, 217, 218, 219, 231, 253, 259. The total scan time was 1.5 s.

12 of the 70 samples analyzed by both GC-FID and GC-MS displayed poor peak identification in the m/z 198 methyldibenzothiophenes (MDBTs) chromatograms due to lacking or interfering peaks. These samples are therefore not plotted in figures that include MDBTs. In the Blanknuten locality, this includes the lower–middle Muen Member (five samples), lower Blanknuten Member (one sample), and the Tschermakfjellet Formation (one sample). In the Skrukkefjellet locality, this includes the lower–middle Muen Member (two samples), the lower Blanknuten Member (one sample), the upper Blanknuten Member (one sample), and the Tschermakfjellet Formation (one sample).

The oils from the NO 7324/8-1 *Wisting Central*, NO 7324/7-2 *Hanssen*, NO 7220/11-1 *Alta* (DST-A and DST-B) discoveries were previously analyzed in the same organic geochemical laboratories at the Department of Geosciences, University of Oslo, using the above GC instruments (Lerch et al., 2018). Specifically for the oils, the saturate, aromatic and polar (resins and asphaltenes) fractions were separated prior to GC-MS analysis using the method outlined by Bastow et al. (2007) but by using hexane instead of pentane as solvent (Lerch et al., 2018). The oil from the NO 7120/1-3 *Gohta* discovery was also analyzed using the procedures above but was not included in the study by Lerch et al. (2018).

The Norwegian Geochemical Standards North Sea Oil - 1 (NSO-1) and Svalbard Rock - 1 (SR-1) maintained by the NPD were also analyzed and are included as references for peak identification (Dahlgren et al., 1998; Weiss et al., 2000). The NSO-1 consists of Upper Jurassic-sourced crude oil from the Oseberg Field (e.g., Pedersen et al., 2006). The NSO-1 was analyzed at regular intervals to check for analytical consistency and peak identification and shows low variance (mean C_{23}tri/30$\alpha\beta$ = 0.10 ± 0.005, SD, n = 5). The SR-1 represents outcrop mudstone material assigned to the lower Botneheia Formation and is commonly considered to represent the Muen Member (Brekke et al., 2014; Dahlgren et al., 1998), although recent evidence strongly suggests that the SR-1 was sampled from the underlying Vendomdalen Member (Wesenlund et al., 2022). Compounds identified from GC-FID and GC-MS analyses (Table 6.2) were quantified by manual baseline interpretation and peak height measurements. The peak heights were then used to calculate the GC-derived parameters.

Values reported as X ± Y represent the arithmetic mean (X) and the SD (Y). Delta degrees of freedom = 1. Values reported as A–B represent the minimum (A) to maximum (B) value.

6.4 Results

6.4.1 Rock-Eval logs and source potential index

The samples from the Vendomdalen Member (facies F0) exhibit a kerogen type II/III composition and show good mean petroleum potential (PP) = (7.80 ± 1.22 mg HC/g rock) (Figs. 6.3 and 6.4). This unit spans the lowermost c. 42 m of the Blanknuten section (the unit was not sampled in the Skrukkefjellet section), resulting in a minimum SPI = 0.82 Mg HC/m² (Fig. 6.5). Samples from the overlying lower–middle Muen Member consists of mudstone facies F1, contain kerogen type III to II/III and thus have the lowest source rock quality of the samples from the Botneheia Formation (Fig. 6.3). These facies F1 mudstones are present within a c. 34 m thick unit in the Blanknuten section (level 42–76 m; Fig. 6.4) and a c. 33 m thick unit in the Skrukkefjellet section (level 0–33 m; Fig. 6.4). Using their mean PP from the Blanknuten (4.57 ± 2.27 mg HC/g rock) and Skrukkefjellet (2.79 ± 1.42 mg HC/g rock) sections, they yield a SPI = 0.39 Mg HC/m² and SPI = 0.23 Mg HC/m², respectively (Fig. 6.5). Both sections show an abrupt positive change in kerogen richness (TOC, S2) and quality (higher HI, lower OI) directly above the contact between the lower–middle and upper Muen members (Fig. 6.4). This corresponds to a transition from F1 to F2 mudstone facies, where samples from the upper Muen Member and the overlying lower Blanknuten Member both consists of mudstone facies F2. Combined, the F2 samples of these units yield a high SPI (2.22 Mg HC/m²) in

Table 6.2: Name and labels of selected *n*-alkanes, isoprenoids, biomarkers, phenanthrenes and thiophenes investigated in this study. The name and label pairs are based on Weiss et al. (2000). The compound labeled 30§ probably represents an unidentified rearranged terpane (George et al., 2007). The labels X and Y represent two unidentified compounds useful for correlation but without specified affinity, see Section 6.4.4 and Section 6.5.2 for description and discussion respectively.

Fraction		Label
Bulk GC-FID	C_x *n*-alkane	*n*-C_x
	Pristane	Pr
	Phytane	Ph
m/z 191	$C_{23}H_{42}$ tricyclic terpane	C_{23}tri
	$C_{24}H_{44}$ tricyclic terpane	C_{24}tri
	$C_{24}H_{42}$ tetracyclic terpane	C_{24}tet
	$C_{25}H_{46}$ tricyclic terpane (R + S)	C_{25}tri
	$C_{26}H_{48}$ tricyclic terpane (R + S)	C_{26}tri
	$C_{28}H_{50}$ tricyclic terpane (R + S)	C_{28}tri
	$C_{29}H_{54}$ tricyclic terpane (R + S)	C_{29}tri
	$C_{30}H_{56}$ tricyclic terpane (R + S)	C_{30}tri
	18α(H)-22,29,30-trisnorneohopane	Ts
	Unidentified rearranged terpane	30§
	17α(H)-22,29,30-trisnorhopane	Tm
	17α(H), 21β(H)-28,30-bisnorhopane	28αβ
	17α(H), 21β(H)-30-norhopane	29αβ
	Unidentified compound	X
	18α(H)-30-norneohopane	29Ts
	15α-methyl-17α(H)-27-norhopane (diahopane)	30d
	17β(H), 21α(H)-30-norhopane (normoretane)	29βα
	18α(H)-oleanane	30O
	17α(H), 21β(H)-hopane	30αβ
	$C_{30}H_{54}$ Δ13(18)-hopene	30D13
	17β(H), 21α(H)-hopane (moretane)	30βα
	Unidentified compound	Y
	Gammacerane	30G
	17α(H), 21β(H), 22(S)-homohopane	31αβS
	17α(H), 21β(H), 22(S)-homohopane	31αβR
	17α(H), 21β(H), 22(S)-bishomohopane	32αβS
	17α(H), 21β(H), 22(R)-bishomohopane	32αβR
	17α(H), 21β(H), 22(S)-trishomohopane	33αβS
	17α(H), 21β(H), 22(R)-trishomohopane	33αβR
	17α(H), 21β(H), 22(S)-tetrakishomohopane	34αβS
	17α(H), 21β(H), 22(R)-tetrakishomohopane	34αβR
	17α(H), 21β(H), 22(S)-pentakishomohopane	35αβS
	17α(H), 21β(H), 22(R)-pentakishomohopane	35αβR
	24-ethyl-5α(H), 14α(H), 17α(H), 20(S)-cholestane	29ααS
m/z 217	13β(H), 17α(H), 20(S)-cholestane (diasterane)	27dβS
	13β(H), 17α(H), 20(R)-cholestane (diasterane)	27dβR
	24-ethyl-5α(H), 14α(H), 17α(H), 20(S)-cholestane (reg. sterane)	29ααS
	24-ethyl-5α(H), 14β(H), 17β(H), 20(R)-cholestane (reg. sterane)	29ββR
	24-ethyl-5α(H), 14β(H), 17β(H), 20(S)-cholestane (reg. sterane)	29ββS
	24-ethyl-5α(H), 14α(H), 17α(H), 20(R)-cholestane (reg. sterane)	29ααR
m/z 218	24-methyl-5α(H), 14β(H), 17β(H), 20(R)-cholestane	27ββR
	24-methyl-5α(H), 14β(H), 17β(H), 20(S)-cholestane	27ββS
	24-ethyl-5α(H), 14β(H), 17β(H), 20(R)-cholestane	28ββR
	24-ethyl-5α(H), 14β(H), 17β(H), 20(S)-cholestane	28ββS
	24-propyl-5α(H), 14β(H), 17β(H), 20(R)-cholestane	29ββR
	24-propyl-5α(H), 14β(H), 17β(H), 20(S)-cholestane	29ββS
m/z 178	Phenanthrene	P
m/z 192	3- or 2- or 9- or 1-methylphenanthrene	3- or 2- or 9- or 1-MP
m/z 198	4- or 3- or 2- or 1-methyldibenzothiophene	4- or 3- or 2- or 1-MDBT

the Blanknuten locality (level 76-93; Figs. 6.4 and 6.5).

The overall largest recorded SPI (2.53 Mg HC/m^2) for a single stratigraphic unit is seen in the samples from the middle Blanknuten Member in the Skrukkefjellet locality (level 51–66; Fig. 6.4), which consists of mudstone facies F3 (Fig. 6.5). The SPI abruptly decreases in the samples from the overlying upper Blanknuten Member, which include samples of both mudstone facies F2 and F4. A complete section was not measured for the Tschermakfjellet Formation. Thus, the SPI is not determined for the few samples collected from this unit, which all consists of mudstone facies F1 samples (Fig. 6.5). However, the SPI is nonetheless expected to be poor based on the low PP values (Fig. 6.4).

The bulk phosphatic succession, ranging from the base of the upper Muen Member to the top upper Blanknuten Member, is c. 40 m thick in the Blanknuten section (level 76–117 m; Fig. 6.4) and c. 38.5 m (level 32.5–71 m; Fig. 6.4) in the Skrukkefjellet section. The mean PP of the bulk phosphatic succession in the Blanknuten locality (47.33 ± 15.55 mg HC/g TOC) and the Skrukkefjellet locality (47.32 ± 23.49 mg HC/g TOC) results in a SPI = 4.73 Mg HC/m^2 and SPI = 4.55 Mg HC/m^2 respectively (Fig. 6.5). These SPIs are substantially larger than those derived from the successions of the Vendomdalen and lower–middle Muen members, even though they have similar thicknesses (Fig. 6.4). For all stratigraphic units, Tmax is slightly lower in the Skrukkefjellet locality (443 ± 2.53 °C) relative to the Blanknuten locality (445 ± 1.67 °C) and shows insignificant coupling with organic facies variations (Fig. 6.4).

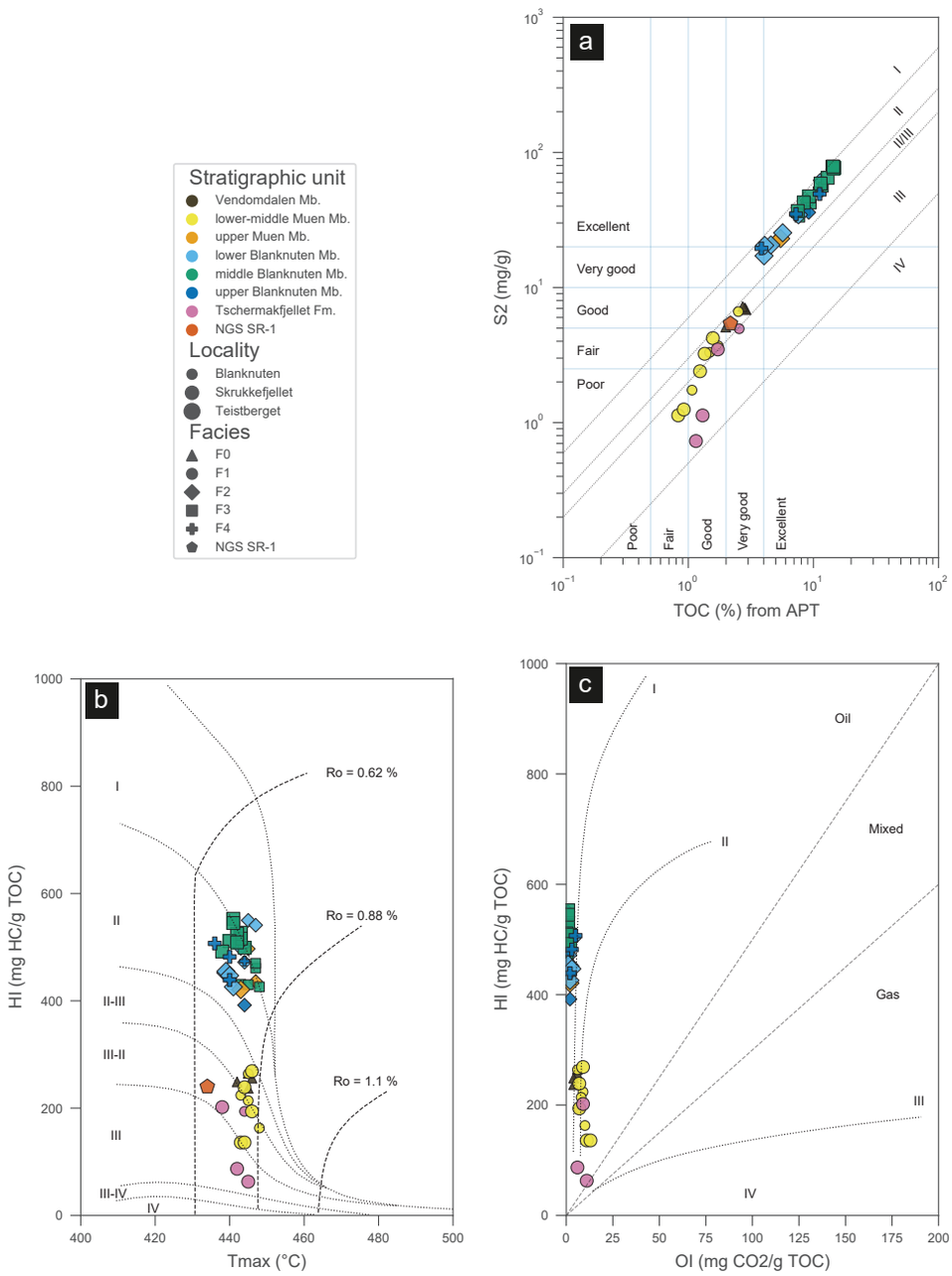

Figure 6.3: Binary plots including modified Van Krevelen diagrams of selected Rock-Eval parameters. **(a)** S_2 vs. TOC from APT. **(b)** HI vs. Tmax. **(c)** HI vs. OI.

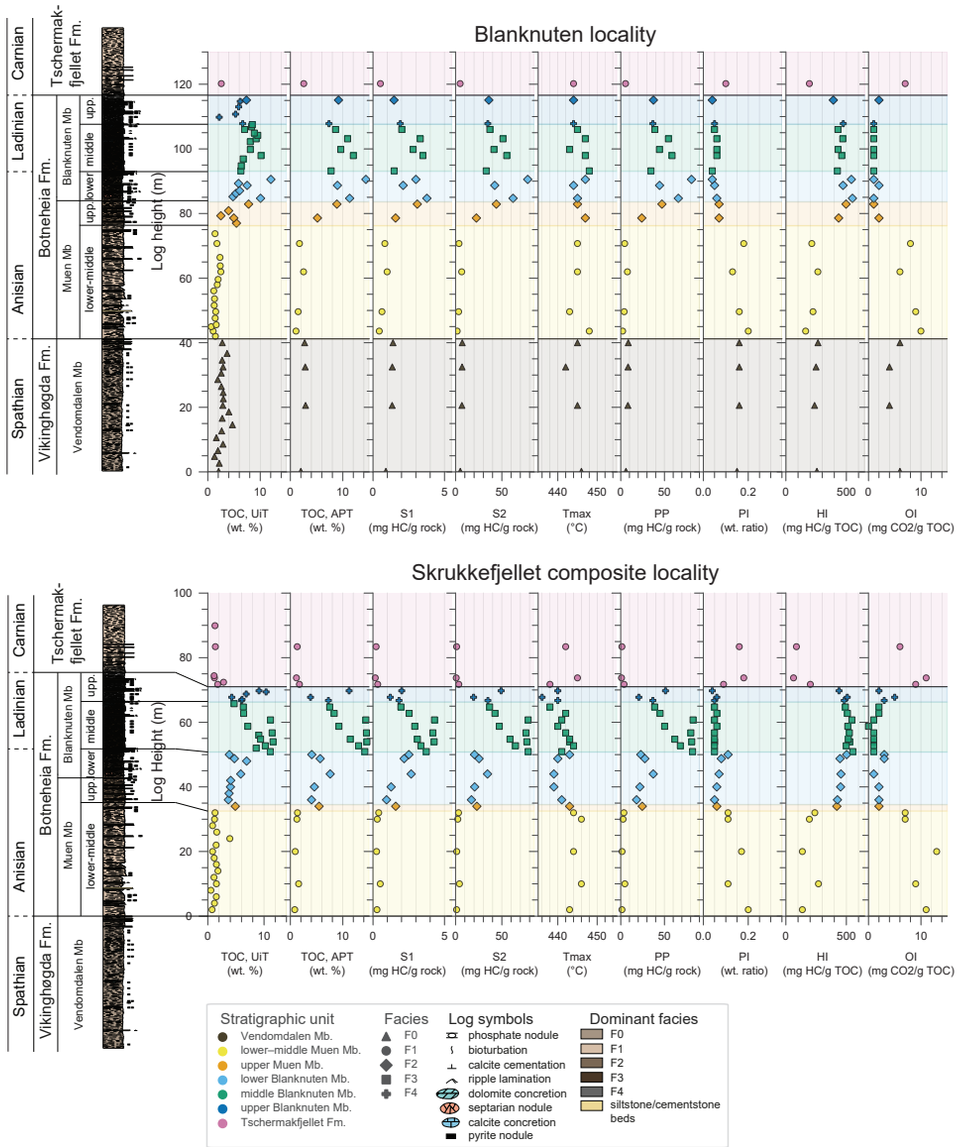

Figure 6.4: Geochemical logs of selected Rock-Eval parameters from the Blanknuten and Skrukkefjellet localities. The TOC log using UiT data and lithostratigraphic logs are collected from Wesenlund et al. (2022) and Wesenlund et al. (2021). Both lithostratigraphic logs represent the Blanknuten section as no lithostratigraphic log was made for the Skrukkefjellet composite section. However, the excellently exposed outcrops allow lithostratigraphic correlation with high confidence.

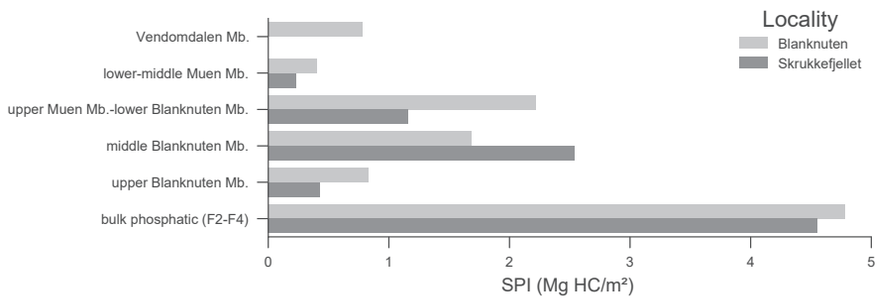

Figure 6.5: Bar chart of the SPI values for each stratigraphic unit. The Tschermakfjellet Formation is not included as no thickness was determined for this unit. The Vendomdalen Member was not sampled in the Skrukkefjellet locality and is therefore not included for this locality.

6.4.2 Visual kerogen description

Each of the four samples examined by APT for visual kerogen content represent a formal stratigraphic unit investigated in this study (Fig. 6.6). They all show dominance of amorphous organic matter (AOM). The sample from the Vendomdalen Member (facies F0) shows weak fluorescence from the AOM groundmass and encapsulation of white/yellow algae and bright yellow/orange sporomorphs. While algae identification was difficult, prasinophytes appear to be present, in addition to thin particles of woody material.

The sample from the lower–middle Muen Member (facies F1) shows higher relative content of herbaceous, woody and coaly organic matter (Fig. 6.6). The AOM groundmass exhibited a very dull orange fluorescence and encapsulation of bright yellow and white/yellow fluorescing algae along with fluorescing orange sporomorphs. The algae were predominantly characterized by prasinophytes and small acritarchs. Bisaccates were the most abundant identified sporomorph, however, due to degradation, they appear very thin and pale in transmitted light.

The sample from the middle Blanknuten member (facies F3) shows abundant bituminite (classified under fluoramorphinite) with white/yellow fluorescing wisps of algae and exinite. Bituminite encapsulation of kerogen occurs, however algae (including acritarchs and prasinophytes) and sporomorphs were identified in the dull orange-fluorescing bituminite groundmass. SCI in transmitted light could not be determined for this sample due to the bituminite encapsulation (Fig. 6.6).

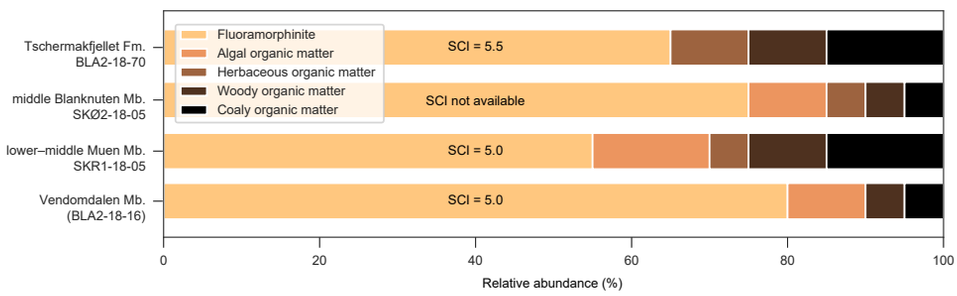

Figure 6.6: Bar chart of the maceral composition of the formal stratigraphic units, showing their contrasting organic facies. Hebamorphinite was not observed in any of the samples.

The sample from Tschermakfjellet Formation (facies F1) at the Blanknuten section shows a weak orange fluorescing AOM matrix containing abundant orange fluorescing sporomorphs and bright yellow algae. Some sporomorphs exhibit thinned walls due to high degree of degradation. In this sample, the algae were included within the kerogen estimate for AOM, because algae could only be identified in the AOM groundmass using ultraviolet light. Additionally, the algae were predominantly acritarchs, and smaller acritarchs were slightly more abundant than prasinophytes.

6.4.3 GC-FID

n-alkane chromatograms and waxiness

Terrestrial higher-plant waxes may serve as a significant source of hydrocarbons, resulting in bitumen enriched in *n*-C_{23} to *n*-C_{31} (Bourbonniere and Meyers, 1996). In contrast, algal marine organic matter typically contributes to the shorter chain *n*-alkanes. The *n*-alkane envelope and the terrigenous/aquatic ratio (TAR), which represents the sum of *n*-C_{16}, *n*-C_{17} and *n*-C_{18} divided by the sum of *n*-C_{27}, *n*-C_{29} and *n*-C_{31}, is therefore useful to investigate wax content and terrestrial vs. marine organic matter contributions (Bourbonniere and Meyers, 1996). However, thermal maturation, biodegradation and/or weathering may significantly alter the original *n*-alkane envelope and overprint the initial organic facies signature (Peters et al., 2005a).

Figure 6.7 shows a heatmap of stratigraphically ordered GC-FID analyzed samples (rows) and identified aliphatic compounds (columns) from the resulting GC-FID fingerprints. The samples of the Vendomdalen Member (facies F0) in the Blanknuten locality display flat or right-skewed unimodal *n*-alkane envelopes (max. mode = C_{15}) and exhibit moderate TAR values of low vari-

ability (0.21 ± 0.02) (not shown). The lithostratigraphic boundary between the Vendomdalen and Muen members records a clear-cut reconfiguration of isoprenoids and *n*-alkanes (Fig. 6.7). The samples of the lower-middle Muen Member (facies F1) exhibit semi-unimodal *n*-alkane envelopes (max. mode = *n*-C_{20}) in both the Blanknuten and Skrukkefjellet sections (Fig. 6.7) and record the highest TAR within the Botneheia Formation (0.34 ± 0.07). The TAR of the samples of the upper Muen Member (facies F2; 0.18 ± 0.05) and those of the lower Blanknuten Member (also facies F2; 0.22 ± 0.09) are lower (max. mode = *n*-C_{15}) and shows notably more asymptotic *n*-alkane envelopes (Fig. 6.7). The samples of the middle Blanknuten Member (facies F3) show similar but less variable TAR (0.17 ± 0.05) as the underlying mudstone facies (i.e., F2). This unit also shows the highest relative abundance of lighter HCs (max. mode = *n*-C_{13}) and a highly asymptotic decline in *n*-alkanes with increasing carbon number (Fig. 6.7). The samples of the upper Blanknuten Member (facies F2/F4) show a lower TAR (0.13 ± 0.07) but relatively higher abundance of heavier *n*-alkanes (max. mode = C_{15}) and varying *n*-alkane envelope patterns (Fig. 6.7). The samples of the Tschermakfjellet Formation (facies F1) shows prominent column bleed due to overall low *n*-alkane concentrations (not shown) and the highest TAR (0.55 ± 0.20) exemplified by relatively high abundancy of waxy *n*-alkanes (Fig. 6.7).

n-alkane/isoprenoid ratios

The Pr/*n*-C_{17} and Ph/*n*-C_{18} ratios are commonly used to infer redox conditions and terrestrial vs. marine organic matter input in both source rock extracts and oils, but are susceptible to alteration by thermal maturation and/or biodegradation (Connan and Cassou, 1980; Shanmugam, 1985). The samples of the Vendomdalen Member (facies F0) record the greatest Pr/*n*-C_{17} (1.88 ± 0.23) and Ph/*n*-C_{18} (1.38 ± 0.26) ratios within the sample set, suggesting mixed organic sources (Fig. 6.8). The samples of the lower–middle Muen Member (facies F1) show lower Pr/*n*-C_{17} (1.08 ± 0.25) and Ph/*n*-C_{18} ratios (0.64 ± 020) (Fig. 6.8), possibly reflecting deposition during slightly more oxidized conditions and/or increased terrestrial organic matter input. The samples of the overlying upper Muen (Pr/*n*-C_{17}= 1.27 ± 0.21, Ph/*n*-C_{18} = 0.85 ± 0.12) and the lower Blanknuten Members (Pr/*n*-C_{17}= 1.47 ± 0.45, Ph/*n*-C_{18} = 0.93 ± 0.26), both facies F2, indicate increased marine organic matter input and/or reducing conditions. The samples of the middle Blanknuten Member (facies F3) shows Pr/*n*-C_{17} = 1.25 ± 0.31 and Ph/*n*-C_{18} = 1.03 ± 0.19, thus recording the most reducing conditions and/or greatest abundancy of marine organic matter content of all the investigated units (Fig. 6.8). The Samples of the upper Blanknuten Member (facies F2/F4) record Pr/*n*-C_{17} = 0.87 ± 0.22 and Ph/*n*-C_{18} = 0.64 ± 0.23 and are thus comparable to the samples of the underlying unit (i.e., facies F3) but indicate an increase in terrestrial organic matter input and/or

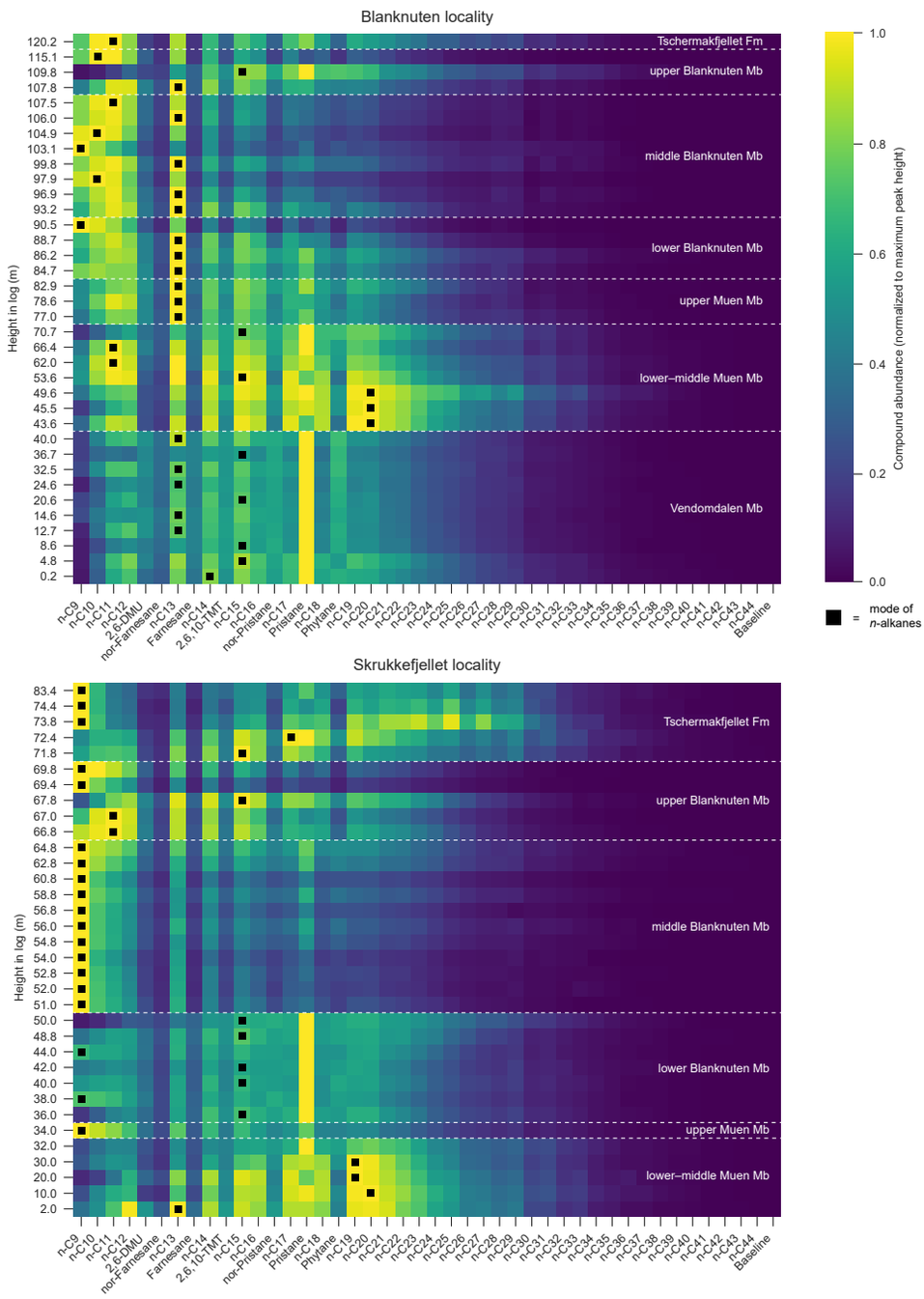

Figure 6.7: GC-FID heatmaps of the Blanknuten and Skrukkefjellet localities, showing the *n*-alkane and isoprenoid distribution for all the samples used in this study. Each row represents a GC-FID chromatogram and are positioned based on their relative stratigraphic height as shown in the Y-axis. All the chromatograms are scaled in between [0,1] using min–max feature scaling, where 0 and 1 represents the chromatogram baseline and maximum *n*-alkane or acyclic isoprenoid peak respectively.

oxidizing conditions, similar to what is documented in the samples of the lower Blanknuten Member (facies F2) (Fig. 6.8). The samples of the Tschermakfjellet Formation (facies F1) record Pr/*n*-C_{17} = 1.03 ± 0.19 and Ph/*n*-C_{18} = 0.50 ± 0.12, suggesting deposition during oxidized conditions and/or a significant increase of terrestrial organic matter input (Fig. 6.8).

The *Alta* (Pr/*n*-C_{17} = 1.12–1.13, Ph/*n*-C_{18} = 0.82–0.83) and *Hanssen* (Pr/*n*-C_{17} = 1.21, Ph/*n*-C_{18} = 0.72) oils plot in the mixed organic matter zone (Fig. 6.8). These oils correlate best with extracts of the F2–F4 phosphogenic samples of the Botneheia Formation. The *Wisting Central* and *Gohta* oils were not included in this part of the study due to a lack of *n*-alkanes in the former sample and a missing GC-FID analysis of the latter.

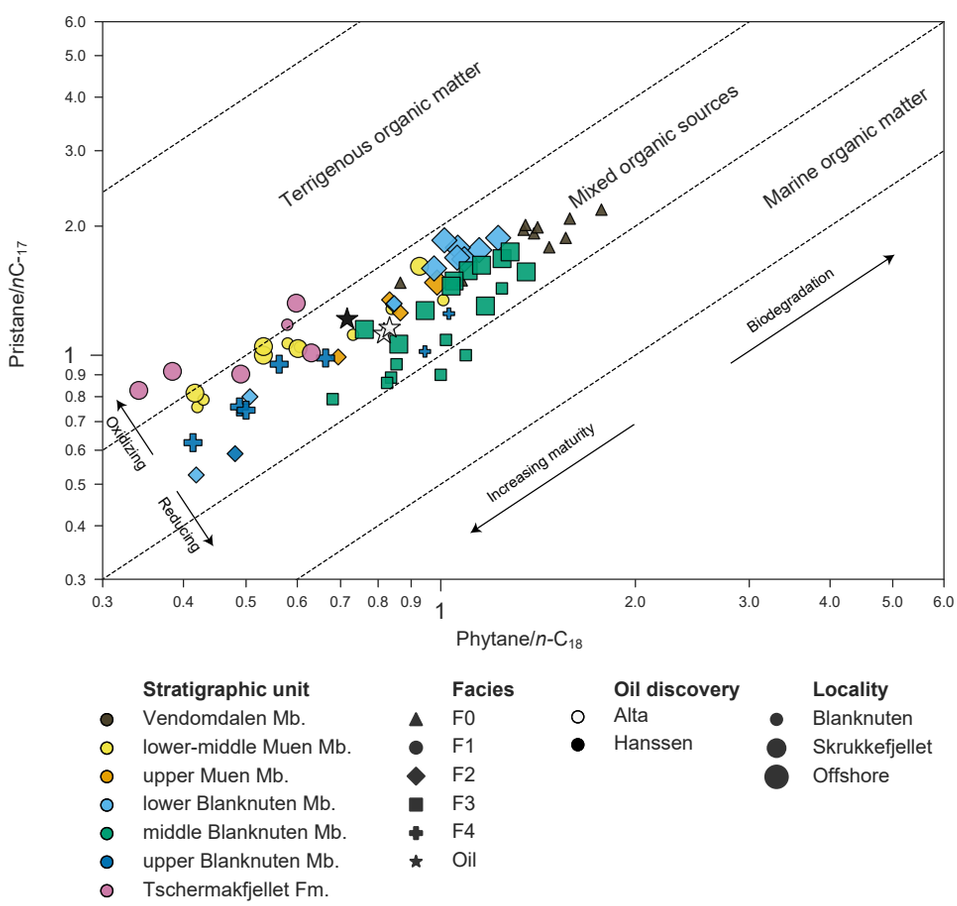

Figure 6.8: Binary plot of Pr/*n*-C_{17} vs. Ph/*n*-C_{18}. The fields implying paleoredox, organic matter type and depositional environments are based on Connan and Cassou (1980) and Shanmugam (1985).

6.4.4 GC-MS

m/z 191 terpane fingerprint

The m/z 191 fingerprint provides a valuable first impression of the terpane distribution of the defined stratigraphic units, facies and investigated oils (Fig. 6.9). In all, but one sample, C_{30} hopane (30αβ) is the most abundant compound among the defined compounds identified (Fig. 6.10). The deviating F2 sample, which is the only facies F2 mudstone sample from the upper Blanknuten Member, records an extreme C_{23}tri peak resulting in a C_{23}tri/30αβ ratio of 1.54 (Fig. 6.10). This sample is further discussed in Section 6.5.1.

Samples of the Vendomdalen Member (facies F0) record abundant C_{23}–C_{30} tricyclic terpanes (Fig. 6.9). An unidentified peak X eluting directly before 30αβ is markedly greater for this stratigraphic unit compared to all the other stratigraphic units and shows the highest concentrations (relative to 30αβ) of the tentatively identified peak 30D13 and the unidentified peak Y (Fig. 6.9). The samples from the lower–middle Muen Member (facies F1) show remarkably less C_{23}–C_{30} tricyclic terpanes. The samples of the upper Muen and lower Blanknuten members (facies F2) record a clear increase in all C_{23}–C_{30} tricyclic terpanes, which are further elevated in the samples of the overlying middle Blanknuten Member (facies F3). The samples of the upper Blanknuten Member (facies F2/F4) show more variable m/z 191 terpane fingerprints but are mostly comparable to the F3 samples (compare Figs. 6.9 and 6.10). Samples of the Tschermakfjellet Formation (facies F1) record a strong decrease in C_{23}–C_{30} tricyclics, and thus resemble the values documented in the samples of the lower–middle Muen Member (which also consist of facies F1 mudstones; Fig. 6.9). Gammacerane (30G) or bisnorhopane (28αβ) were not unequivocally identified in any of the mudstone extracts from Edgeøya.

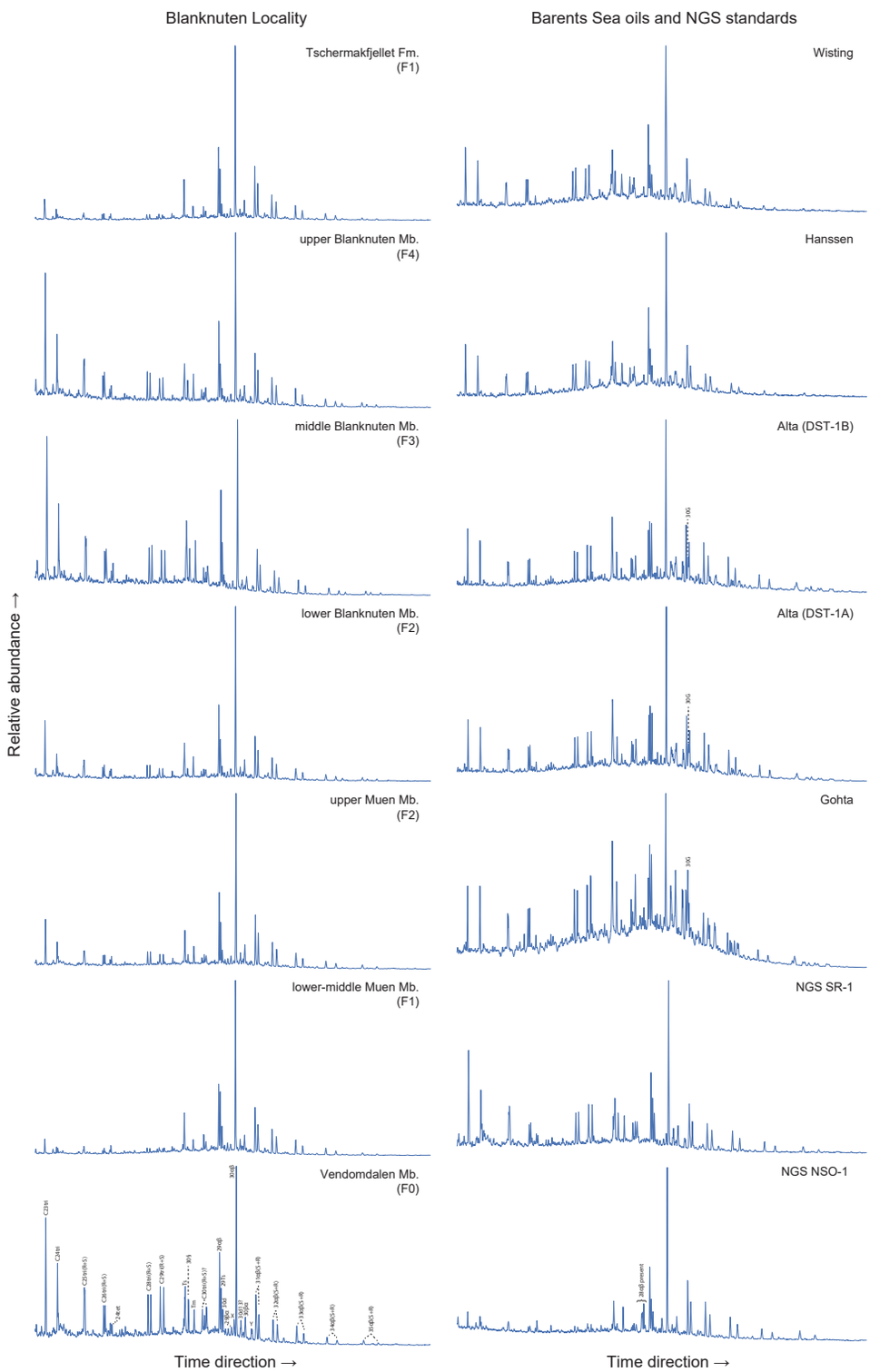

Figure 6.9: m/z 191 terpane fingerprints from the Blanknuten locality representing all the stratigraphic units and oils investigated in this study. The geochemical standards SR-1 and NSO-1 were analyzed and included for peak identification and quantification.

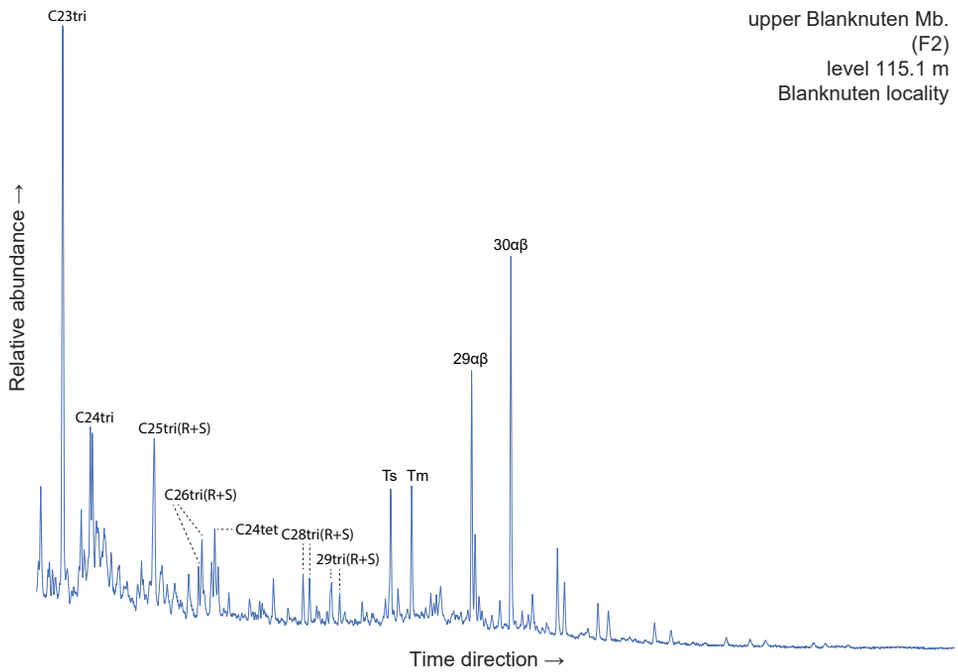

Figure 6.10: m/z 191 terpane fingerprint of the single F2 sample from the upper Blanknuten Member, Blanknuten locality. Note the extreme C_{23}tri peak that exceeds the 30αβ peak.

The SR-1 shows elevated C_{23}–C_{30} tricyclic terpanes and correlates best with m/z = 191 fingerprint of the Vendomdalen Member samples (Fig. 6.9). The *Alta* oils are virtually equal with each other and record abundant tricyclic terpanes. The *Gohta* oil also shows increased relative amounts of C_{23}–C_{30} tricyclic terpanes and an elevated and noisy baseline. As previously observed by Matapour et al. (2019), the *Alta/Gohta* oils show evidence of gammacerane (30G) that partly co-elute with the 22αβR homohopane (Fig. 6.9). 28αβ were not detected for the *Alta/Gohta* oils. The *Wisting Central/Hanssen* oils both show a good correlation with each other for the C_{23}–C_{30} tricyclic terpane distribution, and 30G or 28αβ were not detected.

Source facies biomarkers

The scaled (100%) C_{27}ββ(R + S)–C_{28}ββ(R + S)–C_{29}ββ(R + S) sterane distribution (Fig. 6.11a) is commonly applied to investigate the terrestrial vs. marine organic matter input of source rock extracts and oils (Huang and Meinschein, 1979; Shanmugam, 1985). The C_{28}ββ(R + S)/C_{29}ββ(R + S) ratio in source rocks with primarily marine organic matter also increases with increasing geological age (Grantham and Wakefield, 1988). Similarly, the extended tricyclic terpane

ratio (ETR) = (C_{28}tri + C_{29}Tri)/Ts has been used to distinguish Triassic vs. Jurassic oils (Holba et al., 2001). These distributions and ratios may thus be combined to evaluate source rock facies and ages of Barents Sea oils and condensates (Lerch et al., 2017).

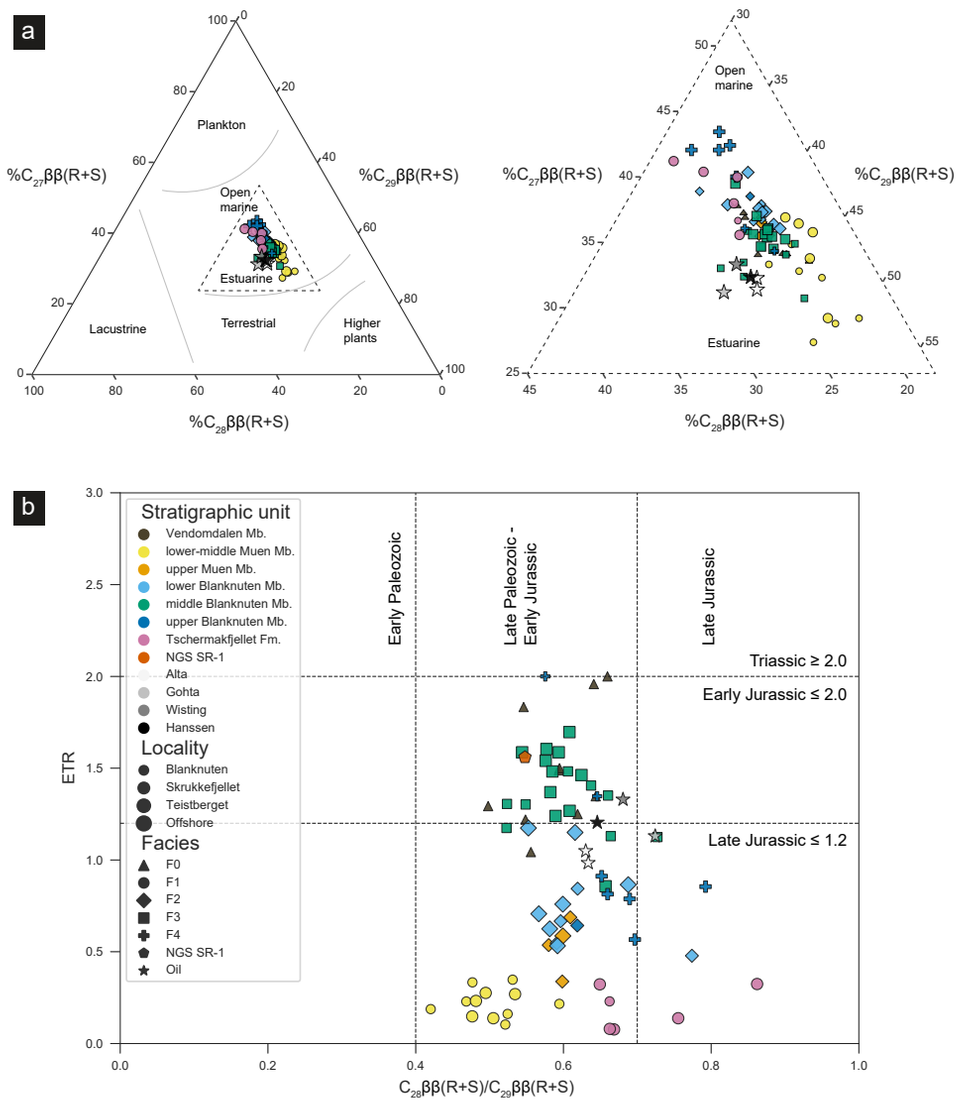

Figure 6.11: (a) Ternary plot of the $C_{27}\beta\beta$(R + S)–$C_{28}\beta\beta$(R + S)–$C_{29}\beta\beta$(R + S) distribution, implying organic matter input. Modified from Huang and Meinschein (1979) and Shanmugam (1985). The dashed ternary plot to the right corresponds to the highlighted area as shown in the left ternary plot. **(b)** Binary plot of the $C_{28}\beta\beta$(R + S)/$C_{29}\beta\beta$(R + S) ratio (Grantham and Wakefield, 1988) vs. the ETR (Holba et al., 2001).

The $C_{28}\beta\beta$(R + S)/$C_{29}\beta\beta$(R + S) ratios of the entire dataset (0.61 ± 0.08) indicate a Late Paleozoic to Early Jurassic age for most of the extracts and all the oils analyzed in this study (Fig. 6.11b). This age-specific ratio apparently shows no consistent trend in the data set. The samples of the Vendomdalen Member (Spathian; facies F0), for example, record significantly larger ratios (0.59 ± 0.05) than those of the lower–middle Muen Member (Anisian; facies F1) (0.50 ± 0.04). However, within the Botneheia Formation mudstones, the ratio clearly increases upwards in the unit. The samples of the Tschermakfjellet Formation (Carnian; facies F1) record the highest $C_{28}\beta\beta$(R + S)/$C_{29}\beta\beta$(R + S) ratio in the sample set (0.71 ± 0.08). The oils range in between 0.63–0.72.

The samples of the Vendomdalen Member (facies F0) have the highest ETR (1.49 ± 0.33) (Fig. 6.11). The ETR abruptly decreases in the overlying lower–middle Muen Member (facies F0) (0.22 ± 0.08). The upper Muen Member samples (facies F2) (0.54 ± 0.15) and the lower Blanknuten Member samples (facies F2) (0.75 ± 0.23) partly group together. The middle Blanknuten Member samples (facies F3) mark a further increase in ETR (1.37 ± 0.21) but decrease upwards into the upper Blanknuten Member (facies F2/F4) (0.99 ± 0.47). The extracts of the Tschermakfjellet Formation (facies F1) record a relatively low ETR (0.20 ± 0.11), resembling the ETR of the lower–middle Muen Member samples. The oils range in between 0.98–1.33.

Yurchenko et al. (2018) showed that high vs. low C_{26}tri/C_{24}tet ratios and low vs. high 29αβ/30αβ ratios were useful to identify shaly vs. calcareous source rocks within the phosphatic Middle–Upper Triassic Shublik Formation in the North Slope Basin, northern Alaska. This study applies the C_{24}tet/30αβ ratio (Lerch et al., 2016b) rather than C_{26}tri/C_{24}tet, but both ratios essentially represent a "C_{24} tetracyclic index" (Peters et al., 2005a) used to evaluate source rock lithology (e.g., Connan et al., 1986). The C_{24}tet/30αβ ratio could potentially be maturity-independent and age-specific for Paleozoic–Triassic vs. Jurassic oils in the Barents Sea (Lerch et al., 2016b; Lerch et al., 2017). The samples of the Vendomdalen Member (facies F0) show intermediate C_{24}tet/30αβ ratios (0.06 ± 0.01) with no noticeable transition into the lower–middle Muen Member (facies F1) (0.06 ± 0.009). The samples of the upper Muen and lower Blanknuten members (both facies F2) show intermediate C_{24}tet/30αβ ratios (0.06 ± 0.02 and 0.06 ± 0.03 respectively), while the middle Blanknuten Member (facies F3) samples record an increased ratio of 0.08 ± 0.02. The samples of the upper Blanknuten Member (facies F2/F4) are the highest among the mudstone extracts (0.09 ± 0.02). The samples of the Tschermakfjellet Formation (facies F1) record a low C_{24}tet/30αβ ratio (0.04 ± 0.004). The SR-1 and the oils show higher C_{24}tet/30αβ ratios ranging between 0.06–0.13.

The 29αβ/30αβ ratios recorded in the samples of the Vendomdalen Member

(facies Fo; 0.41 ± 0.06) are low and comparable to those of lower–middle Muen Member (facies F1; 0.42 ± 0.05) Fig. 6.12. The samples of the upper Muen (Facies F2; 0.48 ± 0.09), lower Blanknuten (Facies F2; 0.53 ± 0.08) and middle Blanknuten (Facies F3; 0.56 ± 0.05) members show intermediate values, while samples from the upper Blanknuten Member exhibit the highest ratios in the sample set (Facies F2/F4; 0.62 ± 0.10). The SR-1 (0.43) and the oils display relatively low values (0.31–0.50).

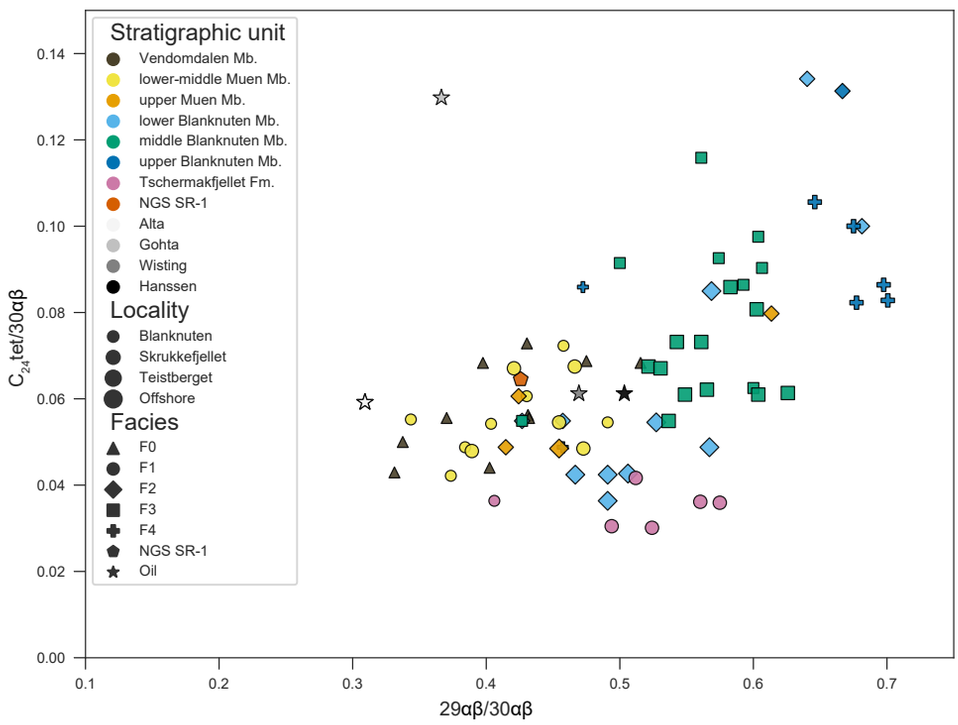

Figure 6.12: Binary plot of the 29αβ/30αβ ratio (Peters et al., 2005a) vs. the C_{24}tet/30αβ ratio (Mello et al., 1988). Lower and higher values typically represent clay-rich vs. clay-poor mudstones respectively (Peters et al., 2005a).

Yurchenko et al. (2018) also demonstrated that high vs. low dia/(dia + reg) steranes and high vs. low 30d/(30d + 30αβ) ratios correlated well with shaly vs. calcareous lithologies in the Shublik Formation. In the present study, samples of the Vendomdalen Member (facies Fo) show relatively high dia/(dia + reg) ratios (0.50 ± 0.02), in strong contrast to all the mudstones of the Botneheia Formation (Fig. 6.13). Samples of the lower–middle Muen Member (facies F1) and those of the upper Blanknuten Member (facies F2/F4) show the highest (0.35 ± 0.03) and lowest (0.30 ± 0.05) dia/(dia + reg) steranes ratios, respectively. Samples of the Tschermakfjellet Formation (facies F1) record intermediate ratios (0.37 ± 0.04), which strongly overlap with those of the lower–middle Muen Member (facies F1). The SR-1 and the oils show high values

(0.40–0.54), mostly comparable to the ratios recorded in the Vendomdalen Member (facies F0) (Fig. 6.13).

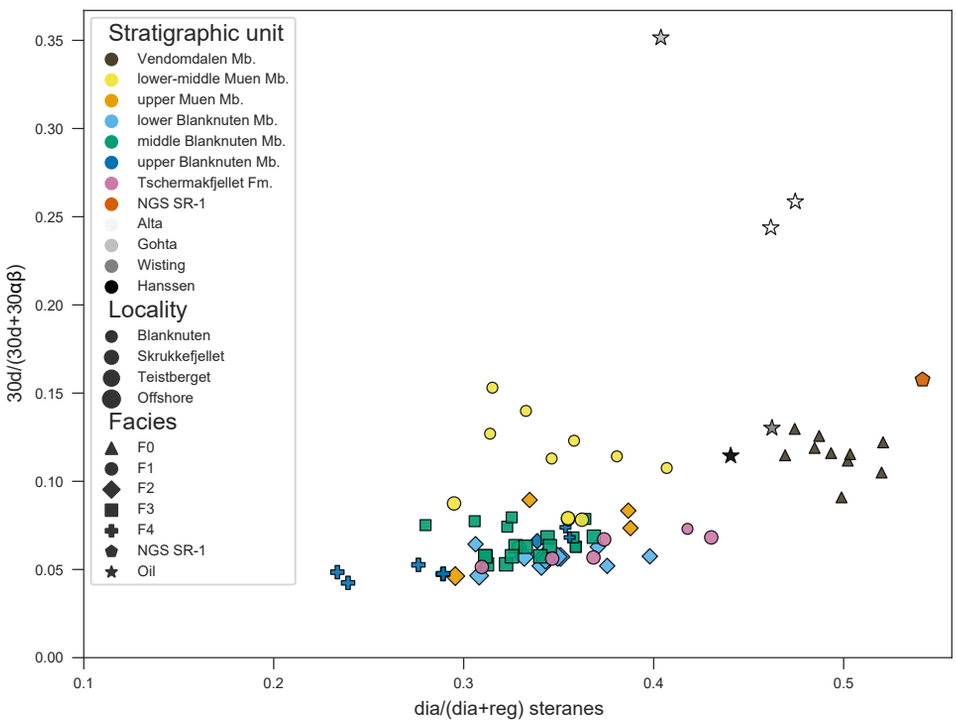

Figure 6.13: Binary plot of the 30d/(30d + 30αβ) ratio (e.g., Yurchenko et al., 2018) vs. the dia/(dia + reg) steranes ratio (e.g., Peters et al., 2005a). dia/(dia + reg) steranes = (27dβS + 27dβR)/(27dβS + 27dβR + 29ααS + 29ββR + 29ββS + 29ααR). Lower and higher values indicate clay-poor vs. clay-rich mudstones respectively (Peters et al., 2005a).

The 30d/(30d + 30αβ) ratios of samples from the Vendomdalen Member (facies F0; 0.12 ± 0.01) and the lower–middle Muen Member (facies F1; 0.11 ± 0.03) are overall high (Fig. 6.13). Samples from the upper Muen Member (facies F2; 0.07 ± 0.02), lower Blanknuten Member (facies F2; 0.06 ± 0.005), and the middle Blanknuten Member (facies F3; 0.07 ± 0.01) show intermediate 30d/(30d + 30αβ) ratios. Samples of the upper Blanknuten Member (facies F2/F4; 0.06 ± 0.01) and the Tschermakfjellet Formation (facies F1; 0.06 ± 0.01) show low 30d/(30d + 30αβ) ratios. The SR-1 (0.16) and the oils exhibit a wide range of 30d/(30d + 30αβ) ratios (0.11–0.35) (Fig. 6.13).

The C_{29}tri/C_{28}tri ratio (Lorenson et al., 2009) and the (C_{23}-C_{29})tri/30αβ ratio (Mello et al., 1988) have previously been used as correlation and source parameters. The C_{29}tri/C_{28}tri ratios vs. the (C_{23}-C_{29})tri/30αβ ratios of samples of the Vendomdalen Member (facies F0; 1.13 ± 0.08 vs. 1.55 ± 0.31) show clear

separation from the overlying lower–middle Muen Member samples (facies F1; 0.93 ± 0.21 vs. 0.30 ± 0.09) (Fig. 6.14). The upper Muen Member samples (facies F2; 0.80 ± 0.02 vs. 0.70 ± 0.21) and lower Blanknuten Member samples (facies F2; 0.93 ± 0.21 vs. 0.99 ± 0.51) are generally similar with mostly intermediate values. The samples of the middle Blanknuten Member (facies F3; 0.79 ± 0.08 vs. 1.54 ± 0.37) and the upper Blanknuten Member (facies F2/F4; 0.66 ± 0.12 vs. 1.77 ± 0.47) show high and highest tricyclic terpane content, respectively, and low and lowest C_{29}tri/C_{28}tri ratios, respectively (Fig. 6.14). Samples of the Tschermakfjellet Formation (facies F1; 0.92 ± 0.18 vs. 0.24 ± 0.14) are equivalent to the lower–middle Muen Member samples. The SR-1 sample (1.22 vs. 1.71) and the oils (1.04–1.17 vs. 1.25–2.42) directly overlap with the samples of the Vendomdalen Member (facies F0).

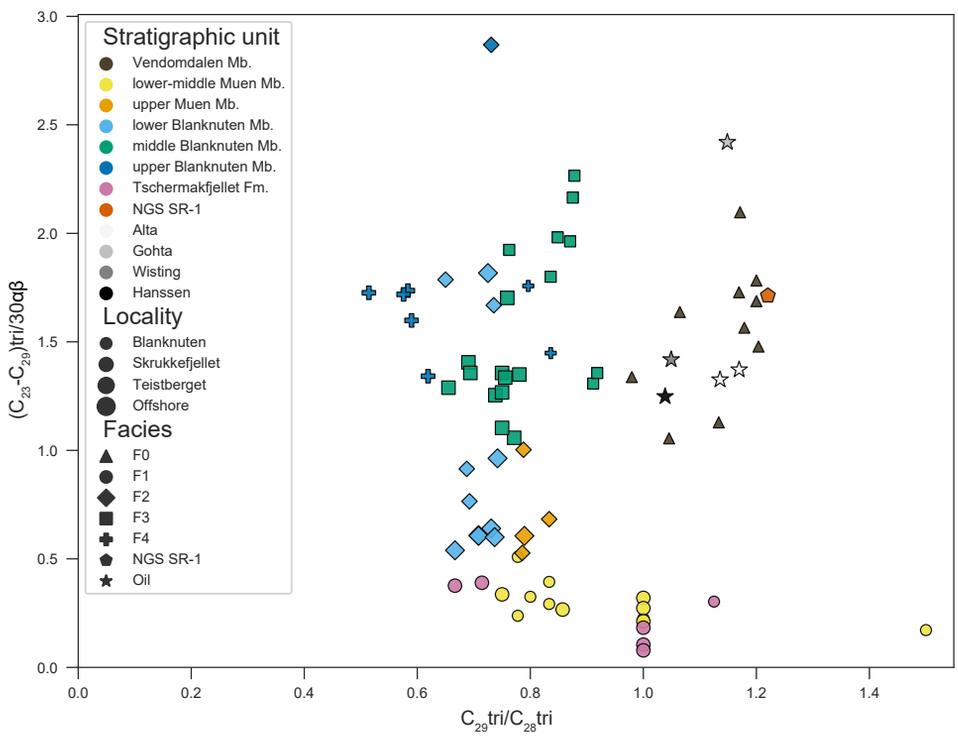

Figure 6.14: Binary plot of the C_{29}tri/C_{28}tri ratios (Lorenson et al., 2009) vs. the (C_{23}–C_{29})tri/30αβ ratios (Mello et al., 1988) used for correlation.

The Pr/Ph ratio retrieved from the GC-FID chromatograms and the sum of 4-, 3-, 2-, 1-MDBTs over the sum of 2-, 3-, 9-, 1-methylphenanthrenes (MPs) (MDBTs/MPs) are commonly used in tandem to interpret source facies (Hughes et al., 1995; Radke et al., 2001). The Vendomdalen Member samples (facies F0) shows relatively low Pr/Ph (1.60 ± 0.11) and MDBTs/MPs ratios (0.09 ± 0.03) (Fig. 6.15). The lower–middle Muen Member samples (facies F1) record similar

MDBTs/MPs ratios (0.11 ± 0.02), but a higher Pr/Ph ratio (1.87 ± 0.18). The samples of the upper Muen and lower Blanknuten members (both facies F2) return to slightly lower Pr/Ph ratios (1.75 ± 0.05 and 1.81 ± 0.11, respectively), and the latter shows an abrupt increase and variability in the MDBTs/MPs ratio (0.21 ± 0.08). The samples from the middle Blanknuten Member (facies F3) record the lowest Pr/Ph ratios (1.58 ± 0.15) and highest MDBTs/MPs ratios (0.40 ± 0.09) among all the analyzed extracts. The upper Blanknuten Member samples (facies F2/F4) generally show intermediate but variable Pr/Ph and MDBTs/MPs ratios (1.75 ± 0.22 and 0.21 ± 0.08 respectively) that group mostly with the lower Blanknuten Member samples (facies F2). The Tschermakfjellet Formation samples (facies F1) show low MDBTs/MPs ratios (0.09 ± 0.04) but the highest Pr/Ph ratios (2.39 ± 0.21) in the sample set (Fig. 6.15). The SR-1 shows virtually identical Pr/Ph and MDBTs/MPs ratios to those recorded in the Vendomdalen Member. The *Alta* oils record relatively low Pr/Ph ratios (1.45–1.47) and elevated MDBTs/MPs ratios (0.26–0.27), contrasting the notably higher Pr/Ph ratios (1.77–1.61) and lower MDBTs/MPs ratios (both 0.15) of the *Wisting Central/Hanssen* oils (Fig. 6.15). The *Gohta* oil exhibits an elevated MDBTs/MPs ratio = 0.42 (not shown).

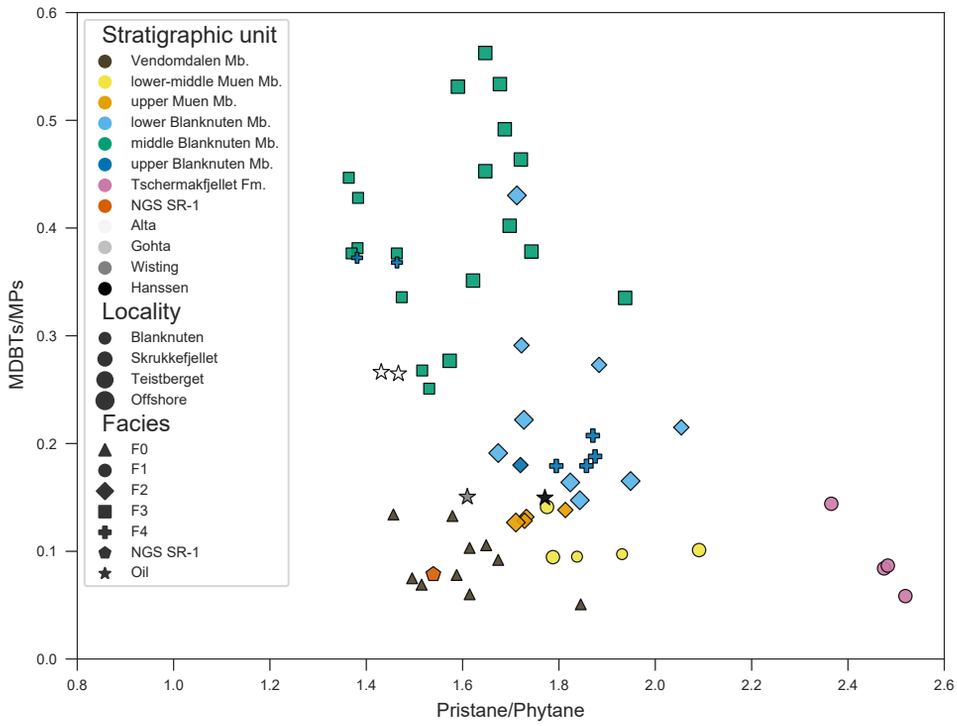

Figure 6.15: Binary plot of the MDBTs/MPs ratios vs. Pr/Ph ratios used for determining source rock lithology and depositional environment (Hughes et al., 1995; Radke et al., 2001). Higher vs. lower MDBTs/MPs ratios indicate calcareous vs. shaly source rocks respectively, while higher vs. lower Pr/Ph ratios indicate oxidizing vs. reducing benthic redox potential respectively (Hughes et al., 1995).

Thermal maturity biomarkers

As the entire Botneheia and the lower Tschermakfjellet formations were sampled in both the early mature Blanknuten section and in the immature to early mature Skrukkefjellet section, it is possible to document maturity contrast between these localities. The Lower Triassic Vendomdalen Member was only sampled in the Blanknuten locality and a comparison between the Blanknuten and Skrukkefjellet sections for this particular unit is therefore not possible.

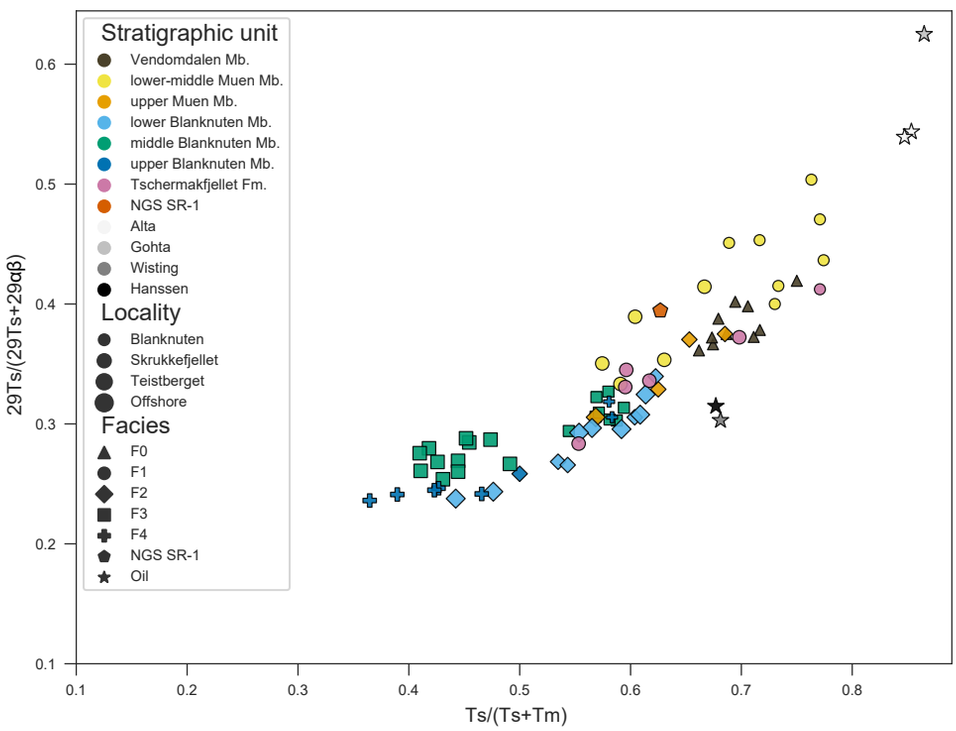

Figure 6.16: Binary plot of the thermal maturity parameters 29Ts/(29Ts + 29αβ) (Peters et al., 2005a) vs. Ts/(Ts + Tm) (Seifert and Moldowan, 1978). Higher values for both ratios indicate higher thermal maturity.

17α(H)-22,29,30-trisnorhopane (Tm) is thermally unstable relative to 18α(H)-22,29,30-trisnorneohopane (Ts), resulting in an increase in the Ts/(Ts + Tm) ratio with greater thermal maturation (Seifert and Moldowan, 1978). Transformation from Tm to Ts may also occur, but this is speculative (Peters et al., 2005a). The 29Ts/(29Ts + 29αβ) maturity parameter has similar properties as the Ts/(Ts + Tm) ratio (Peters et al., 2005a). The samples from the Vendomdalen Member show elevated Ts/(Ts + Tm) vs. 29Ts/(29Ts + 29αβ) ratios (facies F0; 0.70 ± 0.03 vs. 0.38 ± 0.02), generally overlapping with samples from the lower–middle Muen Member (facies F1; 0.69 ± 0.07 vs. 0.41 ± 0.05) and the upper Muen Member (facies F2; 0.63 ± 0.05 vs. 0.34 ± 0.03) (Fig. 6.16). The lower Blanknuten Member samples (facies F2; 0.56 ± 0.06 vs. 0.29 ± 0.03), middle Blanknuten Member samples (facies F3; 0.50 ± 0.07 vs. 0.29 ± 0.02) and upper Blanknuten Member (facies F2/F4; 0.47 ± 0.08 vs. 0.26 ± 0.03) all display significantly lower ratios. The Tschermakfjellet Formation samples (facies F1; 0.64 ± 0.08 vs. 0.35 ± 0.04) exhibit values similar to the lower–middle Muen Member samples (facies F1). When grouped by stratigraphic unit, it is apparent that the mean of both ratios is consistently higher in the Blanknuten section than in the Skrukkefjellet section (Fig. 6.17).

The SR-1 (0.63 vs. 0.39) is equivalent to the values recorded in samples of mudstone facies F0 and F1 (Fig. 6.16). The *Alta/Gohta* oils clearly document the largest ratios in the sample set (0.85–0.86 vs. 0.54–0.62), while the *Wisting Central* (0.68 vs. 0.30) and *Hanssen* (0.68 vs. 0.31) oils group with each other and the extracts (Fig. 6.16).

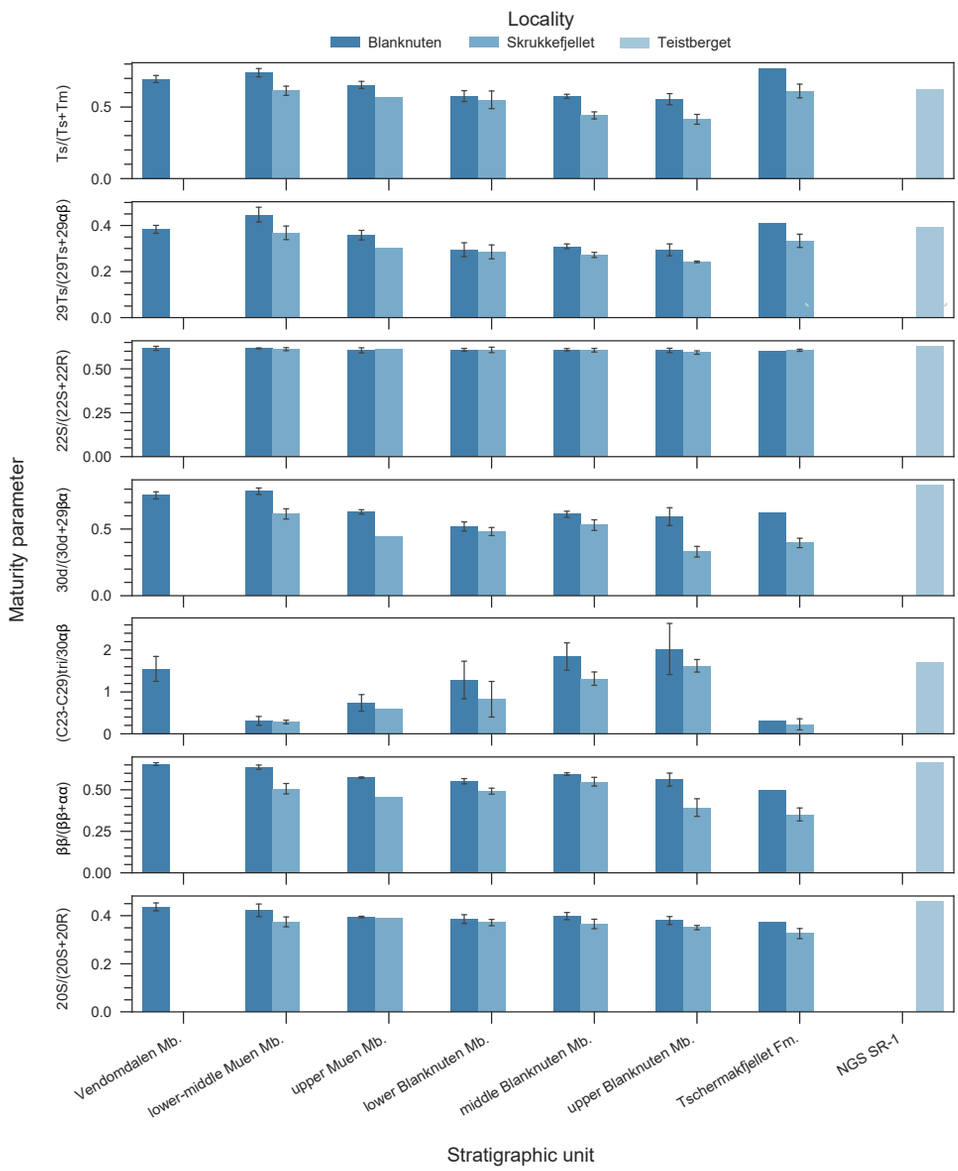

Figure 6.17: Bar charts of mean values and standard deviation (error bars) of biomarker-derived thermal maturity parameters for all the stratigraphic units compared by locality. Note the dominantly lower maturity ratios for the Skrukkefjellet locality relative to the Blanknuten locality for the specific stratigraphic units.

The 22S/(22S + 22R) ratio of the C_{31} homohopanes is a thermal maturity parameter specific for the immature–early mature oil window with isomerization equilibrium at c. 0.6 (Seifert and Moldowan, 1980). Also, the 30d/(30d + 29βα) ratio is useful as a maturity parameter as diahopane (30d) is thermally more stable relative to normoretan (29βα) (Cornford et al., 1986). However, both ratios are shown to be affected by source facies (Peters et al., 2005a). The 22S/(22S + 22R) ratio of the entire sample set range between 0.54–0.65 (0.61 ± 0.02), thus not showing any significant location-specific difference between the extracts (Figs. 6.17 and 6.18).

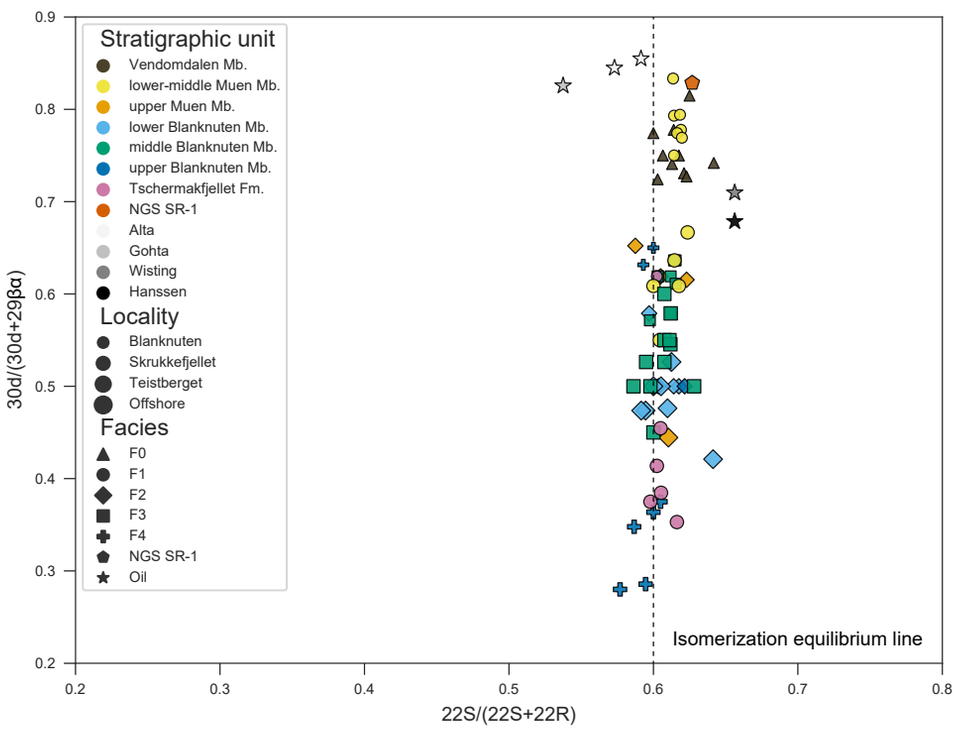

Figure 6.18: Binary plot of the thermal maturity parameters 22S/(22S + 22R) of the C_{31} homohopanes (Seifert and Moldowan, 1980) vs. the 30d/(30d + 29ba) (Cornford et al., 1986). The 22S/(22S + 22R) ratios reach equilibrium at c. 0.6, indicating early maturity (Seifert and Moldowan, 1980).

In contrast, the 30d/(30d + 29βα) ratio shows elevated values for samples of the Vendomdalen Member (facies F0; 0.75 ± 0.03) and the lower–middle Muen Member (facies F1; 0.71 ± 0.09) (Fig. 6.18). All the phosphatic mudstone facies (F2, F3 and F4) generally exhibit low 30d/(30d + 29βα) ratios, i.e., the samples of the upper Muen (0.58 ± 0.09), the lower Blanknuten (0.50 ± 0.04), the middle Blanknuten (0.56 ± 0.05), and the upper Blanknuten members (0.43 ± 0.15). The samples from the Tschermakfjellet Formation (facies F1) record low 30d/(30d + 29βα) ratios (0.43 ± 0.10; Fig. 6.18). The different

stratigraphic units investigated at the Blanknuten locality show consistently higher mean 30d/(30d + 29βα) ratios than for the equivalent units at the Skrukkefjellet locality (Fig. 6.17). The SR-1 (0.83) and the oils (0.68–0.85) are all comparable to the values obtained from the mudstone extracts from the Vendomdalen (facies F0) and the lower–middle Muen members (facies F1) (Fig. 6.18).

The ββ/(ββ + αα) steranes vs. 20S/(20S + 20R) steranes ratios of samples of the Vendomdalen Member (facies F0; 0.66 ± 0.01 vs. 0.44 ± 0.02) are the highest in the dataset, showing some overlap with those of the lower–middle Muen Member (facies F1; 0.58 ± 0.07 vs. 0.40 ± 0.04) (Fig. 6.19). The samples of the upper Muen Member (facies F2; 0.54 ± 0.06 vs. 0.39 ± 0.004), the lower Blanknuten Member (facies F2; 0.51 ± 0.04 vs. 0.38 ± 0.02) and the middle Blanknuten Member (facies F3; 0.57 ± 0.03 vs. 0.38 ± 0.02) show variable degree of overlap. The samples of the upper Blanknuten Member (facies F2/F4; 0.46 ± 0.10 vs. 0.36 ± 0.02) and the Tschermakfjellet Formation (facies F1; 0.38 ± 0.07 vs. 0.33 ± 0.03) are clearly lower than the bulk of the sample set. The SR-1 is surprisingly high (0.66 vs. 0.46) as it is expected to show an immature source signal (Dahlgren et al., 1998). The oils group well together, ranging from 0.57–0.60 and 0.41–0.44 for the ββ/(ββ + αα) and 20S/(20S + 20R) ratios, respectively (Fig. 6.19).

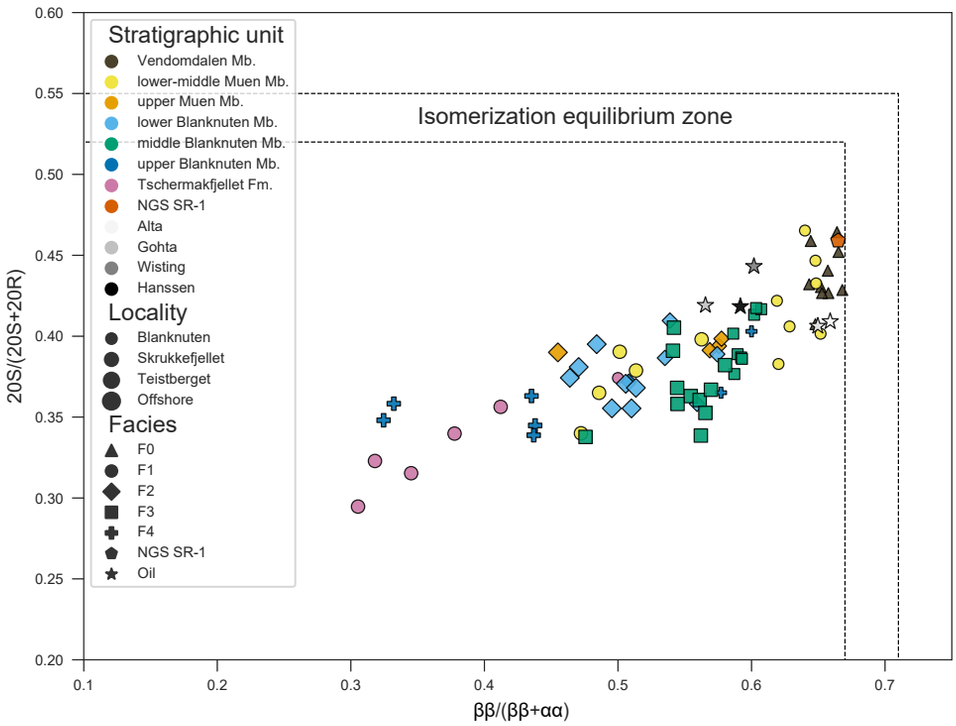

Figure 6.19: Binary plot of the thermal maturity parameters 20S/(20S + 20R) steranes vs. the bb/(bb + aa) steranes (Seifert and Moldowan, 1986). 20S/(20S + 20R) steranes = 29ααS/(29ααS + 29ββR). ββ/(ββ + αα) steranes = (29ββR + 29ββS)/(29ββR + 29ββS + 29ααS + 29ααR). Higher values for both ratios indicate higher thermal maturity. The isomerization equilibrium threshold indicates samples that are minimum peak mature.

The methylphenanthrene ratio (MPR) and the methylphenanthrene index 1 (MPI-1) (Radke et al., 1982) calibrated to vitrinite reflectance (VR) values—i.e. %Rm MPR and %Rc MPI-1—enable direct maturity comparisons of oils/bitumen and rocks (Radke, 1988). The %Rm MPR vs. %Rc MPI-1 binary plot of samples of the Vendomdalen Member (facies F0; 0.71 ± 0.03 % vs. 0.74 ± 0.03 %) shows that %Rc MPR values for this facies are relatively low compared to the remaining sample set (Fig. 6.20). The samples of the lower–middle Muen Member (facies F1; 0.83 ± 0.04 % vs. 0.73 ± 0.04 %), upper Muen Member (facies F2; 0.83 ± 0.03 % vs. 0.71 ± 0.02 %), lower Blanknuten Member (facies F2; 0.81 ± 0.03 % vs. 0.71 ± 0.03 %), middle Blanknuten Member (facies F3; 0.78 ± 0.02 % vs. 0.69 ± 0.02 %), and the upper Blanknuten Member (facies F2/F4; 0.80 ± 0.02 % vs. 0.68 ± 0.02 %) are similar. The Tschermakfjellet Formation samples (facies F1; 0.86 ± 0.03 % vs. 0.73 ± 0.02 %) correlate best with facies F1 samples of the lower–middle Muen Member (Fig. 6.20). The SR-1 (0.77 % vs. 0.74 %) shows intermediate values. None of the mudstone

extracts overlap with the Ro isolines from the Blanknuten and Skrukkefjellet localities (Fig. 6.20), which represent measured vitrinite values from these localities (see Wesenlund et al., 2021). The *Wisting Central/Hanssen* (1.00–1.01 % vs. 0.83–0.85 %) and the *Alta/Gohta* oils (0.92–0.98 % vs. 0.89–0.92 %) show the highest values, forming a separated group in the dataset.

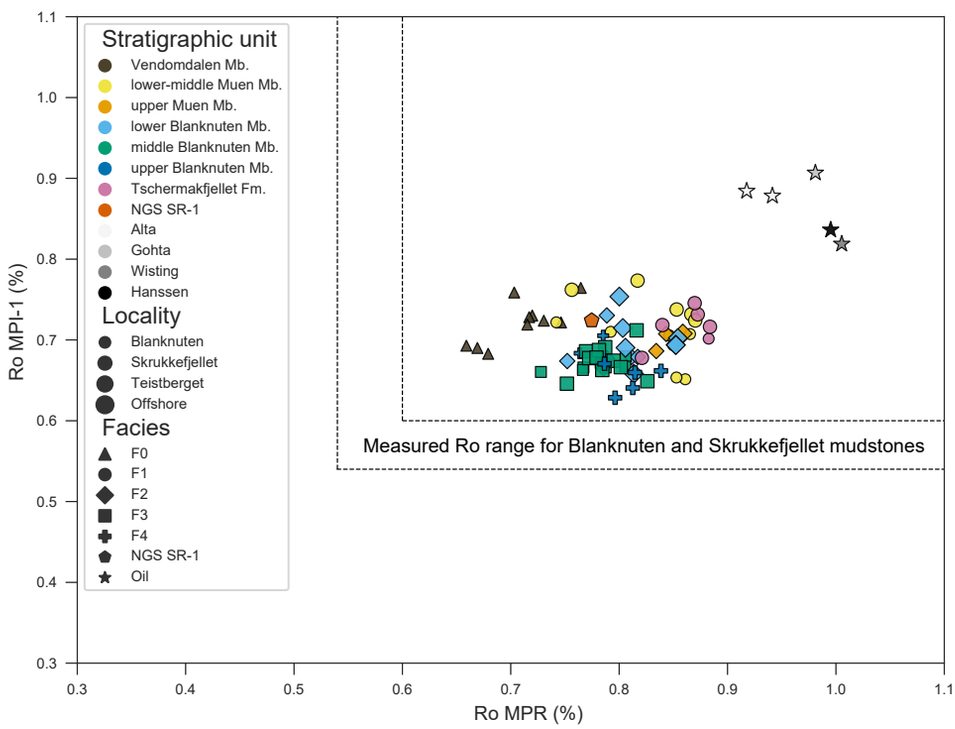

Figure 6.20: Binary plot of the thermal maturity parameters MPR and MPI-1 (Radke et al., 1982) calibrated to VR values (Radke, 1988). The isolines represent the average measured VR between the Blanknuten (mean 0.60 %) and Skrukkefjellet (mean 0.54 %) localities (Wesenlund et al., 2021).

The methylphenanthrene distribution factor 1 (MPDF1) and methylphenanthrene distribution factor 2 (MPDF2) and their calibration against vitrinite reflectance—i.e., %Ro MPDF1 and %Ro MPDF1—were introduced to bypass potential non-linearity problems associated with the MPI-1 parameter (Kvalheim et al., 1987). A binary plot of %RoMPDF1 vs. %RoMPDF2 shows that samples from the Vendomdalen Member (facies F0; 0.75 ± 0.04 % vs. 0.54 ± 0.02), lower–middle Muen Member (facies F1; 0.78 ± 0.04 % vs. 0.60 ± 0.06 %), upper Muen Member (facies F2; 0.74 ± 0.05 % vs. 0.61 ± 0.03 %), lower Blanknuten Member (facies F2; 0.72 ± 0.04 % vs. 0.58 ± 0.04 %), middle Blanknuten Member (facies F3; 0.66 ± 0.03 % vs. 0.55 ± 0.03 %) and upper Blanknuten Member (facies F2/F4; 0.67 ± 0.04 % vs. 0.58 ± 0.05 %) generally overlap (Fig. 6.21). The Tschermakfjellet Formation samples (facies F1; 0.83

± 0.04 % vs. 0.66 ± 0.02 %) correlate best with those of the lower–middle Muen Member (also facies F1). The SR-1 (0.77 % vs. 0.59 %) group mostly with the lower–middle Blanknuten samples (facies F2). Of the two ratios, the %RoMPDF2 shows good correspondence to the measured Ro values from the Blanknuten and Skrukkefjellet localities. The %RoMPDF1 vs. %RoMPDF2 ratios are significantly higher for the oils (0.91–0.93 % vs. 0.68–0.73 %) and form a separate group (Fig. 6.21).

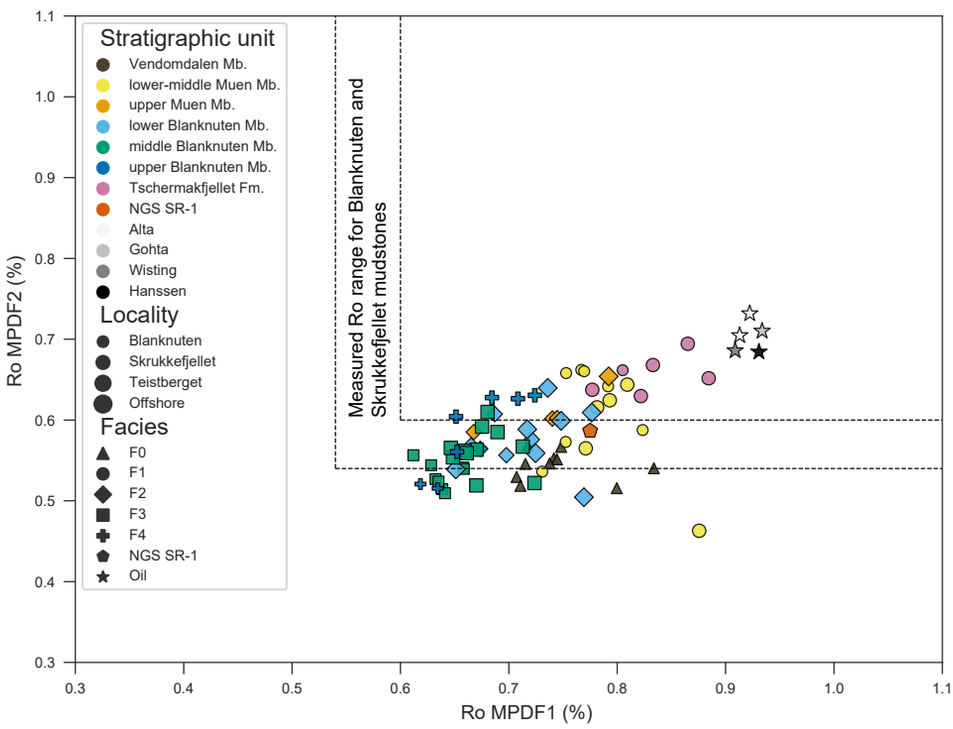

Figure 6.21: Binary plot of the thermal maturity parameters MPDF1 and MPDF2 and their Ro calibrations (Kvalheim et al., 1987). The isolines represent the average measured VR between the Blanknuten (mean 0.60 %) and Skrukkefjellet (mean 0.54 %) localities (Wesenlund et al., 2021).

Summary logs

A log panel of selected source- and maturity-related parameters from the Blanknuten and Skrukkefjellet localities are shown in Figure 6.22 to illustrate important organic chemostratigraphic trends. The TOC log exhibits a positive trend upwards through the Vendomdalen Member, abruptly shifting to slightly lower values across the boundary to the Botneheia Formation. In both sections, the TOC content increases upwards from the base of lower–middle Muen Member and upwards through the lower and middle Blanknuten members. From

here, the TOC log shows a negative incline until the top of the upper Blanknuten Member. Across the boundary to the overlying Tschermakfjellet Formation, the TOC content is low, returning to values like the lower–middle Muen Member. The TIC log increases upwards in both sections with a maximum in the upper Blanknuten Member, then abruptly decreasing into the lowermost Tschermakfjellet Formation. The Pr/Ph log decreases upwards within the Vendomdalen Member, showing an abrupt increase across the boundary to the Botneheia Formation. In both sections, the Pr/Ph log decreases upwards with a minimum in the middle Blanknuten Member, then increasing upwards and especially within the lower Tschermakfjellet Formation. The ETR shows overall the same stratigraphic development as the TOC log but with a significantly more abrupt geochemical transition at the boundary between the Vendomdalen Member and Botneheia Formation. The C_{24}tet/30$\alpha\beta$ and 29$\alpha\beta$/30$\alpha\beta$ logs do not change significantly across the boundary between the Vikinghøgda and Botneheia formations but exhibit an upwards-increasing trend within the Botneheia Formation. The dia/(dia + reg) log displays substantial negative and positive shifts at the boundaries between the Vikinghøgda and Botneheia formations, and between the Botneheia and Tschermakfjellet formations, respectively. The Ts/(Ts + Tm), 29Ts/(29Ts + 29$\alpha\beta$) and Ro MPR logs all display the same stratigraphic development with each other, i.e., a clear positive excursion at the boundary between the Vendomdalen and lower–middle Muen members, overall decrease upwards within the Botneheia Formation, and a positive excursion across the top Botneheia Formation boundary into the Tschermakfjellet Formation.

6.5 Discussion

6.5.1 Lower–Upper Triassic mudstones

Source rock generation potential

The calculated SPI and the pyrolysis results of the various mudstone-dominated units clearly show that the combined phosphogenic mudstone units (composed of facies F2–F4) of the Middle Triassic by far represent the best source rock interval in both sections (Fig. 6.5). This fits the results of previous work (Abay et al., 2018; Bjorøy et al., 2009; Krajewski, 2013; Mørk and Bjorøy, 1984; Wesenlund et al., 2021). Based on the SPI values (Fig. 6.5), any liquid hydrocarbon contributions from the Lower Triassic Vendomdalen Member mudstones and the non-phosphatic lower–middle Muen Member mudstones should be small relative to the bulk phosphatic unit (the combined F2–F4 facies succession). Still, the Vendomdalen Member has a SPI that equals c. 17 % of the bulk phosphatic unit. If the bulk phosphatic unit or the lateral facies

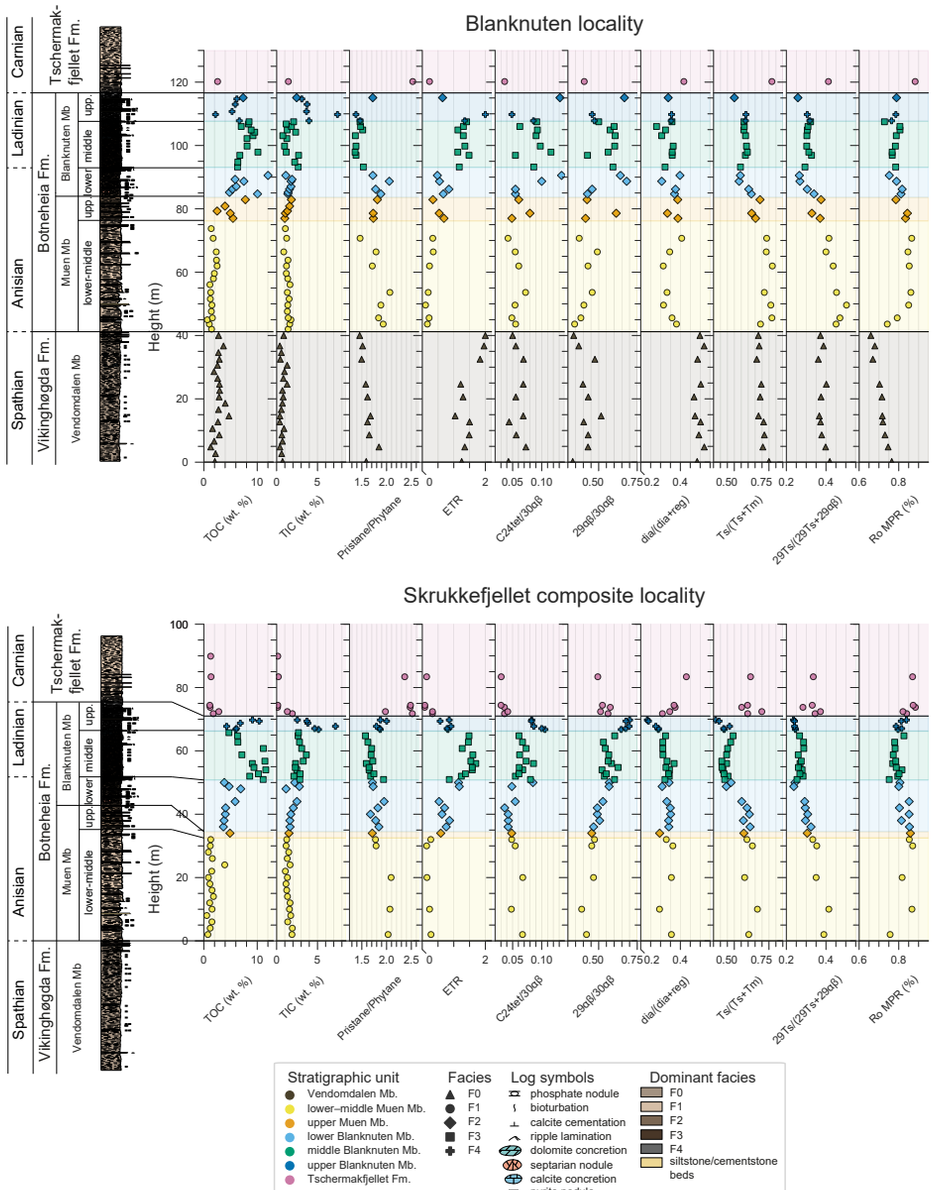

Figure 6.22: Selected geochemical logs of the investigated stratigraphic units. The lithostratigraphic log, TOC and TIC values are collected from Wesenlund et al. (2022) and Wesenlund et al. (2021).

equivalents (i.e., the Steinkobbe Formation) were active source rocks on the northern Barents Shelf, it is plausible that any contribution from the Lower Triassic Vendomdalen Member, or the offshore equivalent in the Steinkobbe Formation, would dominantly be of the same phase. The discovery of an oil-filled ammonite in the Vendomdalen Member in central Spitsbergen (Pedersen et al., 2020) and in the Blanknuten Member in the Blanknuten section (Smelror and Sollid, 2007) clearly proves that both these units are able to generate liquid hydrocarbons.

The vertical and lateral maturity contrast of the investigated units, in both, the Blanknuten and Skrukkefjellet localities, is shown to be negligible (Figs. 6.3 and 6.4) (Wesenlund et al., 2021). Hydrocarbon generation and expulsion from these units should therefore be virtually synchronous. It has been suggested that any major oil accumulations on the northern NBS are most likely sourced by Middle Triassic phosphatic mudstones with some potential contributions from Lower Triassic mudstones (NPD, 2017). Hence, an expelled hydrocarbon mixture sourced from Lower and Middle Triassic mudstones could potentially influence source- and age-specific biomarker characterization of oils or extracts derived from the northern NBS.

Since the lower–middle Muen Member mudstones (facies F1) generally show kerogen type III to III–II (Figs. 6.3 and 6.4) and a low SPI value (Fig. 6.5), they might have insignificant liquid hydrocarbon expulsion potential. Limited liquid hydrocarbon generation potential is also considered for the mudstones of the Tschermakfjellet Formation, which is dominated by mudstone facies F1 and show good richness, but poor to fair remaining generation potential (Figs. 6.3 and 6.4). Thus, this unit is commonly regarded as a gas prone source rock at best (Abay et al., 2018; Mørk and Bjorøy, 1984).

Organic facies and preservation potential

A comparison of the pyrolysis data from the Vendomdalen Member mudstones (facies F0) with those of the lower–middle Muen Member (facies F1) shows that they exhibit similar HI values, corresponding to a mixed kerogen type III-II to II-III for both units (Figs. 6.3 and 6.4). Comparable facies relationships between these units were also reported by (Bjorøy et al., 2009; Krajewski, 2013; Mørk et al., 1999b). However, as shown in this study, their principally different maceral composition and abundance of tricyclic terpanes suggest that they in fact are not organic facies equivalents (Figs. 6.6 and 6.9). Tricyclic terpanes are commonly linked with *Tasmanites* algae (Aquino Neto et al., 1992; Philp et al., 1982), and well-preserved *Tasmanites* algae are expected to contribute to the kerogen type I fraction of the OM (Vigran et al., 2008). Greater abundances of *Tasmanites* have previously been reported in the Vendomdalen Member mudstones relative

to the lower–middle Muen Member in the Skrukkefjellet locality (Vigran et al., 2014). These Fo mudstones are also inferred to exhibit a greater maximum HI value and shows evidence of deposition during intermittently euxinic (reducing) benthic conditions, while the lower–middle Muen Member mudstones (F1) were deposited during oxic–dysoxic benthic conditions (Wesenlund et al., 2022). The abundant tricyclic terpanes and greater relative abundance of flouramorphonite in the Vendomdalen Member mudstones (facies Fo) relative to the lower–middle Muen Member may therefore testify to the inferred better preservation potential of marine organic matter during the Spathian.

The Pr/*n*-C_{17} and Ph/*n*-C_{18} ratios also indicate a similar mixed kerogen type II/III for the Vendomdalen Member mudstones (facies Fo) and the lower–middle Muen Member mudstones (facies F1) (Fig. 6.8). However their stratigraphic *n*-alkane and isoprenoid distribution is clearly different and forms a recognizable organic chemostratigraphic boundary (Fig. 6.7). This agrees with former work from the central Spitsbergen and Edgeøya, which shows that Pr/*n*-C_{17} and Ph/*n*-C_{18} ratios are generally higher in mudstones from the Spathian Vendomdalen Member compared with those from the Botneheia Formation (Abdullah, 1999; Brekke et al., 2014). Abdullah (1999) attributed this to reflect variations in depositional conditions rather than organic matter input. Thus, the better Spathian preservation potential relative to the early Anisian in Svalbard, as observed in Edgeøya (Wesenlund et al., 2022), could be a principal cause for their contrasting organic facies.

The upper Muen Member (middle–late Anisian) shows a sudden increase in HI, $C_{27}\beta\beta$(R + S) (%), tricyclic terpanes, and decrease in PP, OI, TAR, and Pr/Ph, conforming to an increase in marine organic matter production and enhanced preservation potential due to upwelling and development of an OMZ (Krajewski, 2008; Krajewski, 2013). This is further supported by a strong increase in extractable organic matter (EOM) and decrease in the saturate/aromatic ratio directly above the base of the upper Muen Member mudstones, inferred to represent an increase in marine OM content (Wesenlund et al., 2021). The mudstones of the upper Muen and lower Blanknuten members (both facies F2) show similar biomarker compositions (Figs. 6.9 and 6.22), in agreement with previous workers that considered these units to have similar organic facies characteristics (Krajewski, 2008; Krajewski, 2013; Wesenlund et al., 2021).

Further, the upper Muen and lower Blanknuten members exhibit numerous event beds (i.e., conglomeratic lag deposits and cemented siltstones) and peloidal packstone layers interbedded within the mudstones (Fig. 6.22). These beds and layers may represent storm episodes and bottom-current winnowing events respectively (Krajewski, 2008; Krajewski, 2013; Mørk et al., 1982; Mørk and Bromley, 2008; Wesenlund et al., 2021). Horizons of *Thalassinoides* burrows within the upper Muen and lower Blanknuten members mudstones (facies F2)

imply within-sediment oxygenation (Krajewski, 2008; Krajewski, 2013). It is therefore intriguing that these F2 mudstones shows significantly greater HI values and notably higher Pr/Ph ratios than the apparently less-bioturbated Vendomdalen Member F0 mudstones (compare Figs. 6.3 and 6.15), perhaps suggesting that the more H-rich TOC in the F2 mudstones was deposited during less reducing (more oxic) conditions.

A similar relationship was also reported in biomarker analyses of Spathian–Anisian mudstones in central Spitsbergen, indicating that the mudstones of the upper Muen to lower Blanknuten members were deposited in more oxic conditions relative to those of the Vendomdalen Member (Abdullah, 1999). It is important to recognize that oil-prone black shales can be bioturbated as evidenced from the Kashpir oil shales in Russia, which contain abundant cm-scale *Planolites* burrows in black shales with TOC = 13.5 wt. % (Riboulleau et al., 2003, , their fig. 3b). More oxygenated water masses during the Anisian relative to the Spathian agrees with Grasby et al. (2016) and Grasby et al. (2020), who suggested that the Lower–Middle Triassic boundary in the TBO records a climate transition from Early Triassic hothouse conditions and stratified oceans with poor productivity to cooler, more ventilated and nutritious oceans that eventually resulted in high primary productivity during the Middle Triassic.

The mudstones of the middle Blanknuten Member (facies F3) show the highest TOC, HI, AOM (%) in and the lowest mode *n*-alkane and OI within the sample set (Figs. 6.4, 6.6, 6.7 and 6.22). Combined with the distribution of the redox proxies Pr/*n*-C_{17}, Ph/*n*-C_{18} and Pr/Ph (Figs. 6.8 and 6.15), it appears that the F3 mudstones contain the greatest amount of absolute and relative marine organic matter and deposition during primarily reducing conditions, in agreement with previous work (Krajewski, 2013; Wesenlund et al., 2021). These mudstones were deposited during euxinic conditions, high productivity, and low sedimentation rates in the early Ladinian, providing excellent conditions for marine organic matter accumulation and preservation (Krajewski, 2013; Krajewski and Weitschat, 2015; Wesenlund et al., 2022; Wesenlund et al., 2021). The abundant tricyclic terpane content (Fig. 6.9) suggests that *Tasmanites* algae contribute significantly to the TOC. The slightly lowered $C_{29}\beta\beta$(R + S) (%) in the facies F3 mudstones relative to the underlying facies F2 mudstones is therefore intriguing (Fig. 6.11). We currently have no explanation for this, however, the redox conditions and detrital content during deposition of these contrasting mudstones were notably different (Wesenlund et al., 2022), perhaps affecting their $C_{27}\beta\beta$(R + S)–$C_{28}\beta\beta$(R + S)–$C_{29}\beta\beta$(R + S) sterane distributions.

The mudstones of the upper Blanknuten Member (facies F2/F4) return to slightly lower TOC and HI, and higher OI and Pr/Ph (Figs. 6.4, 6.6 and 6.22). Combined with the Pr/*n*-C_{17} and Ph/*n*-C_{18} ratios that indicate more oxic condi-

tions (Fig. 6.8), the reducing conditions that prevailed in the TBO during the early Ladinian appears to have diminished during the late Ladinian. This corresponds to the inferred onset of a regressive phase and shallowing of the entire basin, causing increased reworking and oxidization (Krajewski, 2008; Krajewski, 2013). Interestingly, these mudstones show the lowest TAR, highest $C_{29}\beta\beta$(R + S) (%) (Fig. 6.11) and high (C_{23}–C_{29})tri/30$\alpha\beta$ (Fig. 6.14), suggesting that they also contain a high fraction of marine organic matter or *Tasmanites* relative to the underlying F3 mudstones. Krajewski (2013) reports abundant and large *Tasmanites* algae in the topmost mudstones of the Blanknuten Member and attributed these to algal blooms. Similarly, facies-equivalent mudstones of a late Ladinian age with concentrated laminae of *Tasmanites* have been penetrated by shallow cores in Kong Karls Land, c. 250 km east of the Blanknuten section in Edgeøya (Fig. 6.1) (Riis et al., 2008). Large *Tasmanites* (>500 μm) have also been reported in Ladinian–Carnian mudstones and siltstones at Torellneset c. 150 km north of Blanknuten (Fig. 6.1) (Vigran et al., 2008). These authors considered hydrodynamic reworking and sorting as important agents for accumulating and concentrating *Tasmanites* algae. The overall strong marine organic matter signature and extreme C_{23}tri concentration (Fig. 6.10) could therefore be a result of *Tasmanites* that became concentrated due to the long-term shoaling of the TBO during the late Ladinian rather than algal blooms, however both options should be considered.

The mudstones of the Tschermakfjellet Formation (facies F1) exhibit a similar kerogen and bitumen composition as those of the lower–middle Muen Member (also facies F1) (Figs. 6.4, 6.6, 6.8 and 6.9). This suggests that marine organic matter input and preservation potential that prevailed during the late Anisian–Ladinian ceased in favor of terrestrial organic matter input and oxic conditions in the early Carnian. This is well-documented by numerous studies and marks the termination of the circum-Arctic Middle Triassic 2nd order transgressive–regressive sequence (Høy and Lundschien, 2011; Lundschien et al., 2014; Mørk and Bjorøy, 1984). In Edgeøya, the depositional environment changed from open marine shelf conditions to the well-ventilated and pro-deltaic conditions due to the approaching TBO delta system from the southeast (Fig. 6.2). It is therefore surprising that the mudstones of the Tschermakfjellet Formation exhibit a highly marine $C_{27}\beta\beta$(R + S)–$C_{28}\beta\beta$(R + S)–$C_{29}\beta\beta$(R + S) sterane signature that resembles the phosphatic mudstone facies (F2 to F4) of the upper Muen and entire Blanknuten members (Fig. 6.11a). This is, however, not reflected by the pyrolysis results (Figs. 6.1 and 6.3), the maceral composition (Fig. 6.6), and the isoprenoid/*n*-alkane and Pr/Ph ratios (Figs. 6.8 and 6.14). We therefore consider the $C_{27}\beta\beta$(R + S)–$C_{28}\beta\beta$(R + S)–$C_{29}\beta\beta$(R + S) sterane distribution for the samples included in this study to be useful for correlation and characterization, but imprecise to determine minor changes in the source rock depositional environment.

Clay-rich vs. clay-poor source rocks

Clay-rich source rocks promote rearrangement of steranes and hopanes by clay catalyzation (Rubinstein et al., 1975), resulting in, e.g., increased dia/(dia + reg) steranes and 30d/(30d + 30αβ) ratios relative to clay-poor (e.g., calcareous) source rocks. As the mudstones of the Vendomdalen Member (facies F0) show high values of the above ratios, the C_{29}tri/C_{28}tri ratio and have the lowest TIC (wt. %) content in the sample set (Figs. 6.13, 6.14 and 6.22), it appears that the resulting ratios of these mudstones are related to their inferred relatively higher clay content. Indeed, Abdullah (1999) observed higher diasterane/sterane ratios in mudstones of the Vendomdalen Member (1.58 ± 0.10, n = 4) in central Spitsbergen relative to those of the Botneheia Formation (0.71 ± 0.20, n = 7) and attributed their difference to be a result of their clay richness. The C_{29}tri/C_{28}tri ratio introduced in this study thus appears useful to distinguish clay-rich vs. calcareous source rocks (Fig. 6.14), similar to the C_{21}tri/C_{22}tri or C_{23}tri/C_{24}tri ratios as reported by Yurchenko et al. (2018) for the Shublik Formation. The C_{29}tri/C_{28}tri ratios are low for the mudstones of the upper Blanknuten Member (facies F2/F4), probably due to their lack of clays as inferred from their high TIC content (Figs. 6.13, 6.14 and 6.22).

Similarly, the low 29αβ/30αβ ratios for the mudstones of the Vendomdalen Member (facies F0) and the lower–middle Muen Member (facies F1) relative to those of the TIC-rich upper Blanknuten Member (facies F2/F4) effectively shows that the 29αβ/30αβ parameter is generally low and high for clay-rich vs. clay-poor (calcareous) mudstones respectively (Fig. 6.12), in agreement with (Peters et al., 2005a). This ratio is also higher for the highly phosphatic mudstones of the middle Blanknuten Member (facies F3), probably reflecting their overall lack of clays due to their high phosphate and TOC content that are seen to dilute their detrital siliciclastic fraction (Wesenlund et al., 2022). Perhaps more importantly, this shows that clay-poor source rocks should not be regarded as synonymous to carbonate source rocks on the NBS.

The low C_{24}tet/30αβ ratios of the mudstones of the Vendomdalen Member (facies F0), lower–middle Muen Member (facies F1) and Tschermakfjellet Formation (facies F1) relative to the upper Muen Member (Facies F2) and the entire Blanknuten Member (facies F2–F4) agree with their association with clay-rich vs. clay-poor (calcareous or phosphatic) source rocks respectively (compare Figs. 6.12 and 6.22). All these findings discussed above corroborate with Yurchenko et al. (2018),who show that dia/(dia + reg), 30d/(30d + 30αβ), 29αβ/30αβ, C_{24}tet/C_{26}tri, and C_{24}tet/30αβ are useful for distinguishing clay-rich vs. carbonate-rich samples from the facies-equivalent and time-transgressive phosphatic Middle–Upper Triassic Shublik Formation in the North Slope Basin, northern Alaska.

Based on the Pr/Ph vs. MDBTs/MPs plot (Fig. 6.15), all mudstone samples of this study plot as marine mudstones (cf. Hughes et al., 1995), in agreement with their identified facies and inferred depositional environment. Higher (1>) and lower (<1) MDBTs/MPs ratios are also inferred to represent euxinic and anoxic–oxic depositional conditions respectively (Hughes et al., 1995). While none of the samples show such high MDBTs/MPs ratios, those of middle Blanknuten Member mudstones (facies F3) are slightly elevated (Fig. 6.15), possibly an indication of their euxinic depositional setting and availability of reactive sulfur (cf. Hughes et al., 1995). Krajewski (2013) reports an elevated degree of pyritization (DOP) in the middle Blanknuten Member mudstones and argued that pyrite formation was sluggish due to limited reactive iron availability as a result of sediment starvation during the early Ladinian highstand setting. this is supported by Wesenlund et al. (2022), who show markedly lowered concentrations in several conservative lithogenic elements (Ga, Rb, Cs, Th, K, Ti and Nb) and interpreted this as a result of sediment starvation and biogenic dilution due to the highstand phase and high primary productivity. Thus, variable MDBTs/MPs ratios could—in this case—indicate sediment-starved and biogenically diluted siliciclastic source rocks vs. clay-rich siliciclastic source rocks rather than specifically their varying calcite vs. shale content.

Thermal maturity

The investigated maturity sensitive biomarker ratios are commonly used to assess the thermal maturity of source rock extracts and oils, however these ratios are can be strongly influenced by facies variations (Peters et al., 2005a). The 22S/(22S + 22R) homohopane ratio does not appear to be significantly affected by facies variations and shows that the extracts from all the samples from both the Blanknuten and Skrukkefjellet localities are minimum borderline immature to early oil mature (Fig. 6.18). This agrees well with measured VR from the Blanknuten (mean Ro = 0.60 ± 0.03 %) and Skrukkefjellet (mean Ro = 0.54 ± 0.02 %) localities (Wesenlund et al., 2021). On the contrary, the significant spread in the ββ/(ββ + αα) and 20S/(20S + 20R) ratios indicate that the observed facies differences between the lithostratigraphic units affect their grouping (Fig. 6.19). Likewise, the clear variations in the terpane-based thermal maturity parameters Ts/(Ts + Tm), 29Ts/(29Ts + 29αβ), 30d/(30d + 29βα) and (C_{23}–C_{29})tri/30αβ also indicate that these ratios are heavily impacted by facies variations (Figs. 6.14, 6.16 and 6.17). The Botneheia Formation in the Blanknuten and Skrukkefjellet localities is less than 100 m thick in each locality, and as a result, the geothermal gradient within each respective section is likely to have a negligible differential thermal influence on these biomarker-based thermal maturity parameters (Haile et al., 2018; Wesenlund et al., 2021).

Abdullah (1999) reports higher Ts/(Ts + Tm) ratios in mudstones of the

Vendomdalen Member relative to those of the upper Muen to lower Blanknuten members and considered this mainly as a paleoredox effect rather than organic matter input effect, although both options were considered. Lower Tm/(Tm + Ts)—i.e. higher Ts/(Ts + Tm)—are generally expected in mudstones deposited under more reducing conditions (Moldowan et al., 1986; Peters et al., 2005a), but clearly organic matter input must be considered as shown for the contrasting maceral composition and terpane fingerprints between the lower–middle Muen Member and the middle Blanknuten Member (Figs. 6.6 and 6.9).

Considering either the Blanknuten or Skrukkefjellet locality only, the Ts/(Ts + Tm) vs. 29Ts/(29Ts + 29αβ) plot gives the impression that the samples of the lower–middle Muen Member (facies F1) are more mature than those of the middle Blanknuten Member (facies F3) (Fig. 6.16). This is incorrect, as the maturity difference of the lithostratigraphic units within these respective localities is negligible (Wesenlund et al., 2021). The plot also gives the impression that these middle Blanknuten Member samples from the Blanknuten locality are equally mature as those of the lower–middle Muen Member from the Skrukkefjellet locality (Fig. 6.16). This is also incorrect as there is a minor but consistent maturity contrast (ΔRo = 0.06 %) between these localities (Wesenlund et al., 2021). However, if the samples from the same lithostratigraphic level and facies are compared, the true maturity relationship between the Blanknuten and Skrukkefjellet localities is readily observed (Fig. 6.17). It is therefore essential that these ratios are calibrated based on their facies variations when performing these biomarker-based maturity assessments to prevent a third variable problem (Fig. 6.23).

The Ts/(Ts + Tm) and 29Ts/(29Ts + 29αβ) ratios are commonly plotted in tandem to evaluate crude oil maturity (Farrimond, 2019a; George et al., 2007; Jiang et al., 2018; Lerch et al., 2016b), perhaps due to their notable linear correlation (Fig. 6.16). Both parameters are expected to increase similarly with increasing maturation (Peters et al., 2005a). As shown here, variations between these two parameters could simply represent their strong facies dependency (Figs. 6.17 and 6.22). This is problematic if we consider the following scenario: Assume that the Vendomdalen Member and Middle Blanknuten Member (Facies F0 and F3 respectively) are oil-prone and able to generate and migrate liquid hydrocarbons. This is a fair assumption based on the evidence outlined in this study (Figs. 6.3 and 6.4). Additionally, assume that two oil samples (or oil-stained core cuttings), here referred to as oil X and oil Y, are collected somewhere on the northern Barents Shelf and yields different Ts/(Ts + Tm) and 29Ts/(29Ts + 29αβ) ratios (Fig. 6.24). A traditional plot infers a maturity difference between the oil samples. However, it would be practically impossible to determine from the plot, whether the observed maturity contrast is due to a single source rock that expelled liquid hydrocarbons at different maturities, or if there are two different source rocks contributing at equal maturity but

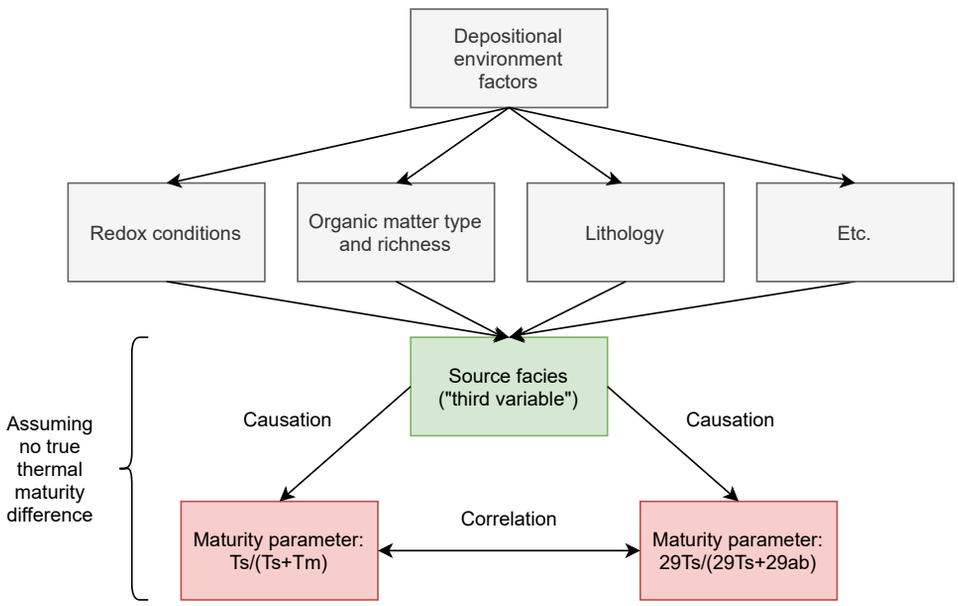

Figure 6.23: Overview of the causal relationship between depositional environment factors resulting in a combined source facies effect and its influence on the correlation between 29Ts/(29Ts + 29αβ) and Ts/(Ts + Tm). In this study, the strong linear correlation between these maturity parameters in the mudstone extracts do not represent a true maturity relationship. Instead, their strong correlation is caused by a source facies effect, representing a third variable problem.

being composed of different organic facies. While this is a hypothetical and presumably unrealistic problem due to the common occurrence of reservoir mixing (e.g., Georgiev et al., 2019), it shows the importance of combining several maturity and facies parameters when evaluating thermal maturity of oils or source extracts.

P and/or MP-based VR parameters have previously been used to evaluate maturity of Barents Sea oils or mudstone extracts from core samples (Abay et al., 2017; Lerch et al., 2016a; Lerch et al., 2018; Matapour et al., 2019). Here we show that calculated VR values of the mudstone extracts in eastern Svalbard are generally not representative of the measured VR values from the same mudstones (Figs. 6.21 and 6.22). Only the MPDF2 maturity parameter is in good agreement with the VR measurements, (Fig. 6.21). The correlation may simply be coincidental. This highlights the importance of calibrating thermal maturity parameters to specific source rock facies, as evaluated vitrinite values from biomarker are overestimated up to 0.3 % Ro compared to direct VR measurements (Fig. 6.20). However, such a calibration is not possible in this study due to the low maturity difference between the two sampled localities.

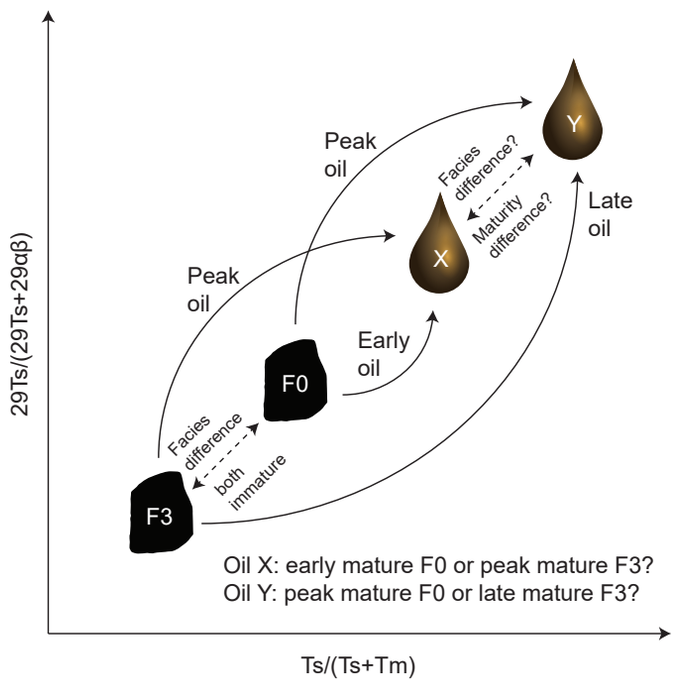

Figure 6.24: A hypothetical problem where the 29Ts/(29Ts + 29αβ) and Ts/(Ts + Tm) ratios of two oils, X and Y, are shown in a binary plot. Due to the possible influence of source facies, oils X and Y could represent two or more source rocks that are equally mature but have different organic facies, or multiple charges of different maturity from a dominating source rock with homogenous biomarker composition, which then would yield a true maturity difference between oils X and Y.

6.5.2 Source–oil and oil–oil correlations

The maturity assessment in this study shows that the mudstone extracts from Edgeøya are dominantly early–peak mature, while the oils are peak mature. A source–oil correlation study of the extracts and samples in this study is therefore considered to be applicable, as the maturity contrast between the extracts and oils are relatively low.

The terpane distribution, $C_{27}\beta\beta$(R + S)–$C_{28}\beta\beta$(R + S)–$C_{29}\beta\beta$(R + S) distribution, $C_{28}\beta\beta$(R + S)/$C_{29}\beta\beta$(R + S) ratios, C_{29}tri/C_{28}tri ratios, (C_{23}-C_{29})tri/30αβ ratios, ETR values, and Pr/Ph ratios of the *Alta/Gohta* and *Wisting Central/Hanssen* oils generally group together with the samples from the Vendomdalen Member (facies F0), the upper Muen Member (facies F2), and the lower–middle Blanknuten Member (facies F2/F3) (Figs. 6.11, 6.14 and 6.15). This indicates that the investigated oils were generated from source rocks that are of similar facies to these mudstones. This agrees with former work that shows a good source–oil correlation between the *Hanssen*, *Wisting Central* and *Gohta* oils

and the Botneheia Formation (Thießen et al., 2019). The most likely source rock equivalent to the Vendomdalen Member and the Botneheia Formation in the commercial acreage of the NBS is the Spathian–Anisian Steinkobbe Formation, which consists of a organic-rich, partly phosphatic, mudstone-dominated succession, 250 m thick in the type section in the Svalis Dome (Isaksen and Bohacs, 1995; Lundschien et al., 2014; Mørk and Elvebakk, 1999). Comparable to this study, the Steinkobbe Formation also exhibit significant variations in TOC (1–9 %) and HI (197–540 mg HC/g TOC) (Abay et al., 2018).

While both the lower Steinkobbe Formation (Spathian) and the middle–upper Steinkobbe Formation (Anisian) are considered to be oil prone (Abay et al., 2018), recent work indicate that the *Wisting Central/Hanssen* oils were dominantly or only sourced by its lower part (Spathian) (Lerch et al., 2018). Based on productivity, redox and water mass restriction proxies derived from trace element enrichments, Wesenlund et al. (2022) suggested that the Botneheia Formation could be genetically unrelated to the Spathian part of the Steinkobbe Formation. The similarity in biomarker composition between the *Wisting Central/Hanssen* oils and the Vendomdalen Member mudstones indicate that they instead could be genetically related. They may thus represent lateral and near-synchronous organic facies equivalents that accumulated during water mass restriction and enhanced preservation in the TBO as a result of the Early Triassic hothouse climate (Grasby et al., 2020; Wesenlund et al., 2022; Wignall et al., 2016). It is therefore questionable if the Botneheia Formation should be considered a younger and time-transgressive facies equivalent to the lower Steinkobbe Formation (Spathian).

The unidentified peak X elutes directly before 30αβ (Fig. 6.9), similar to oleanane, also typically seen to elute directly before 30αβ in 191 m/z chromatograms (e.g., Peters et al., 2005a). However, as oleanane is an age-specific biomarker dominantly seen in Cretaceous or younger strata (Moldowan et al., 1994) it is unlikely that peak X represents oleanane. Still, as peak X appears to be exclusive to the Vendomdalen Member among all the extracts, its abundance appears useful as a criterion to distinguish Spathian vs. Anisian–Ladinian bitumens in Svalbard. Thus, it is speculated that the occurrence of peak X in the *Alta/Gohta* oils is associated with Spathian source contributions. But, on the contrary, the lack of a significant peak X in the (likely) Spathian-sourced *Wisting Central* and *Hanssen* discoveries suggest that peak X is not unequivocally sourced by Spathian source rocks. While it is beyond the scope of this study to perform a chemical structure analysis of peak X, its identification should be performed for further use as a correlation tool.

The dia/(dia + reg) steranes, 30d/(30d + 30αβ), C_{24}tet/30αβ, 29αβ/30αβ and MDBTs/MPs ratios further indicate that the *Wisting Central/Hanssen* oils were generated from dominantly clay-rich source rocks similar to the Vendomdalen

Member (Figs. 6.12, 6.13 and 6.15). However, it is probable that a relative increase in most of these ratios could be due to maturation effects (Peters et al., 2005a). Still, the biomarker fraction of these oils appears to be equally mature as the Vendomdalen Member mudstones based on the 20S/(20S + 20R) and ββ/(ββ + αα) ratios (Fig. 6.19). The biomarker ratios retrieved from these oils could however indicate that they have reached their isomerization threshold, prohibiting further resolution to detect maturity contrasts. The notably higher C_{24}tet/30αβ, 30d/(30d + 30αβ), dia/(dia + reg) and C_{29}tri/C_{28}tri ratios in the *Alta/Gohta* oils (Figs. 6.12 to 6.14 and 6.16) relative to the *Wisting Central/Hanssen* oils could thus indicate a dominantly siliciclastic source rock that are more mature than the *Wisting Central/Hanssen* oils.

The elevated gammacerane content in the *Alta/Gohta* oils may suggest stratified water masses during deposition of its associated source rock (Fig. 6.9) (Sinninghe Damsté et al., 1995). Water mass stratification could have developed due to sluggish Early Triassic oceanic circulation in the TBO (Grasby et al., 2013; Grasby et al., 2016; Grasby et al., 2020; Wignall et al., 2016). Abundant fluvial runoff from the approaching TBO delta system may also have created a halocline that promoted water mass stratification (Høy and Lundschien, 2011; Vigran et al., 2008). Such a scenario would be similar to the present setting of the Black Sea (Demaison and Moore, 1980) or the Bothnian Bay (Liblik and Lips, 2019), and was considered more probable during the Early Triassic compared to the Middle Triassic as local structural elements would probably restrict water flow to a larger extent during the Early Triassic (Leith et al., 1993). However, empirical evidence of gammacerane in proven Early Triassic oil-prone mudstone extracts or oils from the NBS has not been found in this study or by Lerch et al. (2018), suggesting that the *Alta/Gohta* oils could have primarily been sourced from a principally different source rock. A candidate is the dominantly siliciclastic Upper Paleozoic Ørret Formation as previously suggested by Matapour et al. (2019) and Pedersen et al. (2017).

This study considers the biomarker-based thermal maturity parameters (i.e., the Ts/(Ts + Tm), 29Ts/(29Ts + 29αβ), 30d/(30d + 29αβ), ββ/(ββ + αα) steranes and 20S/(20S + 20R) steranes) of the *Wisting Central/Hanssen* oils to be equivalent to the mudstone extract dataset (Figs. 6.16, 6.18 and 6.19). Their similar organic facies indicates that specifically the biomarker fractions in these oils were sourced from early mature source rocks. However, the P-, MP- and MDBT-derived maturity parameters of the oils are significantly larger than all the extracts (Figs. 6.20 and 6.21), suggesting that the biomarker-based maturity parameters of the oils do not reflect the higher maturity that is expected for the *Wisting Central/Hanssen* oils. Moreover, these differences in evaluated maturities from biomarker and aromatic hydrocarbon could suggest mixing of different charges. This is in agreement with Wilhelms and Larter (2004) who also observed that biomarker-based thermal maturity parameters in conven-

tional oil accumulations are typically lower than maturity parameters based on aromatic compounds and attributed this to oil mixing. This conclusion was also made by Matapour et al. (2019) for the *Alta/Gohta* oils and has previously been reported from exploration well 7220/8-1 *Skrugard* in the Johan Castberg Field as well (Matapour and Karlsen, 2018). Leaching of immature–mature organic matter from shallower and less mature sections of the source rock or carrier beds (Farrimond, 2019b) appears less important as the biomarkers ratios in the oils do not indicate immature source rocks (Figs. 6.18 and 6.19). Given the similar groupings in the biomarker-based maturity parameters and the above aromatic-based maturity parameters between the *Wisting Central/Hanssen* and *Alta/Gohta* oils, the oils could represent respective blends of petroleum from different maturities. In addition, the complex interplay between burial, uplift and erosion has undeniably affected the timing of oil generation–migration–accumulation, which additionally could have led to re-migration and mixing of migrated oil (Lerch et al., 2016a; Ohm et al., 2008). It is evident that basin modeling and petroleum systems modeling of the region could provide additional answers to these major uncertainties.

6.6 Conclusion

This study investigates differences in source rock facies and thermal maturity parameters of Lower–Upper Triassic mudstone extracts from Edgeøya (eastern Svalbard) and oils derived from the *Alta*, *Gohta*, *Wisting Central* and *Hanssen* discoveries on the Norwegian Barents Shelf. Source rock–oil and oil–oil correlations were also performed. The investigated *n*-alkanes, acyclic isoprenoids, and biomarkers and their chemostratigraphic development are linked to changing depositional and environmental conditions throughout the Spathian–Carnian, which had major influence on source rock lithology, preservation potential and organic matter richness and type. Furthermore, the coupled facies influence on biomarker-based maturity parameters, especially the Ts/(Ts + Tm) and 29Ts/(29Ts + 29$\alpha\beta$) ratios, clearly show that spurious maturity evaluations are possible due to source facies acting as a third variable. We therefore strongly advice against plotting these two parameters in tandem for maturity evaluations unless their facies differences are taken into consideration.

The Vendomdalen Member (Spathian) of the Lower Triassic Vikinghøgda Formation is likely to generate liquid hydrocarbons, but its generation potential should be considered minor relative to the oil-prone part of the Botneheia Formation: the phosphogenic upper Muen Member and the entire Blanknuten Member. The Vendomdalen Member mudstones were deposited under reducing conditions that were probably more important for accumulating oil-prone organic matter compared to high primary productivity. The lower–middle

Muen Member (Anisian) of the Botneheia Formation and the Tschermakfjellet Formation (Carnian) mudstones were evidently deposited during oxic benthic conditions and contain the highest relative amounts of terrestrial organic matter, resulting in gas prone to mixed gas and oil prone source rocks. The upper Muen Member (Anisian) and the entire Blanknuten Member (Anisian–Ladinian) of the renowned Middle Triassic Botneheia Formation are by far the best oil-prone source rock candidates onshore the NBS. These units reflect deposition during periods of high paleoproductivity and enhanced preservation potential of organic matter as a result of oxygen deficiency triggered by high oxygen demand, and the increased relative sea level limited clastic sediment supply and thus OM dilution.

The performed source–oil and oil–oil correlations indicate that the *Alta/Gohta* and *Wisting Central/Hanssen* oils are of both generated from peak oil mature source rocks, though the saturate biomarker fraction and the aromatic hydrocarbons suggest different levels of maturity. The *Alta/Gohta* oils exhibit a clay-rich source facies and evidence of gammacerane, indicating a siliciclastic source rock most likely deposited during increased water mass restriction. The Early Triassic hothouse climate may represent a possible cause for sluggish ocean circulation and temperature-induced stratification, possibly in combination with a halocline formed due to fluvial runoff from a large delta system prograding into the southern Barents Shelf in the Early Triassic, eventually reaching Svalbard by the Late Triassic. Still, gammacerane has not yet been discovered in Lower Triassic source rock extracts in the southern Barents Shelf or on Svalbard. It may thus possibly be that the *Alta/Gohta* oils were sourced or partly sourced from the Upper Paleozoic Ørret Formation. However, to the best of our knowledge, a source–oil correlation study that provides solid evidence of the Ørret Formation being a source for the *Alta* and/or the *Gohta* discoveries is lacking.

The *Wisting Central/Hanssen* oils, which evidently were sourced from the lower Steinkobbe Formation, show greater similarities to the extracts of the Vendomdalen Member mudstones (both Spathian) than to those of the Botneheia (Anisian–Ladinian) or the Tschermakfjellet formations. This is intriguing, because the Botneheia Formation is typically considered the best facies-equivalent to the Steinkobbe Formation source rock, while the Vendomdalen Member is commonly excluded in such facies comparisons. It therefore appears that the *Wisting Central/Hanssen* oils, which originated from a Spathian-aged source rock, correlate best with age equivalent source rocks in Svalbard. These findings are important, as they demonstrate principally different and possibly climate-controlled source rock depositional environments that have considerable implications for the timing and distribution of oil-prone source rock formation in the region.

The Norwegian Geochemical Standard SR-1, currently assigned to the Muen Member of the lower Botneheia Formation (Anisian), correlates significantly better with the Vendomdalen Member. This strongly indicates that this geochemical standard in fact belong to the latter unit, in agreement with recent work (Wesenlund et al., 2022).

6.7 Acknowledgements

This study forms part of the ARCEx consortium (Research Centre for Arctic Petroleum Exploration), funded by the Research Council of Norway (grant number 228107) and ARCEx partners. We are grateful for additional economic support from Lundin Energy Norway and the Norwegian Petroleum Directorate for the field expedition to Edgeøya. Atle Mørk is thanked for field expedition planning and logistics. The crew at research vessel SS Youexplore by The Dale Oen Experience is thanked for field work logistics. Sofie Bernhardsen is thanked for field assistance and scientific contributions. Trine Dahl, Ingvild Hald and Karina Monsen are thanked for help in the geology lab at UiT–The Arctic University of Norway. Kristian Backer-Owe and Dag Arild Karlsen are thanked for permission to use the organic geochemical lab at the University of Oslo. Kong Haakon den VIIdes utdannelsesfond for norsk ungdom is thanked for additional funding for geochemical analyses. NFiP is thanked for covering travel expenses to UiO.

/7

Synthesis

This chapter synthesizes the findings of Papers I–III to further discuss how the paleoenvironmental conditions fluctuated during the Spathian to Carnian in eastern Svalbard and their implications for understanding the Triassic source rock formation on the NBS. Based on the established lithostratigraphy and chemostratigraphy of Papers I–III, this synthesis presents an evolutionary depositional model focusing on the following ages:

- Spathian
- lower Anisian
- middle–upper Anisian
- lower Ladinian
- upper Ladinian
- lower Carnian

Emphasis is put on the importance of primary productivity, benthic redox conditions and sedimentation rate or lithology, all particularly important for source rock formation. Although the model focuses on eastern Svalbard, comparisons are made to time and facies-equivalent strata, as well as inferred Triassic oils derived from selected discoveries on the NBS. The Svalis Dome area is included

in the discussion as it hosts the type well for Lower–Middle Triassic mudstones on the offshore NBS, thus providing an important reference in terms of the regional stratigraphic development (Mørk and Elvebakk, 1999). Furthermore, the findings of the source–oil correlation performed in Paper III have been addressed.

7.1 Changing depositional conditions and their implications for source rock potential

7.1.1 Spathian

The Spathian mudstones are represented by the Vendomdalen Mb of the Lower Triassic Vikinghøgda Fm, and were investigated in Papers II–III. The Vendomdalen Mb was first defined by Mørk et al. (1999b) in central Spitsbergen, who report that this unit largely consists of silty and dark gray mudstones that are oil- and gas-prone (Facies Fo of Paper II). These source rocks were interpreted to represent "distal shelf deposits, below wave base, with accumulation of marine derived organic material in a low oxic environment" (Mørk et al., 1999b). In Paper II, it is shown that these mudstones are void of bioturbation and record high Mo-TOC and Mo-U ratios, strongly indicating that they were deposited during intense Fe-Mn redox cycling, which previously has been linked with intermittent euxinic conditions (Algeo and Lyons, 2006; Algeo and Maynard, 2008; Algeo and Rowe, 2012; Algeo and Tribovillard, 2009; Tribovillard et al., 2012). Thus, the preservation potential was sufficient to conserve deposited oil-prone OM and form source rocks with liquid hydrocarbon potential (cf. Pedersen et al., 2020).

In western Spitsbergen, the more proximal and time-equivalent mudstone-dominated shallow marine deposits of the Tvillingodden Fm (Spathian) appear to have been deposited during benthic euxinic phases (Wignall et al., 2016). Their study reports that the oxygen deficient conditions did not appear to be related to water depth or terrestrial nutrient supply, i.e., in relationship with high marine productivity and oxygen consumption. In fact, the Early Triassic hothouse conditions and the resulting elevated sea-surface temperatures (e.g., Sun et al., 2012) were voiced as the principle cause (Wignall et al., 2016). The Triassic hothouse conditions have also been inferred to have affected the Lower Triassic strata of the Sverdrup Basin (Grasby et al., 2013; Grasby et al., 2016; Grasby et al., 2020). The combined work of these studies suggests that the northern Pangean margin and the TBO were subjected to sluggish ocean circulation and low nutrient supply, inhibiting marine productivity during the Lower Triassic. This would cause poorly ventilated oceans and less benthic oxygen

supply due to oceanic water mass stratification (i.e., increased preservation potential), perhaps similar to the "superanoxic event" as indicated for the entire Panthalassic Ocean at the Permian–Triassic boundary (Isozaki, 1997).

Paper II shows that productivity proxies (i.e., TIC and EFs of Si, Ba, and P) are low in these Spathian mudstones, conforming to the suggested low productivity during the Spathian. Further, Paper III shows that the biomarker-based lithology proxies of these Spathian mudstones exhibit a clay-rich facies, testifying to their low phosphate and carbonate content. The oxygen deficiency appears therefore to be dominantly ruled by climatic oscillations rather than intrabasinal factors, in agreement with Wignall et al. (2016). Thus, even though marine productivity is considered to have been low or moderate in eastern Svalbard and the sedimentation rate to have been relatively high (Papers II–III), it was still possible to form source rocks with liquid hydrocarbon potential. However, the potential occurrence of a silled or enclosed bay basin setting (Leith et al., 1993; Mørk et al., 1982; Sømme et al., 2018), as well as inherited paleobathymetric relief (Steel and Worsley, 1984), could both potentially limit benthic oxygen supply and contribute to oxygen deficiency.

These findings in Svalbard (and the Sverdrup Basin; Grasby et al., 2016; Grasby et al., 2020) are important, because age-equivalent Spathian mudstones of the lower Steinkobbe Fm on the southern NBS are probable oil-prone source rocks for the *Wisting Central* and *Hanssen* discoveries (Lerch et al., 2018), and perhaps also source contributors for the *Alta* and *Gohta* discoveries (Matapour et al., 2019). Thus, it could be that the oxygen deficit conditions that allowed these source rocks to form on the southern NBS were similarly caused by climate oscillations rather than high metabolic demand, paleobathymetry, salinity-induced water mass stratification, or other intrabasinal factors. If the climate-induced ocean stratification and associated OM preservation were regional and operating on the southern NBS, they could have had major impact on the Spathian and/or Lower Triassic source rock formation throughout the NBS.

7.1.2 lower Anisian

The lower Anisian mudstones are represented by the lower–middle Muen Mb of the Botneheia Fm (Middle Triassic) and were investigated in Papers I–III. The Muen Mb was first defined by Krajewski (2008) and consists of relatively soft, gray–dark gray mudstones (Facies F1 in Papers I–III) that show mixed gas/oil potential (Krajewski, 2013, see also Papers I and III). They have been interpreted to represent mudstones deposited during mainly anoxic conditions (Vigran et al., 2014) and/or during a restricted benthic setting (Lundschien et al., 2014), however deposition during mainly oxygenated benthic conditions

has also been suggested (Krajewski, 2008; Krajewski, 2013). The depositional environment is commonly regarded to have been a deep, restricted shelf (e.g., Lundschien et al., 2014; Mørk et al., 1982; Mørk and Bjorøy, 1984), however Krajewski (2013) attributes these mudstones to represent deposition during a mainly prodeltaic setting and fairly oxygenated benthic conditions related to the emerging TBO delta system in the southeast. In Paper I, it is documented that these mudstones hosted benthic life as evidenced from within-sediment dwellers (*Chondrites*) and surface gracers (*Helminthopsis*), suggesting that the O_2–H_2S (redox) boundary was below the sediment surface, at least episodically. These findings were further substantiated by Paper II, which shows very low to negligible enrichment in common redox proxies (e.g., U, Mo) similar to the PAAS, also suggesting dominantly oxic–dysoxic bottom waters.

This study thus agrees with Krajewski (2013) in that the early Anisian benthic conditions must have been sufficiently oxygenated to the extent that they allowed a low-diversity benthic community and moderate TOC accumulation (Paper I). However, the presence of P-nodules within the lower–middle Muen Mb suggests that elevated marine productivity did occur and was potentially an important factor in accumulating OM (Papers I–III). Still, the relatively high content of woody material, higher Pr/Ph ratios, $C_{29}\beta\beta$(R + S) (%) and lack of C_{23}–C_{29} tricyclic terpanes in these lower Anisian mudstones exemplify higher input and/or preservation of terrestrial OM (Papers I and III). This is a notable contrast to the underlying Vendomdalen Mb, and may thus reflect the remarkable climate change from the Early Triassic hothouse to cooler but more nutrient-rich and ventilated waters that prevailed during the Middle Triassic (Grasby et al., 2016; Grasby et al., 2020; Sun et al., 2012). The oxygen and nutrient supply appears to have caused elevated marine productivity, but not to the extent that benthic oxygen deficiency and associated preservation potential were optimal for marine OM accumulation. Thus, it could be possible that early Anisian productivity was greater than during the Spathian, but that the low preservation potential limited preservation of reactive OM, resulting in overall less oil-prone lower Anisian source rocks (Paper III).

In the Svalis Dome, the mudstones of the lower Anisian succession of the Steinkobbe Fm represent the introduction of a distal and well-ventilated shelf environment (Mørk and Elvebakk, 1999, , their Unit I and lithofacies 3). These medium dark gray–black, organic-rich mudstones contain P-nodules/pebbles and shows a lowering in TOC from the underlying Spathian mudstones. Thus, the Spathian–Anisian boundary may represent a negative TOC excursion spanning from the Svalis Dome to Edgeøya (Papers I–III). It is speculated that this geochemical boundary in the Svalis Dome area represents a transition towards lowered preservation potential but increased marine productivity as a direct consequence of the Early–Middle Triassic climate change (Papers II–III). If so, lower Anisian mudstones may have lowered source potential throughout the

NBS relative to their underlying Spathian counterparts.

7.1.3 middle–upper Anisian

Based on correlations with Vigran et al. (2014), the middle–upper Anisian appear to be best represented by the upper Muen and lower Blanknuten members, both considered facies equivalents in this study (facies F2 mudstones, see Table 2.2). Paper I shows that these mudstones host abundant P-nodules, are significantly darker, brittle, organic-rich, phosphatic and laminated relative to the underlying lower Anisian Facies F1 mudstones, interpreted to mark the onset of intense phosphogenesis, in line with the findings of Krajewski (2008) and Krajewski (2013, , their Units 5–6). However, the occurrence of P-filled *Thalassinoides* burrows (Krajewski, 2013) proves that within-sediment oxygenation did occur, suggesting that the conditions were mainly dysoxic–anoxic and not dominantly euxinic (Paper II). Interestingly, these mudstones show overall greater kerogen quality and richness than the mudstones of the Spathian Vendomdalen Mb (Facies F0), even though they appear to have been deposited during less hospitable conditions based on their overall lack of bioturbation (Paper II). The excellent middle–upper Anisian source rock potential is therefore linked with the increasing marine productivity and associated OMZ development during the Middle Triassic, likely caused by increasingly efficient upwelling and nutrient supply in tandem with rising relative sea levels, also lowering the detrital input (Krajewski, 2013, , see also Papers I–III). Indeed, the elemental chemostratigraphic framework in eastern Svalbard (Paper II) and Mo-EF vs. U-EF trends suggest that the benthic waters were dominantly unrestricted during the mid–late Anisian, which could allow sufficient nutrient supply to sustain the high productivity (Paper II). The accumulated and well-preserved OM appears therefore to be mainly a result of the metabolic O_2 demand that consumed the available O_2 rather than restricted benthic waters formed by ocean stratification or a silled intrabasinal configuration (Paper I–II).

In the Svalis Dome, the middle–upper Anisian is represented by the P-nodule-rich, organic-rich, barite crystal-containing and phosphatic mudstones of the middle–upper Steinkobbe Fm (Mørk and Elvebakk, 1999). The co-occurrence of P-nodule-rich middle–upper Anisian mudstones in Svalbard and the Svalis Dome is regarded to have been formed fairly synchronously and as a result of the regional upwelling and associated marine productivity and phosphogenesis (Papers II–III). This partly disagrees with Lundschien et al. (2014), who considered the Steinkobbe Fm to represent older and time-transgressive (i.e., asynchronous) facies equivalents of the Botneheia Fm. Furthermore, it also disagrees with Leith et al. (1993), who considered the enclosed setting of the TBO more important for OM accumulation than upwelling and OMZ, although the latter was deemed less likely due to the possible obstruction caused by land

mass in the north (Embry, 1993; Embry, 2009; Sømme et al., 2018).

$^{187}Os/^{188}Os$ ratios of upper Anisian mudstones in the Svalis Dome indicate that they were deposited during more restricted water circulation than their age-equivalents in Svalbard, suggesting that basin restriction had implications for benthic redox conditions in the southern TBO (Xu et al., 2009). However, the sample set in Xu et al. (2009) covers only c. 1.2 m of the c. 180 m Anisian succession of the Steinkobbe Fm. The interplay between bioturbated and non-bioturbated phosphogenic mudstones in the middle–upper Anisian mudstones of the Steinkobbe Fm, which contain the highest (but overall variable) TOC values (Mørk and Elvebakk, 1999, , their unit J), could therefore testify to unrestricted depositional conditions in this part of the TBO, as implied for the age- and facies-equivalent mudstones in Svalbard (Paper II).

The abundant P-nodule formation in both Svalbard and the Svalis Dome during the middle–upper Anisian may therefore not necessarily have been due to riverine nutrient supply, which presumably would be important to trigger phosphogenesis in a restricted basin setting (e.g., Høy and Lundschien, 2011; Vigran et al., 2008). Instead, the rising relative sea levels in concert with increased marine productivity serve as an alternative explanation (Krajewski, 2008; Krajewski, 2013). The Pangean Margin north of Svalbard has been portrayed as a marine basin shaped as a large embayment (Fig. 1.5) rather than land mass (Fig. 1.6) during the Early to Late Triassic times (e.g., Eide et al., 2018; Parrish and Curtis, 1982; Twitchett et al., 2004). The former setting could readily allow upwelled and nutrient rich, unrestricted waters to reach the inner shelf (Parrish and Curtis, 1982). Upwelling-induced marine productivity and phosphogenesis, as demonstrated to have occurred during the Middle–Upper Triassic in the Sverdrup Basin (Parrish et al., 2001) and in the Middle Triassic on Svalbard (Krajewski, 2008; Krajewski, 2013), should therefore be strongly considered to have occurred in the Svalis Dome as well. If this is the case, then the increased source potential of the phosphogenic middle–upper Anisian mudstones throughout the NBS, including the Svalis Dome, could primarily be a result of elevated marine productivity and high metabolic demand for O_2, leading to the development of an OMZ, and secondly due to water mass restriction (Paper II).

7.1.4 lower Ladinian

The lower Ladinian mudstones are represented by the middle Blanknuten Mb of the Botneheia Fm (Krajewski, 2013; Krajewski and Weitschat, 2015), which were investigated in Papers I–III. This part of the Blanknuten Mb was first defined as the Blanknuten Bed by Mørk et al. (1982), then raised to member rank by Mørk et al. (1999a). However, Krajewski (2008, their unit 6) included the underlying

phosphatic and P-nodule-rich succession as a part of the Blanknuten Mb, here termed the lower Blanknuten Mb (based on Krajewski, 2008, see Section 7.1.3). The inconsistent definitions of the base Blanknuten Mb boundary by Krajewski (2008) and Mørk et al. (1999a) were discussed in Paper I, concluding that the definition by (Krajewski, 2008) should be used for future reference. This is important, as the lithostratigraphic lower boundary of the Blanknuten Mb boundary has implications on the spatiotemporal distribution of the Blanknuten Mb (Paper I).

In eastern Svalbard, the middle Blanknuten Mb consists of Facies F3 mudstones and is considered the stratigraphic sub-unit with the highest source potential (Papers I–III). These mudstones host the highest amount of absolute bitumen and absolute and relative aromatic hydrocarbons of the sample set, suggesting that their OM content is highly marine (Paper I). Indeed, visual kerogen analyses and pyrolysis products of these mudstones yield a high proportion of fluoramorphinite and the highest HI values of the sample set, respectively (Paper III). These mudstones exhibit the highest paleoproductivity and phosphate proxies, suggesting that marine productivity was intense and the highest among the studied mudstone units (Paper II). Likewise, the paleoredox proxies are high in these mudstones and indicate deposition during dominantly euxinic conditions (Paper II), in agreement with Krajewski (2013).

These mudstones correspond to the highstand phase of the Middle Triassic TR sequence and have been associated with the Ladinian maximum flooding surface (MFS). This MFS reached at least the Ludlovskaya-1 well in the South Barents Basin in Russia (Gilmullina et al., 2021) and shows that detrital input was significantly lowered in the TBO (Klausen et al., 2015), including Svalbard (Krajewski, 2013, see also Papers II–III). Thus, it is probable that the low sedimentation rate (i.e., OM condensation) during deposition of these organic-rich muds in the Svalbard area had a substantial role in increasing their TOC. Furthermore, the highstand phase could increase the upwelling and thereby nutrient supply, promoting increased primary production and phosphogenesis. The combination of high productivity, high preservation potential as a result of the high O_2 demand, and low detrital input all appear to have contributed to the excellent source rock potential of the lower Ladinian mudstones (Papers I–III).

In The Svalis Dome, the age-equivalent Ladinian mudstones of inferred prodeltaic origin are assigned to the Snadd Fm mudstones, and they are are typically not considered oil-prone source rocks (Abay et al., 2018). However, it should be mentioned that selected intervals of the Ladinian part of the Snadd Fm show TOC = 6 % and HI ranging between 300–500 mg HC/g TOC (Henriksen et al., 2011b). Still, the introduction of these prodeltaic and dominantly gas-prone mudstones blanketed the underlying strata during the arrival of the TBO delta,

effectively putting an end to the deposition of the widespread oil-prone source rocks of the Steinkobbe Fm (Lundschien et al., 2014).

7.1.5 upper Ladinian

The upper Ladinian mudstones are represented by the upper Blanknuten Mb of the Botneheia Fm, which were investigated in Papers I–III. The upper Blanknuten Member consists of Facies F2 and F4 mudstones, where the latter is exclusive to this stratigraphic unit and is more abundant than the former (Paper I). The transition from the middle to upper Blanknuten Mb (i.e., from facies F3 to F2/F4 mudstones) shows an abrupt positive TIC excursion that serves as a clear criterion to demarcate these stratigraphic units (Paper I). This is linked with the onset of elevated calcite content in these F4 mudstones, which again is tied to abundant, minute bivalves within this fossil-rich stratigraphic unit (Hurum et al., 2014; Mørk and Bromley, 2008, see also Papers I–II). The increased TIC content is at the expense of the clay fraction, resulting in lowered dia/(dia + reg) steranes, 29αβ/30αβ and C_{24}tet/30αβ ratios (Paper III). The upper Blanknuten Mb also marks the reintroduction of phosphatized *Thalassinoides* burrows, greater relative amounts of terrestrial OM, and generally lower bitumen and kerogen content, all in contrast to the underlying F3 mudstones of the middle Blanknuten Mb (Papers I–III).

These observations indicate that the Middle Triassic upwelling, marine OM production and phosphogenesis were still ongoing during the late Ladinian, in agreement with Krajewski (2013) and Krajewski and Weitschat (2015). However, the generally stable benthic euxinic conditions during the early Ladinian became intermittent euxinic in the late Ladinian as evidenced from high Mo concentrations, the U-EF–Mo-EF relationships, and the Mo/TOC ratios in these upper Ladinian mudstones (Paper II). Similar geochemical signatures were shown in upper Ladinian mudstones cored just offshore Kong Karls Land, easternmost Svalbard (Xu et al., 2014). Therefore, while Krajewski (2013) only considered the middle Blanknuten Mb F3 mudstones to have been deposited during euxinic conditions, it is evident that this is also the case for the upper Blanknuten Mb. The change in benthic euxinic conditions and the relative increase in terrestrial OM content in these oil-prone mudstones are linked with the regressive phase of the Middle Triassic TR sequence and the subsequent shoaling of the basin (Krajewski, 2013, see also Papers I–III).

The upwards increase in element-based grain size proxies (EFs of Zr and Ti) from the middle to upper Blanknuten Mb also indicate increasing hydrodynamic reworking (Paper II). This coincides with the observed layers concentrated in *Tasmanites* algae of age-equivalent mudstones in Svalbard (Riis et al., 2008; Vigran et al., 2008). It must be emphasized that the marine productivity was

still high, resulting in mostly oil-prone source rocks with a calcareous signature (Papers I–III). Thus, elevated marine productivity was the dominant cause for the resulting source potential, while the diminished preservation potential and increased reworking and oxidation explains why these mudstones have less oil potential compared to the underlying middle Blanknuten Mb mudstones.

It should be mentioned that the more proximal depositional conditions during the late Ladinian in Svalbard could have provided increased amounts of river-supplied terrestrial nutrients and freshwater into the basin. Subsequently, these factors may have played an important role in terms of increased primary productivity and water mass restriction through halocline formation during this regressive phase (Høy and Lundschien, 2011; Vigran et al., 2008).

7.1.6 lower Carnian

The lower Carnian mudstones on Svalbard are represented by the Facies F1 mudstones of the Tschermakfjellet Fm (Papers I–III). This unit is considered to demarcate the dominance of the prodeltaic mudstones that formed as a consequence of the continuous progradation of the TBO delta system across the NBS, eventually reaching Svalbard in the Carnian (Leith et al., 1993; Lundschien et al., 2014; Riis et al., 2008). As shown in Paper I, these F1 are equivalent to the lower–middle Muen Mb F1 mudstones, further substantiated by comparing their visual maceral descriptions and biomarker contents (Paper III). Thus, the organic facies of the mudstones from the lowermost Tschermakfjellet Fm are considered similar to those of the lower–middle Muen Mb mudstones (Paper III).

It therefore appears that neither the preservation potential or primary productivity were sufficiently good to accumulate significant quantities of oil-prone OM during the early Carnian in Svalbard. Combined with the overall high Carnian sedimentation rate (Gilmullina et al., 2021), the conditions to accumulate, preserve and concentrate marine OM were generally unfavorable for marine source-rock formation on the NBS (Paper II). However, while the lowermost few meters of this formation may speculatively host borderline oil-prone (kerogen type II/III) source rocks in eastern Svalbard (Paper I and III), they are too insignificant to be considered as liquid hydrocarbon contributors. Still, as these mudstones contain moderate TOC content, the Tschermakfjellet Fm could still host potential gas-prone source rocks in the Svalbard area (Abay et al., 2018; Mørk and Bjorøy, 1984; Mueller et al., 2014).

On the southern NBS, the progradation of the TBO delta system and deposition of prodelta muds and marginal marine sandstones of the Snadd Fm were still ongoing (Gilmullina et al., 2021). The following basins in the western–

northwestern parts of the TBO were still sites of deposition of marine, organic-rich and mudstone successions considered facies-equivalent to the mudstones of the Botneheia Fm:

- The Wandel Sea Basin, northern Greenland (Israrnd Fm) (Alsen et al., 2017; Bjerager et al., 2019)
- The Sverdrup Basin, northern Canada (Hoyle Bay/Murray Harbour formations) (Leith et al., 1993)
- The North Slope Basin, northern Alaska (Shublik Fm) (Parrish et al., 2001)

The lack of extensive and prolific Carnian source rocks on the NBS is therefore attributed to the TBO delta progradation and the change in depositional environment rather than ceased primary productivity and associated O_2 deficiency.

7.2 Source–oil correlation

The bulk bitumen characterization in Paper I combined with the elemental chemostratigraphy in Paper II and the biomarker investigations in Paper III show that the defined lithostratigraphic units exhibit distinct inorganic and organic geochemical assemblages. Papers I–III further cements the fact that their geochemical assemblages reflect changing paleoenvironmental conditions useful to assess and distinguish their source facies (Table 7.1). Thus, in Svalbard, or perhaps the northern NBS, oil–source correlations of migrated oils or bitumen from Triassic source rocks could be performed at the member level or even greater lithostratigraphic resolution.

The performed source–oil correlations with the oils from the southern NBS (see overview of oils in Table 2.3) generally show that the Spathian Vendomdalen Mb—not Middle Triassic Botneheia Fm—correlates the best with the Lower–Triassic-sourced oils contained within the *Wisting Central/Hanssen* discoveries (Paper III). These findings are intriguing, as the mudstones of the Botneheia Fm—not Vendomdalen Mb—typically are considered as the diachronous lateral facies equivalent to the mudstones of the Steinkobbe Fm (e.g., Lundschien et al., 2014; Lutz et al., 2021). As discussed in Papers II–III and this chapter, the Spathian–Anisian boundary marks an important climate change that likely affected the primary productivity and benthic redox potential, ultimately contributing to the abrupt inorganic and organic facies transition at the Vendomdalen Mb–Muen Mb boundary. Thus, the Vendomdalen Mb (Spathian)

and the lower Steinkobbe Fm (Spathian) could be genetically related based on the time-specific occurrence of the Lower Triassic hothouse conditions (Paper II). Similarly, the phosphogenic upper Muen Mb and lower Blanknuten Mb (Both Anisian) would be age- and facies-equivalent and genetically related to the phosphogenic middle–upper Steinkobbe Fm (Anisian), due to the cooler and less restricted Middle Triassic oceans (Paper II). These age-specific climate changes might therefore shed new light on previously reported source facies variations in the Spathian vs. Anisian source rocks of the Steinkobbe Fm (Abay et al., 2018; Isaksen and Bohacs, 1995), with potentially important implications for source–oil correlation in the commercial acreage of the NBS.

Table 7.1: Summary of the investigated lithostratigraphic units in relation to selected geochemical parameters (proxies) useful to interpret benthic oxygen conditions, primary productivity and sedimentation rate/detrital input, and the expected petroleum product during peak maturity. The geochemical values represent the mean ± SD. *The source rock ranking is from best (1) to worst (4), and the upper Muen Mb to upper Blanknuten Mb are ranked equally as they all belong to the same phosphogenic succession and show similar kerogen type. Of the defined lithostratigraphic units, the middle Blanknuten Mb hosts the best source rock succession.

Parameter	Proxy	Vendomdalen Mb	lower–middle Muen Mb	upper Muen Mb	lower Blanknuten Mb	middle Blanknuten Mb	upper Blanknuten Mb	Tschermak-fjellet Fm
Age		Spathian	lower Anisian	middle–upper Anisian	middle–upper Anisian	lower Ladinian	upper Ladinian	lower Carnian
Macroscopic mudstone facies		Fo	F_1	F_2	F_2	F_3	F_2, F_4	F_1
TOC (%)	OM richness	2.70 ± 0.79	1.49 ± 0.64	4.92 ± 1.75	5.90 ± 2.42	8.34 ± 1.93	6.47 ± 2.45	1.72 ± 0.69
HI (mg HC/g TOC)	OM quality	252 ± 12	204 ± 51	451 ± 40	481 ± 46	493 ± 43	459 ± 45	136 ± 72
Kerogen type	OM source	II/III	III to II/III	II	II	II	II	III
U-EF	Redox	3.88 ± 1.24	0.77 ± 0.38	3.43 ± 3.09	5.04 ± 4.07	11.55 ± 3.63	6.22 ± 3.60	1.29 ± 0.44
Mo-EF	Redox	96.90 ± 64.67	1.13 ± 0.90	6.65 ± 3.97	13.79 ± 5.56	31.73 ± 24.43	79.08 ± 53.55	2.20 ± 1.71
Pr/Ph	Redox	1.60 ± 0.11	1.87 ± 0.18	1.75 ± 0.05	1.81 ± 0.11	1.58 ± 0.15	1.75 ± 0.22	2.39 ± 0.21
P-EF	Productivity	1.12 ± 0.19	2.43 ± 2.39	23.51 ± 34.44	64.05 ± 95.29	54.07 ± 27.05	12.40 ± 12.28	0.98 ± 0.29
Ba-EF	Productivity	0.93 ± 0.10	0.76 ± 0.09	0.74 ± 0.09	1.86 ± 0.83	1.79 ± 0.51	1.62 ± 0.64	0.78 ± 0.09
Si-EF	Productivity	1.68 ± 0.06	1.74 ± 0.05	1.85 ± 0.25	2.19 ± 0.79	2.93 ± 0.46	2.63 ± 0.63	1.52 ± 0.12
Al (%)	Detrital input	7.44 ± 0.29	7.06 ± 0.21	6.62 ± 0.67	6.01 ± 1.42	4.18 ± 0.61	4.71 ± 0.95	8.01 ± 0.55
TIC (%)	Carbonate	0.71 ± 0.26	1.39 ± 0.24	1.38 ± 0.31	1.77 ± 0.46	2.23 ± 0.71	4.05 ± 1.56	0.75 ± 0.78
29αβ/30αβ	Carbonate	0.41 ± 0.06	0.42 ± 0.05	0.48 ± 0.09	0.53 ± 0.08	0.56 ± 0.05	0.62 ± 0.10	0.51 ± 0.06
Benthic oxygen conditions	OM preservation	Intermittent euxinic	Oxic–dysoxic	Dysoxic–anoxic	Dysoxic–anoxic	Euxinic	Intermittent euxinic	Oxic
Relative primary productivity	OM generation	Low	Moderate	High	High	Maximum	High	Low
Relative sedimentation rate	OM dilution	High	High	Low	Low	Minimum	Low	High
Main petroleum product		Mixed oil and gas	Mixed oil and gas	Oil	Oil	Oil	Oil	Gas
Source rock ranking*		2	3	1	1	1	1	4

Paper III also shows that biomarker-based thermal maturity parameters, particularly the Ts/(Ts + Tm) and 29Ts/(29Ts + 29αβ) ratios, are highly influenced and correlated with source facies variations. While Triassic source rock extracts from Svalbard show remarkably similar source facies signatures when compared with equivalent pan-Arctic Triassic source rocks or oils (Leith et al., 1993; Thießen et al., 2019), it is stressed that facies effects may significantly affect biomarker-based thermal maturity parameters and thus source–oil or oil–oil correlations in cases where such parameters are used.

7.3 Implications and concluding remarks

Collectively, Papers I–III presented here document changing depositional environments during the Early–Late Triassic, their influence on source rock formation in eastern Svalbard and the NBS (Table 7.1), and their correlation with oils retrieved from the commercial acreage of the NBS. The high sample density, facies descriptions, outcrop observations of excellently exposed strata, and the integration of several organic/inorganic geochemical analyses are shown to liberate a wealth of data that would be impossible with drill cuttings. By using Svalbard as an outcrop analogue, this study has improved the conceptual understanding of the facies distribution and timing of the developing Lower–Upper Triassic source rock depositional environments on the NBS, potentially reducing exploration risk in this relatively underexplored petroleum province.

7.4 Future work

The author recognizes that the interpretations and conclusions made in this study benefit from further investigations and scrutiny. The suggestions below (in no particular order) would provide important knowledge that could verify or further develop the claims made in this study.

A major concern of this study is that it extrapolates regional paleoenvironmental changes in the TBO based on two study localities that are c. 20 km apart. Ideally, time- and facies-equivalent strata onshore Svalbard and in offshore wells on the NBS and in adjacent regions, e.g., the Sverdrup Basin, the North Slope Basin, and the Kotelny Island of the New Siberian Islands should be analyzed as part of the same dataset. The analyses used in this study should subsequently be performed and linked with these localities to address the suggested age- and facies-specific relationships. Furthermore, high resolution biostratigraphy and other dating methods such as Re-Os should ideally be combined to refine the regional and pan-Arctic stratigraphic framework of the Triassic mudstones

(e.g., Xu et al., 2014). This may improve the regional depositional model and timing of Triassic source rock formation and distribution.

It is uncertain how the riverine nutrient supply and fresh water discharge into the basin affected nutrient supply and OM production, as well as water mass stratification due to halocline formation. Their importance relative to the inferred upwelling, marine nutrient supply and OM production during the Middle Triassic has been assessed but essentially remains unsolved. Mapping and/or numerical modeling of Boreal climate, ocean current circulation, water temperatures, ocean anoxic events, fresh water fluxes, and nutrient fluxes within the TBO would indeed provide insight into these fundamentally different source rock-forming processes. These factors could partly be investigated by chemostratigraphic variations in, e.g., $\delta^{18}O_{apatite}$ and $\delta^{13}C$ (Sun et al., 2012). A $\delta^{13}C$ chemostratigraphic study of the Botneheia Fm is currently ongoing at the Natural History Museum at UiO (Engelschiøn et al., 2020).

The unconventional shale oil revolution in the US resulted in a wealth of scientific literature that utilizes microfacies analysis of mudstones (e.g., Percy and Pedersen, 2020; Schieber, 2016). As sedimentation and especially benthic water mass restriction is heavily discussed in this study, it is clear that documenting the microscale sedimentary structure by microfacies analyses would improve the understanding of the hydrodynamic regimes of the defined facies. Furthermore, it would refine the mudstone facies classification of this study and allow significant improvements in determining grain size, sorting, grading, roundness, mineralogy, etc., providing increased insight into the source rock depositional environments with respect to physical sedimentary processes. While several studies exist (Bernhardsen, 2019; Krajewski, 2008; Krajewski, 2013; Vigran et al., 2008; Vigran et al., 2014), microfacies analyses should be included in future studies of the Triassic mudstones.

Detailed biofacies investigations would certainly improve the understanding of the benthic environment and oxygen availability. Implementing high-resolution biofacies models would shed light on the benthic hospitality and thus the OM preservation and accumulation potential. A dedicated and complimentary biofacies study of the Botneheia Fm is currently ongoing at the Natural Historical Museum at UiO (Engelschiøn et al., 2020). Their study applies the same sample set as this study. The results from the two separate, yet complementary studies should be integrated for further refinement of the depositional model for the Triassic mudstones in Svalbard.

The multi-elemental chemostratigraphic framework in Paper II is solely based on whole-rock mudstone samples using WD-XRF and LECO analyses. As discussed in Xu et al. (2012), the total content of redox-sensitive elements in a bulk

mudstone sample can be expressed using Eq. (7.1):

$$\frac{X_{WR}}{Al_{WR}} = \frac{X_{seawater}}{Al_{WR}} + \frac{X_{detrital}}{Al_{WR}} \tag{7.1}$$

where X is the concentration of the redox-sensitive element and WR is the whole-rock composition. The approach used in Paper II could therefore be less than ideal, as inferences of these elements from the detrital fraction—which is unrelated to benthic redox and primary productivity—cannot be ruled out. Future high-resolution chemostratigraphic studies of the investigated succession may benefit from aqua regia digestion of whole-rock samples followed by inductively coupled plasma (ICP)-optical emission spectrometry (OES) or ICP-MS (Xu et al., 2012). Neither of these methods are included in the analytical suite at the geochemical lab at UiT. As WD-XRF analysis could be efficiently performed at UiT at low costs, and the fact that this method is commonly applied in elemental chemostratigraphic studies (Craigie, 2018), it was considered adequate for the purpose of Paper II.

The source–oil correlations are solely based on published work and selected *n*-alkanes, acyclic isoprenoids and biomarkers quantified using SIM-mode. This limited approach could have overlooked potentially important parameters that would have shed new light on the correlation potential between the mudstone extracts and the oils (e.g., $\delta^{13}C$, diamondoids, GCMS/MS-based biomarkers, TA-DMCs, porphyrins, light hydrocarbons). Furthermore, the SIM-mode itself is less than ideal to quantify many of the biomarkers used in Paper III, as SIM-mode is prone to interfering compounds when quantifying selected biomarkers, potentially resulting in erroneous parameter values. However, applying GCMS/MS-mode to quantify selected parameters requires significantly more instrument run-time, a rather costly affair that was not prioritized. The use of the SIM/MS-based data may therefore serve as screening data for future work that aim to quantify and evaluate selected GCMS/MS parameters for paleoenvironmental and/or source–oil correlation studies.

/8

References

Abay, T. B., Karlsen, D. A., Lerch, B., Olaussen, S., Pedersen, J. H., and Backer-Owe, K. (2017). "Migrated Petroleum in Outcropping Mesozoic Sedimentary Rocks in Spitsbergen: Organic Geochemical Characterization and Implications for Regional Exploration." In: *Journal of Petroleum Geology* **40**, pp. 5–36.

Abay, T. B., Karlsen, D. A., and Pedersen, J. H. (2014). "Source Rocks at Svalbard: An Overview of Jurassic and Triassic Formations and Comparison with OffshoreBarents Sea Time Equivalent Source Rock Formations." In: *Search and Discovery*. Article #30372.

Abay, T. B., Karlsen, D. A., Pedersen, J. H., Olaussen, S., and Backer-Owe, K. (2018). "Thermal maturity, hydrocarbon potential and kerogen type of some Triassic–Lower Cretaceous sediments from the SW Barents Sea and Svalbard." In: *Petroleum Geoscience* **24**, pp. 349–373.

Abdullah, W. H. (1999). "Organic facies variations in the Triassic shallow marine and deep marine shales of central Spitsbergen, Svalbard." In: *Marine and Petroleum Geology* **16**, pp. 467–481.

Algeo, T. J. and Li, C. (2020). "Redox classification and calibration of redox thresholds in sedimentary systems." In: *Geochimica Et Cosmochimica Acta* **287**, pp. 8–26.

Algeo, T. J. and Liu, J. S. (2020). "A re-assessment of elemental proxies for paleoredox analysis." In: *Chemical Geology* **540**.

Algeo, T. J. and Lyons, T. W. (2006). "Mo-total organic carbon covariation in modern anoxic marine environments: Implications for analysis of paleoredox and paleohydrographic conditions." In: *Paleoceanography* **21**.

Algeo, T. J. and Maynard, J. B. (2004). "Trace-element behavior and redox facies in core shales of Upper Pennsylvanian Kansas-type cyclothems." In: *Chemical Geology* **206**, pp. 289–318.

Algeo, T. J. and Maynard, J. B. (2008). "Trace-metal covariation as a guide to water-mass conditions in ancient anoxic marine environments." In: *Geosphere* **4**, pp. 872–887.

Algeo, T. J. and Rowe, H. (2012). "Paleoceanographic applications of trace-metal concentration data." In: *Chemical Geology* **324**, pp. 6–18.

Algeo, T. J. and Tribovillard, N. (2009). "Environmental analysis of paleoceanographic systems based on molybdenum-uranium covariation." In: *Chemical Geology* **268**, pp. 211–225.

Algeo, T. J., Kuwahara, K., Sano, H., Bates, S., Lyons, T., Elswick, E., Hinnov, L., Ellwood, B., Moser, J., and Maynard, J. B. (2011). "Spatial variation in sediment fluxes, redox conditions, and productivity in the Permian–Triassic Panthalassic Ocean." In: *Palaeogeography, Palaeoclimatology, Palaeoecology* **308**, pp. 65–83.

Alsen, P., McRoberts, C., Svennevig, K., Bojesen-Koefoed, J., Hovikoski, J., and Piasecki, S. (2017). "The Israd Formation: a Middle Triassic Daonella-bearing, black shale unit in Kilen, North Greenland (with a note on the Triassic in Amdrup Land)." In: *Newsletters on Stratigraphy* **50**, pp. 31–46.

Anaconda Inc. (2021). *Anaconda Software Distribution*. Version 2021.05. URL: `https://docs.anaconda.com/`.

Anell, I., Braathen, A., Olaussen, S., and Osmundsen, P. T. (2013). "Evidence of faulting contradicts a quiescent northern Barents Shelf during the Triassic." In: *first break* **31**, pp. 67–76.

Anell, I., Faleide, J.-I., and Braathen, A. (2016). "Regional tectono-sedimentary development of the highs and basins of the northwestern Barents Shelf." In: *Norwegian Journal of Geology* **96**, pp. 27–41.

Aquino Neto, F. R., Triguis, J., Azevedo, D. A., Rodrigues, R., and Simoneit, B. R. T. (1992). "Organic Geochemistry of Geographically Unrelated Tasmanites." In: *Organic Geochemistry* **18**, pp. 791–803.

Ardakani, O. H., Chappaz, A., Sanei, H., and Mayer, B. (2016). "Effect of thermal maturity on remobilization of molybdenum in black shales." In: *Earth and Planetary Science Letters* **449**, pp. 311–320.

Atar, E., Marz, C., Schnetger, B., Wagner, T., and Aplin, A. (2019). "Local to global controls on the deposition of organic-rich muds across the Late Jurassic Laurasian Seaway." In: *Journal of the Geological Society* **176**, pp. 1143–1153.

Bastow, T. P., Aarssen, B. G. K. van, and Lang, D. (2007). "Rapid small-scale separation of saturate, aromatic and polar components in petroleum." In: *Organic Geochemistry* **38**, pp. 1235–1250.

Berner, R. A. (1984). "Sedimentary Pyrite Formation - an Update." In: *Geochimica Et Cosmochimica Acta* **48**, pp. 605–615.

Berner, R. A. and Raiswell, R. (1983). "Burial of Organic-Carbon and Pyrite Sulfur in Sediments over Phanerozoic Time - a New Theory." In: *Geochimica Et Cosmochimica Acta* **47**, pp. 855–862.

Bernhardsen, S. (2019). "A sedimentological study of the organic-rich Botneheia Formation (Middle Triassic) with emphasis on the ichnogenus Thalassinoides, Edgeøya, Svalbard." MSc thesis. Norwegian University of Science and Technology (NTNU).

Betts, J. and Holland, H. (1991). "The oxygen content of ocean bottom waters, the burial efficiency of organic carbon, and the regulation of atmospheric oxygen." In: *Global and Planetary Change* **5**. Atmospheric Oxygen Variation Through Geologic Time, pp. 5–18.

Bjerager, M., Alsen, P., Hovikoski, J., Lindstrom, S., Pilgaard, A., Stemmerik, L., and Therkelsen, J. (2019). "Triassic lithostratigraphy of the Wandel Sea Basin, North Greenland." In: *Bulletin of the Geological Society of Denmark* **67**, pp. 83–105.

Bjorøy, M., Hall, P. B., Ferriday, I. L., and Mørk, A. (2009). "Triassic Source Rocks of the Barents Sea and Svalbard." In: *Search and Discovery*. Article #40641.

Blinken, A. J. (2021). *Imposition of Further Sanctions in Connection with Nord Stream 2*. URL: https://www.state.gov/imposition-of-further-sanctions-in-connection-with-nord-stream-2/ (visited on 01/10/2022).

Boës, X., Rydberg, J., Martinez-Cortizas, A., Bindler, R., and Renberg, I. (2011). "Evaluation of conservative lithogenic elements (Ti, Zr, Al, and Rb) to study anthropogenic element enrichments in lake sediments." In: *Journal of Paleolimnology* **46**, pp. 75–87.

Bohacs, K. M., Grabowski, G. J., Carroll, A. R., Mankiewicz, P. J., Miskell-Gerhardt, K. J., Schwalbach, J. R., Wegner, M. B., and Simo, J. A. (2005). "Production, Destruction, and Dilution—The Many Paths to Source-Rock Development." In: *Deposition of Organic-Carbon-Rich Sediments: Models*. Vol. 82. SEPM Society for Sedimentary Geology, pp. 61–101.

Borchers, S. L., Schnetger, B., Boning, P., and Brumsack, H. J. (2005). "Geochemical signatures of the Namibian diatom belt: Perennial upwelling and intermittent anoxia." In: *Geochemistry Geophysics Geosystems* **6**.

Bordovskiy, O. (1965). "Accumulation of organic matter in bottom sediments." In: *Marine Geology* **3**. Organic matter in marine sediments, pp. 33–82.

Bourbonniere, R. A. and Meyers, P. A. (1996). "Sedimentary geolipid records of historical changes in the watersheds and productivities of Lakes Ontario and Erie." In: *Limnology and Oceanography* **41**, pp. 352–359.

Brand, A., Allen, L., Altman, M., Hlava, M., and Scott, J. (2015). "Beyond authorship: attribution, contribution, collaboration, and credit." In: *Learned Publishing* **28**, pp. 151–155.

Brekke, T., Krajewski, K. P., and Hubred, J. H. (2014). "Organic geochemistry and petrography of thermally altered sections of the Middle Triassic Botneheia Formation on south-western Edgeøya, Svalbard." In: *Norwegian Petroleum Directorate Bulletin* **11**, pp. 111–128.

Bue, E. P. and Andresen, A. (2014). "Constraining depositional models in the Barents Sea region using detrital zircon U-Pb data from Mesozoic sediments in Svalbard." In: *Sediment Provenance Studies in Hydrocarbon Exploration and Production* **386**, pp. 261–279.

Bugge, T. and Fanavoll, S. (1995). "The Svalis Dome, Barents Sea - a geological playground for shallow stratigraphic drilling." In: *First Break* **13**, pp. 237–251.

Calvert, S. E. and Pedersen, T. F. (2007). "Elemental Proxies for Palaeoclimatic and Palaeoceanographic Variability in Marine Sediments: Interpretation and Application." In: *Developments in Marine Geology*. Ed. by Hillaire–Marcel, C. and De Vernal, A. Vol. 1. Elsevier. Chap. 14, pp. 567–644.

Chen, J. B., Zhao, L. S., Algeo, T. J., Zhou, L., Zhang, L., and Qiu, H. (2019). "Evaluation of paleomarine redox conditions using Mo-isotope data in low-[Mo] sediments: A case study from the Lower Triassic of South China." In: *Palaeogeography, Palaeoclimatology, Palaeoecology* **519**, pp. 178–193.

Connan, J., Bouroullec, J., Dessort, D., and Albrecht, P. (1986). "The microbial input in carbonate-anhydrite facies of a sabkha palaeoenvironment from Guatemala: A molecular approach." In: *Organic Geochemistry* **10**, pp. 29–50.

Connan, J. and Cassou, A. M. (1980). "Properties of gases and petroleum liquids derived from terrestrial kerogen at various maturation levels." In: *Geochimica et Cosmochimica Acta* **44**, pp. 1–23.

Cornford, C., Needham, C., and De Walque, L. (1986). "Geochemical habitat of North Sea oils." In: *Habitat of Hydrocarbons on the Norwegian Continental Shelf, Proceedings of an International Conference*. Ed. by Spencer, A. Graham & Trotman, pp. 39–54.

Craigie, N. W. (2015). "Applications of chemostratigraphy in Middle Jurassic unconventional reservoirs in eastern Saudi Arabia." In: *Geoarabia* **20**, pp. 79–110.

Craigie, N. (2018). *Principles of Elemental Chemostratigraphy*. Advances in Oil and Gas Exploration & Production. Cham: Springer International Publishing, p. 189.

Craigie, N. W., Breuer, P., and Khidir, A. (2016). "Chemostratigraphy and biostratigraphy of Devonian, Carboniferous and Permian sediments encountered in eastern Saudi Arabia: An integrated approach to reservoir correlation." In: *Marine and Petroleum Geology* **72**, pp. 156–178.

Creaney, S. and Passey, Q. R. (1993). "Recurring patterns of total organic carbon and source rock quality within a sequence stratigraphic framework." In: *AAPG Bulletin* **77**, pp. 386–401.

Dahlgren, S., Hanesand, T., Mills, N., Patience, R., Brekke, T., and Sinding-Larsen, R. (1998). "Norwegian Geochemical Standard samples: Svalbard Rock – 1 (NGS SR-1)." In: *Norwegian Geochemical Standards newsletter* **1**.

Dallmann, W. K., ed. (1999). *Lithostratigraphic Lexicon of Svalbard. Upper Palaeozoic to Quaternary bedrock. Review and recommendations for nomenclature use*. Norwegian Polar Institute (NPI), p. 320.

Dallmann, W. K. and Elvevold, S. (2015). "Bedrock geology." In: *Geoscience Atlas of Svalbard*. Ed. by Dallmann, W. Norwegian Polar Institute (NPI). Chap. 7, pp. 133–174.

Demaison, G. J. and Huizinga, B. J. (1991). "Genetic Classification of Petroleum Systems." In: *AAPG Bulletin* **75**, pp. 1626–1643.

Demaison, G. J. and Moore, G. T. (1980). "Anoxic Environments and Oil Source Bed Genesis." In: *AAPG Bulletin* **64**, pp. 1179–1209.

Demaison, G., Holck, J. J., Jones, R. W., and Moore, G. T. (1983). "Predictive Source Bed Stratigraphy: A Guide to Regional Petroleum Occurrence." In: *Proceedings of the 11th World Petroleum Congress (WPC)*. Vol. 2. London: John Wiley & Sons, pp. 1–13.

DNV (2021). *Energy Transition Outlook 2021*. URL: https://eto.dnv.com/2021 (visited on 10/25/2021).

Dow, W. (1977). "Kerogen studies and geological interpretations." In: *Journal of Geochemical Exploration* **7**, pp. 77–79.

Eggimann, D. W., Manheim, F. T., and Betzer, P. R. (1980). "Dissolution and analysis of amorphous silica in marine sediments." In: *Journal of Sedimentary Research* **50**, pp. 215–225.

Eide, C. H., Klausen, T. G., Katkov, D., Suslova, A. A., and Helland-Hansen, W. (2018). "Linking an Early Triassic delta to antecedent topography: Source-to-sink study of the southwestern Barents Sea margin." In: *GSA Bulletin* **130**, pp. 263–283.

Eisenberg, R. and Harris, P. (1995). "Application of chemostratigraphy and multivariate statistical analysis to differentiating bounding stratigraphic surfaces." In: *Carbonate Facies and Sequence Stratigraphy: Practical Applications of Carbonate Models*. Ed. by Pausé, P. and Candelaria, M. Permian Basin Section-SEPM Publication 95-36 / Permian Basin Graduate Center Publication 5-95, pp. 83–102.

Ellis, D. V. and Singer, J. M. (2007). "Gamma Ray Devices." In: *Well Logging for Earth Scientists*. Ed. by Ellis, D. V. and Singer, J. M. Springer Netherlands, pp. 267–288.

Embry, A. (1993). "Crockerland — the northwest source area for the Sverdrup Basin, Canadian Arctic Islands." In: *Norwegian Petroleum Society Special Publications*. Ed. by Vorren, T., Bergsager, E., Dahl-Stamnes, Ø., Holter, E., Johansen, B., Lie, E., and Lund, T. Vol. 2. Elsevier, pp. 205–216.

Embry, A. (2009). "Crockerland – The Source Area for the Triassic to Middle Jurassic Strata of Northern Axel Heiberg Island, Canadian Arctic Islands." In: *Bulletin of Canadian Petroleum Geology* **57**, pp. 129–140.

Engelschiøn, V. S., Wesenlund, F., Hurum, J. H., Hammer, Ø., and Mørk, A. (2020). "East-west depositional trends and fossil preservation in the Middle Triassic Botneheia Fm. on Svalbard." In: *ARCEx Annual Conference 2020*. The Research Centre for Arctic Petroleum Exploration.

England, W. A. and Mackenzie, A. S. (1989). "Some Aspects of the Organic Geochemistry of Petroleum Fluids." In: *Geologische Rundschau* **78**, pp. 291–303.

Faleide, J. I., Gudlaugsson, S. T., and Jacquart, G. (1984). "Evolution of the western Barents Sea." In: *Marine and Petroleum Geology* **1**, pp. 123–150.

Faleide, J. I., Tsikalas, F., Breivik, A. J., Mjelde, R., Ritzmann, O., Engen, Ø., Wilson, J., and Eldholm, O. (2008). "Structure and evolution of the continental margin off Norway and the Barents Sea." In: *Episodes* **31**, pp. 82–91.

Farrimond, P. (2019a). *Rearranged hopanes in petroleum geochemistry*. Integrated Geochemical Interpretation (IGI) Ltd. URL: https://igiltd.com/news/rearranged-hopanes-in-petroleum-geochemistry/ (visited on 01/10/2022).

Farrimond, P. (2019b). "Recognizing the causes ofcomplex (mixed) molecular-maturity signals in oils." In: *29th International Meeting on Organic Geochemistry (IMOG)*. European Association of Organic Geochemists. Gothenburg, Sweden.

Ferriday, T. and Montenari, M. (2016). "Chemostratigraphy and Chemofacies of Source Rock Analogues." In: *Stratigraphy & Timescales*. Ed. by Montenari, M. Vol. 1. Stratigraphy & Timescales. Academic Press. Chap. 3, pp. 123–255.

Filippelli, G. M. (2011). "Phosphate rock formation and marine phosphorus geochemistry: the deep time perspective." In: *Chemosphere* **84**, pp. 759–66.

Fleming, E. J., Flowerdew, M. J., Smyth, H. R., Scott, R. A., Morton, A. C., Omma, J. E., Frei, D., and Whitehouse, M. J. (2016). "Provenance of Triassic

sandstones on the southwest Barents Shelf and the implication for sediment dispersal patterns in northwest Pangaea." In: *Marine and Petroleum Geology* **78**, pp. 516–535.

Francois, R. (1988). "A Study on the Regulation of the Concentrations of Some Trace-Metals (Rb, Sr, Zn, Pb, Cu, V, Cr, Ni, Mn and Mo) in Saanich Inlet Sediments, British-Columbia, Canada." In: *Marine Geology* **83**, pp. 285–308.

Garcia, R. J. L., Silva, J. B. da, Abreu, I. M., Soares, S. A. R., Araujo, R. G. O., Souza, E. S. de, Ribeiro, H. J. S., Hadlich, G. M., and Queiroz, A. F. D. (2020). "Application of PCA and HCA in geochemical parameters to distinguish depositional paleoenvironments from source rocks." In: *Journal of South American Earth Sciences* **103**.

George, S. C., Volk, H., Ahmed, M., Pickel, W., and Allan, T. (2007). "Biomarker evidence for two sources for solid bitumens in the Subu wells: Implications for the petroleum prospectivity of the East Papuan Basin." In: *Organic Geochemistry* **38**, pp. 609–642.

Georgiev, S. V., Stein, H. J., Hannah, J. L., Yang, G., Markey, R. J., Dons, C. E., Pedersen, J. H., and di Primio, R. (2019). "Comprehensive evolution of a petroleum system in absolute time: The example of Brynhild, Norwegian North Sea." In: *Chemical Geology* **522**, pp. 260–282.

Gilmullina, A., Klausen, T. G., Paterson, N. W., Suslova, A., and Eide, C. H. (2021). "Regional correlation and seismic stratigraphy of Triassic Strata in the Greater Barents Sea: Implications for sediment transport in Arctic basins." In: *Basin Research* **33**, pp. 1546–1579.

Glørstad-Clark, E., Birkeland, E. P., Nystuen, J. P., Faleide, J. I., and Midtkandal, I. (2011). "Triassic platform-margin deltas in the western Barents Sea." In: *Marine and Petroleum Geology* **28**, pp. 1294–1314.

Glørstad-Clark, E., Faleide, J. I., Lundschien, B. A., and Nystuen, J. P. (2010). "Triassic seismic sequence stratigraphy and paleogeography of the western Barents Sea area." In: *Marine and Petroleum Geology* **27**, pp. 1448–1475.

Goldberg, E. D. and Arrhenius, G. O. S. (1958). "Chemistry of Pacific Pelagic Sediments." In: *Geochimica Et Cosmochimica Acta* **13**, pp. 153–212.

Grabowski, J., Stoykova, K., Wierzbowski, H., and Wójcik-Tabol, P. (2021). "Upper Berriasian chemostratigraphy, clay minerals and calcareous nannofossils of the Barlya section (Western Balkan, Bulgaria): Implications for palaeoclimate and productivity changes, and stratigraphic correlations across the

Alpine Tethys." In: *Palaeogeography, Palaeoclimatology, Palaeoecology* **567**, p. 110252.

Grantham, P. J. and Wakefield, L. L. (1988). "Variations in the Sterane Carbon Number Distributions of Marine Source Rock Derived Crude Oils through Geological Time." In: *Organic Geochemistry* **12**, pp. 61–73.

Grasby, S. E., Beauchamp, B., Embry, A., and Sanei, H. (2013). "Recurrent Early Triassic ocean anoxia." In: *Geology* **41**, pp. 175–178.

Grasby, S. E., Beauchamp, B., and Knies, J. (2016). "Early Triassic productivity crises delayed recovery from world's worst mass extinction." In: *Geology* **44**, pp. 779–782.

Grasby, S. E., Knies, J., Beauchamp, B., Bond, D. P. G., Wignall, P., and Sun, Y. D. (2020). "Global warming leads to Early Triassic nutrient stress across northern Pangea." In: *Geological Society of America Bulletin* **132**, pp. 943–954.

Haile, B. G., Klausen, T. G., Jahren, J., Braathen, A., and Hellevang, H. (2018). "Thermal history of a Triassic sedimentary sequence verified by a multi-method approach: Edgeoya, Svalbard, Norway." In: *Basin Research* **30**, pp. 1075–1097.

Hammer, Ø., Jones, M. T., Schneebeli-Hermann, E., Hansen, B. B., and Bucher, H. (2019). "Are Early Triassic extinction events associated with mercury anomalies? A reassessment of the Smithian/Spathian boundary extinction." In: *Earth-Science Reviews* **195**, pp. 179–190.

Hansen, B. B., Hammer, Ø., and Nakrem, H. A. (2018). "Stratigraphy and age of the Grippia niveau bonebed, Lower Triassic Vikinghøgda Formation, Spitsbergen." In: *Norwegian Journal of Geology* **98**, pp. 175–187.

Helz, G. R., Bura-Nakic, E., Mikac, N., and Ciglenecki, I. (2011). "New model for molybdenum behavior in euxinic waters." In: *Chemical Geology* **284**, pp. 323–332.

Helz, G. R., Miller, C. V., Charnock, J. M., Mosselmans, J. F. W., Pattrick, R. A. D., Garner, C. D., and Vaughan, D. J. (1996). "Mechanism of molybdenum removal from the sea and its concentration in black shales: EXAFS evidence." In: *Geochimica Et Cosmochimica Acta* **60**, pp. 3631–3642.

Henriksen, E., Bjørnseth, H. M., Hals, T. K., Heide, T., Kiryukhina, T., Kløvjan, O. S., Larssen, G. B., Ryseth, A. E., Rønning, K., Sollid, K., and Stoupakova, A. (2011a). "Uplift and erosion of the greater Barents Sea: impact on prospec-

tivity and petroleum systems." In: *Arctic Petroleum Geology*. Ed. by Spencer, A. M., Embry, A. F., Gautier, D. L., Stoupakova, A. V., and Sørensen, K. Vol. 35. Geological Society, London, Memoirs. The Geological Society of London. Chap. 17, pp. 271–281.

Henriksen, E., Ryseth, A. E., Larssen, G. B., Heide, T., Rønning, K., Sollid, K., and Stoupakova, A. V. (2011b). "Tectonostratigraphy of the greater Barents Sea: implications for petroleum systems." In: *Arctic Petroleum Geology*. Ed. by Spencer, A. M., Embry, A. F., Gautier, D. L., Stoupakova, A. V., and Sørensen, K. Vol. 35. Geological Society, London, Memoirs. The Geological Society of London. Chap. 10, pp. 163–195.

Hildred, G., Ratcliffe, K., and Schmidt, K. (2011). "Application of inorganic whole-rock geochemistry to shale resource plays: an example from the Eagle Ford Shale, Texas." In: *Houston Geological Society Bulletin* **53**, pp. 31–38.

Hildred, G. (2012). "Shale Resource Plays in the Horn River Basin, British Columbia, Canada: Using High Resolution Chemostratigraphy to Determine Well-Bore Pathways in Multi-Lateral Drilling Campaigns." In: *Houston Geological Society Bulletin* **55**, 21 and 23.

Holba, A., Ellis, L., Dzou, L., Hallam, A., Masterson, D., Francu, J., and Fincannon, A. (2001). "Extended tricyclic terpanes as age discriminators between Triassic, Early Jurassic and Middle-Late Jurassic oils." In: *20th International Meeting on Organic Geochemistry*.

Hounslow, M. W., Hu, M. Y., Mørk, A., Weitschat, W., Vigran, J. O., Karloukovski, V., and Orchard, M. J. (2008a). "Intercalibration of Boreal and Tethyan time scales: the magnetobiostratigraphy of the Middle Triassic and the latest Early Triassic from Spitsbergen, Arctic Norway." In: *Polar Research* **27**, pp. 469–490.

Hounslow, M. W., Peters, C., Mørk, A., Weitschat, W., and Vigran, J. O. (2008b). "Biomagnetostratigraphy of the Vikinghogda Formation, Svalbard (Arctic Norway), and the geomagnetic polarity timescale for the Lower Triassic." In: *Geological Society of America Bulletin* **120**, pp. 1305–1325.

Høy, T. and Lundschien, B. A. (2011). "Triassic deltaic sequences in the northern Barents Sea." In: *Arctic Petroleum Geology*. Ed. by Spencer, A. M., Embry, A. F., Gautier, D. L., Stoupakova, A. V., and Sørensen, K. Vol. 35. The Geological Society of London. Chap. 249, pp. 249–260.

Huang, W. Y. and Meinschein, W. G. (1979). "Sterols as Ecological Indicators." In: *Geochimica Et Cosmochimica Acta* **43**, pp. 739–745.

Hubred, J. H. (2006). "Thermal Effects of Basaltic Sill Emplacement in Source Rocks on Maturation and Hydrocarbon Generation." MSc thesis. University of Oslo (UiO).

Hughes, W. B., Holba, A. G., and Dzou, L. I. P. (1995). "The Ratios of Dibenzothiophene to Phenanthrene and Pristane to Phytane as Indicators of Depositional Environment and Lithology of Petroleum Source Rocks." In: *Geochimica Et Cosmochimica Acta* **59**, pp. 3581–3598.

Hurum, J., Roberts, A., Nakrem, H., Stenløkk, J., and Mørk, A. (2014). "The first recovered ichthyosaur from the Middle Triassic of Edgeøya, Svalbard." In: *Norwegian Petroleum Directorate Bulletin* **11**, pp. 97–110.

Isaksen, G. H. and Bohacs, K. M. (1995). "Geological Controls of Source Rock Geochemistry Through Relative Sea Level; Triassic, Barents Sea." In: *Petroleum Source Rocks*. Ed. by Katz, B. J. Berlin, Heidelberg: Springer Berlin Heidelberg, pp. 25–50.

Islam, M. R. (2020). *Economically and Environmentally Sustainable Enhanced Oil Recovery*. John Wiley & Sons and Scrivener Publishing LLC, p. 816.

Isozaki, Y. (1997). "Permo-Triassic Boundary Superanoxia and Stratified Superocean: Records from Lost Deep Sea." In: *Science* **276**, pp. 235–238.

Jarvis, I., Burnett, W. C., Nathan, Y., Almbaydin, F. S. M., Attia, A. K. M., Castro, L. N., Flicoteaux, R., Hilmy, M. E., Husain, V., Qutawnah, A. A., Serjani, A., and Zanin, Y. N. (1994). "Phosphorite Geochemistry - State-of-the-Art and Environmental Concerns." In: *Eclogae Geologicae Helvetiae* **87**, pp. 643–700.

Jiang, L., George, S. C., and Zhang, M. (2018). "The occurrence and distribution of rearranged hopanes in crude oils from the Lishu Depression, Songliao Basin, China." In: *Organic Geochemistry* **115**, pp. 205–219.

Jones, B. and Manning, D. A. C. (1994). "Comparison of Geochemical Indexes Used for the Interpretation of Palaeoredox Conditions in Ancient Mudstones." In: *Chemical Geology* **111**, pp. 111–129.

Karlsen, D. A. and Larter, S. R. (1991). "Analysis of Petroleum Fractions by TLC-FID - Applications to Petroleum Reservoir Description." In: *Organic Geochemistry* **17**, pp. 603–617.

Katz, B. J. (2005). "Controlling Factors on Source Rock Development—A Review of Productivity, Preservation, and Sedimentation Rate." In: *The Deposition of Organic-Carbon-Rich Sediments: Models, Mechanisms, and Consequences*.

Vol. 82. SEPM Special Publication. SEPM Society for Sedimentary Geology, pp. 7–16.

Klausen, T. G., Nyberg, B., and Helland-Hansen, W. (2019). "The largest delta plain in Earth's history." In: *Geology* **47**, pp. 470–474.

Klausen, T. G., Ryseth, A. E., Helland-Hansen, W., Gawthorpe, R., and Laursen, I. (2015). "Regional development and sequence stratigraphy of the Middle to Late Triassic Snadd Formation, Norwegian Barents Sea." In: *Marine and Petroleum Geology* **62**, pp. 102–122.

Klausen, T. G. (2013). "Does evidence of faulting contradict a quiescent northern Barents Shelf during the Triassic?" In: *first break* **31**, pp. 69–72.

Koeverden, J. H. van, Karlsen, D. A., and Backer-Owe, K. (2011). "Carboniferous non-marine source rocks from Spitsbergen and Bjørnøya: Comparison with the western Arctic." In: *Journal of Petroleum Geology* **34**, pp. 53–66.

Koeverden, J. H. van, Karlsen, D. A., Schwark, L., Chpitsglouz, A., and Backer-Owe, K. (2010). "Oil-prone Lower Carboniferous coals in the Norwegian Barents Sea: Implications for a Palaeozoic petroleum system." In: *Journal of Petroleum Geology* **33**, pp. 155–182.

Kolodny, Y. (2009). "Phosphorite." In: *Encyclopedia of Paleoclimatology and Ancient Environments*. Ed. by Gornitz, V. Dordrecht: Springer Netherlands, pp. 775–780.

Krajewski, K. P. (2008). "The Botneheia Formation (Middle Triassic) in Edgeøya and Barentsøya, Svalbard: lithostratigraphy, facies, phosphogenesis, paleoenvironment." In: *Polish Polar Research* **29**, pp. 319–364.

Krajewski, K. P. (2013). "Organic matter-apatite-pyrite relationships in the Botneheia Formation (Middle Triassic) of eastern Svalbard: Relevance to the formation of petroleum source rocks in the NW Barents Sea shelf." In: *Marine and Petroleum Geology* **45**, pp. 69–105.

Krajewski, K. P. and Weitschat, W. (2015). "Depositional History of the Youngest Strata of the Sassendalen Group (Bravaisberget Formation, Middle Triassic-Carnian) in Southern Spitsbergen, Svalbard." In: *Annales Societatis Geologorum Poloniae* **85**, pp. 151–175.

Kvalheim, O. M., Christy, A. A., Telnæs, N., and Bjørseth, A. (1987). "Maturity determination of organic matter in coals using the methylphenanthrene distribution." In: *Geochimica et Cosmochimica Acta* **51**, pp. 1883–1888.

LaGrange, M. T., Konhauser, K. O., Catuneanu, O., Harris, B. S., Playter, T. L., and Gingras, M. K. (2020). "Sequence stratigraphy in organic-rich marine mudstone successions using chemostratigraphic datasets." In: *Earth-Science Reviews* **203**, p. 103137.

Larssen, G., Elvebakk, G., Henriksen, L., Kristensen, S.-E., Nilsson, I., Samuelsberg, T., Svånå, T., Stemmerik, L., and Worsley, D. (2002). *Upper Palaeozoic lithostratigraphy of the Southern Norwegian Barents Sea*. Norwegian Petroleum Directorate.

Le Tran, K. and Philippe, B. (1993). "Oil and Rock Extract Analysis." In: *Applied Petroleum Geochemistry*. Ed. by Bordenave, M. Editions Technip. Chap. II.4, pp. 376–394.

Leith, T. L., Weiss, H. M., Mørk, A., Århus, N., Elvebakk, G., Embry, A. F., Brooks, P. W., Stewart, K. R., Pchelina, T. M., Bro, E. G., Verba, M. L., Danyushevskaya, A., and Borisov, A. V. (1993). "Mesozoic hydrocarbon source rocks of the Arctic region." In: *Arctic Geology and Petroleum Potential*. Ed. by Vorren, T. O., Bergsager, E., Dahl-Stamnes, A., Holter, E., Johansen, Å., Lie, Å., and Lund, T. B. NPF Special Publication. Amsterdam: Elsevier, pp. 1–25.

Lerch, B., Karlsen, D. A., Abay, T. B., Duggan, D., Seland, R., and Backer-Owe, K. (2016a). "Regional petroleum alteration trends in Barents Sea oils and condensates as a clue to migration regimes and processes." In: *AAPG Bulletin* **100**, pp. 165–190.

Lerch, B., Karlsen, D. A., Matapour, Z., Seland, R., and Backer-Owe, K. (2016b). "Organic geochemistry of Barents Sea petroleum: Thermal maturity and alteration and mixing processes in oils and condensates." In: *Journal of Petroleum Geology* **39**, pp. 125–148.

Lerch, B., Karlsen, D. A., Seland, R., and Backer-Owe, K. (2017). "Depositional environment and age determination of oils and condensates from the Barents Sea." In: *Petroleum Geoscience* **23**, pp. 190–209.

Lerch, B., Karlsen, D. A., Thiessen, O., Abay, T. B., Soelen, E. E. van, Kurschner, W. M., Planke, S., and Backer-Owe, K. (2018). "Investigations on the use of triaromatic dimethylcholesteroids as age-specific biomarkers in bitumens and oils from Arctic Norway." In: *Organic Geochemistry* **122**, pp. 1–16.

Lewan, M. D. (1984). "Factors controlling the proportionality of vanadium to nickel in crude oils." In: *Geochimica Et Cosmochimica Acta* **48**, pp. 2231–2238.

Liang, L. J., Sun, Y., Beets, C., Prins, M., Wu, F., and Vandenberghe, J. (2013). "Impacts of grain size sorting and chemical weathering on the geochemistry of Jingyuan loess in the northwestern Chinese Loess Plateau." In: *Journal of Asian Earth Sciences* **69**, pp. 177–184.

Liblik, T. and Lips, U. (2019). "Stratification Has Strengthened in the Baltic Sea – An Analysis of 35 y of Observational Data." In: *Frontiers in Earth Science* **7**.

Line, L. H., Jahren, J., and Hellevang, H. (2018). "Mechanical compaction in chlorite-coated sandstone reservoirs - Examples from Middle - Late Triassic channels in the southwestern Barents Sea." In: *Marine and Petroleum Geology* **96**, pp. 348–370.

Logan, A. (2020). *Triassic Period*. URL: https://www.britannica.com/science/Triassic-Period (visited on 10/26/2021).

Lord, G. S., Johansen, S. K., Stoen, S. J., and Mørk, A. (2017). "Facies development of the Upper Triassic succession on Barentsøya, Wilhelmøya and NE Spitsbergen, Svalbard." In: *Norwegian Journal of Geology* **97**, pp. 33–62.

Lorenson, T., Hostettler, F., Rosenbauer, R., Peters, K., Kvenvolden, K., Dougherty, J., Gutmacher, C., Wong, F., and Normark, W. (2009). *Natural Offshore Oil Seepage and Related Tarball Accumulation on the California Coastline—Santa Barbara Channel and the Southern Santa Maria Basin; Source Identification and Inventory*. Tech. rep. U.S. Geological Survey.

Lundschien, B. A., Høy, T., and Mørk, A. (2014). "Triassic hydrocarbon potential in the Northern Barents Sea; integrating Svalbard and stratigraphic core data." In: *Norwegian Petroleum Directorate Bulletin* **11**, pp. 3–20.

Lutz, R., Klitzke, P., Weniger, P., Blumenberg, M., Franke, D., Reinhardt, L., Ehrhardt, A., and Berglar, K. (2021). "Basin and petroleum systems modelling in the northern Norwegian Barents Sea." In: *Marine and Petroleum Geology* **130**, p. 105128.

Magoon, L. B. and Dow, W. G. (1994). "The Petroleum System." In: *The Petroleum System - From Source to Trap*. Ed. by Magoon, L. B. and Dow, W. G. AAPG. Chap. 1, pp. 3–24.

Mansour, A., Gentzis, T., Carvajal-Ortiz, H., Tahoun, S. S., Elewa, A. M., and Mohamed, O. (2020). "Source rock evaluation of the Cenomanian Raha Formation, Bakr oil field, Gulf of Suez, Egypt: Observations from palynofacies, RGB-based sporomorph microscopy, and organic geochemistry." In: *Marine and Petroleum Geology* **122**.

Matapour, Z. and Karlsen, D. A. (2018). "Ages of Norwegian oils and bitumen based on age-specific biomarkers." In: *Petroleum Geoscience* **24**, pp. 92–101.

Matapour, Z., Karlsen, D. A., Lerch, B., and Backer-Owe, K. (2019). "Petroleum occurrences in the carbonate lithologies of the Gohta and Alta discoveries in the Barents Sea, Arctic Norway." In: *Petroleum Geoscience* **25**, pp. 50–70.

Mello, M. R., Gaglianone, P. C., Brassell, S. C., and Maxwell, J. R. (1988). "Geochemical and biological marker assessment of depositional environments using Brazilian offshore oils." In: *Marine and Petroleum Geology* **5**, pp. 205–223.

Moldowan, J. M., Sundararaman, P., and Schoell, M. (1986). "Sensitivity of Biomarker Properties to Depositional Environment and or Source Input in the Lower Toarcian of Southwest Germany." In: *Organic Geochemistry* **10**, pp. 915–926.

Moldowan, J. M., Dahl, J., Huizinga, B. J., Fago, F. J., Hickey, L. J., Peakman, T. M., and Taylor, D. W. (1994). "The Molecular Fossil Record of Oleanane and Its Relation to Angiosperms." In: *Science* **265**, pp. 768–771.

Mongenot, T., Tribovillard, N.-P., Desprairies, A., Lallier-Vergès, E., and Laggoun-Defarge, F. (1996). "Trace elements as palaeoenvironmental markers in strongly mature hydrocarbon source rocks: the Cretaceous La Luna Formation of Venezuela." In: *Sedimentary Geology* **103**, pp. 23–37.

Morford, J. L. and Emerson, S. (1999). "The geochemistry of redox sensitive trace metals in sediments." In: *Geochimica Et Cosmochimica Acta* **63**, pp. 1735–1750.

Mørk, A., Dallmann, W. K., Dypvik, H., Johannessen, E. P., Larssen, G. B., Nagy, J., Nøttvedt, A., Olaussen, S., Pčelina, T. M., and Worsley, D. (1999a). "Mesozoic lithostratigraphy." In: *Lithostratigraphic Lexicon of Svalbard*. Ed. by Dallmann, W. K. Norwegian Polar Institute, pp. 127–214.

Mørk, A., Egorov, A. Y., and Embry, A. F. (1994). "Base Olenekian and base Anisian sequence boundaries produced by Triassic circumpolar 'synchronous' transgressions." In: *1992 proceedings: international conference on Arctic margins, Anchorage, Alaska, September 1992*. Ed. by Thurston, D. K. and Fujita, K. US. Department of the Interior, Mineral Management Service, pp. 9–14.

Mørk, A. and Elvebakk, G. (1999). "Lithological description of subcropping Lower and Middle Triassic rocks from the Svalis Dome, Barents Sea." In: *Polar Research* **18**, pp. 83–104.

Mørk, A., Elvebakk, G., Forsberg, A. W., Hounslow, M. W., Nakrem, H. A., Vigran, J. O. S., and Weitschat, W. (1999b). "The type section of the Vikinghøgda Formation: a new Lower Triassic unit in central and eastern Svalbard." In: *Polar Research* **18**, pp. 51–82.

Mørk, A., Knarud, R., and Worsley, D. (1982). "Depositional and diagenetic environments of the Triassic and Lower Jurassic succession of Svalbard." In: *Arctic geology and geophysics: Proceedings of the Third International Symposium on Arctic Geology*. Ed. by Embry, A. F. and Balkwill, H. R. Canadian Society of Petroleum Geologists Memoir 8, pp. 371–398.

Mørk, A. (2015). "Historical Geology - Triassic." In: *Geoscience Atlas of Svalbard*. Ed. by Dallmann, W. 148. Norwegian Polar Institute (NPI). Chap. 6-7, pp. 133–174.

Mørk, A. and Bjorøy, M. (1984). "Mesozoic source rocks on Svalbard." In: *Proceedings of the North European Margin Symposium (NEMS '83), organized by the Norwegian Petroleum Society and held at the Norwegian Institute of Technology (NTH) in Trondheim 9–11 May*. Ed. by Spencer, A. M. Petroleum Geology of the North European Margin. Springer Netherlands, pp. 371–382.

Mørk, A. and Bromley, R. G. (2008). "Ichnology of a marine regressive systems tract: the Middle Triassic of Svalbard." In: *Polar Research* **27**, pp. 339–359.

Mørk, A., Embry, A., and Weitschat, W. (1989). "Triassic transgressive-regressive cycles in the Sverdrup Basin, Svalbard and the Barents Shelf." In: *Correlation in Hydrocarbon Exploration*. Ed. by Collinson, J. Graham and Trotman, pp. 113–130.

Mueller, S., Veld, H., Nagy, J., and Kürschner, W. M. (2014). "Depositional history of the Upper Triassic Kapp Toscana Group on Svalbard, Norway, inferred from palynofacies analysis and organic geochemistry." In: *Sedimentary Geology* **310**, pp. 16–29.

Muller, R., Klausen, T. G., Faleide, J. I., Olaussen, S., Eide, C. H., and Suslova, A. (2019). "Linking regional unconformities in the Barents Sea to compression-induced forebulge uplift at the Triassic-Jurassic transition." In: *Tectonophysics* **765**, pp. 35–51.

Nagy, J., Hess, S., Dypvik, H., and Bjærke, T. (2011). "Marine shelf to paralic biofacies of Upper Triassic to Lower Jurassic deposits in Spitsbergen." In: *Palaeogeography, Palaeoclimatology, Palaeoecology* **300**, pp. 138–151.

Nicolaisen, J. B., Elvebakk, G., Ahokas, J., Bojesen-Koefoed, J. A., Olaussen, S., Rinna, J., Skeie, J. E., and Stemmerik, L. (2019). "Characterization of Upper Palaeozoic Organic-Rich Units in Svalbard: Implications for the Petroleum Systems of the Norwegian Barents Shelf." In: *Journal of Petroleum Geology* **42**, pp. 59–78.

Niebuhr, B. (2005). "Geochemistry and time-series analyses of orbitally forced Upper Cretaceous marl–limestone rhythmites (Lehrte West Syncline, northern Germany)." In: *Geological Magazine* **142**, pp. 31–55.

Nogrady, B. (2021). "Most fossil-fuel reserves must remain untapped to hit 1.5 °C warming goal." In: *Nature* **597**, pp. 316–317.

Norges Bank Investment Management (2021). *Dette er Oljefondet*. URL: https://www.nbim.no/no/oljefondet/om-oljefondet/ (visited on 10/21/2021).

Norlex Project (2012). *Standard Lithostratigraphy of Offshore Norway*. URL: https://timescalefoundation.org/resources/NW_Europe_Lex/stratchart_files/StandardLithostratigraphicWallchartOffshoreNorway.pdf (visited on 10/21/2021).

norskpetroleum.no (2021). *Exploration activity*. URL: https://www.norskpetroleum.no/en/exploration/exploration-activity/ (visited on 10/21/2021).

Norwegian National Committee for Research Ethics in Science and Technology (2014). *Forskningsetisk vurdering av petroleumsforskning (Saksnr. 2014/3)*. URL: https://www.forskningsetikk.no/om-oss/komiteer-og-utvalg/nent/uttalelser/vedrorende-forskningsetisk-vurdering-av-petroleumsforskning-saksnr-20143/ (visited on 10/21/2021).

Norwegian Petroleum Directorate (2017). *Geological assessment of petroleum resources in eastern parts of Barents Sea North*.

Norwegian Petroleum Directorate (2021a). *Factpages*. URL: https://factpages.npd.no/en/ (visited on 10/21/2021).

Norwegian Petroleum Directorate (2021b). *Factpages - Steinkobbe Formation*. URL: https://factpages.npd.no/en/strat/pageview/litho/formations/158 (visited on 10/21/2021).

Ogata, K., Mulrooney, M. J., Braathen, A., Maher, H., Osmundsen, P. T., Anell, I., Smyrak-Sikora, A. A., and Balsamo, F. (2018). "Architecture, deformation style and petrophysical properties of growth fault systems: the Late Triassic

deltaic succession of southern Edgeøya (East Svalbard)." In: *Basin Research* **30**, pp. 1042–1073.

Ohm, S. E., Karlsen, D. A., and Austin, T. J. F. (2008). "Geochemically driven exploration models in uplifted areas: Examples from the Norwegian Barents Sea." In: *AAPG Bulletin* **92**, pp. 1191–1223.

Osmundsen, P. T., Braathen, A., Rød, R. S., and Hynne, I. B. (2014). "Styles of normal faulting and fault-controlled sedimentation in the Triassic deposits of Eastern Svalbard." In: *Norwegian Petroleum Directorate Bulletin* **11**, pp. 61–79.

Pang, H., Pan, B., Garzanti, E., Gao, H., Zhao, X., and Chen, D. (2018). "Mineralogy and geochemistry of modern Yellow River sediments: Implications for weathering and provenance." In: *Chemical Geology* **488**, pp. 76–86.

Parrish, J. T., Droser, M. L., and Bottjer, D. J. (2001). "A Triassic upwelling zone: The Shublik Formation, Arctic Alaska, USA." In: *Journal of Sedimentary Research* **71**, pp. 272–285.

Parrish, J. and Curtis, R. (1982). "Atmospheric circulation, upwelling, and organic-rich rocks in the Mesozoic and Cenozoic eras." In: *Palaeogeography, Palaeoclimatology, Palaeoecology* **40**, pp. 31–66.

Paterson, N. W., Mangerud, G., and Mørk, A. (2017). "Late Triassic (early Carnian) palynology of shallow stratigraphical core 7830/5-U-1, offshore Kong Karls Land, Norwegian Arctic." In: *Palynology* **41**, pp. 230–254.

Paterson, N. W., Mangerud, G., Cetean, C. G., Mørk, A., Lord, G. S., Klausen, T. G., and Mørkved, P. T. (2016). "A multidisciplinary biofacies characterisation of the Late Triassic (late Carnian–Rhaetian) Kapp Toscana Group on Hopen, Arctic Norway." In: *Palaeogeography, Palaeoclimatology, Palaeoecology* **464**, pp. 16–42.

Pčelina, T. M. and Korčinskaja, M. V. (2008). "Palaeogeographic reconstructions of the Russian Boreal areas and Svalbard during the Triassic." In: *Polar Research* **27**, pp. 491–494.

Pedersen, J., Brunstad, H., Kristensen, T., and Primio, R. di (2017). "The 7120/1-3 Gohta Oil Discovery - Opening up a Permian Petroleum System on the Loppa High, SW Barents Sea." In: *28th International Meeting on Organic Geoschemistry (IMOG)*. European Association of Organic Geochemists. Florence, Italy.

Pedersen, J., Hammer, E., Bernhardsen, S., Engelschiøn, V., Hansen, B., Hurum, J., Hammer, Ø., Hansen, G., and Nyjordet, B. (2020). "Verdens første oljeboring på fossil blekksprut!" In: *NGF Oslo meetings Autumn 2020*.

Pedersen, J. H., Karlsen, D. A., Backer-Owe, K., Lie, J. E., and Brunstad, H. (2006). "The geochemistry of two unusual oils from the Norwegian North Sea: implications for new source rock and play scenario." In: *Petroleum Geoscience* **12**, pp. 85–96.

Pedersen, T. F. and Calvert, S. E. (1990). "Anoxia vs productivity - what controls the formation of organic-carbon-rich sediments and sedimentary-rocks?" In: *AAPG Bulletin* **74**, pp. 454–466.

Percy, E. L. and Pedersen, P. K. (2020). "Detailed facies analysis of Cenomanian–Turonian organic-rich mudstones: Implications for depositional controls on source rocks." In: *The Depositional Record* **6**, pp. 409–430.

Peters, K. E. (1986). "Guidelines for Evaluating Petroleum Source Rock Using Programmed Pyrolysis." In: *AAPG Bulletin* **70**, pp. 318–329.

Peters, K. E., Walters, C. C., and Moldowan, J. M. (2005a). "Biomarkers and Isotopes in Petroleum Systems and Earth History." In: *The Biomarker Guide*. Vol. 2. Cambridge University Press.

Peters, K. E., Walters, C. C., and Moldowan, J. M. (2005b). "Biomarkers and Isotopes in the Environment and Human History." In: *The Biomarker Guide*. 2nd ed. Vol. 1. Cambridge University Press.

Peters, K. E. and Cassa, M. R. (1994). "Applied Source Rock Geochemistry." In: *The Petroleum System - From Source to Trap*. Ed. by Magoon, L. B. and Dow, W. G. AAPG. Chap. 5, pp. 93–120.

Philp, R. P., Gilbert, T. D., and Russell, N. J. (1982). "Characterization by Pyrolysis-Gas Chromatography-Mass Spectrometry of the Insoluble Organic Residues Derived from the Hydrogenation of Tasmanites Sp Oil-Shale." In: *Fuel* **61**, pp. 221–226.

Potter, P. E., Maynard, J. B., and Depetris, P. J. (2005). *Mud and Mudstones*. Springer-Verlag Berlin Heidelberg, p. 297.

Qin, Z. Y., Yang, X., and Jiang, M. M. (1985). "Chemostratigraphic Correlation of the Middle and Upper Proterozoic between the Yanshan and Shennongjia Basins." In: *Precambrian Research* **29**, pp. 77–91.

Radke, M., Vriend, S. P., and Schaefer, R. G. (2001). "Geochemical. characterization of lower toarcian source rocks from NW Germany. Interpretation of aromatic and saturated hydrocarbons in relation to depositional environment and maturation effects." In: *Journal of Petroleum Geology* **24**, pp. 287–307.

Radke, M. (1988). "Application of aromatic compounds as maturity indicators in source rocks and crude oils." In: *Marine and Petroleum Geology* **5**, pp. 224–236.

Radke, M., Welte, D. H., and Willsch, H. (1982). "Geochemical study on a well in the Western Canada Basin: relation of the aromatic distribution pattern to maturity of organic matter." In: *Geochimica et Cosmochimica Acta* **46**, pp. 1–10.

Raiswell, R., Buckley, F., Berner, R. A., and Anderson, T. F. (1988). "Degree of pyritization of iron as a paleoenvironmental Indicator of bottom-water oxygenation." In: *Journal of Sedimentary Petrology* **58**, pp. 812–819.

Ramirez-Montoya, E., Madhavaraju, J., and Monreal, R. (2021). "Geochemistry of the sedimentary rocks from the Antimonio and Río Asunción formations, Sonora, Mexico: Implications for weathering, provenance and chemostratigraphy." In: *Journal of South American Earth Sciences* **106**, p. 103035.

Riboulleau, A., Baudin, F., Deconinck, J. F., Derenne, S., Largeau, C., and Tribovillard, N. (2003). "Depositional conditions and organic matter preservation pathways in an epicontinental environment: the Upper Jurassic Kashpir Oil Shales (Volga Basin, Russia)." In: *Palaeogeography, Palaeoclimatology, Palaeoecology* **197**, pp. 171–197.

Riis, F., Lundschien, B. A., Høy, T., Mørk, A., and Mørk, M. B. E. (2008). "Evolution of the Triassic shelf in the northern Barents Sea region." In: *Polar Research* **27**, pp. 318–338.

Rohatgi, A. (2021). *Webplotdigitizer: Version 4.5*. URL: https://automeris.io/WebPlotDigitizer.

Rosenberg, Y. O., Reznik, I. J., Vinegar, H. J., Feinstein, S., and Bartov, Y. (2021). "Comparing natural and artificial thermal maturation of a Type II-S source rock, Late Cretaceous, Israel." In: *Marine and Petroleum Geology* **124**, p. 104773.

Rothwell, R. G. and Croudace, I. W. (2015). "Twenty Years of XRF Core Scanning Marine Sediments: What Do Geochemical Proxies Tell Us?" In: *Micro-XRF Studies of Sediment Cores: Applications of a non-destructive tool for the envi-*

ronmental sciences. Ed. by Croudace, I. W. and Rothwell, R. G. Developments in Paleoenvironmental Research. Dordrecht: Springer Netherlands. Chap. 2, pp. 25–102.

Rubinstein, I., Sieskind, O., and Albrecht, P. (1975). "Rearranged Sterenes in a Shale - Occurrence and Simulated Formation." In: *Journal of the Chemical Society-Perkin Transactions 1*, pp. 1833–1836.

Sanei, H., Ardakani, O. H., Akai, T., Akihisa, K., Jiang, C. Q., and Wood, J. M. (2020). "Core versus cuttings samples for geochemical and petrophysical analysis of unconventional reservoir rocks." In: *Scientific Reports* **10**.

Schatz, W. (2005). "Palaeoecology of the Triassic black shale bivalve Daonella—new insights into an old controversy." In: *Palaeogeography, Palaeoclimatology, Palaeoecology* **216**, pp. 189–201.

Schieber, J. (2016). "Mud re-distribution in epicontinental basins - Exploring likely processes." In: *Marine and Petroleum Geology* **71**, pp. 119–133.

Schoepfer, S. D., Shen, J., Wei, H., Tyson, R. V., Ingall, E., and Algeo, T. J. (2015). "Total organic carbon, organic phosphorus, and biogenic barium fluxes as proxies for paleomarine productivity." In: *Earth-Science Reviews* **149**, pp. 23–52.

Schou, L., Mørk, A., and Bjorøy, M. (1984). "Correlation of source rocks and migrated hydrocarbons by GC-MS in the Middle Triassic of Svalbard." In: *Organic Geochemistry* **6**, pp. 513–520.

Scikit-learn (2021). *sklearn.decomposition.PCA*. URL: https://scikit-learn.org/stable/modules/generated/sklearn.decomposition.PCA.html (visited on 01/14/2022).

SciPy (2021). *scipy.cluster.hierarchy.linkage*. URL: https://docs.scipy.org/doc/scipy/reference/reference/generated/scipy.cluster.hierarchy.linkage.html#scipy.cluster.hierarchy.linkage (visited on 01/14/2022).

Scott, C. and Lyons, T. W. (2012). "Contrasting molybdenum cycling and isotopic properties in euxinic versus non-euxinic sediments and sedimentary rocks: Refining the paleoproxies." In: *Chemical Geology* **324**, pp. 19–27.

seaborn (2021). *seaborn.clustermap*. URL: https://seaborn.pydata.org/generated/seaborn.clustermap.html (visited on 01/14/2022).

Seifert, W. and Moldowan, J. (1978). “Applications of steranes, terpanes and monoaromatics to the maturation, migration and source of crude oils.” In: *Geochimica et Cosmochimica Acta* **42**, pp. 77–95.

Seifert, W. and Moldowan, J. (1980). “The effect of thermal stress on source-rock quality as measured by hopane stereochemistry.” In: *Physics and Chemistry of the Earth* **12**, pp. 229–237.

Seifert, W. and Moldowan, J. (1986). “Use of biological markers in petroleum exploration.” In: *Methods in Geochemistry and Geophysics*. Ed. by Johns, R. Elsevier, pp. 261–290.

Selley, R. C. and Sonnenberg, S. A. (2015). *Elements of Petroleum Geology*. 3rd ed. Elsevier, p. 507.

Shanmugam, G. (1985). “Significance of Coniferous Rain Forests and Related Organic-Matter in Generating Commercial Quantities of Oil, Gippsland Basin, Australia.” In: *AAPG Bulletin* **69**, pp. 1241–1254.

Silva, R. L., Carlisle, C. A. M., and Wach, G. (2017). “A new TOC, Rock-Eval, and carbon isotope record of Lower Jurassic source rocks from the Slyne Basin, offshore Ireland.” In: *Marine and Petroleum Geology* **86**, pp. 499–511.

Sinninghe Damsté, J. S., Kenig, F., Koopmans, M. P., Koster, J., Schouten, S., Hayes, J. M., and Deleeuw, J. W. (1995). “Evidence for Gammacerane as an Indicator of Water Column Stratification.” In: *Geochimica Et Cosmochimica Acta* **59**, pp. 1895–1900.

Smelror, M. and Sollid, K. (2007). “Blekkspruter fulle av olje.” In: *GEO* **2**, pp. 28–29.

Sømme, T. O., Dore, A. G., Lundin, E. R., and Torudbakken, B. O. (2018). “Triassic-Paleogene paleogeography of the Arctic: Implications for sediment routing and basin fill.” In: *AAPG Bulletin* **102**, pp. 2481–2517.

Song, J., Littke, R., Maquil, R., and Weniger, P. (2014). “Organic facies variability in the Posidonia Black Shale from Luxembourg: Implications for thermal maturation and depositional environment.” In: *Palaeogeography, Palaeoclimatology, Palaeoecology* **410**, pp. 316–336.

Steel, R. J. and Worsley, D. (1984). “Svalbard’s post-Caledonian strata — an atlas of sedimentational patterns and palaeogeographic evolution.” In: *Petroleum Geology of the North European Margin*. Ed. by Spencer, A. M. Graham and Trotman. Chap. 8, pp. 209–135.

Stemmerik, L. and Worsley, D. (2005). "30 years on - Arctic Upper Palaeozoic stratigraphy, depositional evolution and hydrocarbon prospectivity." In: *Norwegian Journal of Geology* **85**, pp. 151–168.

Sun, Y., Joachimski, M. M., Wignall, P. B., Yan, C., Chen, Y., Jiang, H., Wang, L., and Lai, X. (2012). "Lethally hot temperatures during the Early Triassic greenhouse." In: *Science* **338**, pp. 366–70.

Szmytkiewicz, A. and Zalewska, T. (2014). "Sediment deposition and accumulation rates determined by sediment trap and 210Pb isotope methods in the Outer Puck Bay (Baltic Sea)." In: *Oceanologia* **56**, pp. 85–106.

Taylor, K. G. and Macquaker, J. H. S. (2014). "Diagenetic alterations in a silt- and clay-rich mudstone succession: an example from the Upper Cretaceous Mancos Shale of Utah, USA." In: *Clay Minerals* **49**, pp. 213–227.

Taylor, S. and McLennan, S. (1985). *The Continental Crust: Its Composition and Evolution*. London: Blackwell Scientific Publishers, p. 312.

Thießen, O., Weiss, H., Smelror, M., and Sollid, K. (2019). "Triassic oil from the Botneheia Formation of Svalbard and oil–oil correlation with recent Norwegian Barents Sea discoveries." In: *29th International Meeting on Organic Geochemistry (IMOG)*. European Association of Organic Geochemists. Gothenburg, Sweden.

Thöle, H., Bornemann, A., Heimhofer, U., Luppold, F. W., Blumenberg, M., Dohrmann, R., and Erbacher, J. (2019). "Using high-resolution XRF analyses as a sequence stratigraphic tool in a mudstone-dominated succession (Early Cretaceous, Lower Saxony Basin, Northern Germany)." In: *The Depositional Record* **6**, pp. 236–258.

Tissot, B. P. and Welte, D. H. (1984). *Petroleum Formation and Occurrence*. 2nd ed. Springer-Verlag Berlin Heidelberg, p. 702.

Tribovillard, N., Algeo, T. J., Baudin, F., and Riboulleau, A. (2012). "Analysis of marine environmental conditions based on molybdenum–uranium covariation—Applications to Mesozoic paleoceanography." In: *Chemical Geology* **324-325**, pp. 46–58.

Tribovillard, N., Algeo, T. J., Lyons, T., and Riboulleau, A. (2006). "Trace metals as paleoredox and paleoproductivity proxies: An update." In: *Chemical Geology* **232**, pp. 12–32.

Tsikalas, F., Uncini, G., Mavilla, N., Staine, I., Casaglia, F., Leutscher, J., Gennaro, M., Arrigoni, V., Gustafsson, L.-E., Galimberti, R., and Daturi, C. (2018). "Goliat Discovery - A Knowledge-Based Approach, Persistence and the First Commercial Oil Development in the Norwegian Arctic." In: *Search and Discovery*. Article #20415.

Twitchett, R., Krystyn, L., Baud, A., Wheeley, J., and Richoz, S. (2004). "Rapid marine recovery after the end-Permian mass-extinction event in the absence of marine anoxia." In: *Geology* **32**, pp. 805–808.

Tyson, R. (2001). "Sedimentation rate, dilution, preservation and total organic carbon: some results of a modelling study." In: *Organic Geochemistry* **32**, pp. 333–339.

Tyson, R. V. (1995). *Sedimentary Organic Matter. Organic facies and palynofacies*. Springer Dordrecht, p. 615.

U.S. Energy Information Administration (2021). *Short-term energy outlook*. URL: `https://www.eia.gov/outlooks/steo/report/global_oil.php` (visited on 01/10/2022).

Van der Weijden, C. H. (2002). "Pitfalls of normalization of marine geochemical data using a common divisor." In: *Marine Geology* **184**, pp. 167–187.

Vigran, J. O., Mørk, A., Forsberg, A. W., Weiss, H. M., and Weitschat, W. (2008). "Tasmanites algae-contributors to the Middle Triassic hydrocarbon source rocks of Svalbard and the Barents Shelf." In: *Polar Research* **27**, pp. 360–371.

Vigran, J. O., Mangerud, G., Mørk, A., Bugge, T., and Weitschat, W. (1998). "Biostratigraphy and sequence stratigraphy of the Lower and Middle Triassic deposits from the Svalis Dome, Central Barents Sea, Norway." In: *Palynology* **22**, pp. 89–141.

Vigran, J. O., Mangerud, G., Mørk, A., Worsley, D., and Hochuli, P. A. (2014). *Palynology and geology of the Triassic succession of Svalbard and the Barents Sea*. Geological Survey of Norway Special Publication. Norwegian Geological Survey, p. 270.

Walters, C. C. (2006). "The Origin of Petroleum." In: *Practical Advances in Petroleum Processing*. Ed. by Hsu, C. S. and Robinson, P. R. New York, NY: Springer New York, pp. 79–101.

Wang, Y.-P., Zou, Y.-R., Shi, J.-T., and Shi, J. (2018). "Review of the chemometrics application in oil-oil and oil-source rock correlations." In: *Journal of Natural Gas Geoscience* **3**, pp. 217–232.

Waples, D. W. and Curiale, J. A. (1999). "Oil–Oil and Oil–Source Rock Correlations." In: *Exploring for Oil and Gas Traps*. Ed. by Beaumont, E. A. and Foster, N. H. Vol. 3. AAPG.

Wedepohl, K. H. (2004). "The composition of Earth's upper crust, natural cycles of elements, natural resources." In: *Elements and their compounds in the environment*. Ed. by Merian, E., Anke, M., Ihnat, M., and Stoeppler, M. 2nd ed. Weinheim: WILEY-VCH Verlag GmbH & Co. KGaA, pp. 3–16.

Weiss, H., Wilhelms, A., Mills, N., Scotchmer, J., Hall, P., Lind, K., and Brekke, T. (2000). *NIGOGA - The Norwegian Industry Guide to Organic Geochemical Analyses*. Report.

Weitschat, W. and Lehmann, U. (1983). "Stratigraphy and ammonoids from the Middle Triassic Botneheia Formation (Daonella Shales) of Spitsbergen." In: *Mitteilungen Geologisch–Paläontologisches Institut der Universität Hamburg* **54**, pp. 27–54.

Welsby, D., Price, J., Pye, S., and Ekins, P. e. a. (2021). "Unextractable fossil fuels in a 1.5 °C world." In: *Nature* **597**, pp. 230–234.

Wesenlund, F., Grundvåg, S. A., Engelschiøn, V. S., Thießen, O., and Pedersen, J. H. (2022). "Multi-elemental chemostratigraphy of Triassic mudstones in E astern Svalbard: implications for source rock formation in front of the World's largest delta." Accepted in *The Depositional Record* pending copyediting.

Wesenlund, F., Grundvåg, S.-A., Engelschiøn, V. S., Thießen, O., and Pedersen, J. H. (2021). "Linking facies variations, organic carbon richness and bulk bitumen content – A case study of the organic-rich Middle Triassic shales from eastern Svalbard." In: *Marine and Petroleum Geology* **132**. 105168.

Wickham, H. (2014). "Tidy Data." In: *Journal of Statistical Software* **59**, pp. 1–23.

Wignall, P. B., Bond, D. P. G., Sun, Y. D., Grasby, S. E., Beauchamp, B., Joachimski, M. M., and Blomeier, D. P. G. (2016). "Ultra-shallow-marine anoxia in an Early Triassic shallow-marine clastic ramp (Spitsbergen) and the suppression of benthic radiation." In: *Geological Magazine* **153**, pp. 316–331.

Wilhelms, A. and Larter, S. (2004). "Shaken but not always stirred. Impact of petroleum charge mixing on reservoir geochemistry." In: *Understanding*

Petroleum Reservoirs: Towards an Integrated Reservoir Engineering and Geochemical Approach. Ed. by Cubitt, J. M., England, W., and Larter, S. R. Vol. 237. Special Publications. London: Geological Society, pp. 27–35.

Wołkowicz, S., Graniczny, M., Wołkowicz, K., and Urban, H. (2017). "History of the oil industry in Poland until 1939." In: *History of Geoscience: Celebrating 50 Years of INHIGEO*. Ed. by Mayer, W., Clary, R. M., Azuela, L. F., Mota, T. S., and Wołkowicz, S. Vol. 442. Special Publications. London: Geological Society of London, pp. 401–411.

Wright, A. M., Spain, D., and Ratcliffe, T. K. (2010). "Application of Inorganic Whole Rock Geochemistry to Shale Resource Plays." In: *The Canadian Unconventional Resources and International Petroleum Conference*. SPE-137946-MS. Calgary, Alberta, Canada: Society of Petroleum Engineers (SPE).

Xu, G. P., Hannah, J. L., Bingen, B., Georgiev, S., and Stein, H. J. (2012). "Digestion methods for trace element measurements in shales: Paleoredox proxies examined." In: *Chemical Geology* **324**, pp. 132–147.

Xu, G. P., Hannah, J. L., Stein, H. J., Mørk, A., Vigran, J. O., Bingen, B., Schutt, D. L., and Lundschien, B. A. (2014). "Cause of Upper Triassic climate crisis revealed by Re-Os geochemistry of Boreal black shales." In: *Palaeogeography Palaeoclimatology Palaeoecology* **395**, pp. 222–232.

Xu, G., Hannah, J. L., Stein, H. J., Bingen, B., Yang, G., Zimmerman, A., Weitschat, W., Mørk, A., and Weiss, H. M. (2009). "Re–Os geochronology of Arctic black shales to evaluate the Anisian–Ladinian boundary and global faunal correlations." In: *Earth and Planetary Science Letters* **288**, pp. 581–587.

Yurchenko, I. A., Moldowan, J. M., Peters, K. E., Magoon, L. B., and Graham, S. A. (2018). "The role of calcareous and shaly source rocks in the composition of petroleum expelled from the Triassic Shublik Formation, Alaska North Slope." In: *Organic Geochemistry* **122**, pp. 52–67.

Zhang, F. F., Romaniello, S. J., Algeo, T. J., Lau, K. V., Clapham, M. E., Richoz, S., Herrmann, A. D., Smith, H., Horacek, M., and Anbar, A. D. (2018). "Multiple episodes of extensive marine anoxia linked to global warming and continental weathering following the latest Permian mass extinction." In: *Science Advances* **4**.

Zhang, J., Zeng, Y., and Slatt, R. (2019). "XRF (X-ray fluorescence) applied to characterization of unconventional Woodford Shale (Devonian, U.S.A.) lateral well heterogeneity." In: *Fuel* **254**.

Zhao, J., Jin, Z., Jin, Z., Geng, Y., Wen, X., and Yan, C. (2016). "Applying sedimentary geochemical proxies for paleoenvironment interpretation of organic-rich shale deposition in the Sichuan Basin, China." In: *International Journal of Coal Geology* **163**, pp. 52–71.

Zuchuat, V., Sleveland, A. R. N., Twitchett, R. J., Svensen, H. H., Turner, H., Augland, L. E., Jones, M. T., Hammer, Ø., Hauksson, B. T., Haflidason, H., Midtkandal, I., and Planke, S. (2020). "A new high-resolution stratigraphic and palaeoenvironmental record spanning the End-Permian Mass Extinction and its aftermath in central Spitsbergen, Svalbard." In: *Palaeogeography, Palaeoclimatology, Palaeoecology* **554**.